

https://dspace.org/

Chemical and structural studies of substituted transition metal carbonyl complexes

Harris, Gillian Wendy

2015-01-23
http://hdl.handle.net/10539/16724

Downloaded from a DSpace repository. https://dspace.org/

CHEMICAL AND STRUCTURAL STUDIES OF SUBSTITUTED TRANSITION METAL CARBONYL COMPLEXES

by

Gillian Wendy Harris

A Thesis Submitted to the Faculty of Science,
University of the Witwatersrand, Johannesburg,
for the Degree of Doctor of Philosophy.

November 1984

ABSTRACT

Catalytic routes were employed to prepare isonitrile (RNC) and phosphine (PR_3) substituted derivatives of monomeric and dimeric transition metal carbonyl complexes, representative new derivatives being characterized by single crystal X-ray crystallography.

Isonitrile derivatives of $(\eta^6\text{-Arene})Cr(CO)_3$ and $(\eta^5C_5H_5)$-$Mn(CO)_3$ were synthesized by catalysed substitution reactions, catalysts being $[(\eta^5C_5Me_5)Rh(CO)]_2$ and/or PdO. The structures of two of the new derivatives, $(\eta\text{-}C_6H_5CCMe)Cr(CO)_2(CNBu^t)$, and $(\eta^5C_5H_5)Mn(CO)_2(CNBu^t)$, were determined by X-ray crystallography, and stereochemical information obtained used in explaining anomalous IR spectra of these complexes.

X-ray crystallography was employed to establish the substitution geometry of the di-isonitrile derivative of iron pentacarbonyl, $Fe(CO)_3(CNMe)_2$. The molecular structure was unable to account for anomalies in the IR spectrum.

A chemical and structural study was undertaken of isonitrile and phosphine derivatives of $Re_2(CO)_{10}$. The use of PdO to catalyse the reaction between $Re_2(CO)_{10}$ and RNC enabled the facile syntheses of the isonitrile derivatives $Re_2(CO)_{10-n}(CNR)_n$ (n = 1-4). These new derivatives were fully characterized by IR, ^1H NMR and *mass spectroscopy*. X-ray crystallography established the structures of a series of representative compounds, $Re_2(CO)_9(CNBu^t)$, $Re_2(CO)_8(CNC_6H_3Me_2\text{-}2,6)_2$, $Re_2(CO)_7(CNMe)_3$ and $Re_2(CO)_6(CNC_6H_3Me_2\text{-}2,6)_4$. The structures of two analogous manganese carbonyl isonitrile derivatives, $Mn_2(CO)_8(CNBu^t)_2$ and $Mn_2(CO)_6(CNC_6H_3Me_2\text{-}2,6)_4$, were also investigated by X-ray crystallography. Differences observed in the IR and ^1H NMR spectra of the di-isonitrile derivatives of *rhenium and manganese* carbonyl could be explained in terms of the observed molecular structures. The stereochemistry of the mono- to tetra-isonitrile substituted derivatives are discussed in terms of electronic and steric factors.

Attempts were made to extend the Pd-catalysed carbonyl substitution reaction of $Re_2(CO)_{10}$ to phosphine ligands. Although the catalysed reaction with PR_3 is much less facile than with RNC, this route was successfully employed in the synthesis of mono- and

di-substituted phosphine derivatives, $Re_2(CO)_{10-n}(PR_3)_n$ (n = 1,2). The X-ray crystal structure of diax$[Re_2(CO)_8(PMe_2Ph)_2]$ was determined. A correlation was established between IR spectral data and substitution geometry for $M_2(CO)_8(L)_2$ (M = Re,Mn) complexes.

This study demonstrated the synthetic utility of transition metal-catalysed routes to substituted metal carbonyl derivatives. X-ray crystallography was shown to be a powerful tool in the rationalization, in terms of structure, of certain observed properties of these complexes.

DECLARATION

I hereby declare that the work presented in this thesis was carried out exclusively by myself under the supervision of Professor J.C.A Boeyens and Dr. N.J. Coville.

This thesis has neven been submitted for a degree in any other university.

G.W. Harris

1 November 1984

ACKNOWLEDGEMENTS

I should like to express my sincere thanks to the following:-

- Professor J.C.A. Boeyens and Dr. N.J. Coville, my supervisors, for their guidance and enthusiasm.
- Professor G.J. Kruger, for advice on crystallographic problems in Professor Boeyens' absence.
- Mr. J. Albain, for the collection of the X-ray data.
- Mr. D.C. Levendis, for assistance with computing problems.
- Dr. M.O. Albers, for helpful advice on certain synthetic aspects, and for running the FTIR spectra.
- Dr. P.R. Boshoff, for running the mass spectra.
- Professor I.S. Butler, and Mr. P.D. Harvey, of McGill University, Montreal, for communicating the results of their Raman studies on the $Re_2(CO)_{10-n}(CNR)_n$ (n = 1-4) complexes prepared as part of this work.
- Mrs. A. Maritz, for typing this thesis.
- Mrs. M. Crabb and Mrs. R. Hillier, for the labelling of the ORTEP diagrams.

Finally, I wish to acknowledge the financial support from the University of the Witwatersrand, and the South African Council for Scientific and Industrial Research.

In addition, I should like to express my gratitude to

- Mr. M.I.J. Maneef, of Birbeck College, University of London, for use of the EMPMDS program.
- Drs. D.S. Moss, R.A. Palmer and B.J. Howlin, of Birkbeck College, University of London, for advice on crystallographic and computing problems.

and Professor. T.L. Blundell, of Birkbeck College, for the use of the College Computing facilities.

PREFACE

It is not for nothing that the scholar invented the Ph.D. thesis as his principal contribution to literary form. The Ph.D. thesis is the perfect image of his world. It is work done for the sake of doing work - perfectly conscientious, perfectly laborious, perfectly irresponsible.

- Archibald MacLeish
(*The Irresponsibles*)

TABLE OF CONTENTS

ACKNOWLEDGEMENTS			v
LIST OF TABLES			xix
LIST OF FIGURES			xxv
LIST OF ABBREVIATIONS AND SYMBOLS			xxxi
I.	Introduction		1
II	Catalytic Synthesis and characterization of Isonitrile Derivatives of (η^6-Arene)$Cr(CO)_3$		5
	2.1	Introduction	5
	2.2	Result	7
	2.2.1	Reaction of (η^6-Arene)$Cr(CO)_3$ complexes with isonitriles	7
	2.2.2	Reaction of ($\eta^6-C_6H_5CO_2Me$)$Cr(CO)_3$ with 2,6-$Me_2C_6H_3NC$, in the presence of Iron Dimer Catalysts	8
	2.2.3	Formation of by-products of the type $Cr(CO)_{6-n}(CNC_6H_3Me_2\text{-}2,6)_n$ (n = 3,4) in the reaction of ($\eta^6-C_6H_5CO_2Me$)-$Cr(CO)_3$ with 2,6-$Me_2C_6H_3NC$	10
	2.3	Spectroscopic properties of (η^6Arene)$Cr(CO)_2$-*(CNR) complexes*	11
	2.3.1	Infra Red	11
	2.3.2	Proton Nuclear Magnetic Resonance	11
	2.3.3	Mass Spectrum of ($\eta^6-C_6H_5CO_2Me$)-$Cr(CO)_2(CNBu^t)$	11
	2.4	Experimental	14
	2.4.1	The catalysed synthesis of [($\eta^6-C_6H_5X$)-$Cr(CO)_2(CNR)$] (X = H, Cℓ, CO_2Me; R = Bu^t, 2,6-$Me_2C_6H_3$)	14
	2.4.2	Reaction of ($\eta^6-C_6H_5CO_2Me$)$Cr(CO)_3$ with 2,6-$Me_2C_6H_3NC$, with catalyst $[CpFe(L)_2]_2$ (Cp = C_5H_5, $C_5H_4CO_2Me$, C_5Me_5; L = CO; Cp = C_5H_5, L = 2,6-$Me_2C_6H_3NC$) and co-catalyst PdO	14
	2.4.3	Preparation of $[(C_5H_4CO_2Me)Fe(CO)_2]_2$	15
	2.4.4	Reaction of $[(C_5H_4CO_2Me)Fe(CO)_2]_2$ with ^tBuNC (1:1 Ratio)	15

	2.4.5	Reaction of $[(C_5H_4CO_2Me)Fe(CO)_2]_2$ with ^tBuNC (1:2 Ratio)	16
III	The Modification of $(\eta^6C_6H_5CO_2Me)Cr(CO)_3$ by Ligands L		19
	3.1	Introduction	19
	3.2	The Structure of $(\eta^6C_6H_5CO_2Me)Cr(CO)_3$	19
	3.2.1	Ligand geometry	20
	3.2.2	Conformation	20
	3.2.3	Cr-C bond lengths	23
	3.2.4	Ring C-C bond lengths	23
	3.2.5	Planrity of Ring	23
	3.2.6	Cr-C-O bond angles	24
	3.2.9	Packing considerations	24
	3.3	The structural effect of substitution of CO by Ligand L	24
	3.3.1	Ligand geometry	24
	3.3.2	Conformation	25
	3.3.3	Influence of electronic nature of L on Cr-C bond lengths	25
	3.3.4	Ring C-C bond lengths	25
	3.3.5	Planarity of Ring	25
	3.3.6	Cr-C-C and Cr-C-R bond angles (L = CR)	26
	3.3.7	Packing, and Steric Factors	26
	3.4	X-ray Crystallographic Studies of $(\eta^6C_6H_5CO_2Me)Cr(CO)_2L$ complexes	27
	3.4.1	OC-Cr-CO and OC-Cr-L angles	27
	3.4.2	*Conformation; An exception*	27
	3.4.3	Trends in Cr-C bond lengths	31
	3.4.4	*Ring* C-C bond lengths	31
	3.4.5	Ring planarity and bending of CO_2Me group	31
	3.4.6	Cr-C-O and [illegible] nd angles (L = CR)	32
	3.4.7	Conform[illegible] ligand L	32
	3.5	Conclusion	32
IV	The Crystal and Molecular Structure of $(\eta^6C_6H_5CO_2Me)$-$Cr(CO)_2(CNBu^t)$		33
	4.1	Introduction	33

4.2	Discussion of the Structure of $(\eta^5C_6H_5CO_2Me)$-$Cr(CO)_2(CNBu^t)$		33
	4.2.1	OC-Cr-CO and OC-Cr-CN angles	40
	4.2.2	Conformation	40
	4.2.3	Cr-C bond lengths	40
	4.2.4	Ring C-C bond lengths	41
	4.2.5	Ring planarity and bending of CO_2ME group	41
	4.2.6	Cr-C-CO and Cr-C-N bond angles	42
	4.2.7	Conformation of the $CNBu^t$ ligand	42
4.3	Unusual Structural Features of $(\eta^6C_6H_5CO_2Me)$-$Cr(CO)_2(CNBu^t)$		42
	4.3.1	Staggered Conformation	42
	4.3.2	Position of ^tBuNC vis-á-vis CO_2Me	42
	4.3.3	Bending of the ^tBuNC ligand	43
	4.3.4	Intra- and Inter-molecular Interactions	43
4.4	Experimental		43
	4.4.1	Data collection	43
	4.4.2	Structure Solution and Refinement	44
V	Catalytic Synthesis and Characterization of Isonitrile Derivatives of $(\eta^5C_5H_5)Mn(CO)_3$		48
5.1	Introduction		48
5.2	Results and Discussion		49
	5.2.1	PdO-catalysed reaction of $(\eta^5C_5H_5)$-$Mn(CO)_3$ with isonitriles	49
	5.2.2	Characterization of $(\eta^5C_5H_5)Mn(CO)_2$-(CNR) products	49
		(a) Infra red	49
		(b) Proton Nuclear Magnetic Resonance	50
		(c) Mass spectrum of $(\eta^5C_5H_5)$-$Mn(CO)_2(CNBu^t)$	50
5.3	Experimental - preparation of $(\eta^5C_5H_5)Mn(CO)_2$-(CNR), (R = Bu^t, $C_6H_5CH_2$, C_6H_{11}, $C_6H_3Me_2$-2,6, Me)		50
VI	The Modification of $(\eta^5C_5H_5)Mn(CO)_3$ by Ligands L		54
6.1	Introduction		54
6.2	The Structure of $(\eta^5C_5H_5)Mn(CO)_3$		54

	6.2.1	Ligand geometry and conformation	54
	6.2.2	Conformation	55
	6.2.3	*Mn-C-ring* and *Mn-CO* bond lengths	55
	6.2.4	Ring planarity and C-C bond lengths	55
	6.2.5	Mn-C-O bond angles	55
	6.2.6	Packing considerations	55
6.3	X-ray Crystallographic Studies of $(\eta^5C_5H_5)$-$Mn(CO)_2L$ complexes		57
	6.3.1	OC-Mn-CO and OC-Mn-L angles	57
	6.3.2	Molecular Conformation	57
	6.3.2	Mn-C-ring and Mn-CO bond lengths	58
	6.3.4	Ring C-C bond lengths	58
	6.3.5	Mn-C-O bond angles	62
	6.3.6	Packing and Steric Factors	62
6.4	Conclusion		63
VII	The Crystal and Molecular Structure of $(\eta^5C_5H_5)Mn(CO)_2(CNBu^t)$		64
7.1	Introduction		64
7.2	Discussion of the Structure of $(\eta^5C_5H_5)Mn(CO)_2(CNBu^t)$		64
	7.2.1	OC-Mn-CO and OC-Mn-CN angles	64
	7.2.2	Molecular Conformation	64
	7.2.3	Mn-C bond lengths	71
	7.2.4	Ring planarity and C-C bond lengths	71
	7.2.5	M-C-O and M-C-N bond angles	71
	7.2.6	Conformation of the $CNBu^t$ ligand	72
	7.2.7	Packing	72
7.3	Experimental		73
	7.3.1	Data collection	73
	7.3.2	Structure Solution and Refinement	73
VIII	Anomalous Infra Red Spectra of (Arene)$Cr(CO)_2$-(CNR) and $(\eta^5C_5H_5)Mn(CO)_2$(CNR) complexes		78
8.1	Introduction		78
8.2	IR spectral studies of $(\eta^6C_6H_5CO_2Me)Cr(CO)_2$-$(CNBu^t)$ and $(\eta^5C_5H_5)Mn(CO)_2(CNBu^t)$ in different solvents		79

8.3 Structural data on $(\eta^6-C_6H_5CO_2Me)Cr(CO)_2(CNBu^t)$ and $(\eta^5-C_5H_5)Mn(CO)_2(CNBu^t)$ from X-ray Crystallographic Studies 81

8.4 Structural data on $(\eta^5-C_5H_5)Ru(CNBu^t)_2I$ from an X-ray Crystallographic study 87

8.5 The solid state IR spectrum and crystal structure of $(\eta^6-C_6H_5CO_2Me)Cr(CO)_2(CMC_6H_3Me_2-2,6)$ 87

8.6 Possible explanations for the anomalous IR data 88

8.6.1 Conformers in solution 88

8.6.2 Solid state effects 89

8.6.3 Lowering of molecular symmetry by bent isonitrile 90

8.7 Conclusion 90

IX *The Geometry of* $Fe(CO)_{5-n}(L)_n$ ($n = 1,2$) Structures, and the Crystal and Molecular Structure of $Fe(CO)_3(CNMe)_2$ 91

9.1 Introduction 91

9.2 The Geometry of $Fe(CO)_4L$ structures 92

9.2.1 Axial versus Equatorial Site Preference of L 92

9.2.2 *Distortions to the tbp geometry* 93

9.2.3 Fe-CO bond length trends 98

9.2.4 Fe-C-O bond angles 99

9.3 The Geometry of $Fe(CO)_3(L)_2$ Structures 100

9.3.1 Geometry, tbp, distorted tbp, spy 100

9.3.2 Ligand site preferences - ax-ax, ax-eq, eq-eq 101

9.3.3 *Fe-CO bond length trends* 105

9.3.4 Fe-C-O bond angles 106

9.4 The Crystal and Molecular Structure of $Fe(CO)_3(CNMe)_2$ 107

9.4.1 Anomalous Infra Red Data 107

9.4.2 Discussion of the Structure 108

9.5 Experimental 113

9.5.1 Data Collection 113

9.5.2 Structure Solution and Refinement 113

X Derivatives of dirhenium decacarbonyl - a survey of the Literature 118

10.1 Introduction 118

10.2 Reactions of $Re_2(CO)_{10}$ with phosphines (and arsines) 120

10.2.1 *Thermal reactions* 121

10.2.2 Photochemical reactions 122

10.2.3 Amine-oxide assisted reactions 123

10.2.4 *Comment on product formulations* 123

10.3 The reaction of $Re_2(CO)_{10}$ with ^{13}CO 123

10.4 Photochemical reaction of $Re_2(CO)_{10}$ with isonitriles 124

10.5 Amine-oxide assisted reaction of $Re_2(CO)_{10}$ with nitriles 124

10.6 Photochemical reactions of $Re_2(CO)_{10}$ with olefins 125

10.6.1 The photochemical reaction of $Re_2(CO)_{10}$ with olefins in hexane solution 125

10.6.2 The photochemical reaction of $Re_2(CO)_{10}$ with 1,3-butadiene 126

10.6.3 The photochemical reaction of $Re_2(CO)_{10}$ with 1,3,5-cycloheptatriene 131

10.6.4 The photochemical reactions of $Re_2(CO)_{10}$ with 1-alkenes and 2-alkenes and further reactions of the products 131

10.7 Photochemical raction of $Re_2(CO)_{10}$ with R_2SiH_2 138

10.8 The photochemical reaction of $Re_2(CO)_{10}$ with H_2 138

10.9 Photochemical reaction of $Re_2(CO)_{10}$ with water 138

10.10 N-donor ligand derivatives of $Re_2(CO)_{10}$ 139

10.10.1 Trimethylamine-N-oxide-induced reactions of $Re_2(CO)_{10}$ with N-donor liganda 139

10.10.2 Photolytic reactions of $Re_2(CO)_{10-n}L_n$ (n = 1,2, L = N-donor ligand) 140
10.10.3 Preparation of $(\mu\text{-H})Re_2(CO)_8(\mu\text{-}NC_5H_4)$, and subsequent reactions with donor ligands 140
(a) Thermal reactions with ligand L 140
(b) Reaction with Me_3NO in the presence of ligand L 141
(c) Photochemical reactions with ligand L 141
10.10.4 Preparation of bis-N-donor-ligand derivatives of $Re_2(CO)_{10}$ 141
10.11 Dirhenium carbonyl carbene complexes 142
10.12 Thermal reaction of $Re_2(CO)_{10}$ with acetylenes 143
10.13 Formation of $[cis\text{-}Re_2(CO)_9(CHO)]^-$ from $Re_2(CO)_{10}$ 143
10.14 Formation of $Et_4N^+[cis\text{-}Re_2(CO)_9H]^-$ from $Re_2(CO)_{10}$ 145
10.15 Quaternary Ammonium Borohydride reductions of $Re_2(CO)_{10}$ 145
10.16 Conclusion 145
XI Catalytic Synthesis and Characterization of Isonitrile Derivatives of Dirhenium Decacarbonyl 147
11.1 Introduction 147
11.2 Catalyst Testing 148
11.3 PdO-catalysed reaction of $Re_2(CO)_{10}$ with isonitriles 151
11.4 Characterization of the dirhenium carbonyl isonitrile derivatives 155
11.4.1 Infra Red Spectroscopy 155
11.4.2 Proton Nuclear Magnetic Resonance Spectroscopy 164
11.4.3 Raman Spectroscopy 165
11.4.4 Mass Spectroscopy 169
(a) Mass spectrum of $Re_2(CO)_8(CNBu^t)$ 169
(b) Mass spectrum of $Mn_2(CO)_8(CNBu^t)_2$ 174
(c) Mass spectrum of $Re_2(CO)_8(C.I\text{-}C_6H_3Me_2\text{-}2,6)_2$ 179

11.5 Mechanism of the reaction of $M_2(CO)_{10}$ (M = Re, Mn) with isonitriles 184

11.5.1 Mechanism of the PdO-catalysed reaction between $Re_2(CO)_{10}$ and Bu^tNC to give $Re_2(CO)_9(CNBu^t)$ - ^{13}CO labelling study 184

11.5.2 Kinetic studies of the reaction of $M_2(CO)_{10}$ (M = Mn,Re) with Bu^tNC 184

11.6 Experimental 185

11.6.1 Catalyst testing 185

11.6.2 PdO-catalysed synthesis of $Re_2(CO)_{10-n}(CNR)_n$ (n = 1-3, R = Bu^t, $C_6H_5CH_2$, C_8H_{11}; n = 1-4, R = 2,6-$Me_2C_6H_3$, Me) 186

11.6.3 PdO-catalysed synthesis of $Re_2(CO)_8(CNBu^t)(CNC_6H_3Me_2$-2,6) 186

11.6.4 PdO-catalysed reaction of $Re_2(CO)_{10}$ and $Re_2(^{13}CO)_{10}$ with Bu^tNC (1:1:2 ratio) 186

XII The Modification of $Re_2(CO)_{10}$ by Ligands L 188

12.1 Introduction 188

12.1 The Structure of $Re_2(CO)_{10}$ 188

12.2.1 The Re-Re bond length 189

12.2.2 THe Re-CO bond lengths 191

12.2.3 Molecular Conformation 192

12.2.4 OC-Re-CO bond angles 193

12.2.5 Re-C-O bond angles 194

12.2.6 Packing 195

12.3 Ringing the changes: the effects of ligand substitution on molecular geometry 195

12.3.1 The Re-Re bond length 195

(a) Bond order 195

(b) Electronic nature of ligands 197

(c) Steric factors 198

(d) Bridging ligands 198

12.3.2 The Re-CO bond lengths 199

12.3.3 Molecular Conformation 200

12.3.4 Re-CO bond angles 200

12.3.5 Re-C-O bond angles 200

12.3.6 Packing 200

XIII X-ray Crystallographic Studies of Dirhenium Decacarbonyl Derivatives - a Survey of the Literature 202

13.1 Introduction 202

13.2 Literature Structures 203

13.2.1 Structures without bridging ligands 203

(a) Mono-substitution: eq-$Re_2(CO)_9(L)$, L = CH(OMe); C(OR)-$(SiPh_3)$; R = Me, Et 203

(b) Di-substitution: 1,2-ax,eq-$Re_2(CO)_8[C(OEt)(SiPh_3)]_2$ 206

13.2.2 Structures with bridging ligands 208

(a) A bridging olefin - $Re_2(CO)_8$-$[\mu\text{-}(\eta^2,\eta^2C_4H_6)]$ 208

(b) A bridging carbene - $Re_2(CO)_8$-$[\mu\text{-}(\eta^1,\eta^3CH\cdot C^1\cdot CMe_2)]$ 208

(c) $Re_2(CO)_8(\mu\text{-}NC_5H_4)(\mu\text{-}H)$ and Re_2-$(CO)_7(ONMe_3)(\mu\text{-}NC_5H_4)(\mu\text{-}H)$ 208

(d) $Re_2(CO)_8[\mu\text{-}SiPh_2]_2$, $Re_2(CO)_8(H)_2$-$[\mu\text{-}SiPh_2]$, $Re_2(CO)_7(H)_2[\mu\text{-}SiEt_2]_2$ and $Re_2(CO)_6(H)_4[\mu\text{-}SiEt_2]_2$ 209

(e) $Re_2(CO)_8[\mu\text{-}C(OMe)(C_6H_4Me\text{-}p)]_2$ 211

(f) $(CO)_4Re[\mu\text{-}C(SiPh_3)O\overline{(OEt)Re(CO)}_3$-$[C(OEt)(SiPh_3)]$ - a carbonyl-ligand bonded derivative of 1,2-ax,eq-$Re_2(CO)_8[C(OEt)(SiPh_3)]_2$ 211

(g) $Re_2(CO)_8[\mu\text{-}(C(SiPh_3)(CO))](\mu\text{-}H)$, and $Re_2(CO)_8[\mu\text{-}(CPh)](\mu\text{-}Br)$ 211

(h) $Re_2(CO)_8(\mu\text{-}H)_2$ - an Re-Re double bond? 212

(i) An $Re_2(CO)_8(\mu\text{-}H)_2$ derivative - $Re_2(CO)_6(\mu\text{-}H)_2[\mu\text{-}Ph_2PCH_2PPh_2]$ 213

(j) $Re_2(CO)_6(\mu\text{-}H)(\mu\text{-}NCHMe)[\mu\text{-}Ph_2P$-$CH_2PPh_2]$ - a derivative of Re_2-$(CO)_6(\mu\text{-}H)_2[\mu\text{-}Ph_2PCH_2PPh_2]$ 214

(k) $Re_2(CO)_6(\mu\text{-}H)(\mu\text{-}OH)[\mu\text{-}Ph_2PCH_2\text{-}PPh_2]$ - a formal derivative of $Re_2(CO)_6(\mu\text{-}H)_2(\mu\text{-}Ph_2PCH_2PPh_2]$ 214

(l) $[Re_2(CO)_4(PhCOPh)_3(CNCH_2SO_2C_6H_4\text{-}Me\text{-}p)_2]$, and $[Re_2(CO)_4(PhCOPh)_4]$ 215

13.3 Assessment 216

13.3.1 The Re-Re bond length 216

13.3.2 The Re-CO bond lengths 217

13.3.3 Molecular Conformation 217

13.3.4 OC-Re-CO bond angles 217

13.3.5 Re-C-O bond angles 217

13.3.6 Packing 217

XIV X-ray Crystallographic studies of isonitrile derivatives of $M_2(CO)_{10}$ (M = Re,Mn) 218

14.1 Introduction 218

14.2 X-ray Crystallographic 220

14.2.1 Structure of $\ldots NBu^t)$ (I) 220

14.2.2 Structure of $Re_2\ldots_8(CNC_6H_3Me_2\text{-}2,6)_2$- (II) 223

14.2.3 Structure of $Mn_2(CO)_8(CNBu^t)_2$ (V) 228

14.2.4 Structure of $Re_2(CO)_7(CNMe)_3$ (III) 228

14.2.5 Structure of $Re_2(CO)_8(CNC_6H_3Me_2\text{-}2,6)_4$- (IV) 238

14.2.6 Structure of $Mn_2(CO)_6(CNC_6H_3Me_2\text{-}2,6)_4$- (VI) 243

14.3 Structural Trends 243

14.3.1 The M-M bond length 252

14.3.2 The M-CO bond lengths 252

14.3.3 Molecular Conformation 254

14.3.4 C-M-C and M-M-Ceq bond angles 256

14.3.5 M-C-O, M-C-N and M-N-C bond angles 256

14.3.6 Packing 259

14.4 Relating structure to chemical reactivity 261

14.5 Experimental 262

14.5.1 Data collection 262

14.5.2 Structure solution and refinement 263

14.5.3 *Refinement problems with* $Mn_2(CO)_6$- $CNC_6H_3Me_2\text{-}2,6)_4$ (VI) 267

XV The Reaction between dirhenium decacarbonyl and phosphine ligands 280

15A. Introduction 280

15B *Discussion of the IR spectral data of* $Re_2(CO)_{10-n}(PR_3)_n$ (n = 1-4) complexes 280

15B.1 Introduction 280

15B.2 $Re_2(CO)_9PR_3$) complexes 282

15B.3 $Re_2(CO)_8(PR_3)_2$ complexes 288

15B.4 $Re_2(CO)_7(PR_3)_3$ complexes 293

15B.5 $Re_2(CO)_6(PR_3)_4$ complexes 296

15B.6 *Conclusion* 296

15C A Survey of Kinetic and Mechanistic Studies 297

15D.1 Synthesis and characterization of $Re_2(CO)_{10-n}(PR_3)_n$ (n = 1,2) derivatives 303

15D.2 Experimental 313

15D.2.1 Synthesis of $Re_2(CO)_{10-n}(PR_3)_n$ (n = 1,2) *from the reation of* $Re_2(CO)_{10}$ and PR_3 in the presence of Pd-catalysts 313

15D.2.2 Synthesis of $Re_2(CO)_{10-n}(PR_3)_n$ (n = 1,2) by the NMe_3O-assisted reaction of $Re_2(CO)_{10}$ with PR_3 in CH_2Cl_2 313

15D.2.3 Preparation of an isomer of $Re_2(CO)_8(PMe_2Ph)_2$ 313

15D.2.4 Preparation of an isomer of $Re_2(CO)_8(PMePh_2)_2$ 314

15E The Crystal and Molecular Structure of diax-$[Re_2(CO)_8(PMe_2Ph)_2]$ 314

15E.1 Introduction 314

15E.2 Discussion of related $Mn_2(CO)_{10-n}(PR_3)_n$ (n = 1,2) structures 315

15E.3 Discussion of the structure of diax-$[Re_2(CO)_8(PMe_2Ph)_2]$ 316

15E.3.1 Diaxial phosphine substitution 316

15E.3.2 The Re-Re, Re-P and Re-CO bond lengths 320

	15E.3.3 Molecular Conformation	324
	15E.3.4 P-Re-CO, OC-Re-CO and Re-Re-CO bond angles	324
	15E.3.5 Re-C-O bond angles	327
	15E.3.6 Packing	327
15E.4	Experimental	328
	15E.4.1 Data collection	328
	15E.4.2 Structure solution and refinement	330
XVI	Conclusion	334
Appendix A	The Sources of Chemicals used in this study	337
	(A) General Chemicals	337
	(B) Catalysts	337
	(C) Other Sources	337
Appendix B	General Experimental Details	339
	(a) Synthetic Methods	339
	(b) Solvents	339
	(c) Instrumentation	339
	(d) X-ray data collection	340
	(e) Crystallographic Computing Programs	340
	(f) Crystallographic R-indices	341
Appendix C	Torsional Angles for the $M_2(CO)_{10-n}(L)_n$ Structures	342
	(I) $Re_2(CO)_9(CNBu^t)$	343
	(II) $Re_2(CO)_8(CNC_6H_3Me_2\text{-}2,6)_2$	343
	(III) $Re_2(CO)_7(CNMe)_3$	344
	(IV) $Re_2(CO)_6(CNC_6H_3Me_2\text{-}2,6)_4$	344
	(V) $Mn_2(CO)_8(CNBu^t)_2$	345
	(VI) $Mn_2(CO)_6(CNC_6H_3Me_2\text{-}2,6)_4$	345
	(VII) diax$[Re_2(CO)_8(PMe_2Ph)_2]$	346
Appendix D	Structure Factor Tables - Bound as a separate volume (105 pages)	
	List of contents	347
Appendix E	List of Publications	348
Appendix F	Molecular Mechanics Calculations	349
References		350

LIST OF TABLES

			PAGE
Table 2.1	:	Spectroscopic data for the (η^6-Arene)Cr-(CO)$_2$(CNR) complexes	12
Table 2.2	:	Analytical data for the (η^6-Arene)Cr(CO)$_2$-(CNR) complexes	17
Table 2.3	:	Spectroscopic data for the Cr(CO)$_{6-n}$-(CNC$_6$H$_3$Me$_2$-2,6)$_n$ (n = 3,4) complexes	17
Table 2.4	:	Analytical data for [(C$_5$H$_4$CO$_2$Me)Fe(CO)$_2$]$_2$ and derivatives	18
Table 2.5	:	Spectroscopic data for [(C$_5$H$_4$CO$_2$Me)Fe-(CO)$_2$]$_2$ and derivatives	18
Table 3.1	:	*X-ray Crystal Structures of* (η^6C$_6$H$_5$CO$_2$Me)-Cr(CO)$_2$L complexes	28
Table 3.2	:	Principal geometric characteristics of (η^6-C$_6$H$_5$CO$_2$*Me*)Cr(CO)$_2$L complexes	29
Table 4.1	:	Bond lengths for (η^6-C$_6$H$_5$CO$_2$Me)Cr(CO)$_2$-(CNBu^t)	36
Table 4.2	:	*Bond angles for* (η^6-C$_6$H$_5$CO$_2$Me)Cr(CO)$_2$-(CNBu^t)	36
Table 4.3	:	Bond parameters involving hydrogen atoms for (η^6-C$_6$H$_5$CO$_2$Me)Cr(CO)$_2$(CNBu^t)	37
Table 4.4	:	Deviations of atoms from the plane defined by the six C-atoms of the arene ring in (η^6-C$_6$H$_5$CO$_2$Me)Cr(CO)$_2$(CNBu^t)	37
Table 4.5	:	Principal geometric characteristics of (η^6-C$_6$H$_5$CO$_2$Me)Cr(CO)$_2$(CNBu^t)	39
Table 4.6	:	Crystal data and details of structural analysis for (η^6-C$_6$H$_5$CO$_2$Me)Cr(CO)$_2$(CNBu^t)	45
Table 4.7	:	*Fractional Atomic Co-ordinates for* (η^6-C$_6$H$_5$CO$_2$Me)Cr(CO)$_2$(CNBu^t)	46
Table 4.8	:	Anisotropic Thermal Parameters for the non-*hydrogen atoms of* (η^6-C$_6$H$_5$CO$_2$Me)Cr(CO)$_2$-(CNBu^t)	47

			PAGE
Table 5.1	:	Analytical data for the $(\eta^5C_5H_5)Mn(CO)_2$-(CNR) complexes	51
Table 5.2	:	Spectroscopic data for the $(\eta^5C_5H_5)Mn$-$(CO)_2(CNR)$ complexes	52
Table 6.1	:	X-ray Crystal structures of $(\eta^5C_5H_5)Mn$-$(CO)_2L$ complexes	59
Table 6.2	:	Principal geometric characteristics of $(\eta^5C_5H_5)Mn(CO)_2L$ complexes	60
Table 7.1	:	Bond lengths for $(\eta^5C_5H_5)Mn(CO)_2(CNBu^t)$	67
Table 7.2	:	Bond angles for $(\eta^5C_5H_5)Mn(CO)_2(CNBu^t)$	67
Table 7.3	:	Bond parameters involving hydrogen atoms for $(\eta^5C_5H_5)Mn(CO)_2(CNBu^t)$	68
Table 7.4	:	Deviations of atoms from the plane defined by the 5 C-atoms of the cyclo-pentadienyl ring of $(\eta^5C_5H_5)Mn(CO)_2$-$(CNBu^t)$	69
Table 7.5	:	Principal geometric characteristics of $(\eta^5C_5H_5)Mn(CO)_2(CNBu^t)$	70
Table 7.6	:	Crystal data and details of structural analysis for $(\eta^5C_5H_5)Mn(CO)_2(CNBu^t)$	75
Table 7.7	:	Fractional atomic co-ordinates for $(\eta^5C_5H_5)Mn(CO)_2(CNBu^t)$	76
Table 7.8	:	Anisotropic thermal parameters for the non-hydrogen atoms of $(\eta^5C_5H_5)Mn(CO)_2(CNBu^t)$	77
Table 8.1	:	IR spectral study of $[(\eta^6C_6H_5CO_2Me)Cr(CO)_2$-$(CNBu^t)$ in different solvents	82
Table 8.2	:	IR spectral study of $(C_5H_5)Mn(CO)_2(CNBu^t)$ in different solvents	83
Table 9.1	:	X-ray Crystal Structures of $Fe(CO)_4L$ Complexes	94
Table 9.2	:	Geometric data for the ax-L-$Fe(CO)_4$ tbp structures	96
Table 9.3	:	X-ray Crystal Structures of $Fe(CO)_3LL'$ Structures	102
Table 9.4	:	Geometric data for $Fe(CO)_3LL'$ Structures	103
Table 9.5	:	Bond lengths for $Fe(CO)_3(CNMe)_2$	112

		PAGE
Table 9.6 :	Bond angles for $Fe(CO)_3(CNMe)_2$	112
Table 9.7 :	Crystal data and details of structural analysis for $Fe(CO)_3(CNMe)_2$	115
Table 9.8(a):	Fractional atomic co-ordinates for the non-hydrogen atoms of $Fe(CO)_3(CNMe)_2$	116
Table 9.8(b):	Fractional atomic co-ordinates and isotropic temperature factors for the hydrogen atoms of $Fe(CO)_3(CNMe)_2$	116
Table 9.9 :	Anisotropic temperature factors for the non-hydrogen atoms of $Fe(CO)_3(CNMe)_2$	117
Table 10.1 :	Re-Re bonded *dimeric products from the* photochemical reaction of $Re_2(CO)_{10}$ and olefins in hexane solution	128
Table 11.1 :	Effect of potential catalysts on the reaction $Re_2(CO)_{10} + Bu^tNC \longrightarrow Re_2(CO)_9(CNBu^t) + CO$	150
Table 11.2 :	Reaction conditions and product yields for the PdO catalysed syntheses of the complexes $Re_2(CO)_{10-n}(CNR)_n (n = 1-4)$	153
Table 11.3 :	Reaction times at 55°C for the uncatalysed and PdO-catalysed reaction $Re_2(CO)_{10} + RNC \longrightarrow Re_2(CO)_9(CNR) + CO$	154
Table 11.4 :	Analytical data for the $Re_2(CO)_{10-n}(CNR)_n$ (n = 1-4) complexes	156
Table 11.5 :	Infra Red Data of the complexes $Re_2(CO)_{10-n}(CNR)_n$ (n = 1-4)	157
Table 11.6 :	^1H NMR data of the complexes $Re_2(CO)_{10-n}(CNR)_n$; n = 1-4)	166
Table 11.7 :	Mass spectral data for $Re_2(CO)_9(CNBu^t)$	170
Table 11.8 :	Mass spectral data for $Mn_2(CO)_8(CNBu^t)_2$	175
Table 11.9 :	Mass spectral data for the complex $[Re(CO)_4(CNC_6H_3Me_2\text{-}2,6)]_2$	180
Table 13.1 :	X-ray Crystal Structures of dirhenium decacarbonyl derivatives, with a direct Re-Re bond	204

PAGE

Table 13.2 : Average values of the Re-Re-C bond angles for the eq-$Re_2(CO)_9$(Carbene) structures (i) - (iii) 207

Table 14.1 : Bond lengths for $Re_2(CO)_9(CNBu^t)$(I) 226

Table 14.2 : Bond angles for $Re_2(CO)_9(CNBu^t)$ (I) 227

Table 14.3 : Bond lengths for $Re_2(CO)_8(CNC_6H_3Me_2$-2,6)$_2$ (II) 231

Table 14.4 : Bond angles for $Re_2(CO)_8(CNC_6H_3Me_2$-2,6)$_2$(II) 232

Table 14.5 : Bond lengths for $Mn_2(CO)_8(CNBu^t)_2$ (V) 235

Table 14.6 : Bond angles for $Mn_2(CO)_8(CNBu^t)_2$ (V) 236

Table 14.7 : Bond lengths for $Re_2(CO)_7(CNMe)_3$ (III) 241

Table 14.8 : Bond angles for $Re_2(CO)_7(CNMe)_3$ (III) 242

Table 14.9 : Bond lengths for $Re_2(CO)_6(CNC_6H_3Me_2$-2,6)$_4$ (IV) 246

Table 14.10 : Bond angles for $Re_2(CO)_6(CNC_6H_3Me_2$-2,6)$_4$ (IV) 249

Table 14.11 : Bond lengths for $Mn_2(CO)_6(CNC_6H_3Me_2$-2,6)$_4$ (IV) 250

Table 14.12 : Bond angles for $Mn_2(CO)_6(CNC_6H_3Me_2$-2,6)$_4$ (IV) 251

Table 14.13 : Metal-metal bond length data for the complexes $M_2(CO)_{10}(CNR)_n$ (a) M = Re, n = 0-4; (b) M = Mn, n = 0,2,4 253

Table 14.14 : Average M-C bond length data for the complexes $M_2(CO)_{10}(CNR)_n$ (a) M = Re, n = 0-4; (b) M = Mn, n = 0,2,4 255

Table 14.15 : Average M-M-C bond angle data for the complexes $M_2(CO)_{10-n}(CNR)_n$ (a) M = Re, n = 0-4; (b) M = Mn, n = 0,2,4 257

Table 14.16 : Average cis C-M-C bond angle data for the complexes $M_2(CO)_{10-n}(CNR)_n$ (a) M = Re, N = 0-4; (b) M = Mn, n = 0,2,4 258

Table 14.17 : Average bond data for the M-C-O, M-C-N and C-N-C bond angles of the complexes $M_2(CO)_{10-n}(CNR)_n$ (a) M = Re, n = 0-4; (b) M = Mn, n = 0,2,4 260

		PAGE
Table 14.18 :	Crystal data and details of structure analyses for the $Re_2(CO)_{10-n}(CNR)_n$ (n = 1-4) complexes (I - IV)	264
Table 14.19 :	Crystal data and details of structure analyses for the $Mn_2(CO)_{10-n}(CNR)_n$ (n = 2,4) complexes (V,VI)	266
Table 14.20 :	Final atomic co-ordinates, and isotropic temperature factors of the C-atoms, for $Re_2(CO)_9(CNBu^t)$ (I)	268
Table 14.21 :	Final atomic co-ordinates, and isotropic temperature factors of the C-atoms, for $Re_2(CO)_8(CNC_6H_3Me_2\text{-}2,6)_2$(II)	269
Table 14.22 :	Final atomic co-ordinates, and isotropic temperature factors of the C-atoms, for $Re_2(CO)_7(CNMe)_3$(III)	271
Table 14.23 :	Final atomic co-ordinates, and isotropic temperature factors of the C-atoms, for $Re_2(CO)_6(CNC_6H_3Me_2\text{-}2,6)_4$(IV)	272
Table 14.24(a):	Final atomic co-ordinates of the non-H atoms for $Mn_2(CO)_8(CNBu^t)_2$(V)	273
Table 14.24(b):	Final atomic co-ordinates and isotropic temperature factors of the Hydrogen atoms, for $Mn_2(CO)_8(CNBu^t)_2$(V)	274
Table 14.25 :	Final atomic co-ordinates, and isotropic temperature factors of the non-C atoms, for $Mn_2(CO)_6(CNC_6H_3Me_2\text{-}2,6)_4$(VI)	275
Table 14.26 :	Anisotropic temperature factors for the non-C atoms of $Re_2(CO)_9(CNBu^t)$(I)	276
Table 14.27 :	Anisotropic temperature factors for the non-C atoms of $Re_2(CO)_8(CNC_6H_3Me_2\text{-}2,6)_2$ (II)	276
Table 14.28 :	Anisotropic temperature factors for the non-C atoms of $Re_2(CO)_7(CNMe)_3$(III)	277
Table 14.29 :	Anisotropic temperature factors for the non-C atoms of $Re_2(CO)_6(CNC_6H_3Me_2\text{-}2,6)_4$ (IV)	277

		PAGE
Table 14.30 :	Anisotropic temperature factors for the non-H atoms of $Mn_2(CO)_8(CNBu^t)_2$(V)	278
Table 14.31 :	Anisotropic temperature factors for the non-C atoms of $Mn_2(CO)_6(CNC_6H_3Me_2\text{-}2,6)_4$ (VI)	279
Table 15.1 :	IR spectral data of $M_2(CO)_9(L)$ (M = Mn, Re; L = AsR_3, PR_3) complexes	285
Table 15.2 :	IR spectral data of $M_2(CO)_8(L)_2$ (M = Mn, Re; L = AsR_3, PR_3) complexes	287
Table 15.3 :	IR spectral data of $Re_2(CO)_7(PR_3)_3$ complexes	295
Table 15.4 :	Correlation between IR data and molecular geometry for $M_2(CO)_8(L)_2$ complexes	298
Table 15.5 :	Details of catalytic syntheses of $Re_2(CO)_{10-n}(PR_3)_n$ (n = 1,2) complexes	305
Table 15.6 :	IR spectral data for the $Re_2(CO)_{10-n}(PR_3)_n$ (n = 1,2) derivatives	306
Table 15.7 :	IR spectral data for the C$\ell Re(CO)_3(PR_3)_2$ complexes	306
Table 15.8 :	Crystal data and selected bond parameters for $Mn_2(CO)_{10-n}(PR_3)_n$ structures (n = 1,2)	317
Table 15.9 :	Bond lengths for diax$[Re_2(CO)_8(PMe_2Ph)_2]$ (VII)	321
Table 15.10 :	Bond angles for diax$[Re_2(CO)_8(PMe_2Ph)_2]$ (VII)	322
Table 15.11 :	Average bond length and bond angle data for diax$[Re_2(CO)_8(PMe_2Ph)_2]$ (VII)	323
Table 15.12 :	Least squares planes for phenyl rings in diax$[Re_2(CO)_8(PMe_2Ph)_2]$(VII)	329
Table 15.13 :	Crystal data and details of structure analysis for diax$[Re_2(CO)_8(PMe_2Ph)_2]$(VII)	331
Table 15.14 :	Final atomic co-ordinates and isotropic temperature factors for the C and O atoms, of diax$[Re_2(CO)_8(PMe_2Ph)_2]$(VII)	332
Table 15.15 :	Anisotropic temperature factors for the Re and P atoms of diax$[Re_2(CO)_8(PMe_2Ph)_2]$ (VII)	332

LIST OF FIGURES

		PAGE
Figure 2.1 :	Fragmentation pattern for [(η^6-Arene)-$Cr(CO)_2(CNBu^t)$]	13
Figure 3.1 :	The three possible conformations for $(C_6H_5R)Cr(CO)_3$: I. Staggered, IIa. anti-eclipsed, and IIb. syn-eclipsed	21
Figure 3.2 :	Two sets of three hybrid orbitals of $Cr(CO)_3$: (a) empty, (b) filled	21
Figure 3.3.a:	Ring polarization with electron-accepting substituent A results in the anti-eclipsed conformation IIa for $(C_6H_5A)Cr(CO)_3$	22
Figure 3.3.b:	Ring polarization with electron-donating substituent D results in the syn-eclipsed conformation IIb for $(C_6H_5D)Cr(CO)_3$	22
Figure 3.4 :	Anti-eclipsed conformation of (η^6-$C_6H_5CO_2$-Me)$Cr(CO)_2L$ complex, viewed down ligand tripod onto arene ring	30
Figure 3.5 :	Unusual staggered conformation of the (η^6-$C_6H_5CO_2Me$)$Cr(CO)_2$(CNCOPh) molecule, viewed down ligand tripod onto arene ring	30
Figure 4.1 :	An ORTEP view of the (η^6-$C_6H_5CO_2Me$)$Cr(CO)_2$-$CNBu^t$) molecule, showing the numbering system	34
Figure 4.2 :	An ORTEP view of the unit cell of (η^6-$C_6H_5CO_2Me$)$Cr(CO)_2(CNBu^t)$, looking down the c-axis	35
Figure 4.3 :	Conformation of the (η^6-$C_6H_5CO_2Me$)$Cr(CO)_2$-$(CNBu^t)$ molecule, viewed down ligand tripod onto arene ring	41
Figure 5.1 :	Fragmentation pattern for (η^5-C_5H_5)Mn-$(CO)_2(CNBu^t)$	53
Figure 6.1 :	Conformation of (η^5-C_5H_5)$Mn(CO)_3$, looking down onto the (C_5H_5) ring	56
Figure 6.2 :	Ring C-C bond lengths in (η^5-C_5H_5)$Mn(CO)_3$	56

PAGE

Figure 6.3 : Ring C-C bond lengths in $(\eta^5C_5H_5)Mn(CO)_2(CCMe)$ 63

Figure 7.1 : ORTEP view of the $(\eta^5C_5H_5)Mn(CO)_2(CNBu^t)$ molecule, showing the numbering system 65

Figure 7.2 : ORTEP view of the unit cell of $(\eta^5C_5H_5)Mn(CO)_2(CNBu^t)$, looking down the b-axis 66

Figure 7.3 : Ring C-C bond lengths in $(\eta^5C_5H_5)Mn(CO)_2(CNBu^t)$ 72

Figure 8.1 : Solid state IR spectra (KBr) of $(\eta^6C_6H_5CO_2Me)Cr(CO)_2(CNR)$ (a) R = $C_6H_3Me_2$-2,6, (b) R = Bu^t 80

Figure 8.2 : Sideways ORTEP view of the $(\eta^6C_6H_5CO_2Me)Cr(CO)_2(CNBu^t)$ molecule 84

Figure 8.3 : Sideways ORTEP view of the $(\eta^5C_5H_5)Mn(CO)_2(CNBu^t)$ molecule 85

Figure 8.4 : Diagram illustrating the conformation of the $CNBu^t$ ligand in $(\eta^6C_6H_5CO_2Me)Cr(CO)_2(CNBu^t)$ ((a) and (c)) and $(\eta^5C_5H_5)Mn(CO)_2(CNBu^t)$ ((b) and (d)) 86

Figure 9.1 : An ORTEP view of the $Fe(CO)_3(CNMe)_2$ molecule, showing the numbering system used 110

Figure 9.2 : An ORTEP view of the unit cell of $Fe(CO)_3(CNMe)_2$ looking down the b-axis 111

Figure 10.1 : Possible Re-Re bonded dimeric olefin derivatives of $Re_2(CO)_{10}$ (a) octacarbonyl-μ-olefinyl-μ-hydride-dirhenium, (b) enneacarbonyl-η-olefin-dirhenium 127

Figure 10.2 : Re-Re bonded dimeric products of $Re_2(CO)_{10}$ with olefins in hexane solution 128

Figure 10.3 : Re-Re bonded dimeric products from the photochemical reactions of $Re_2(CO)_{10}$ with 1,3 butadiene 132

Figure 10.4 : Re-Re bonded dimeric products from the photochemical reaction of $Re_2(CO)_{10}$ with 1,3,5-cycloheptatetriene 132

PAGE

Figure 10.5 : Products from photolysis reactions of $Re_2(CO)_{10}$ with 1-alkenes and 2-alkenes 133

Figure 10.6 : Dipolar addition product, $(\mu\text{-H})(\mu\text{-CH=CH}_2)\text{-Re}_2(CO)_8(PMe_3)$ 133

Figure 10.7 : Dirhenium carbonyl (μ-carbene) derivatives 137

Figure 10.8 : Products of reaction of $(\mu\text{-H})(\mu\text{-trans-CH=CHMe})Re_2(CO)_8$ with acetylene 137

Figure 10.9 : Possible dipolar addition products, $(\mu\text{-H})(\mu\text{-C=CPh})Re_2(CO)_8(PMe_3)$ 137

Figure 10.10: The two isomers of 1,2-*ax,eq*-$Re_2(CO)_8$-$[C(OEt)SiPh_3][C(OEt)C_6H_4Me]$ 144

Figure 11.1 : Synthetic routes to the mixed-isonitrile derivative, $Re_2(CO)_8(CNBu^t)(CNC_6H_3Me_2$-2,6) 154

Figure 11.2 : IR spectra of (a) eq-$Re_2(CO)_9(CNBu^t)$ and (b) ax-$Mn_2(CO)_9(PMe_2Ph)$ 158

Figure 11.3(a): FTIR spectrum of 1,2-dieq-$Re_2(CO)_8$-$(CNC_6H_3Me_2$-2,6$)_2$ 161

Figure 11.3(b): FTIR spectrum of 1,1-cis-dieq-$Re_2(CO)_8$-$(CNBu^t)_2$ 162

Figure 11.4 : Plot of $\delta(CH_x)$ (x = 2,3) vs n(RNC) for the $Re_2(CO)_{10-n}(CNR)_n$ (n = 1-4) complexes 167

Figure 11.5 : Newman projection of the possible cis-equatorial conformational isomers of $M_2(CO)_7(CNR)_3$ (M = Re,Mn), as viewed down the M-M bond 168

Figure 11.6 : Isomers of $Mn_2(CO)_8(CNBu^t)_2$ (A) 1,1-cis-dieq, and (B) 1,2-dieq 168

Figure 11.7(a): Dimeric fragmentation pattern for Re_2-$(CO)_9(CNBu^t)$ 172

Figure 11.7(b): Monomeric fragmentation pattern for $Re_2(CO)_9(CNBu^t)$ 173

Figure 11.8(a): Dimeric fragmentation pattern for Mn_2-$(CO)_8(CNBu^t)_2$ 177

		PAGE
Figure 11.8(b):	Monomeric fragmentation pattern for $Mn_2(CO)_8(CNBu^t)_2$	178
Figure 11.9(b):	Dimeric fragmentation pattern for $[Re(CO)_4(CNC_6H_3Me_2\text{-}2,6)]_2$	182
Figure 11.9(b):	Monomeric fragmentation path for $[Re(CO)_4(CNC_6H_3Me_2\text{-}2,6)]_2$	183
Figure 13.1 :	Schematic representation of the structure of $(CO)_4Re[\mu\text{-}C(SiPh_3)C\overline{O(OEt)}]\overline{Re}[C(OEt)\text{-}(SiPh_3)]$	212
Figure 14.1 :	The two possible structures of $Re_2(CO)_9(CNR)$ (Ia) equatorial substitution, (Ib) axial substitution	221
Figure 14.2 :	Newman projections of possible conformations of $M_2(CO)_8(CNR)_2$ (M = Re, Mn), as viewed down the M-M axis	221
Figure 14.3 :	Newman projections of possible conformations of $Re_2(CO)_7(CNR)_3$, as viewed down the Re-Re axis	222
Figure 14.4 :	Newman projections of possible conformations of $M_2(CO)_6(CNR)_4$ (M = Re, Mn), as viewed down the M-M axis	222
Figure 14.5 :	ORTEP view of the $Re_2(CO)_9(CNBu^t)$ molecule (I), showing the numbering system used	224
Figure 14.6 :	ORTEP view of the unit cell of $Re_2(CO)_9(CNBu^t)$ (I), looking down the b-axis	225
Figure 14.7 :	ORTEP view of the $Re_2(CO)_8(CNC_6H_3Me_2\text{-}2,6)_2$ molecule (II) showing the numbering system used	229
Figure 14.8 :	ORTEP view of the unit cell of $Re_2(CO)_8(CNC_6H_3Me_2\text{-}2,6)_2$ (II), looking down the b-axis	230
Figure 14.9 :	ORTEP view of the $Mn_2(CO)_8(CNBu^t)_2$ molecule (V), showing the numbering system used	233

		PAGE
Figure 14.10:	ORTEP view of the unit cell of $Mn_2(CO)_8(CNBu^t)_2$(V), looking down the b-axis	234
Figure 14.11:	ORTEP view of the $Re_2(CO)_7(CNMe)_3$ molecule (III), showing the numbering system used	239
Figure 14.12:	ORTEP view of the unit cell of $Re_2(CO)_7(CNMe)_3$(III), looking down the b-axis	240
Figure 14.13:	ORTEP view of the $Re_2(CO)_6(CNC_6H_3Me_2\text{-}2,6)_4$ molecule (IV), showing the numbering system used	244
Figure 14.14:	ORTEP view of the unit cell of $Re_2(CO)_6(CNC_6H_3Me_2\text{-}2,6)_4$(IV), looking down the b-axis	245
Figure 14.15:	ORTEP view of the $Mn_2(CO)_6(CNC_6H_3Me_2\text{-}2,6)_4$ molecule (VI), showing the numbering system used	248
Figure 14.16:	ORTEP view of the unit cell of $Mn_2(CO)_6(CNC_6H_3Me_2\text{-}2,6)_4$(VI), looking down the b-axis	249
Figure 15.1 :	Possible isomers for $M_2(CO)_9(L)$ complexes	284
Figure 15.2 :	Possible isomers for $M_2(CO)_8(L)_2$ complexes	286
Figure 15.3 :	Possible isomers for 1,2,2-$M_2(CO)_7(L)_3$ complexes	294
Figure 15.4 :	Schematic representation of the mechanism for the formation of diax-$Re_2(CO)_8(PR_3)_2$ (IIA)	310
Figure 15.5 :	ORTEP view of the diax$[Re_2(CO)_8(PMe_2Ph)_2]$ molecule (VII), showing the numbering system used	318
Figure 15.6 :	ORTEP view of the unit cell of diax-$[Re_2(CO)_8(PMe_2Ph)_2]$(VII), looking down the b-axis	319
Figure 15.7 :	Newman projection of diax$[Re_2(CO)_8(PMe_2Ph)_2]$ looking down the Re(1)-Re(2) bond	325

PAGE

Figure 15.8 : Newman projections of diax[$Re_2(CO)_8(PMe_2Ph)_2$], showing conformation of phosphine groups relative to eq carbonyl ligands 325

(a) Newman projection of diax[$Re_2(CO)_8(PMe_2Ph)_2$], looking down the P(1)-Re(1)-Re(2)-P(2) axis 325

(b) Newman projection of ax[$Re(CO)_4(PMe_2Ph)$] fragments 326

(i) looking down the P(1)-Re(1) bond 326

(ii) looking down the Re(2)-P(2) bond 325

LIST OF ABBREVIATIONS AND SYMBOLS

IR	infra red
NMR	nuclear magnetic resonance
UV	ultra violet
MS	mass spectroscopy
TLC	thin layer chromatography
FT	Fourier Transform
MO	Molecular Orbital
Mr	molecular weight
Dc	calculated density
U	unit cell volume ($\AA^3$)
μ	linear absorption co-efficient (cm^{-1})
s.o.f.	site occupancy factor
mp	melting point
ν	frequency (cm^{-1})
M	metal atom
L	ligand
R	alkyl or aryl group
X	arene ring substituent, or halogen atom
/C	activated carbon support
RNC	isonitrile
TEABH	tetraethylammonium borohydride
THF	tetrahydrofuran
TMS	tetramethylsilane
py	pyridine
phen	phenanthroline
biquin	biquinoline
bipy	bipyridyl
xylyl	*2,6-dimethylphenyl* ($2,6\text{-}Me_2C_6H_3$)
Me	methyl
Et	*ethyl*
Pr	propyl
Bu	butyl
Ph	phenyl
Cp	cyclopentadienyl

n	normal
i	iso
t	tertiary
o	ortho
m	meta
p	para
tbp	trigonal bipyramidal
spy	square pyramidal
ax	axial
eq	equatorial
ap	apical
bs	basal

With reference to IR spectra:-

s	strong
m	medium
w	weak
sh	shoulder
sp	sharp
br	broad
v	very

With reference to NMR spectra:-

s	singlet
d	doublet
t	triplet
m	multiplet

With reference to symmetry:-

m	mirror (plane)
$\bar{1}$	centre of symmetry

I. INTRODUCTION

Organometallic chemistry is dominated by the chemistry of metal carbonyl complexes. Due to the catalytic potential of such complexes, the study of their chemical and physical properties continues to be an area of active interest. One important reaction type relating to metal carbonyl complexes is the carbonyl substitution reaction. However, carbonyl substitution reactions of transition metal carbonyl complexes are often difficult to achieve, and owing to the lack of facile synthetic methods of bringing about such reactions, substituted transition metal carbonyl complexes are not always accessible for further chemical and structural studies.

Some years ago a facile process to induce CO substitution of transition metal carbonyl complexes by ligands in the presence of catalysts was discovered in these laboratories. Use of this catalytic route enables substituted metal carbonyl derivatives to be prepared under mild thermal conditions. This thesis in part presents further attempts at exploring the potential of this reaction type, using specifically isonitrile (RNC) as a probe ligand.

The isonitrile ligand is potentially an extremely useful ligand for investigating the effect of ligand substitution on transition metal carbonyl complexes. Electronically, RNC is very similar to CO, the two ligands being isoelectronic. Further, the steric bulk of the isonitrile ligands is generally not as great as to be an impediment to multiple substitution of metal carbonyl complexes.

Catalysts for the reaction of transition metal carbonyl complexes with isonitriles that were investigated in this study include supported metals eg. Pd/C, $Pd/CaCO_3$, metals, and metal oxides, and the iron dimer $[(\eta^5-C_5R_5)Fe(CO)_2]_2$ ($R = H$, Me) with PdO as co-catalyst. Such catalytic synthetic methods have indeed provided access to isonitrile-substituted transition metal carbonyl complexes, and spectroscopic and crystallographic studies of these novel products have been undertaken.

In particular X-ray crystallographic studies were undertaken on representative metal carbonyl isonitrile derivatives,

(i) to determine the substitution geometry,
(ii) to investigate the effect of ligand substitution on molecular structure
and (iii) to enable a correlation to be established between IR spectral data and substitution geometry.

These studies have provided the basis for the bulk of the material contained in this thesis.

The systems investigated in this study are (η^6Arene)Cr-$(CO)_3$/RNC, ($\eta^5C_5H_5$)Mn$(CO)_3$/RNC, Fe$(CO)_5$/RNC, and $M_2(CO)_{10}$/L, M = Re, Mn, L = RNC, PR_3. In chs. II and V respectively, the catalytic syntheses of (η^6Arene)Cr$(CO)_2$(CNR) and ($\eta^5C_5H_5$)Mn$(CO)_2$(CNR) derivatives are described. Chs. III and VI respectively give brief surveys of the ($\eta^6C_6H_5CO_2Me$)-$Cr(CO)_2$ L and ($\eta^5C_5H_5$)Mn$(CO)_2$ L complexes for which X-ray crystal structures have been reported in the Literature, while Chs. IV and VII respectively describe the X-ray crystal and molecular structures of the two representative isonitrile derivatives, ($\eta^6C_6H_5CO_2Me$)Cr$(CO)_2$($CNBu^t$) and ($\eta^5C_5H_5$)Mn$(CO)_2$($CNBu^t$). Finally, ch. VIII discusses the anomalous IR data for the (η^6Arene)Cr$(CO)_2$(CNR) and ($\eta^5C_5H_5$)Mn$(CO)_2$(CNR) derivatives.

In ch. IX, a brief literature survey of $Fe(CO)_{5-n}(L)_n$ (n = 0-2) complexes for which a crystal structure has been reported is given. Against this background, the X-ray crystal and molecular structure of $Fe(CO)_3(CNMe)_2$ is discussed. This structure was primarily undertaken in an attempt to explain the anomalous IR data of $Fe(CO)_3(CNR)_2$ complexes. This aspect is discussed.

The remaining Chs. (X-XV) are concerned with the detailed chemical and structural study undertaken of $Re_2(CO)_{10-n}(L)_n$ (L = CNR, n = 1-4; L = PR_3, n = 1,2) complexes. To place this study in perspective, a literature

survey of derivatives of $Re_2(CO)_{10}$ is presented in Ch. X. Further, a survey of X-ray crystallographic studies of dirhenium decacarbonyl derivatives reported in the Literature, is given in ch. XIII.

Chs. XI and XIV are concerned with the $Re_2(CO)_{10}$/RNC system. Ch. XI describes the catalytic synthesis of $Re_2(CO)_{10-n}(CNR)_n$ (n = 1-4) derivatives, and discusses the chemical and spectroscopic properties of these complexes.

To set the stage for the X-ray crystal studies, the structural modification of $Re_2(CO)_{10}$ by ligands L is discussed in ch. XII in terms of the electronic and/or steric nature of L, relative to that of CO. The results of the X-ray crystal and molecular structures of a series of $Re_2(CO)_{10-n}(CNR)_n$ (n = 1-4) complexes are then discussed in ch. XIV. The isonitrile-derivatives studied in ch. XIV are $Re_2(CO)_9(CNBu^t)$, $Re_2(CO)_8(CNC_6H_3Me_2\text{-}2,6)_2$, $Re_2(CO)_7(CNMe)_3$ and $Re_2(CO)_6(CNC_6H_3Me_2\text{-}2,6)_4$. The X-ray structures of the related manganese complexes, $Mn_2(CO)_8(CNBu^t)_2$ and $Mn_2(CO)_6(CNC_6H_3Me_2\text{-}2,6)_4$, are also presented in ch. XIV.

Ch. XV, which is divided into subsections (A-E) deals with the $Re_2(CO)_{10}/PR_3$ system. The introductory Section 15A outlines the content of the subsequent sections. Section 15B discusses the IR spectral data reported in the Literature for compounds of the type $M_2(CO)_{10-n}(PR_3)_n$ (M = Re, Mn, n = 1-4). In particular, the correlation between IR data and molecular geometry is investigated. A summary of the kinetic and mechanistic studies on the reaction of $Re_2(CO)_{10}$ with phosphine ligands, which has been extensively investigated by several groups, is given in Section 15C. An extension of the catalytic methods to phosphine ligands is covered in Section 15D, where the synthesis and characterization of $Re_2(CO)_{10-n}(PR_3)_n$ (n = 1,2) derivatives is described. The formation of geometric isomers of $Re_2(CO)_8(PR_3)_2$ is discussed in terms of synthetic routes and the steric bulk of the phosphine ligand. The X-ray crystal and molecular structure of diax$[Re_2(CO)_8(PMe_2Ph)_2]$ is presented in Section 15E.

Finally, ch. XVI, the Conclusion, sums up the foregoing work, and gives a brief assessment of what has been achieved. Suggestions for further work related to this study are made.

Appendix A lists the sources of chemicals used in this study. In Appendix B, general experimental details are given, relating to (a) synthetic methods, (b) solvents, (c) instrumentation, (d) X-ray data collection, (e) Crystallographic Computing Programs used, and (f) definition of the Crystallographic R-indices. Appendix C gives the torsional angles for the $M_2(CO)_{10-n}(CNR)_n$ (M = Re, n = 1-4, M = Mn, n = 2,4) structures of ch. XIV and for *diax*-$[Re_2(CO)_8(PMe_2rn)_2]$ (Section 15E). A listing of the Structure Factor Tables for all the ten X-ray crystal structures is to be found in Appendix D, bound as a separate volume.

The literature surveys (which include X-ray structural data accessed from the Cambridge Crystallographic Data Base) presented in this thesis are considered complete up until December 1983, but mention has been made of pertinent publications that have appeared in 1984.

II. CATALYTIC SYNTHESIS AND CHARACTERIZATION OF ISONITRILE DERIVATIVES OF (η^6-ARENE)$Cr(CO)_3$

2.1 Introduction

Interest in complexes of the type (η^6-Arene)$Cr(CO)_3$ has been stimulated by the demonstrated ability of such compounds to catalyse reactions such as the hydrogenation of olefins.[1] Replacement of a CO group by other ligands L such as phosphines, arsines, stibines and isonitriles, significantly affects the catalytic properties of the (η^6-Arene)$Cr(CO)_2L$ complexes.[2] Consequently there is an interest in routes to such substituted complexes.

In an attempt to combine the advantages of homogeneous and heterogeneous catalysts, an ($\eta^6C_6H_5CO_2Me$)$Cr(CO)_2$ moeity has been bound to a polymer support through an isonitrile *functionality*.[3] Hence there is an interest in such isonitrile-substituted complexes.

Use has been made of arene chromium carbonyl complexes in organic chemistry. Arene chromium dicarbonyl chelates (synthesized photochemically[4a]) have been used to prepare chiral amines in good yields.[4b] The $Cr(CO)_2L$ unit (L = CO, CS, PR_3) has been shown to increase reactivity, enhance selectivity, or protect the substituents of complexed arene rings with respect to alkylation.[5] The arene ligand can be removed by refluxing (Arene)$Cr(CO)_3$ with py,[6] and the [$(py)_3Cr(CO)_3$] generated can be recycled to prepare (Arene)$Cr(CO)_3$ complexes (*vide infra*). The replacement of L = $C_6H_4Me_2$-p from L $Cr(CO)_3$ by C_6H_6 is catalysed by L'$Cr(CO)_3$ (L' = C_6Me_6) without L' replacement. Arene tricarbonyl complexes, obtained by the reaction of Arene and $Cr(CO)_6$ (*vide infra*), react with nucleophiles to form adducts and subsequently treated with trifluoroacetic acid under carbon monoxide, give substituted cyclohexadienes or, after oxidation, substituted arenes and $Cr(CO)_6$, thereby providing a route to such dienes and arenes in a cyclic process.[7]

Although most simple arenes react with $Cr(CO)_6$ to give (η^6-Arene)$Cr(CO)_3$ complexes,[8] the reaction is slow, the removal of high-boiling solvents or excess arene from the

product may be difficult, and a complex apparatus[10] is required to prevent sublimation of $Cr(CO)_6$ from the reaction vessel. These problems have been overcome by the reported "solvent-assisted" reaction between $Cr(CO)_6$ and a variety of arenes, in a dibutyl ether-tetrahydrofuran (THF) solvent mix,[11] thereby making (η^6-Arene)$Cr(CO)_3$ complexes easily accessible for further studies. Another reported successful synthetic method employs the reaction in refluxing dioxane of the arene and $[(NH_3)_3Cr(CO)_3]$,[12] which does not cause sublimation problems, thereby eliminating the need for special apparatus or solvents. In a similar method, $[(py)_3Cr(CO)_3]$ is reacted with arene in the presence of boron trifluoridediethyl ether in boiling ether.[6,13]

Replacement of CO in (η^6-Arene)$Cr(CO)_3$ complexes by an isonitrile ligand, RNC, to give (η^6-Arene)$Cr(CO)_2(CNR)$ derivatives, has been achieved by direct[14] or indirect[15,16] (involving photolysis of (η^6-Arene)$Cr(CO)_3$ with KCN, to give $K^+[(\eta^6\text{Arene})Cr(CO)_2(CN)]^-$, followed by reaction with RCℓ) photochemical methods. Photochemical methods have been employed to prepare chiral (η^6-Arene)Cr(CO)(CNR)(PR_3)[5] and (η^6-Arene)Cr(CO)(CS)(PR_3)[17] complexes. Direct substitution of an (η^6-Arene)$Cr(CO)_3$ complex with $P(OEt)_3$ has been achieved by electrochemical techniques[18] (reported since this work was completed). However, no thermal synthesis of (η^6-Arene)$Cr(CO)_2(CNR)$ complexes is known. Further, thermochemical studies[19] have shown that under typical thermal reaction conditions required to induce Cr-CO bond cleavage, displacement of the arene ring from the $Cr(CO)_3$ moiety by ligand(s) L, becomes a competing process, leading to reactant decomposition, or formation of $Cr(CO)_3L_n$ (n ≈ 1,3) complexes.

Hence a catalyst was sought to bring about the substitution of CO by RNC in (η^6-Arene)$Cr(CO)_3$ complexes, under mild thermal conditions. To function effectively, the requirement of such a catalyst would be the ability to lower the activation energy for the Cr-Co bond cleavage process, without also reducing that of the competing Cr-

Arene displacement reaction. The iron dimer, $[(\eta^5C_5H_5)Fe(CO)_2]_2$, in the presence of suitable donor ligands (e.g. PR_3, RNC), is known to catalyse the replacement of CO ligands on transition metal complexes.[3n,11] Further, $[(\eta^6C_5H_5)Fe(CO)_2]_2$, together with co-catalysts such as PdO, PtO_2, Pd/C or $Pd/CaCO_3$, has been shown to successfully catalyse reactions between metal carbonyls and isonitriles.[12]

The reaction of $(\eta^6C_6H_5X)Cr(CO)_3$ (X = H, Cℓ, CO_2Me, Me) with isonitriles RNC (R = Bu^t, 2,6-$Me_2C_6H_3$), using as catalysts compounds of the type $[CpFe(CO)_2]_2$ (Cp = C_5H_5, $C_5H_4CO_2$Me, C_5Me_5), together with PdO co-catalyst, were studied in order to explore the potential of this synthetic route. Variation of the arene substituent X allows the effect on the reaction of electron-donating or withdrawing properties to be investigated.

2.2 Results and Discussion

2.2.1 Reaction of $(\eta^6$-Arene$)Cr(CO)_3$ complexes with isonitriles

The reaction between $(\eta^6C_6H_5X)Cr(CO)_3$ (X = H, Cℓ, CO_2Me, Me) and RNC (R = Bu^t, 2,6-$Me_2C_6H_3$) in refluxing degassed heptane is catalysed by the iron dimer, $[(\eta^5C_5Me_5)Fe(CO)_2]_2$, and co-catalyst PdO, to yield the required substitution product, $(\eta^6C_6H_5X)Cr(CO)_2(CNR)$, in moderate to good yields. In the absence of catalyst, or in the presence of $[(\eta^5C_5Me_5)Fe(CO)_2]_2$ or PdO separately, less than 5% product formation was observed by IR spectroscopy even after long reaction times (6 h).

Reactions were slower with 2,6-$Me_2C_6H_3NC$ than with ^tBuNC [e.g. $(\eta^6C_6H_5CO_2Me)Cr(CO)_2(CNC_6H_3Me_2$-2,6), 80% yield, 6 h, cf. $(\eta^6C_6H_5CO_2Me)Cr(CO)_2(CNBu^t)$, 90% yield, 10 min.] For both isonitrile ligands, reaction times were dependent on the substituent X of the co-ordinated arene ring. As expected, reaction time was found to increase with arenes with electron-releasing X-groups [e.g. $(\eta^6C_6H_5CO_2Me)Cr(CO)_2(CNC_6H_3Me_2$-2,6), 80% yield, 6 h, cf. $(\eta^6C_6H_5Me)Cr(CO)_2(CNC_6H_3Me_2$-2,6), 50% yield, 18 h]. This trend is in keeping with the increased metal-CO bond strength, reflected, for instance in the ν(CO) stretching frequencies of the starting materials (e.g. IR(hexane): $(\eta^6C_6H_5CO_2Me)Cr(CO)_3$: 1991

and 1928 cm^{-1}; $(\eta^6C_6H_6)Cr(CO)_3$: 1983 and 1915 cm^{-1}; and $(\eta^6C_6H_5Me)Cr(CO)_3$: 1975 and 1906 cm^{-1}).

With the electron-withdrawing ring substituent X = CO_2Me, the consequent weakening of the Cr-(η^6Arene) bond[19] allows the arene ring to be eliminated during the reaction of $(\eta^6C_6H_5CO_2Me)Cr(CO)_3$ with $2,6\text{-}Me_2C_6H_3NC$, resulting in the formation of products of the type $Cr(CO)_{6-n}(CNC_6H_3Me_2\text{-}2,6)_n$ (n = 3,4) (*vide infra*). This is not observed with the electron-donating ring substituent X = Me, where the Cr-(η^6Arene) bond is stronger.[19]

2.2.2 *Reaction of $(\eta^6C_6H_5CO_2Me)Cr(CO)_3$ with $2,6\text{-}Me_2C_6H_3NC$, in the Presence of Iron Dimer Catalysts*

The reaction between $(\eta^6C_6H_5CO_2Me)Cr(CO)_3$ and $2,6\text{-}Me_2C_6H_3NC$, was investigated in the presence of iron dimer catalysts. The most efficient catalyst was found to be an $[(\eta^5C_5Me_5)Fe(CO)_2]_2$/PdO mixture (*vide infra*).

Although the unsubstituted iron dimer $[(\eta^5C_5H_5)Fe(CO)_2]_2$, together with Pd/O, catalyses the reaction, under the reaction conditions the iron dimer itself rapidly undergoes CO substitution to $[(\eta^5C_5H_5)Fe(CNC_6H_3Me_2\text{-}2,6)_2]_2$.[21] The modification of the iron dimer catalyst can readily be detected during the reaction by IR spectroscopy. Further, PdO is a poor catalyst for the reaction (2.1)[22] $[(\eta^5C_5H_5)Fe(CO)_2]_2 + nRNC \rightarrow [(\eta^5C_5H_5)_2Fe_2(CO)_{4-n}(CNR)_n] + nCO$ (n = 1,2) (2.1) and is thus not responsible for the substitution reaction observed. Hence the addition of either $[(\eta^5C_5H_5)Fe(CO)_2]_2$ or $[(\eta^5C_5H_5)Fe(CNC_6H_3Me_2\text{-}2,6)_2]_2$ (independently synthesized[21]) to reaction mixtures of $[(\eta^6C_6H_5CO_2Me)Cr(CO)_3$ and $CNC_6H_3Me_2\text{-}2,6$, resulted in the same rate of formation of $(\eta^6C_6H_5CO_2Me)Cr(CO)_2(CNC_6H_3Me_2\text{-}2,6)$, as determined by IR spectroscopy. (ca. 15% product formation was observed for both reactions after 8 h).

The ring-substituted iron dimer, $[(\eta^5C_5H_4CO_2Me)Fe(CO)_2]_2$, with PdO, was also tried as a catalyst for this reaction, but IR data indicated that although initially product substitution was more rapid than with $[(\eta^5C_5H_5)Fe(CO)_2]_2$/PdO catalyst, the reaction rates soon inverted, and

after ca. 3 h, the reaction with $[(\eta^5C_5H_4CO_2Me)Fe(CO)_2]_2$/PdO as catalyst ceased. This result can be explained in terms of the increased ability of the $[(\eta^5C_5H_4CO_2Me)Fe(CO)_2]_2$ complex to undergo CO substitution since electron-withdrawing groups on the ring enhance *the substitution reaction.*[23] Consistent with this proposal are the results of the reaction between $[(\eta^5C_5H_4CO_2Me)Fe(CO)_2]_2$ and ^{t}BuNC. (vide infra)

In refluxing benzene, a 1:2 reaction between $[(\eta^5C_5H_4CO_2Me)Fe(CO)_2]_2$ and ^{t}BuNC rapidly (<15 min) gave $[(\eta^5C_5H_4CO_2Me)_2Fe_2(CO)_3(CNBu^t)]$, and more slowly, $[(\eta^5C_5H_4CO_2Me)Fe(CO)(CNBu^t)]_2$ (50% isolated yield, 4 h.) A 1:1 reaction between $[(\eta^5C_5H_4CO_2Me)Fe(CO)_2]_2$ and ^{t}BuNC in refluxing benzene gave predominately $[(\eta^5C_5H_4CO_2Me)_2Fe_2(CO)_3(CNBu^t)]$, and some $[(\eta^5C_5H_4CO_2Me)Fe(CO)(CNBu^t)]_2$, indicative of the facile nature of multiple CO substitution. *(These new iron dimer derivatives* have been completely characterized, and the pertinent analytical and spectral data are reported in Section 2.4.4.) By contrast, the reaction between $[(\eta^5C_5H_5)Fe(CO)_2]_2$ and ^{t}BuNC under identical reaction conditions, gives only $[(\eta^5C_5H_5)_2Fe_2(CO)_3(CNBu^t)]$, in near quantitative yield,[24] and trace amounts (<2%) of $[(\eta^5C_5H_5)Fe(CO)(CNBu^t)]_2$.[25] Under our reaction conditions (ie. large excess of RNC), it can be anticipated that multiple CO substitution of $[(\eta^5C_5H_4CO_2Me)Fe(CO)_2]_2$ by RNC eventually occurs, presumably leading to catalyst deactivation.

To avoid this problem of catalyst substitution, the use as a catalyst of the pentamethyl derivative, $[(\eta^5C_5Me_5)Fe(CO)_2]_2$, was investigated. Owing to the electron-donating nature of the methyl substituents on the cyclopentadienyl ring, this dimer is inert to CO substitution.[21] An $[(\eta^5C_5Me_5)Fe(CO)_2]_2$/PdO mixture was found to be a convenient, though not highly active catalyst for the substitution of $(\eta^5C_6H_5CO_2Me)Cr(CO)_3$ with $CNC_6H_3Me_2$-2,6, *and this catalytic* method was employed in the synthesis of other $(\eta^5$Arene$)Cr(CO)_2$(CNR) derivatives (vide supra). Further, it was possible to isolate the unsubstituted dimer catalyst, $[(\eta^5C_5Me_5)Fe(CO)_2]_2$,

at the end of the reaction, thereby confirming the above hypothesis.

2.2.3 Formation of by-products of the type $Cr(CO)_{6-n}(CNC_6H_3Me_2\text{-}2,6)_n$ (n = 3,4) in the reaction of $(\eta^6\text{-}C_6H_5CO_2Me)Cr(CO)_3$ with $2,6\text{-}Me_2C_6H_3NC$

A feature of the (catalysed) reaction between $(\eta^6\text{-}C_6H_3CO_2Me)Cr(CO)_3$ and $2,6\text{-}Me_2C_6H_3NC$ was the formation of products resulting from the cleavage of the (η^6-Arene)-Cr bond. In the $[(\eta^5\text{-}C_5Me_5)Fe(CO)_2]_2$/PdO catalysed reaction between $(\eta^6\text{-}C_6H_5CO_2Me)Cr(CO)_3$ and $2,6\text{-}Me_2C_6H_3NC$, $C_6H_5CO_2Me$, together with complexes of the type $[Cr(CO)_{6-n}(CNC_6H_3Me_2\text{-}2,6)_n]$ (n = 3,4) were isolated (total yield of ring-cleavage by-products ca. 5%) from the reaction mixture by column chromatography, in addition to the major substitution product, $(\eta^6\text{-}C_6H_5CO_2Me)Cr(CO)_2(CNC_6H_3Me_2\text{-}2,6)$ (70% yield, 6 h). The by-products $[Cr(CO)_{6-n}(CNC_6H_3Me_2\text{-}2,6)_n]$ (n = 3,4) were characterized by independent synthesis from $[Cr(CO)_6]$ and $2,6\text{-}Me_2C_6H_3NC$ in the presence of PdO as catalyst.[26] (Pertinent IR and NMR spectral data for these complexes are given in Section 2.4.2.)

The electron withdrawing CO_2Me arene ring substituent results in a weakening of the Cr-(η^6-Arene) bond,[13] and the consequent displacement of the arene ring in the side reaction (2.2) $(C_6H_5CO_2CH_3)Cr(CO)_3 + 3(2,6\text{-}Me_2C_6H_3NC) \rightarrow [Cr(CO)_3(CNC_6H_3Me_2\text{-}2,6)_3] + C_6H_5CO_2Me$ (2.2). The tetra-substituted derivative, $[Cr(CO)_2(CNC_6H_3Me_2\text{-}2,6)_4]$, is however unexpected and could arise from two potential pathways:- (a) displacement of the arene ligand to give $[Cr(CO)_3(CNC_6H_3Me_2\text{-}2,6)_3]$ (Reaction (2.2.)), followed by catalytic displacement of CO to give $[Cr(CO)_2(CNC_6H_3Me_2\text{-}2,6)_4]$,[26] or (b) formation of $[(\eta^6\text{-}C_6H_5CO_2Me)Cr(CO)_2(CNC_6H_3Me_2\text{-}2,6)]$, followed by displacement of the arene ring by isonitrile.

A blank reaction between $(\eta^6\text{-}C_6H_5CO_2Me)Cr(CO)_3$ and $2,6\text{-}Me_2C_6H_3NC$, in the absence of catalyst, indicated that ca. 5% $[(\eta^6\text{-}C_6H_5CO_2Me)Cr(CO)_2(CNC_6H_3Me_2\text{-}2,6)]$, as well as ca. 15% ring cleavage products had formed in 6 h, as detected by IR spectroscopy. This suggests that the major, if not exclusive pathway to formation of the $[Cr(CO)_{6-n}$-

$(CNC_6H_3Me_2\text{-}2,6)_n]$ ($n \approx 3,4$) derivatives is via a thermal non-catalytic route. Further, the reaction between $[(\eta^6C_6H_5CO_2Me)Cr(CO)_2(CNC_6H_3Me_2\text{-}2,6)]$ and 2,6-$Me_2C_6H_3NC$ in both the absence (no reaction) and presence of catalyst (<1% ring cleavage) under similar reaction conditions rules out the possibility that the ring-cleavage derivatives are formed in secondary reactions via the decomposition of the product. The significant feature of the above experiments is the finding that catalytic cleavage of an (η^6Arene)-Cr bond does not take place under our reaction conditions.

2.3 Spectroscopic properties of $(\eta^6\text{Arene})Cr(CO)_2(CNR)$ complexes

2.3.1 Infra Red

The IR data (Table 2.1) for the $(\eta^6\text{Arene})Cr(CO)_2(CNR)$ complexes show anomalous behaviour. Whereas two ν(CO) and one ν(NC) stretching frequencies are predicted, two ν(CO) and two ν(NC) absorption were observed in both solution and the solid state (except for $(\eta^6C_6H_5CO_2Me)Cr(CO)_2(CNC_6H_3Me_2\text{-}2,6)$, which has one ν(NC) and two ν(CO) bands in solution, and one ν(NC) and three ν(CO) bands in the solid state). This phenomenon will be discussed in Chapter VIII.

2.3.2 Proton Nuclear Magnetic Resonance

The ^{1}H NMR data (Table 2.1) for the $(\eta^6\text{Arene})Cr(CO)_2(CNR)$ complexes gave the expected resonances (number, position).

2.3.3 Mass Spectrum of $(\eta^6C_6H_5CO_2Me)Cr(CO)_2(CNBu^t)$

Mass spectra gave fragments consistent with the structural formulation proposed. A typical example is shown in Fig. 2.1, which indicates the fragmentation pattern (together with peak intensities and metastable peaks) for the mass spectrum of $(\eta^6C_6H_5CO_2Me)Cr(CO)_2(CNBu^t)$. The fragmentation pattern is in agreement with that reported for related complexes.[138] The loss of the CO ligands precedes loss of ^{t}BuNC, indicative of the stronger σ-donor ability of ^{t}BuNC than CO. The ^{t}Bu-group is lost before the CN linkage.[27] The arene ligand is the last to be lost.

Table 2.1: Spectroscopic data for the (η^6-Arene)Cr(CO)$_2$(CNR) complexes

Complex	IR(cm^{-1})[a]		^{1}H NMR (ppm)[b]			
	ν(NC)	ν(CO)	RNC(Me)	RNC(C_6H_n)	Arene(Me)	Arene(C_6H_n)
(η^6-C_6H_5Me)Cr(CO)$_2$($CNBu^t$)	2038, 2002	1921, 1883	1.39	–	2.09	4.99
(η^6-C_6H_6)Cr(CO)$_2$($CNBu^t$)	2046, 2028	1942, 1894	1.38	–	–	5.43
(η^6-$C_6H_5Cℓ$)Cr(CO)$_2$($CNBu^t$)	2095, 2060	1933, 1893	1.42	–	–	5.01,5.05
(η^6-$C_6H_5CO_2Me$)Cr(CO)$_2$($CNBu^t$)[c,d]	2102, 2060	1937, 1894	1.40	–	3.83	4.99-5.78[e]
(η^6-C_6H_5Me)Cr(CO)$_2$($CNC_6H_3Me_2$-2,6)	2050, 2010	1916, 1888	2.17	6.83	2.38	4.97
(η^6-C_6H_6)Cr(CO)$_2$($CNC_6H_3Me_2$-2,6)	2040, 1992	1916, 1874	2.37	7.00	–	5.12
(η^6-$C_6H_5CO_2Me$)Cr(CO)$_2$($CNC_6H_3Me_2$-2,6)[f,g]	2060	1938, 1902	2.37	6.63	3.81	5.02-5.98[e]

[a] Recorded in hexane

[b] Recorded in $CDCℓ_3$ relative to TMS

[c] ν(COOMe) ≈ 1720 cm^{-1}

[d] IR(KBr), ν(NC): 2090, 2060 (sh); ν(CO): 1908, 1856, ν(COOMe): 1700 cm^{-1}

[e] *Multiplet*

[f] ν(COOMe) ≈ 1725 cm^{-1}

[g] IR(KBr), ν(NC): 2070; ν(CO): 1904, 1855, 1840; ν(COOMe): 1715 cm^{-1}

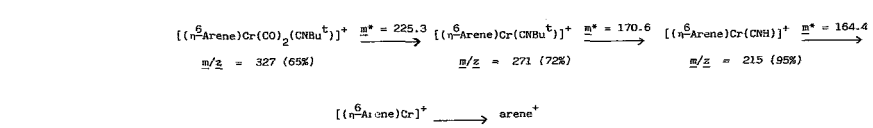


FIGURE 2.1 Fragmentation pattern for $[(\eta^6\text{Arene})Cr(CO)_2(CNBu^t)]$. Fragments and intensity data refer to the samples with $\eta^6\text{Arene} = \eta^6C_6H_5CO_2Me$. The spectrum was recorded at 48°C and all fragments with m/z <110 are not reported.

2.4 Experimental

2.4.1 The catalysed synthesis of $[(\eta^6\text{-}C_6H_5X)Cr(CO)_2(CNR)]$ (X = H, Cℓ, CO_2Me, Me; R = Bu^t, 2,6-$Me_2C_6H_3$)

$(\eta^6\text{-}C_6H_5CO_2CH_3)Cr(CO)_3$ and $(\eta^6\text{-}C_6H_5Cℓ)Cr(CO)_3$ were prepared by the method of Mahaffy and Pauson.[11a]

$[(\eta^6\text{-}C_6H_5X)Cr(CO)_3]$ (1.00 mmol), catalyst $[(\eta^5\text{-}C_5Me_5Fe(CO)_2]_2$ (20 mg) and co-catalyst PdO (20 mg), and 2,6-$Me_2C_6H_3NC$ (1.3 mmol), or ^tBuNC (1.1 mmol), were combined in freshly distilled heptane (15 mℓ) the mixture was heated at reflux (100°C), and the reaction was monitored by TLC (silica; eluent : hexane-diethyl ether (30%)) and IR spectroscopy (2200-1700cm^{-1} region). On completion of the reaction (or when no further changes were apparent (R = Bu^t), or after 18 h (R = 2,6-$Me_2C_6H_3$)), the reaction mixture was allowed to cool and the product isolated by column chromatography (2 cm x 40 cm column, silica ; gradient elution with hexane-diethyl ether mixtures). The column was run, and the product collected, under nitrogen, using deoxygenated eluent solutions, as the products tend to be air-sensitive, especially in solution. Recrystallization from dichloromethane-hexane solution gave the required product as yellow or orange crystalline material. (Table 2.2). Product yields were generally >60%. Even in the solid state, the $(\eta^6\text{-}C_6H_6)Cr(CO)_2(CNR)$ derivatives decomposed on exposure to air, as evidenced by the change in colour from yellow to lime green.

2.4.2 Reaction of $(\eta^6\text{-}C_6H_5CO_2Me)Cr(CO)_3$ with 2,6-$Me_2C_6H_3NC$, with catalyst $[CpFe(L)_2]_2$ (Cp = C_5H_5, $C_5H_4CO_2Me$, C_5Me_5; L = CO; Cp = C_5H_5, L = 2,6-$Me_2C_6H_3NC$), and co-catalyst PdO

$(\eta^6\text{-}C_6H_5CO_2Me)Cr(CO)_3$ (1.00 mmol), catalyst $[CpFe(L)_2]_2$ (20 mg) and co-catalyst PdO (20 mg), and 2,6-$Me_2C_6H_3NC$ (1.3 mmol), were combined in freshly distilled heptane (15 mℓ), the mixture was heated at reflux (100°C), and the reaction was monitored by IR spectroscopy and TLC (as above). On completion of the reaction, or when no further changes were apparent, column chromatography (as above) was used to

isolate the product(s), which were purified by recrystallization from dichloromethane-hexane solutions. In addition to the main substitution product, $(\eta^6\text{-}C_6H_5CO_2Me)Cr(CO)_2(CNC_6H_3Me_2\text{-}2,6)$, arene-ring displacement products of the type $Cr(CO)_{6-n}(CNC_6H_3Me_2\text{-}2,6)_n$ ($n = 3,4$), were obtained. These products were characterized by IR and ^1H NMR spectroscopy (Table 2.3).

2.4.3 Preparation of $[(C_5H_4CO_2Me)Fe(CO)_2]_2$

$C_5H_4CO_2Me$ was synthesized from $C\ell CO_2Me$, according to the method of Peters.[28]

A mixture of $[Fe(CO)_5]$ (8 mℓ, 0.06 mol), octane (100 mℓ), and $C_5H_4CO_2Me$ (3 g, 0.024 mol), was degassed and the reaction mixture refluxed (120°C) under argon for 24 h. The mixture was cooled in ice, prior to filtering, and yielded 1.7 g (32%) of deep purple product. Cleavage with I_2 yielded $(C_5H_4CO_2Me)Fe(CO)_2I$ as a black crystalline material. Analytical and spectral data for these compounds are given in Tables 2.4 and 2.5 respectively.

2.4.4 Reaction of $[(C_5H_4CO_2Me)Fe(CO)_2]_2$ with ^tBuNC (1:1 Ratio

$[(C_5H_4CO_2Me)Fe(CO)_2]_2$ (0.47 g, 1.00 mmol) was dissolved in benzene (20 mℓ), and to this was added ^tBuNC (130 μℓ, 1.2 mmol). The solution was then brought to reflux (80°C). The reaction was monitored by TLC (silica; eluent : benzene-diethyl ether (20%)). The reaction was allowed to proceed for 3 h, during which time TLC indicated the formation of three products, with Rf-values of 0.34, 0.60 and 0.75 (trace). The products were separated by column chromatography (2 cm x 40 cm column, silica; eluent : benzene - diethyl ether (20%)), and purified by filtration and recrystallization from benzene-hexane solution. The lower brown band (Rf 0.60) yielded the monosubstituted maroon complex $[(C_5H_4CO_2Me)_2Fe_2(CO)_3(CNBu^t)]$ (70%), while the upper green band (Rf 0.37) gave disubstituted $[(C_5H_4CO_2Me)Fe(CO)(CNBu^t)]_2$ (< 10%), as a bottle green solid. Analytical and spectral data for these complexes are given in Tables 2.4 and 2.5 respectively. The trace product (Rf 0.75)

was present in insufficient amount to be isolated.

2.4.5 Reaction of $[(C_5H_4CO_2Me)Fe(CO)_2]_2$ with ^tBuNC (1:2 Ratio)

$[(C_5H_4CO_2Me)Fe(CO)_2]_2$ (0.47g, 1.00 mmol) was dissolved in benzene (20 mℓ), and to this was added ^tBuNC (112 μℓ, 1.00 mmol). The solution was then brought to reflux (80°C). The reaction was monitored by IR spectroscopy. The formation of the monosubstituted $[(C_5H_4CO_2Me)_2Fe_2(CO)_3(CNBu^t)]$ was judged to be complete after 15 min. Further ^tBuNC (150 μℓ, 1.33 mmol) was added. The progress of the reaction was monitored by TLC (as above). The reaction was allowed to proceed for 4 h, but complete conversion to the disubstituted product had not occured in this time. The reaction was stopped and the solvent removed in vacuo. The products were separated by column chromatography (see above) and purified by recrystallisation from benzene-hexane solution. The lower brown band (Rf 0.60) yielded maroon $[(C_5H_4CO_2Me)_2Fe_2(CO)_3(CNBu^t)]$ (< 5%). The upper green band (Rf 0.41) gave 0.28g (50%) of green $[(C_5H_4CO_2Me)Fe(CO)(CNBu^t)]_2$. (See Tables 2.4 and 2.5). The trace product (Rf 0.75) was not collected.

TABLE 2.2: Analytical data for the (η^6Arene)$Cr(CO)_2$(CNR) complexes

Complex	Colour	mp (°C)	Elemental analysis (Found (calcd.) (%))		
			C	H	N
($\eta^6C_6H_5Me$)$Cr(CO)_2(CNBu^t)$	yellow	77–78	59.5(59.4)	5.82(6.01)	4.92(4.94)
($\eta^6C_6H_5Cl$)$Cr(CO)_2(CNBu^t)$	yellow	86–88	51.4(51.4)	4.68(4.61)	4.63(4.61)
($\eta^6C_6H_5CO_2Me$)$Cr(CO)_2(CNBu^t)$	red	84–85	54.8(55.0)	5.19(5.20)	4.35(4.28)
($\eta^6C_6H_5Me$)$Cr(CO)_2(CNC_6H_3Me_2$-2,6)	orange	99–100	66.1(65.2)	5.26(5.17)	5.10(4.23)
($\eta^6C_6H_5CO_2Me$)$Cr(CO)_2(CNC_6H_3Me_2$-2,6)	red	73	60.4(60.8)	4.58(4.57)	3.80(3.73)

TABLE 2.3: Spectroscopic data for the $Cr(CO)_{6-n}(CNC_6H_3Me_2$-2,6$)_n$ (n = 3,4) complexes

Complex	IR (cm^{-1})[a]		^{1}H NMR (ppm)[b]	
	ν(NC)	ν(CO)	$C_6H_3(CH_3)_2$-2,6	$C_6H_3(CH_3)_2$-2,6
$Cr(CO)_3(CNC_6H_3Me_2$-2,6$)_3$	2134(w), 2060(m)	1954(s), 1904(s)	2.23(s)	6.69, 6.68(d)
$Cr(CO)_2(CNC_6H_3Me_2$-2,6$)_4$	2125(w), 2050(s),	1899(s), 1875(sh),	2.38,	6.74, 6.72(d)
	1984(s)		2.34(d)	

[a] Recorded in $CHCl_3$

[b] Recorded in C_6D_6, relative to TMS

TABLE 2.4: Analytical data for $[(C_5H_4CO_2Me)Fe(CO)_2]_2$ and derivatives

Complex	Colour	mp(°C)	Elemental analysis (Found (Calcd.)(%))			
			C	H	N	I
$[(C_5H_4CO_2Me)Fe(CO)_2]_2$	purple	>330	46.4(46.0)	2.94(3.00)	-	-
$(C_5H_4CO_2Me)Fe(CO)_2I$	black	75-76	30.4(29.9)	2.05(1.95)	-	35.5(35.1)
$[(C_5H_4CO_2Me)_2Fe_2(CO)_3(CNBu^t)]$	maroon	70-71	50.4(50.3)	4.55(4.41)	2.60(2.67)	-
$[(C_5H_4CO_2Me)Fe(CO)(CNBu^t)]_2$	bottle green	>330	54.9(53.8)	5.84(5.56)	4.36(4.83)	-

TABLE 2.5: Spectroscopic data for $[(C_5H_4CO_2Me)Fe(CO)_2]_2$ and derivatives

Complex	IR (cm^{-1})[a]				^1H NMR (ppm)[b]		
	ν(NC)	ν(CO)(terminal)	ν(CO)(bridging)	ν(COOMe)	$C(CH_3)_3$	$C_5H_4CO_2CH_3$	$C_5H_4CO_2CH_3$
$[(C_5H_4CO_2Me)Fe(CO)_2]_2$	-	2012(s),1974(m)	1790(s)	1720(m)	-	3.80(s)	4.35 and 4.90(m)
$(C_5H_4CO_2Me)Fe(CO)_2I$	-	2052(s),2012(s)	-	1730(m)	-	3.84(s)	3.79 and 5.00(m)
$[(C_5H_4CO_2Me)_2Fe_2(CO)_3(CNBu^t)]$	2136(m)	1964(m)	1760(s)	1713(m)	0.79(s)	3.70(s)	4.46 and 5.04(m)
$[(C_5H_4CO_2Me)Fe(CO)(CNBu^t)]_2$	2120(m),2000(w)	-	1754(s)	1720(m)	0.94(s)	3.80(s)	4.41 and 5.10(m)

[a] *Recorded in CH_2Cl_2*

[b] Recorded om C_6D_6, relative to TMS

III. THE MODIFICATION OF $(\eta^6C_6H_5CO_2Me)Cr(CO)_3$ BY LIGANDS L

3.1 Introduction

A typical example of a half-sandwich metal carbonyl compound is $(\eta^6C_6H_6)Cr(CO)_3$. The crystal and molecular structure (at 78°K) of this complex has been determined by Rees and Coppens[13] using X-ray and neutron diffraction techniques. The molecule exhibits a "piano-stool" arrangement of the (η^6-Arene) and the $Cr(CO)_3$ unit, with the conformation of the carbonyl ligands with respect to the carbon atoms of the Arene ring staggered.

Considerable interest has been shown in complexes of the type $(\eta^6$-Arene$)Cr(CO)_3$, owing to the catalytic potential of such compounds.[1-3] It is possible to modify the chemistry of *(Arene)$Cr(CO)_3$ in two ways:-*

(i) by varying the arene ligand

or (ii)by the substitution of CO by ligand L (eg. RNC, CS, PR_3). Further, if the $(\eta^6C_6H_6)$ ring is replaced by a ring containing an *electron-withdrawing* group, eg. $\eta^6C_6H_5CO_2Me$, the stability of the complex (to air oxidation) increases,[12c] making such substituted derivatives more accessible for study.

The complex $(\eta^6C_6H_5CO_2Me)Cr(CO)_3$,[14] and a wide range of ligand substituted derivatives, $(\eta^6C_6H_5CO_2Me)Cr(CO)_2L$, have been previously investigated by X-ray *crystallographic* techniques.[14,31-35] Unlike the unsubstituted $(\eta^6C_6H_6)Cr(CO)_3$, the parent compound $(\eta^6C_6H_5CO_2Me)Cr(CO)_3$ adopts an eclipsed conformation of the carbonyl ligands *with respect* to the C-atoms of the arene ring, as do most of the $(\eta^6C_6H_5CO_2Me)$-$Cr(CO)_2L$ derivatives. This, and the effect of the ligand L on molecular structure, can be rationalized in terms of *electronic effects*.

3.2 The Structure of $(\eta^6C_6H_5CO_2Me)Cr(CO)_3$

The crystal and molecular structure of $(\eta^6C_6H_5CO_2Me)Cr(CO)_3$ was first determined by Carter, McPhail and Sim[14a] in 1967 (R-value of 14.1%) and in 1976 redetermined by *Saillard and*

Grandjean[36b] (R-value of 3.4%), improving the accuracy of bond parameter data.

3.2.1 Ligand geometry

The $(\eta^6\text{-}C_6H_5CO_2Me)Cr(CO)_3$ molecule has the typical "piano-stool" geometry, with the three OC-Cr-CO angles being equal within experimental error (av. 88.2(1)°).

3.2.2 Conformation

There are three ssible conformations for a mono-*substituted arene complex of the type* $(C_6H_5R)Cr(CO)_3$ (Fig. 3.1), viz. staggered (I), anti-eclipsed (IIa), i.e. ortho and para C-atoms of ring eclipsed, and syn-eclipsed (IIb), i.e. C-atom bearing substituent R, and meta C-atoms of ring eclipsed

From electronic considerations,[33-38] it is possible to predict the most favourable conformation for a given $(\eta^6\text{-}C_6H_5R)Cr(CO)_3$ complex. According to the hybridization model, the $Cr(CO)_3$ unit has three filled hybrid orbitals collinear with the Cr-CO bonds and three empty hybrids, directed in an octahedral arrangement, with the empty hybrids staggering the Cr-CO bonds (Fig. 3.2). The $Cr(CO)_3$ group will orient itself such that the empty set of hybrid orbitals (a) are pointed towards regions of high electron density, and the filled set of hybrid orbitals (b) towards regions of low electron density on the arene ring. The charge distribution on the arene ring is dependent on the electronic nature of the ring substituent R. Case a: If R is an electron-acceptor A, the $Cr(CO)_3$ group will orient itself with the empty trio of orbitals (a) pointing towards the electron rich ipso and meta positions, and the filled trio of orbitals (b) towards the electron deficient ortho and para positions, giving the anti-eclipsed conformation (IIa). (Fig. 3.3a). Case b: If R is an electron-donor D, the $Cr(CO)_3$ group will orient itself with the empty trio of orbitals (a) pointing towards the electron rich ortho and para positions, and the filled trio of orbitals (b) towards the electron deficient ipso and meta positoins, giving the syn-eclipsed conformation (IIb) (Fig. 3.3b).

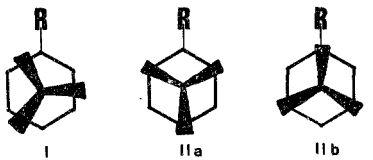


Figure 3.1 The three possible conformations for (C_6H_5R)-$Cr(CO)_3$: I. staggered, IIa. anti-eclipsed, and IIb. syn-ecl psed.



Figure 3.2 Two sets of three hybrid orbitals of $Cr(CO)_3$: (a) empty, (b) filled.

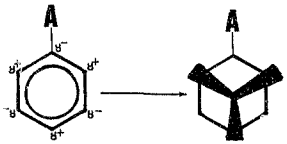


Figure 3.3a Ring polarization with electron-accepting substituent A results in the anti-eclipsed conformation IIa for $(C_6H_5A)Cr(CO)_3$

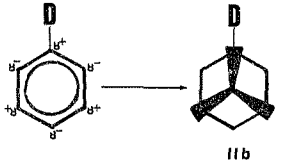


Figure 3.3b Ring polarization with electron-donating substituent D results in the syn-eclipsed conformation IIb for $(C_6H_5D)Cr(CO)_3$

Hence for $(\eta^6C_6H_5R)Cr(CO)_3$ complexes, electron-withdrawing R-groups favour the anti-eclipsed conformation (IIa), and electron-releasing R-groups the syn-eclipsed conformation (IIb). However, steric factors may favour a staggered conformation (I), especially if bulky groups are present.[24,28] Further, since the rotation barrier in many $(\eta^6C_6H_5R)Cr(CO)_3$ complexes is not expected to be very large if the R-group is neither strongly electron-withdrawing or -releasing,[37] packing forces may be the determining factor in the conformation adopted in the solid state.

In the case of $(\eta^6C_6H_5CO_2Me)Cr(CO)_3$, since the CO_2Me group is [illegible]tron-withdrawing, the anti-eclipsed conformation [illegible]ich the substitutuert resides on a non-eclip[illegible], would be expected. This is indeed the conformation found in the crystal.[38]

3.2.3 *Cr-C bond lengths*

The av. values for the Cr-CO and Cr-C-ring bond lengths are 1.842(3)Å and 2.217(3)Å respectively. The distance between the chromium atom and the centre of gravity of the arene ring, Cr-Aren , is 1.7144(4)Å.[34b]

3.2.4 Ring C-C bond lengths

In the unsubstituted complex, $(\eta^6C_6H_6)Cr(CO)_3$, which has a staggered conformation, there is a lowering of the benzene-ring symmetry from D_{3h} to C_{3v}; the C-C bonds of the arene ring alternate in length, with the three non-eclipsed C-C bonds (av. 1.406(1)Å) shorter than the three eclipsed C-C bonds (av. 1.423(1)Å).[39] This effect has been rationalized in terms of Molecular Orbital (MO) Theory, which demonstrates that the observed bond lengths correlate well with electron overlap populations.[39,38]

However, in the eclipsed $(\eta^6C_6H_5CO_2Me)Cr(CO)_3$ molecule, the C-C bonds of the arene ring are uniform within the error limits (av. 1.407(4)Å).[38b]

3.2.5 Planarity of Ring

The arene ring in $(\eta^6C_6H_5CO_2Me)Cr(CO)_3$ is essentially planar.[38b] In the case of $(\eta^6C_6H_6)Cr(CO)_3$, the ring H-atoms

are displaced an av. of 0.03Å from the plane of the benzene ring towards the Cr-atom.[39] This slight bending of the hydrogen atoms towards the metal atom has been ascribed to better metal-ring orbital overlap.[38] This effect is not apparent in $(\eta^6-C_6H_5CO_2Me)Cr(CO)_3$, but the α-C-atom of the substituent is bent 0.010(3)Å towards the Cr-atom.[39b]

3.2.6. Cr-C-O bond angles

In $M(CO)_n$ (n = 2,3,4) groups, the M-C-O fragments are expected to be bent (ca. 5° deviation from linearity) due to the different occupation of the two anti-bonding π* orbitals on a carbonyl ligand.[38] The carbonyl ligands in $(\eta^6-C_6H_5CO_2Me)Cr(CO)_3$ are slightly bent, with Cr-C-O angles ranging from 178.0 to 179.3° (av. 178.8(3)°).[39b] The slight difference in Cr-C-O angles within the $Cr(CO)_3$ group (although equal within experimental error) could be due to crystal packing forces, or to the influence of other groups within the molecule which lower the symmetry of the $M(CO)_3$ group from C_{3v}.[39]

3.2.7 Packing considerations

$(\eta^6-C_6H_5CO_2Me)Cr(CO)_3$ crystallizes in the triclinic centrosymmetric space group $C\bar{1}$, with four molecules in the unit cell. The molecules pack with the arene rings parallel, the separation between the adjacent benzene planes of 3.38Å being very close to the graphite distance of 3.35Å.[39a] There are no unusually short non-bonded contacts, but intermolecular repulsions could result in minor deviations from the ideal geometry.

3.3 The structural effect of substitution of CO by ligand L

The electronic nature of the ligand L, relative to CO, may result in structural changes in the $(\eta^6-C_6H_5CO_2Me)Cr(CO)_2L$. With bulky L groups, steric factors may also be important.

3.3.1 Ligand geometry

Although the "piano-stool" arrangement is retained, the OC-Cr-CO angle may differ significantly from the OC-Cr-L angles. If L is a better π-acceptor than CO, an increase in the OC-Cr-CO angle, and a diminution of the OC-Cr-L angles is expected.[38]

3.3.2 Conformation

Since the electronic preference for a conformation is governed by the electronic nature of the arene substituent, the ligand substituted derivatives (η^6-$C_5H_5CO_2Me$)$Cr(CO)_2L$ would be expected to have the same conformation as the parent molecule (η^6-$C_6H_5CO_2Me$)$Cr(CO)_3$, viz. anti-eclipsed (IIa).

However, as mentioned previously, where the barrier to ring rotation is not large, packing forces may determine the molecular conformation in the crystal.[37]

Exceptions to the predicted conformation may also be caused by steric factors,[38] particularly if the L group is bulky. A staggered conformation may better accomodate a sterically demanding L group, by minimizing intramolecular repulsive interactions.

3.3.3 Influence of electronic nature of L on Cr-C bond lengths

The electronic nature of the ligand L, relative to CO, effects the Cr-C bond lengths in (η^6-$C_6H_5CO_2Me$)$Cr(CO)_2L$. Specifically, if the ligand L is a stronger ligand than CO, i.e. stronger σ-donor and π-acceptor properties than CO, a shortening of the Cr-CR (L ≈ CR) bond (relative to the Cr-CO bond lengths in (η^6-$C_6H_5CO_2Me$)$Cr(CO)_3$) is expected, with a concomitant lengthening of the Cr-CO bonds, and of the Cr-C ring bond lengths, and the Cr-arene distance, relative to these Cr-C distances in (η^6-$C_6H_5CO_2Me$)$Cr(CO)_3$. However, with a ligand L which is a poorer π-acceptor than CO, the inverse trends in Cr-C bond lengths are expected.[40]

3.3.4 Ring C-C bond lengths

The ring C-C bonds are expected to be uniform, as in (η^6-$C_6H_5CO_2Me$)$Cr(CO)_3$. Small differences may result from differences in the polarization of the electron denisty of specific carbon atoms of the ring by the $Cr(CO)_2L$ group itself.[37] The $[Cr(CO)_3]$ unit has been shown to exert an electron-withdrawing effect upon arene rings which is approximately equal to that of the nitro group.[41]

3.3.5 Planarity of Ring

The arene ring is expected to be essentially planar, as for (η^6-$C_6H_5CO_2Me$)$Cr(CO)_3$. The ring substituent may bend

slightly towards the Cr-atom, as in $(\eta^6-C_6H_5CO_2Me)Cr(CO)_3$, or may bend away from the Cr-atom. A bending away from the Cr-atom may be in an attempt to minimize repulsive intramolecular interactions. The bending of the ring substituent may also be influenced by intermolecular interactions. Steric factors are likely to be more dominant with bulky ligands L.

3.3.6 Cr-C-O and Cr-C-R bond angles (L = CR)

Non-linearity of Cr-C-O fragments is expected for $Cr(CO)_2$ groups, as for $Cr(CO)_3$ groups.[39] Linearity would only be expected for M(CO). This applies also to other ligands such as CNR,NO. Different Cr-C-O angles within the $Cr(CO)_2$ group (often equal within experimental error) could be due to crystal packing forces, or to the influence of other groups within the molecule which lower the symmetry. Steric constraints and crystal packing forces may cause the Cr-C-R (L = CR) angle to deviate from linearity.

3.3.7 Packing, and Steric factors

Packing considerations could be important in determining the overall conformation of the molecule. Packing forces may also be responsible for small deviations from ideal geometry within the molecule.

For a ligand of the type L = CRR', the magnitude and direction of the bending of the ligand (ie. the deviation of the C-R-R' angle from linearity, and whether the R' group bends in towards the two CO groups, or outwards away from the carbonyls), is probably determined largely by intramolecular and intermolecular interactions, and the influence of crystal packing forces. Steric factors are likely to be particularly dominant in determining the ligand conformation when there is no very strong electronic conformation preference, eg. for isonitrile ligands, L = CNR, MO calculations indicate[42] that the energy difference between the linear (C-N-R = 180°) and slightly bent (C-N-R = 167-171°) conformations is small, although the linear conformation is slightly more stable electronically. Here steric factors may dominate, especially with bulky R-groups.

3.4 X-ray Crystallographic Studies of $(\eta^6-C_6H_5CO_2Me)Cr(CO)_2L$ complexes

The $(\eta^6-C_6H_5CO_2Me)Cr(CO)_2L$ complexes for which X-ray crystal and molecular structures have been reported in the literature are listed in Table 3.1. Note that the compound $(\eta^6-C_6H_5CO_2Me)$-$Cr(CO)_2(CNCOC_6H_5)$ has two crystal morphologies, a triclinic form (A), and a monoclinic form (B), both of which, however, have very similar molecular structure.[16]

Table 3.2 summarizes the principal geometric characteristics of the above complexes. Trends and special features will be discussed.

The electronic nature of the ligand L is an important factor influencing molecular geometry, through the σ-donor and π-acceptor properties of L relative to CO. For the ligands L of interest, the order of increasing σ-donor strength is CSe>CS>CNR>CNCOR>CO, and of increasing π-acceptor ability is CSe>CS>CNCOR>CO>CNR>PR_3.[40,42,43] However, the PF_3 ligand does not fall into the PR_3 class with PPh_3, being a stronger π-acceptor than CO.[44]

3.4.1 OC-Cr-CO and OC-Cr-L angles

All the $(\eta^6-C_6H_5CO_2Me)Cr(CO)_2L$ complexes have the usual "piano-stool" geometry. The order of increasing OC-Cr-CO angle, and decreasing av. OC-Cr-L angle for ligands L, relative to the av. OC-Cr-CO angle in $(\eta^6-C_6H_5CO_2Me)Cr(CO)_3$ of 88.3(1)°, is PPh_3, CO, PF_3, CS, CSe, which parallels the order of increasing π-acceptor ability.

3.4.2 *Conformation; An exception*

The complexes $(\eta^6-C_6H_5CO_2Me)Cr(CO)_2L$ (L = PPh_3, CO, CS, CSe), all have the anti-eclipsed conformation as expected, with small angles of eclipse at the ortho and para positions (Fig 3.4). However, for L = PF_3, the angles of eclipse are large (av. 18.1°)[16] and the conformation can be described as "off-anti-eclipsed."

With the exception of L = PPh_3, the ligand L (L = CSe, CS, PF_3) occupies the ortho position with the angle of eclipse (a) (Fig 3.4), where L has moved away from the CO_2Me

TABLE 3.1: X-ray Crystal Structures of (η^6-$C_6H_5CO_2Me$)$Cr(CO)_2L$ complexes

Complex	Space Group, Z	Reference
(η^6-$C_6H_5CO_2Me$)$Cr(CO)_3$	$C\bar{1}$, 4	30
(η^6-$C_6H_5CO_2Me$)$Cr(CO)_2CS$	$P\bar{1}$, 2	31
(η^6-$C_6H_5CO_2Me$)$Cr(CO)_2CSe$	$P\bar{1}$, 2	32
(η^6-$C_6H_5CO_2Me$)$Cr(CO)_2PPh_3$	$P2_1/n$, 4	33
(η^6-$C_6H_5CO_2Me$)$Cr(CO)_2PF_3$	$P\bar{1}$, 2	34
(η^6-$C_6H_5CO_2Me$)$Cr(CO)_2$(CNCOPh)	$P\bar{1}$, 2 (Form A) $P2_1/c$, 4 (Form B)	16

TABLE 3.2: Principal geometric characteristics (distances, Å; Angles, °) of (π-$C_6H_5CO_2Me$)$Cr(CO)_2L$ complexes

L	PPh_3	$CNCOPh$	CO	PF_3	CS	CSe
Conformation	Anti-eclipsed	Staggered	Anti-eclipsed	Off-anti-eclipsed	Anti-eclipsed	Anti-eclipsed
Angles of eclipse. a,b,c [a]		-	4.3,4.9,4.2	17.6,17.7,19.0	0,6.0,1.5	1.7,5.4,2.5
Ring planarity	Planar	Planar	Planar	Planar	Planar	Planar
Deviation of α-C [b]	c	c	+0.010(3)	+0.083(11)	+0.037(3)	0°
av Ring C-C	1.399(5)	c	1.407(4)	1.399(15)	1.401(4)	1.40(2)
Cr-Arene	1.695(1) [d]	c	1.714(1)	1.698(2)	1.730(1)	1.742(1)
av Cr-C ring	2.198(4)	c	2.217(2)	2.201(10)	2.226(2)	2.232(11)
av Cr-CO	1.823(4)	c	1.842(3) [e]	1.833(11)	1.848(3)	1.862(11)
Cr-L	2.337(1)	1.85(1)	c	2.132(3)	1.797(2)	1.786(11)
OC-Cr-CO	85.3(1)	c	88.7(1) [e]	89.4(5)	90.9(1)	91.0(6)
av OC-Cr-L	90.1(1) [d]	c		88.6(5)	85.7(1)	84.9(5)
av Cr-C-O	176.6(3) [d]	c	176.8(3) [e]	177.7(7)	176.9(2)	177.1(7)
Cr-C-R [f]	-	178.8(9)		-	178.0(2)	179.0(7)

[a] See Fig 3.4

[b] Deviation of α-C of $-CO_2Me$ from mean plane of arene ring; + indicates towards Cr atom, - away from Cr atom

[c] Not quoted in reference

[d] Ref. 34

[e] av value for the three CO ligands

[f] Applicable for ligand type L = CR

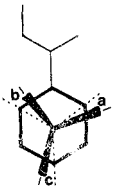


Figure 3.4 Anti-eclipsed conformation of $(\eta^6C_6H_5CO_2Me)Cr(CO)_2L$ complex, viewed down ligand tripod onto arene ring, showing angles of eclipse, a, b and c, at ortho positions and para C-atom respectively

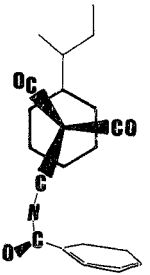


Figure 3.5 Unusual staggered conformation of the $(\eta^6C_6H_5CO_2Me)Cr(CO)_2(CNCOPh)$ molecule, viewed down ligand tripod onto arene ring. (Both A and B forms the same structurally).

substituent, presumedly for steric reasons. This could also account for the larger angle of eclipse (a) of 17.6° observed for L = PF_3. However, for L = PPh_3, the PPh_3 ligand occupies the ortho position with angle of eclipse (b).

There is one exception: the $(\pi^6-C_6H_5CO_2Me)Cr(CO)_2(CNCOPh)$[16] molecule has a staggered conformation (in both A and B forms) (Fig 3.5). Further, the relation of the ligand tripod to the arene substituent differs from all the other structures; if viewed down the ligand tripod onto the arene ring, the -OMe group points to the right, and not to the left, as is usual. (Fig 3.5,cf. Fig 3.4). The $CNCOC_6H_5$ group is anti-parallel to the CO_2Me substituent. Steric considerations could be responsible for the overall conformation, and crystal packing forces probably also play a role.

3.4.3 Trends in Cr-C bond lengths

For the complexes $(\pi^6-C_6H_5CO_2Me)Cr(CO)_2L$, (L = CSe, CS, PF_3, PPh_3, CO), the order of increasing Cr-CO bond length and of increasing Cr-C-ring and Cr-arene distances, is PPh_3, PF_3, CO, CS, CSe, which is the same as the order of increasing π-acceptor strength of the ligands L. This is also reflected in the Cr-CR (L = CR, R = Se, S, O, NCOPh) bond lengths CNCOPh<CO<CS<CSe. Note that the Cr-PF_3 bond (2.132(3)Å) is considerably shorter than the Cr-PPh_3 bond (2.337(1)Å), indicating that the PF_3 ligand, unlike PPh_3, is a good π-acceptor.[14]

3.4.4 Ring C-C bond lengths

The ring C-C bond lengths are consistent within a structure, and from structure to structure (ca. 1.40Å).

3.4.5 Ring planarity and bending of CO_2Me group

In all cases, the arene ring is planar, with the α-C atom of the CO_2Me group either planar with the ring (L = CSe), or bending in slightly towards the Cr-atom (L = CS, PF_3, CO).

3.4.6 Cr-C-O and Cr-C-R bond angles (L = CR)

For all the complexes, the Cr-C-O angles deviate slightly for linearity (ca. 177°), as expected. The Cr-C-R angles (L = CR, R = Se, S, NCOPh), are also slightly bent (178 - 179°).

3.4.7 Conformation of the ligand L

In the complex (η^6-$C_6H_5CO_2Me$)Cr(CO)$_2$(CNCOPh),[16] the isonitrile ligand is bent, with a C-N-C angle of 168(1)°. This probably reflects steric and packing requirements.

3.5 Conclusion

From the foregoing analyses, it is apparent that structural variations in (η^6-$C_6H_5CO_2Me$)Cr(CO)$_2$L derivatives, relative to the parent (η^6-$C_6H_5CO_2Me$)Cr(CO)$_3$, may be rationalized by considering the influence of the electronic nature of the ligand L, relative to CO.

However, steric factors and the role of crystal packing forces should not be ignored, and these may account for exceptions encountered, as well as small deviations from ideal geometry.

IV. THE CRYSTAL AND MOLECULAR STRUCTURE OF (η^6-$C_6H_5CO_2Me$)Cr-($CO)_2(CNBu^t$)

4.1 Introduction

An X-ray crystal study of (η^6-$C_6H_5CO_2Me$)$Cr(CO)_2(CNBu^t$), was undertaken as part of an investigation into the anomalous IR spectra exhibited by certain complexes of this type. It was hoped that the X-ray study might provide a structural basis for the rationalization of the anomalous IR data. The IR spectra in relation to the structure, will be discussed separately in Chapter VIII.

(η^6-$C_6H_5CO_2Me$)$Cr(CO)_2(CNBu^t$) crystallizes in the triclinic centrosymmetric space group $P\bar{1}$, with two molecules in the unit cell. Fig. 4.2 shows a view of the unit cell looking down the c-axis. A view of the molecule, looking down the ligand tripod onto the arene ring is shown in Fig. 4.1, together with the numbering system used in the analysis.

Bond lengths and bond angles, and bond parameters involving hydrogen atoms, are given in Table 4.1, 4.2 and 4.3 respectively. Table 4.4 lists the deviations ($\AA$) of the atoms from the mean plane through the ring C-atoms (C(1)-C(6)).

4.2 Discussion of the Structure of (η^6-$C_6H_5CO_2Me$)$Cr(CO)_2(CNBu^t$)

The structure of the (η^6-$C_6H_5CO_2Me$)$Cr(CO)_2(CNBu^t$) molecule will be discussed in relation to the structures of related (η^6-$C_6H_5CO_2Me$)$Cr(CO)_2L$ complexes (Table 3.2), following the scheme of analysis previously employed. Any irregularities observed will be examined in greater detail, and possible causes considered (section 4.3). The principal geometric characteristics of (η^6-$C_6H_5CO_2Me$)$Cr(CO)_2(CNBu^t$) are summarized in Table 4.5

Since the electronic nature of the ligand L has an important influence on structure, it should be noted that the $CNBu^t$ ligand is a better σ-donor and a poorer π-acceptor than CO, but a better π-acceptor than PR_3.[41a]

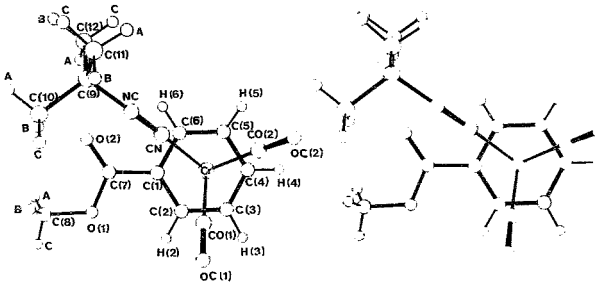


Figure 4.1 An ORTEP[45] view of the $(\eta^6-C_6H_5CO_2Me)Cr(CO)_2(CNBu^t)$ molecule, showing the numbering system

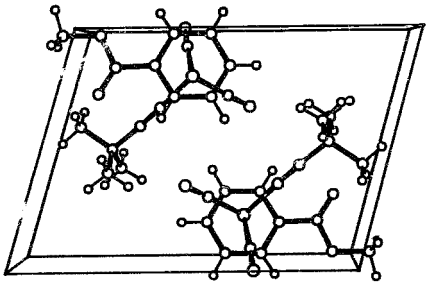


Figure 4.2 An ORTEP[43] view of the unit cell of (η^6-$C_6H_5CO_2Me$)$Cr(CO)_2$(CNBu^t), looking down the c-axis

TABLE 4.1: Bond lengths (Å) for (η^6-$C_6H_5CO_2Me$)Cr(CO)$_2$($CNBu^t$)

Cr-C(1)	2.190(4)	C(1)-C(2)	1.410(7)
Cr-C(2)	2.198(4)	C(2)-C(3)	1.405(8)
Cr-C(3)	2.207(5)	C(3)-C(4)	1.404(7)
Cr-C(4)	2.190(5)	C(4)-C(5)	1.407(9)
Cr-C(5)	2.224(5)	C(5)-C(6)	1.381(7)
Cr-C(6)	2.212(5)	C(6)-C(1)	1.420(6)
Cr-CO(1)	1.827(4)	CO(1)-OC(1)	1.159(5)
Cr-CO(2)	1.836(3)	CO(21-OC(2)	1.157(4)
Cr-CN	1.940(5)	CN-NC	1.155(6)
C(1)-C(7)	1.486(7)	NC-C(9)	1.451(6)
C(7)-O(1)	1.346(5)	C(9)-C(10)	1.524(6)
C(7)-O(2)	1.201(6)	C(9)-C(11)	1.512(8)
O(1)-C(8)	1.448(6)	C(9)-C(12)	1.523(6)

TABLE 4.2: Bond angles (°) for (η^6-$C_6H_5CO_2Me$)Cr(CO)$_2$($CNBu^t$)

Cr-CO(1)-OC(1)	178.3(3)	CO(1)-Cr-CO(2)	86.2(2)
Cr-CO(2)-OC(2)	177.9(3)	CO(1)-Cr-CN	90.7(2)
Cr-CN-NC	177.3(4)	CO(2)-Cr-CN	90.2(2)
NC-CN-C(9)	166.8(4)	C(1)-Cr-CO(1)	112.7(1)
CN-C(9)-C(10)	106.9(4)	C(2)-Cr-CO(1)	89.0(2)
CN-C(9)-C(11)	107.1(4)	C(3)-Cr-CO(1)	93.4(2)
CN-C(9)-C(12)	108.4(4)	C(4)-Cr-CO(1)	122.1(2)
C(10)-C(9)-C(11)	111.9(5)	C(5)-Cr-CO(1)	159.0(2)
C(11)-C(9)-C(12)	112.2(4)	C(6)-Cr-CO(1)	150.1(1)
C(12)-C(9)-C(10)	110.1(4)	C(1)-Cr-CO(2)	161.1(2)
C(6)-C(1)-C(2)	119.2(4)	C(2)-Cr-CO(2)	149.1(2)
C(1)-C(2)-C(3)	119.8(4)	C(3)-Cr-CO(2)	112.6(2)
C(2)-C(3)-C(4)	120.0(5)	C(4)-Cr-CO(2)	89.7(2)
C(3)-C(4)-C(5)	120.1(5)	C(5)-Cr-CO(2)	95.2(2)
C(4)-C(5)-C(6)	119.9(4)	C(6)-Cr-CO(2)	123.6(2)
C(5)-C(6)-C(1)	120.7(5)	C(1)-Cr-CN	90.3(2)
C(7)-C(1)-C(2)	122.7(4)	C(2)-Cr-C	120.4(2)
C(7)-C(1)-C(6)	118.1(4)	C(3)-Cr-CN	157.0(2)
C(1)-C(7)-O(2)	124.6(4)	C(4)-Cr-CN	147.1(2)
C(1)-C(7)-O(1)	112.0(4)	C(5)-Cr-CN	110.2(2)
O(1)-C(7)-O(2)	123.4(4)	C(6)-Cr-CN	86.5(2)
C(7)-O(1)-C(8)	115.3(4)	C(1)-Cr-C(2)	37.5(2)
Cr-C(1)-C(2)	71.6(2)	C(1)-Cr-C(3)	67.3(2)
Cr-C(1)-C(6)	72.0(2)	C(1)-Cr-C(4)	79.8(2)
Cr-C(2)-C(1)	70.9(2)	C(1)-Cr-C(5)	67.0(2)
Cr-C(2)-C(3)	71.7(3)	C(1)-Cr-C(6)	37.6(1)
Cr-C(3)-C(2)	71.1(3)	C(2)-Cr-C(3)	37.2(2)
Cr-C(3)-C(4)	70.7(3)	C(2)-Cr-C(	67.4(2)
Cr-C(4)-C(3)	72.0(3)	C(2)-Cr	79.1(2)
Cr-C(4)-C(5)	72.7(3)	C(2)-	67.2(2)
Cr-C(5)-C(4)	70.1(3)	C(3)-C	37.2(2)
Cr-C(5)-C(6)	71.4(3)	C(3)-Cr	66.7(2)
Cr-C(6)-C(5)	72.3(3)	C(3)-Cr-C(	78.7(2)
Cr-C(6)-C(1)	70.3(3)	C(4)-Cr-C(5)	37.2(2)
Cr-C(1)-C(7)	127.3(3)	C(4)-Cr-C(6)	66.5(2)
		C(5)-Cr-C(6)	36.3(2)

TABLE 4.3: Bond parameters involving hydrogen atoms for $(\eta^6C_6H_5CO_2Me)Cr(CO)_2(CNBu^t)$

a) Bond lengths (Å)

C(2)-H(2)	0.97(4)	C(10)-H(10A)	0.97(5)
C(3)-H(3)	0.99(5)	C(10)-H(10B)	0.94(4)
C(4)-H(4)	0.98(4)	C(10)-H(10C)	1.07(4)
C(5)-H(5)	0.99(4)	C(11)-H(11A)	0.98(5)
C(6)-H(6)	0.96(5)	C(11)-H(11B)	0.97(4)
C(8)-H(8A)	0.95(5)	C(11)-H(11C)	0.95(4)
C(8)-H(8B)	0.91(4)	C(12)-H(12A)	1.00(4)
C(8)-H(8C)	1.03(4)	C(12)-H(12B)	0.96(5)
		C(12)-H(12C)	0.94(4)

b) Bond angles (°)

C(1)-C(2)-H(2)	118(3)	Cr-C(2)-H(2)	124(2)
C(3)-C(2)-H(2)	122(3)	Cr-C(3)-H(3)	125(2)
C(2)-C(3)-H(3)	117(2)	Cr-C(4)-H(4)	129(2)
C(4)-C(3)-H(3)	123(2)	Cr-C(5)-H(5)	131(2)
C(3)-C(4)-H(4)	119(2)	Cr-C(6)-H(6)	131(2)
C(5)-C(4)-H(4)	121(2)	O(1)-C(8)-H(8A)	110(3)
C(4)-C(5)-H(5)	121(3)	O(1)-C(8)-H(8B)	110(3)
C(6)-C(5)-H(5)	119(3)	O(1)-C(8)-H(8C)	105(3)
C(5)-C(6)-H(6)	121(2)	C(9)-C(10)-H(10A)	104(2)
C(1)-C(6)-H(6)	119(2)	C(9)-C(10)-H(10B)	108(2)
H(10A)-C(10)-H(10B)	104(4)	C(9)-C(10)-H(10C)	110(2)
H(10B)-C(10)-H(10C)	119(3)	C(9)-C(11)-H(11A)	111(2)
H(10C)-C(10)-H(10A)	111(3)	C(9)-C(11)-H(11B)	109(4)
H(11A)-C(11)-H(11B)	105(4)	C(9)-C(11)-H(11C)	111(3)
H(11B)-C(11)-H(11C)	111(3)	C(9)-C(12)-H(12A)	112(2)
H(11C)-C(11)-H(11A)	109(4)	C(9)-C(12)-H(12B)	106(2)
H(12A)-C(12)-H(12B)	114(4)	C(9)-C(12)-H(12C)	112(2)
H(12B)-C(12)-H(12C)	105(4)	H(8A)-C(8)-H(8B)	116(4)
H(12C)-C(12)-H(12A)	108(4)	H(8B)-C(8)-H(8C)	118(3)
		H(8C)-C(8)-H(8A)	98(3)

TABLE 4.4: Deviations (Å) of atoms from the plane defined by the six C-atoms (C(1)-C(6)) of the arene ring[a] in $(\eta^6C_6H_5CO_2Me)Cr(CO)_2(CNBu^t)$

Atom	Deviation from Plane (Å)
Cr	1.6975
C(1)	0.0147
C(2)	-0.0046
C(3)	-0.0132
C(4)	0.0209
C(5)	-0.0107

TABLE 4.4 (Continued)

Atom	Deviation from Plane (Å)
C(6)	-0.0071
H(2)	0.0905
H(3)	0.0572
H(4)	0.0468
H(5)	-0.0285
H(6)	-0.0387
C(7)	0.0787
O(1)	0.0621
O(2)	0.1447
C(8)	0.1376
H(8A)	-0.5468
H(8B)	0.9869
H(8C)	-0.2454
CO(1)	2.7746
CO(2)	2.8316
OC(1)	3.4511
OC(2)	3.5666
CN	2.7731
NC	3.3754
C(9)	3.8288
C(10)	3.8186
C(11)	2.8604
C(12)	5.2473
H(10A)	4.0513
H(10B)	2.9222
H(10C)	4.5454
H(11A)	3.0944
H(11B)	1.9744
H(11C)	2.8530
H(12A)	5.8888
H(12B)	4661
H(12C)	5.2949

[a] Equation of the plane defined by C(1)-C(6):

0.0478x + 1.1172y + 6.5952z = 1.6293

TABLE 4.4 (Continued)

Atom	Deviation from Plane (Å)
C(6)	-0.0071
H(2)	0.0905
H(3)	0.0572
H(4)	0.0468
H(5)	-0.0285
H(6)	-0.0387
C(7)	0.0787
O(1)	0.0621
O(2)	0.1447
C(8)	0.1376
H(8A)	-0.5468
H(8B)	0.9869
H(8C)	-0.2454
CO(1)	2.7746
CO(2)	2.8316
OC(1)	3.4511
OC(2)	3.5666
CN	2.7731
NC	3.3754
C(9)	3.8288
C(10)	3.8186
C(11)	2.8604
C(12)	5.2473
H(10A)	4.0513
H(10B)	2.9232
H(10C)	4.5484
H(11A)	3.0944
H(11B)	1.9744
H(11C)	2.8500
H(12A)	5.8888
H(12B)	5.4661
H(12C)	5.2949

[a] Equation of the plane defined by C(1)-C(6):

0.0478x + 1.1172y + 6.5952z = 1.6293

TABLE 4.5: Principal geometric characteristics (distances, Å; angles, °) of $(\eta^6-C_6H_5CO_2Me)Cr(CO)_2(CNBu^t)$

Conformation	*Staggered*
Ring planarity	Planar
Deviation of α-C	0.079, towards the Cr-atom
av Ring C-C	1.405(7)
Cr-Arene	1.697(1)
av Cr-C-ring	2.204(7)
av Cr-CO	1.833(4)
Cr-CN	1.940(5)
OC-Cr-CO	86.2(2)
av OC-Cr-CN	90.5(2)
av Cr-C-O	178.1(3)
Cr-C-N	177.3(4)
C-N-C	166.8(4)

4.2.1 OC-Cr-CO and OC-Cr-CN angles

The molecule has the usual "piano-stool" arrangement of ligands. Within the ligand tripod, the OC-Cr-CO angle is 86.2(2)°, and the av. OC-Cr-CN angle 90.5(2)°. These values are intermediate between those for (η^6-$C_6H_5CO_2Me$)-$Cr(CO)_2(PPh_3)$ [OC-Cr-CO, 85.3(1)°, and av. OC-Cr-P, 90.1(1)°][31] and (η^6-$C_6H_5CO_2Me$)$Cr(CO)_3$ [av. OC-Cr-CO, 88.2(1)°],[18b] as expected, since $CNBu^t$ is a poorer π-acceptor than CO, but a stronger π-acceptor than PPh_3.[31a]

4.2.2 Conformation

(η^6-$C_6H_5CO_2Me$)$Cr(CO)_2(CNBu^t)$ is an exception to the electronic conformation preference, since the molecule adopts a staggered conformation in the crystal. However, the relation of the ligand tripod to the arene ring is normal (Fig 3.4) (ie. when viewed down the ligand tripod onto the arene ring the -OMe group points to the left), but the $CNBu^t$ ligand which is parallel to the ring substituent has moved towards the CO_2Me group. (The angle between Cr-CN and Cr-C(1) (bearing substituent) projected on the plane of the arene ring is 37.7°). The "angles of eclipse" (Fig 4.3) are less than the ideal 30° for a symmetrical staggered conformation (av. 21.3°), placing the conformation intermediate between staggered and the "off-anti-eclipsed" of the (η^5-$C_6H_5CO_2Me$)$Cr(CO)_2PF_3$ structure (av. 18.1°).[34] However, in the latter structure, the PF_3 ligand has moved away from the CO_2Me substituent. The only other isonitrile derivative, (η^6-$C_6H_5CO_2Me$)$Cr(CO)_2(CNCOC_6H_5)$,[14] also has a staggered structure, but the CNR ligand is anti-parallel to the CO_2Me group (Fig 3.5).

4.2.3 Cr-C bond lengths

The av. Cr-CO bond length, and the av. Cr-C ring and Cr-Arene distances of 1.833(4), 2.204(5) and 1.697(1)Å respectively, are intermediate between the values of 1.823(4), 2.198(4) and 1.695(1)Å and 1.842(3), 2.217(2) and 1.716(1)Å for (η^6-$C_6H_5CO_2Me$)$Cr(CO)_2PPh_3$[33] and (η^6-$C_6H_5CO_2Me$)$Cr(CO)_3$[18b]

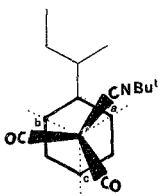


Figure 4.3 Conformation of the (η^6-$C_6H_5CO_2Me$)$Cr(CO)_2(CNBu^t)$ molecule, viewed down ligand tripod onto arene ring. The "angles of *eclipse*" at the ortho and para positions, are a, 22.3°, c, 22.8°, and b, 18.9°, respectively.

respectively, as expected. (π-acceptor strength CO>CNR>PR_3 [3a]). The longer Cr-CN bond length of 1.940(5)Å also reflects the poor π-acceptor property of the CNR ligand relative to CO. Note that the Cr-CO, Cr-C ring and Cr-arene distances are very similar to those for (η^6-$C_6H_5CO_2Me$)$Cr(CO)_2(PF_3)$(1.833(11), 2.201(10) and 1.698(2)Å respectively.)[3a]

4.2.4 Ring C-C bond lengths

The ring C-C bond lengths (av. 1.405(7)Å) are similar to those in the related structures.

4.2.5 Ring planarity and bending of CO_2Me-group

The arene ring is essentially planar, with the α-C-atom of the arene substituent bending slightly towards the Cr-atom, as observed for other (η^6-$C_6H_5CO_2Me$)$Cr(CO)_2L$ (L = CO,[3b] CS,[3] PF_3[3a]) *ctures.*

4.2.6 Cr-C-O and Cr-C-N bond angles

As expected,[39] the Cr-C-O angles deviate slightly from linearity (av. 178.1(3)°). The Cr-C-N group is also slightly bent, with a Cr-C-N angle of 177.3(4)°.

4.2.7 Conformation of the $CNBu^t$ ligand

In $(\eta^6-C_6H_5CO_2Me)Cr(CO)_2(CNBu^t)$, the isonitrile ligand is bent, with a C-N-C angle of 166.8(4)°, similar to that of 168(1)° observed for $(\eta^6-C_6H_5CO_2Me)Cr(CO)_2(CNCOC_6H_5)$.[16] The $CNBu^t$ ligand bends outwards, away from the carbonyls, towards the CO_2Me ring substituent. (see Fig. 8.2, ch.VIII).

4.3 Unusual Structural Features of $(\eta^6-C_6H_5CO_2Me)Cr(CO)_2(CNBu^t)$

The structure of $(\eta^6-C_6H_5CO_2Me)Cr(CO)_2CNBu^t)$ has been discussed above in terms of its similarity to related $(\eta^6-C_6H_5CO_2Me)Cr(CO)_2L$ structures. However, the molecule possesses certain unusual features, which will be considered in more detail, and possible reasons for irregularities discussed.

4.3.1 Staggered Conformation

On electronic grounds, an anti-eclipsed conformation would have been predicted, as is found for the complexes $(\eta^6-C_6H_5CO_2Me)Cr(CO)_2L$ (L = CO,[36b] CS,[11] CSe,[12] PPh_3[13]). The staggered conformation (Fig. 4.1) adopted by the $(\eta^6-C_6H_5CO_2Me)-Cr(CO)_2(CNBu^t)$ molecule is thus unexpected. However, from theoretical calculation, the energy barrier between the eclipsed and staggered conformation is not expected to be substantial.[37,38] It is unlikely that the movement from the eclipsed position originates from steric factors, since the PPh_3 ligand adopts the eclipsed geometry, and the steric bulk of the ^tBuNC group is expected to be less than that of the PPh_3 ligand.[44] Note, however, that the PPh_3 group eclipses the ortho position on the COMe side of the COOMe ring substituent, whereas the ^tBuNC ligand lies on the C=O side.

4.3.2. Position of ^tBuNC vis-á-vis CO_2Me

In $(\eta^6-C_6H_5CO_2Me)Cr(CO)_2(CNBu^t)$, the $CNBu^t$ ligand is parallel to the CO_2Me ring substituent (Fig. 4.1). In

contrast to the "off-anti-eclipsed" conformation of $(\eta^6C_6H_5CO_2Me)Cr(CO)_2(PF_3)$, where the PF_3 ligand has moved away from the CO_2Me group (angle between Cr-PF_3 and Cr-C(CO_2Me) projected on the plane of the arene ring is 77.6°),[14] the $CNBu^t$ ligand has moved towards the CO_2Me group (angle between Cr-$CNBu^t$ and Cr-C(CO_2Me) in projection is 37.7°). In the other reported isonitrile derivative, $(\eta^6C_6H_5CO_2Me)Cr(CO)_2(CNCOC_6H_5)$, the conformation is also staggered, but the $Cr(CO)_2L$ tripod has a completely different orientation relative to the $C_6H_5CO_2Me$ ring (Fig. 3.5), and the $CNCOC_6H_5$ and CO_2Me groups are antiparallel.[16]

4.3.3 Bending of the ^{t}BuNC ligand

The ^{t}BuNC ligand bends out towards the CO_2Me ring substituent (see Fig. 8.2), with a C-N-C angle of 166.8(4)°. This aspect is discussed further in in relation to the anomalous IR data (ch. II) of the $Cr(CO)_2(CNR)$ complexes.

4.3.4 Intra- and Inter- molecular Interactions

It is possible that the molecular geometry observed (both the position of the $CNBu^t$ ligand relative to the ring, and the bending out of the $CNBu^t$ ligand towards the CO_2Me group) could be due to an interaction between O(2) and a H-atom of the ^{t}Bu group. Although there are no exceptionally short non-bonding intermolecular distances, weak intramolecular (e.g. O(2)...H(8A), 2.55Å) and intermolecular (e.g. O(2)...H(10C) 2.75Å) interactions are possible. The unusual structural features observed may, however, be a consequence of purely packing considerations in the crystal.

4.4 Experimental

4.4.1 Data collection

The complex $(\eta^6C_6H_5CO_2Me)Cr(CO)_2(CNBu^t)$ was prepared as described in ch. II. Red crystals were obtained by slow recrystallization from dichloromethane-hexane under nitrogen at 15°C. Despite the crystalline appearance in ordinary light, examination under polarized light characterized most

of the material as polycrystalline. Suitable single-crystal fragments of diffraction quality could be cut from the large specimens. Preliminary investigation was done by standard Weissenberg and precession photography. Refined cell constants were obtainid during data collection on a Philips PW1100 four-circle diffractometer using graphite-monochromated MoKα radiation (λ = 0.7107Å) at room temperature (20°C). Lorentz and polarization corrections were applied, but no corrections for absorption were made as the linear absorption coefficient μ was only 3.50 cm^{-1}. Crystal data and details of the structure analysis are summarized in Table 4.6.

4.4.2 Structure Solution and Refinement

Structure analysis and refinements were carried out by using the program SHELX.[44a] Initial co-ordinates for the chromium atom were derived from a Patterson synthesis and difference Fourier syntheses yielded positions first for all 21 non-hydrogen atoms, and after least-squares refinement of these, also for the 17 hydrogen atoms. Positional parameters for all atoms and anisotropic temperature factors for non-hydrogen atoms were refined by full-matrix least-squares analyses. The hydrogen atoms were assigned a common isotropic temperature factor, which refined to the value of 0.0784(27)Å^2. Least-squares refinement was considered complete when all parameter shifts were less than 0.5σ. At this stage the conventional R was 0.0418. Unit weights were used, and scattering factors for Cr^0 were taken from "International Tables for X-ray Crystallography."[44b] Anomalous dispersion corrections[44c] for chromium were made. Fractional atomic co-ordinates, and anisotropic thermal parameters for the non-hydrogen atoms are listed in Tables 4.7 and 4.8 respectively. A listing of the Structure Factors is to be found in Appendix D.

TABLE 4.5: Crystal data and details of structural analysis for $(\eta^6-C_6H_5CO_2Me)Cr(CO)_2(CNBu^t)$

Formula	$CrC_{15}H_{17}NO_4$
Mr	327.30
Crystal dimensions (mm)	0.16 x 0.16 x 0.14
Space Group	$P\bar{1}$ (No 2)
a(Å)	12.812(6)
b(Å)	9.314(5)
c(Å)	6.807(3)
α(°)	97.28(3)
β(°)	87.94(3)
γ(°)	106.02(3)
U(Å^3)	774.47
Z	2
Dc(gcm^{-3})	1.44
F(000)	168.99
μ(cm^{-1})	3.50
λ(Å)	MoKα (0.7107)
Scan mode	ω/2θ
Range (°)	$3 \leq \theta \leq 23$
Scan width (°)	1.20
Scan speed (°s^{-1})	0.04
Range of hkl	± h, ± k, + l
Measured intensities	2147
Unique reflections	2115
Internal consistency R-index	0.3358
Omitted reflections	-
R (R = Rw)	0.0418

TABLE 4.7: Fractional Atomic Co-ordinates for $(\eta^6-C_6H_5CO_2Me)Cr(CO)_2^-$ $(CNBu^t)$

Atom	x/a	y/b	z/c
Cr	0.3658(0)	0.2001(1)	0.4679(1)
C(1)	0.2524(3)	0.1541(5)	0.2213(6)
C(2)	0.2814(4)	0.0211(5)	0.2408(6)
C(3)	0.3914(4)	0.0227(6)	0.2384(7)
C(4)	0.4723(4)	0.1571(6)	0.2202(7)
C(5)	0.4434(4)	0.2885(6)	0.1933(7)
C(6)	0.3353(4)	0.2873(5)	0.1949(6)
C(7)	0.1380(4)	0.1618(5)	0.2306(6)
C(8)	-0.0456(4)	0.0259(7)	0.2639(9)
C(9)	0.1778(3)	0.5196(5)	0.7383(6)
C(10)	0.0615(4)	0.4223(7)	0.7540(10)
C(11)	0.1906(5)	0.6187(7)	0.5746(8)
C(12)	0.2156(5)	0.6098(6)	0.9378(7)
CO(1)	0.3224(3)	0.0703(4)	0.6535(5)
CO(2)	0.4873(3)	0.2861(4)	0.6244(5)
OC(1)	0.2965(2)	-0.0132(3)	0.7704(4)
OC(2)	0.5619(2)	0.3369(3)	0.7267(4)
O(1)	0.0676(2)	0.0274(4)	0.2513(5)
O(2)	0.1105(3)	0.2741(4)	0.2218(5)
CN	0.2926(3)	0.3380(5)	0.6081(6)
NC	0.2450(3)	0.4180(4)	0.6863(6)
H(2)	0.224 (3)	-0.066 (5)	0.270 (6)
H(3)	0.408 (3)	-0.071 (4)	0.265 (5)
H(4)	0.549 (3)	0.157 (4)	0.224 (6)
H(5)	0.500 (3)	0.383 (4)	0.174 (6)
H(6)	0.315 (3)	0.376 (4)	0.175 (5)
H(8A)	-0.065 (3)	0.066 (4)	0.154 (6)
H(8B)	-0.060 (3)	0.071 (4)	0.385 (6)
H(8C)	-0.088 (3)	-0.085 (5)	0.224 (6)
H(10A)	0.019 (3)	0.495 (4)	0.777 (6)
H(10B)	0.040 (3)	0.372 (5)	0.627 (6)
H(10C)	0.054 (3)	0.358 (4)	0.876 (6)
H(11A)	0.144 (3)	0.687 (5)	0.599 (6)
H(11B)	0.165 (3)	0.557 (4)	0.451 (6)
H(11C)	0.263 (3)	0.676 (5)	0.563 (6)
H(12A)	0.205 (3)	0.544 (4)	1.046 (6)
H(12B)	0.177 (3)	0.685 (5)	0.959 (6)
H(12C)	0.289 (3)	0.663 (4)	0.936 (6)

TABLE 4.8: Anistropic Thermal Parameters ($Å^2$) for the non-hydrogen[a] atoms of (n^6-$C_6H_5CO_2Me$)Cr(CO)$_2$($CNBu^t$)

Atom	U11	U22	U33	U23	U13	U12
Cr	0.0442(3)	0.0421(3)	0.0471(3)	-0.0027(2)	-0.0010(2)	0.0203(2)
C(1)	0.059 (3)	0.050 (3)	0.037 (2)	-0.004 (2)	-0.002 (2)	0.022 (2)
C(2)	0.070 (3)	0.049 (3)	0.045 (2)	-0.007 (2)	-0.004 (2)	0.023 (2)
C(3)	0.083 (4)	0.062 (3)	0.057 (3)	-0.013 (2)	-0.002 (2)	0.042 (3)
C(4)	0.063 (3)	0.084 (4)	0.060 (3)	0.000 (3)	0.014 (2)	0.040 (3)
C(5)	0.064 (3)	0.070 (3)	0.060 (3)	0.011 (2)	0.013 (2)	0.025 (3)
C(6)	0.066 (3)	0.061 (3)	0.045 (2)	0.010 (2)	0.003 (2)	0.026 (2)
C(7)	0.061 (3)	0.055 (3)	0.037 (2)	0.004 (2)	0.008 (2)	0.017 (2)
C(8)	0.061 (3)	0.088 (4)	0.071 (4)	-0.006 (3)	-0.008 (3)	0.016 (3)
C(9)	0.049 (2)	0.050 (2)	0.055 (3)	-0.009 (2)	-0.003 (2)	0.027 (2)
C(10)	0.055 (3)	0.084 (4)	0.086 (4)	-0.013 (3)	-0.001 (3)	0.021 (3)
C(11)	0.096 (4)	0.073 (4)	0.069 (3)	0.002 (3)	-0.007 (3)	0.040 (3)
C(12)	0.068 (3)	0.071 (3)	0.060 (3)	-0.015 (3)	-0.007 (3)	0.027 (3)
CO(1)	0.049 (2)	0.048 (2)	0.050 (2)	-0.009 (2)	-0.011 (2)	0.018 (2)
CO(2)	0.053 (2)	0.049 (2)	0.062 (2)	0.001 (2)	-0.001 (2)	0.021 (2)
OC(1)	0.088 (2)	0.066 (2)	0.062 (2)	0.015 (1)	-0.002 (1)	0.016 (2)
OC(2)	0.061 (2)	0.069 (2)	0.098 (3)	-0.003 (2)	-0.026 (2)	0.011 (1)
O(1)	0.056 (2)	0.065 (2)	0.066 (2)	0.001 (2)	-0.004 (2)	0.016 (2)
O(2)	0.067 (2)	0.060 (2)	0.093 (3)	0.004 (2)	-0.015 (2)	0.030 (2)
CN	0.046 (2)	0.053 (3)	0.049 (2)	0.001 (2)	-0.005 (2)	0.018 (2)
NC	0.060 (2)	0.063 (2)	0.063 (2)	-0.010 (2)	-0.002 (2)	0.036 (2)

[a] The hydrogen atoms were assigned a common isotropic temperature factor, which refined to the value of 0.0784(27)$Å^2$.

V. CATALYTIC SYNTHESIS AND CHARACTERIZATION OF ISONITRILE DERIVATIVES OF $(\eta^5C_5H_5)Mn(CO)_3$

5.1 Introduction

Direct displacement of CO in $(\eta^5C_5H_5)Mn(CO)_3$ by donor ligands L to give $(\eta^5C_5H_5)Mn(CO)_2L$ is extremely difficult to achieve by thermal means.[47] Consequently the synthetic routes presently available to synthesize $(\eta^5C_5H_5)Mn(CO)_2L$ complexes employ photochemical[47] or Me_3NO induced[48] techniques.

With isonitrile ligands (L = RNC), preparation of $(\eta^5C_5H_5)Mn(CO)_2(CNR)$ derivatives has involved photochemical methods. Irradiation of $(\eta^5C_5H_5)Mn(CO)_3$ in the presence of THF (tetrahydrofuran) or KCN yields $(\eta^5C_5H_5)Mn(CO)_2(THF)$[49] or $K^+[(\eta^5C_5H_5)Mn(CO)_2CN]^-$[52a], which on reaction with RNC[36,51] or RX(X = I, Cℓ, Br)[15b,c,52,53] *yields the desired product* $(\eta^5C_5H_5)Mn(CO)_2(CNR)$. $(\eta^5C_5H_5)Mn(CO)_2(CNBu^t)$ has also been obtained *from the photolysis of* $(\eta^5C_5H_5)Mn(CO)_2[C\,Ph_2]$ and ^tBuNC in THF solution.[51] To date, isolation of the apparently *unstable* $(\eta^5C_5H_5)Mn(CO)(CNR)_2$ derivatives has not been achieved.[36] Tri-substituted derivatives, $(\eta^5C_5H_5)Mn(CNR)_3$, *have also been reported*, and have been synthesized either by irradiation of $(\eta^5C_5H_5)Mn(CO)_3$ and RNC in THF,[35] or from $[Mn(CNC_6H_5)_6]I$ and $Na[C_5H_5]$.[54]

The complex, $(\eta^5C_5H_4Me)Mn(CO)_2(CNBu^t)$ has been catalytically synthesized by electrochemical techniques.[55] However, this reaction involves the displacement of acetonitrile (and not CO) from $(\eta^5C_5H_4Me)Mn(CO)_2(NCMe)$ by Bu^tNC, and consequently still necessitates the use of photochemical, or Me_3NO-induced techniques in the synthesis of the acetonitrile derivative. To date no thermal displacement reactions of CO on $(\eta^5C_5H_5)Mn(CO)_3$ by isonitriles have been reported.

Since PdO has been found to be an effective catalyst for the direct displacement of CO by RNC on several metal carbonyl complexes,[26,56] the thermal reaction between $(\eta^5C_5H_5)Mn(CO)_3$ and a variety of RNC ligands, with PdO as catalyst, was investigated.

5.2 Results and discussion

5.2.1 PdO catalysed reaction of $(\eta^5C_5H_5)Mn(CO)_3$ with isonitriles

PdO was found to be an effective, though not highly active catalyst for the reaction of $(\eta^5C_5H_5)Mn(CO)_3$ with isonitrile ligands (RNC), allowing for the synthesis, under moderate thermal reaction conditions, of a series of $(\eta^5C_5H_5)Mn(CO)_2(CNR)$ substituted complexes. Product yields varied from poor (MeNC) to excellent ($C_6H_{11}NC$) (*Table* 5.1). By contrast, the thermal uncatalysed reaction did not proceed under the identical experimental conditions.

Since the catalyst mixture $[(\eta^5C_5H_5)Fe(CO)_2]_2$/PdO was found to catalyse related substitution reactions between isonitriles and metal carbonyl complexes,[44] and was applied successfully to the reaction between $(\eta^6\text{Arene})Cr(CO)_3$ and RNC (*see ch II*), the catalytic potential of an iron dimer-PdO mixture was investigated for the reaction of $(\eta^5C_5H_5)Mn(CO)_3$ with ^{t}BuNC. However, it was found that the reaction rates observed either for the use of a catalyst mixture (iron dimer/PdO) or for PdO alone (equal amounts of Pd in both reactions) are the same.

The PdO-catalysed synthetic route can be extended to *related systems*. For example, the reaction between $(\eta^5C_5H_5)V(CO)_4$ and ^{t}BuNC in toluene in the presence of PdO (110°C, 4 h) yielded a yellow product identified as $(\eta^5C_5H_5)V(CO)_3(CNBu^t)$ [IR(hexane), ν(NC): 2100(w), ν(CO): 1970(s), 1904 (sh,sp), 1892 (vs) cm^{-1}] by comparison with the IR spectra of $(\eta^5C_5H_5)V(CO)_3(PR_3)$ *complexes*.[47] *The* thermal reaction in the absence of PdO (110°C, 4 h) gave only recovered starting material, $(\eta^5C_5H_5)V(CO)_4$.

5.2.2 Characterization of $(\eta^5C_5H_5)Mn(CO)_2(CNR)$ products

The isonitrile complexes $(\eta^5C_5H_5)Mn(CO)_2(CNR)$ have been fully characterized by IR and NMR spectroscopy. (Table 5.2).

(a) Infra Red

The IR spectra of $(\eta^5C_5H_5)Mn(CO)_2(CNR)$ complexes are *expected to show two* ν(CO) and one ν(NC) stretching vibration.

This has been observed previously for RNC = MeNC[33] and CNCOPh[14b,c], and was also observed for the complexes with RNC = $C_6H_5CH_2NC$, 2,6-$Me_2C_6H_3NC$, and MeNC prepared in this study. However, for RNC = Bu^tNC and $C_6H_{11}NC$, two ν(NC) (and two ν(CO)) vibrations were observed in both the solid state and solution. This phenomenon of observing more IR active ν(NC) bands than expected has also been detected in a series of $(\eta^6\text{Arene})Cr(CO)_2(CNBu^t)$ complexes (see ch II), and will be discussed in ch VIII.

(b) Proton Nuclear Magnetic Resonance

The ^1H NMR spectra of the $(\eta^5C_5H_5)Mn(CO)_2(CNR)$ complexes (Table 5.2) are as expected, and show no unusual features.

(c) Mass spectrum of $(\eta^5C_5H_5)Mn(CO)_2(CNBu^t)$

The fragmentation pattern of the complex $(\eta^5C_5H_5)Mn(CO)_2(CNBu^t)$ is shown in Fig. 5.1, together with peak intensities. Loss of the CO ligands precedes loss of the $CNBu^t$, and the Bu^t fragment is lost before the CN linkage.[37] The cyclopentadienyl ring is lost last. Such a fragmentation pattern is typical of half-sandwich metal carbonyl complexes, and has been observed for other $(\eta^5C_5H_5)Mn(CO)_2(CNR)$ complexes.[38]

5.3 Experimental-preparation of $(\eta^5C_5H_5)Mn(CO)_2(CNR)$, (R = Bu^t, $C_6H_5CH_2$, C_6H_{11}, $C_6H_3Me_2$-2,6,Me)

$(\eta^5C_5H_5)Mn(CO)_3$ (2 mmol) and PdO (30 mg) were added to toluene (10 mℓ) and the solution heated to reflux (110°C). The appropriate RNC (5 mmol) was then added to the reaction vessel, and the reaction monitored by TLC (Silica; eluent: hexane, or hexane/$CH_2Cℓ_2$ (10%)). The reaction was allowed to proceed for 6 h (except in the case R = Me, where the reaction time was 24 h), after which heating was stopped and the product isolated by column chromatography. (Silica, 2cm x 40 cm column). Gradient elution, starting with hexane (to remove unreacted starting material) and gradually increasing the proportion of $CH_2Cℓ_2$ to 50% in a $CH_2Cℓ_2$/hexane mixture, was employed. Recrystallization from $CH_2Cℓ_2$/hexane gave the desired products as yellow solids (Table 5.1).

TABLE 5.1: Analytical data for the $(\eta^5C_5H_5)Mn(CO)_2(CNR)$ complexes

Complex	Isolated yield(%)[a]	M.p.(°C)	Elemental Analysis (Found Calcd.)(%)		
			C	H	N
$(\eta^5C_5H_5)Mn(CO)_2(CNBu^t)$	60	95-96	55.6(56.0)	5.4(5.5)	5.4(5.4)
$(\eta^5C_5H_5)Mn(CO)_2(CNCH_2C_6H_5)$	70	51-52	61.4(61.4)	4.2(4.1)	4.8(4.8)
$(\eta^5C_5H_5)Mn(CO)_2(CNC_6H_{11})$	95	68-69	58.7(58.9)	5.7(5.7)	4.9(4.9)
$(\eta^5C_5H_5)Mn(CO)_2(CNC_6H_3Me_2\text{-}2,6)$	15	79-80	61.1(62.5)	4.6(4.6)	4.3(4.6)
$(\eta^5C_5H_5)Mn(CO)_2(CNMe)$	5[b]	90-93	49.1(49.8)	3.9(3.7)	5.9(6.5)

[a] After 6 h .

[b] After 24 h.

TABLE 5.2: Spectroscopic data for the $(\eta^5C_5H_5)Mn(CO)_2(CNR)$ complexes

Complex	IR (cm^{-1})[a]		^1H NMR (ppm)[b]		
	ν(NC)	ν(CO)	C_5H_5	C_6H_n	CH_n
$(\eta^5C_5H_5)Mn(CO)_2(CNBu^t)$	2114, 2078	1952, 1907[c]	4.25	–	0.94
$(\eta^5C_5H_5)Mn(CO)_2(CNCH_2C_6H_5)$	2112	1957, 1911	4.23	7.01, 6.99	3.92
$(\eta^5C_5H_5)Mn(CO)_2(CNC_6H_{11})$	2104, 2070(sh)[d]	1954, 1907	4.27	1.29, 1.02	–
$(\eta^5C_5H_5)Mn(CO)_2(CNC_6H_3Me_2\text{-}2,6)$	2080	1954, 1916	4.27	6.71	2.14
$(\eta^5C_5H_5)Mn(CO)_2(CNMe)$	2130	1958, 1907	4.22	–	2.12

[a] Recorded in hexane

[b] Recorded in C_6D_6 relative to TMS.

[c] KBr, ν(NC) 2118, 2072(sh), ν(CO) 1971, 1926 cm^{-1}

[d] sh = shoulder

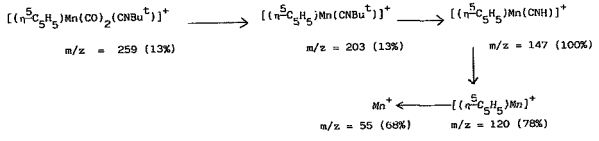


Figure 5.1 Fragmentation pattern for $(\eta^5C_5H_5)Mn(CO)_2(CNBu^t)$

VI. THE MODIFICATION OF $(\eta^5C_5H_5)Mn(CO)_3$ BY LIGANDS L

6.1 Introduction

Considerable interest has been focussed on the half-sandwich *metal carbonyl complex*, $(\eta^5C_5H_5)Mn(CO)_3$, owing to the exceptional stabilizing capacity of $(\eta^5C_5H_5)Mn(CO)_2$ moeity.[47] *This has been explcited in the capture and display of* ligands L. Complexes of the type $(\eta^5C_5H_5)Mn(CO)_2L$ have been detected, isolated and unequivocally characterized, by techniques including X-ray crystallography, for a wide range of exotic and unstable ligands L.

Some twenty $(\eta^5C_5H_5)Mn(CO)_2L$ complexes have been studied by X-ray crystallography.[61-84] In most cases, the $(\eta^5C_5H_5)Mn(CO)_2$ moeity has been used to anchor and display the ligand L, often a carbene, L itself being of prime concern in the structural study, and the geometry around the Mn-atom itself of secondary interest.

However, the substitution in $(\eta^5C_5H_5)Mn(CO)_3$ of a CO for a ligand L, can result in structural modifications in the resulting $(\eta^5C_5H_5)Mn(CO)_2L$ complex, compared to the parent carbonyl, $(\eta^5C_5H_5)Mn(CO)_3$. The structure of $(\eta^5C_5H_5)Mn(CO)_3$ will be discussed in detail, and the structural effect of ligand substitution examined by considering the $(\eta^5C_5H_5)Mn(CO)_2L$ complexes for which X-ray crystal and molecular structures have been reported. Structural trends, and notable exceptions, *will be rationalized in terms of* electronic and steric factors.

6.2 The Structure of $(\eta^5C_5H_5)Mn(CO)_3$

The crystal and molecular structure of $(\eta^5C_5H_5)Mn(CO)_3$ was first determined by Berndt and Marsh in 1963.[59a] *(R value* of 9%), and in 1981 redetermined by Fitzpatrick, le Page, Sedman and Butler[59b]. *(R value of 2.86%), improving the* accuracy of bond parameter data.

6.2.1 Ligand geometry and conformation

The molecule has the typical "piano-stool" geometry, with the OC-Mn-CO angles being equal within experimental error (av. 92.02(9)°[59b]).

6.2.2 Conformation

The (C_5H_5) ring-$(CO)_3$ tripod conformation is shown in Fig. 6.1. Two ring C-atoms (C3 and C5) are eclipsed by two carbonyls (C12 and C13 respectively), while the third CO ligand (C11) eclipses the C1-C2 bond of the ring. The deviations from the fully eclipsed structure destroy possible mirror (m) symmetry of the $(\eta^5C_5H_5)Mn(CO)_3$ molecule.[55b]

6.2.3 Mn-C-ring and Mn-CO bond lengths

The av. values for the Mn-C-ring and Mn-CO bond lengths are 2.124(2) and 1.780(2)Å respectively. The distance between the Mn atom and the centre of gravity of the cyclopentadiene ring, Mn-Cp, is 1.766Å.[55b]

6.2.4 Ring planarity and C-C bond lengths

The (C_5H_5) ring is essentially planar. A notable feature of the (C_5H_5) ring is the non-equivalence of the C-C bonds (see Fig 6.2). This breakdown of the 5-fold ring symmetry in the crystal is indicative of some degree of C-C bond localization. There does not appear to be a correlation between the ring C-C bond lengths and the ring-tripod ligand arrangement, as found for $(\eta^5C_6H_6)Cr(CO)_3$ (see section 3.2.4.)

6.2.5 Mn-C-O bond angles

The av. Mn-C-O bond angle is 178.9(2)°.[55b] Near linearity of M-C-O bonds is predicted for $M(CO)_n$ (n = 2,3) groups.[39] (see section 3.2.6)

6.2.6 Packing considerations

The compound crystallizes in the monoclinic centrosymmetric space group $P2_1/a$, with Z = 4. In general the packing is rather loose,[55] with the shortest non-hydrogen intermolecular contact involving the cyclopentadienyl ring being 3.407Å.[55b]

However, the orientation of the ring with respect to the carbonyl groups is probably determined largely by crystal packing forces, since the intrinsic electronic barrier to rotation of the ring about the molecular axis

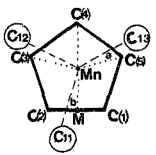


Figure 6.1 Conformation of $(\eta^5-C_5H_5)Mn(CO)_3$, looking down onto the (C_5H_5) ring. (CO C-atoms are circled; M is the mid-point of the C(1)-C(2) bond.) Angles of eclipse, a and b are 7.25 and 5.93° respectively.[3,9b]

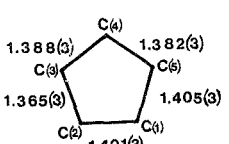


Figure 6.2 Ring C-C bond lengths (Å) in $(\eta^5-C_5H_5)Mn(CO)_3$.[3,9b]

in $(\eta^5C_5H_5)Mn(CO)_3$ is estimated to be very small (ca. 0.008 kJ mol^{-1}).[18] Potential energy calculations[19] have shown that the barrier to ring rotation *in the solid phase* of 7.24 kJ mol^{-1} is due to non-bonded intermolecular C...H and O...H interactions. (eg. O...H distances of 2.48 to 3.08Å).[19a]

Crystal packing forces could also be responsible for minor deviations from ideal geometry observed.

6.3 X-ray Crystallographic Studies of $(\eta^5C_5H_5)Mn(CO)_2L$ complexes

The $(\eta^5C_5H_5)Mn(CO)_2L$ complexes for which X-ray crystal and molecular structures have been reported in the literature are listed in Table 6.1. The principal geometric characteristics of the $(\eta^5C_5H_5)Mn(CO)_2L$ structures are given in Table 6.2. Trends and special features will be discussed.

6.3.1. OC-Mn-CO and OC-Mn-L angles

Although the $(\eta^5C_5H_5)Mn(CO)_2L$ complexes all adopt the "piano-stool" arrangement of ligands, in general the av. OC-Mn-L angle is greater than the OC-Mn-CO angle. The reverse is expected if L is a better π-acceptor than CO.[44] However, in most cases L is a vinylidene, carbene or η^2 olefinic ligand.

Since PR_3 is a *poorer π-acceptor than* CO,[19a] the smaller av. CO-Mn-P (91.6(3)°) than OC-Mn-CO (92.4(4)°) angle seems anomalous. However, the CO-Mn-P angles are *92.7(3) and* 90.5(3)°.[42] The difference could be due to steric repulsions between the bulky PPh_3 group (Tolman cone angle 145°)[83] or crystal packing forces. Hence caution must be exercized in interpreting small bond parameter deviations in terms of electronic effects.

6.3.2 Molecular Conformation

In $(\eta^5C_5H_5)Mn(CO)_3$, one CO ligand eclipses a C-C bond of the (C_5H_5) ring, while the other two carbonyls eclipse ring C-atoms. For $(\eta^5C_5H_5)Mn(CO)_2L$, the ligand L may eclipse a C-C bond or a C-atom of the (C_5H_5) ring. In the cases L = SO_2,[61] PPh_3,[62] $N_2C(CO_2Me)_2$,[64] $\eta^2C_5H_6$,[54] L eclipses a ring C-atom, but for all the

other structures of Table 6.1 (excluding $(\eta^5C_5H_5)Mn(CO)_2$-[PPh_2(OC(Me)(CHC(O)Me)]], where the (C_5H_5) ring is disordered[42]), L eclipses a ring C-C bond. Hence it appears that in general with vinylidene, carbene and η^2-olefinic ligands L, L eclipses a ring C-C bond, and with ligands such as L = PPh_3, L eclipses a ring C-atom. Note also that in $(\eta^5C_5H_5)Mn(CO)(PPh_3)_2$,[16] both PPh_3 ligands, and the CO, near-eclipse ring C-atoms. This phenomenon could possibly have an electronic basis. MO calculation of $(\eta^5C_5H_5)Mn(CO)_2L$ complexes for different ligand types L, might provide information on the electronically most favourable conformation. However, crystal packing forces probably also play a role in determining molecular conformation, especially as the barrier to rotation in complexes of the type $(\eta^5C_5H_5)Mn(CO)_2L$ is predicted to be small.[18]

6.3.3. Mn-C-ring and Mn-CO bond lengths

For the $(\eta^5C_5H_5)Mn(CO)_2L$ structures, the Mn-C-ring bond distances are generally in the range 2.12 to 2.18Å, cf. av. Mn-C-ring of 2.124(2)Å for $(\eta^5C_5H_5)Mn(CO)_3$.[39b] A notable exception is L = SO_2[41] (av. Mn-C-ring 2.090(2)Å). Possibly this could reflect a weaker bonding of the SO_2 ligand to Mn, compensated for by increased Mn-Ring bonding. A weaker bonding of the SO_2 ligand could possibly account for the reported instability of the $(\eta^5C_5H_5)Mn(CO)_2(SO)_2$ complex,[41] which has also been ascribed to steric crowding of the SO_2 and CO ligands.[41]

The Mn-CO bond lengths are generally 1.74 to 1.80Å, comparable to the av. Mn-CO bond length of 1.780(2)Å for the parent complex, $(\eta^5C_5H_5)Mn(CO)_3$.[39b] For ligands such as PPh_3, which is a weaker π-acceptor than CO,[45a] a decrease in Mn-CO bond length relative to $(\eta^5C_5H_5)Mn(CO)_3$ would be expected. This is indeed observed (av. Mn-CO bond lengths of 1.75(2)Å and 1.780(2)Å respectively for $(\eta^5C_5H_5)Mn(CO)_2$-(PPh_3)[42] and $(\eta^5C_5H_5)Mn(CO)_3$[39b]). Further, the Mn-CO bond length in $(\eta^5C_5H_5)Mn(CO)(PPh_3)_2$ is 1.748(9)Å.[16]

6.3.4 Ring C-C bond lengths

The ring C-C bond lengths for the $(\eta^5C_5H_5)Mn(CO)_2L$

TABLE 6.1: X-ray Crystal Structures of $(\eta^5C_5H_5)Mn(CO)_2L$ complexes

Complex	Space Group Z	Reference
$(\eta^5C_5H_5)Mn(CO)_3$	$P2_1/a$, 4	59
$(\eta^5C_5H_5)Mn(CO)_2(SO)_2$	$P2_1/c$, 4	61
$(\eta^5C_5H_5)Mn(CO)_2(PPh_3)$	$P\bar{1}$, 2	62
$(\eta^5C_5H_5)Mn(CO)_2[PPh_2(OC(Me)(CHC(O)Me))]$	$P\bar{1}$, 2	63
$(\eta^5C_5H_5)Mn(CO)_2(PhP(OC(CH_2)CHC(Me)O))$[a]	$P2_1/c$, 4	64
$(\eta^5C_5H_5)Mn(CO)_2(C(O)Ph)]^-[NMe_4]^+$	Tb2a, 16[b]	65
$(\eta^5C_5H_5)Mn(CO)_2[N_2C(CO_2Me)_2]$	$P2_1/n$, 4	66
$(\eta^5C_5H_5)Mn(CO)_2[SC(C_6H_6(Me_2)_2\text{-}2,6)]$	$P2_1/n$, 4	67
$(\eta^5C_5H_5)Mn(CO)_2[C_2C(C_6H_{11})_2]$	$P2_1/c$, 4	68
$(\eta^5C_5H_5)Mn(CO)_2(CCMe_2)$	Pnma, 4[c]	69
$(\eta^5C_5H_5)Mn(CO)_2(CCNPh)$	Pccn, 8	70
$(\eta^5C_5H_5)Mn(CO)_2(CMe_2)$	$Cmc2_1$, 8[c,d]	71
$(\eta^5C_5H_5)Mn(CO)_2(CPh_2)$	[e]	37[f]
$(\eta^5C_5H_5)Mn(CO)_2(CFPh)$	$P2_1/c$, 4	72
$(\eta^5C_5H_5)Mn(CO)_2[C(OEt)Ph]$	$P2_1/c$, 4	73
$(\eta^5C_5H_5)Mn(CO)_2[CFh(C(O)Ph)]$[g]	$P2_1/n$, 4	74
$(\eta^5C_5H_5)Mn(CO)_2[C(OMe)(C_6H_8(CHMe_2)(Me)\text{-}2,5)]$	$P2_1$, 2	75
$(\eta^5C_5H_5)Mn(CO)_2(C(CO_2Me)CHPPh_3)$	$P2_1/a$, 4	76
$[(\eta^5C_5H_5)Mn(CO)_2(CPh)]_2O$	$P2_1/c$, 4	77
$(\eta^5C_5H_5)Mn(CO)_2[\eta^2C(O)CPh_2]$	$P2_1/c$, 4	78
$(\eta^5C_5H_5)Mn(CO)_2[\eta^2CH_2CHC(O)Me]$	$P2_12_12_1$, 4	79
$(\eta^5C_5H_5)Mn(CO)_2[\eta^2CH_2CPhCO_2Me]$	$P2_1/a$, 8[b]	80
$(\eta^5C_5H_5)Mn(CO)_2[\eta^2CHPhCHP(O)(OEt)_2]$	$P\bar{1}$, 4[b]	81
$(\eta^5C_5H_5)Mn(CO)_2(\eta^2C_6H_8)$	$P2_1/c$, 4	82
$(\eta^5C_5H_5)Mn(CO)_2(\eta^2C_7H_8)$	$P2_1/m$, 2[c]	83a
	Pnma, 4[c]	83b[h]
$[(\eta^5C_5H_5)Mn(CO)_2]_2(C_5H_6)$	$P2_1/c$, 4	84

a *Dienediolate group disordered*
b 2 crystallographically independent molecules in the asymmetric unit
c Molecule possesses crystallographic m symmetry
d 2 crystallographically independent half-molecules in the asymmetric unit
e Unpublished structure
f Ref. 41 therein
g *No co-ordinates, or* bond data pertaining to Table 6.2. available
h Redetermined structure

TABLE 6.2 Principal geometric characteristics (bond lengths (Å), bond angles (°) of $(\eta^5-C_5H_5)Mn(CO)_2L$ complexes

L	Mn-C-ring[a]	Mn-CO	C-C(ring)[a]	Mn-C-O	OC-Mn-CO	OC-Mn-L
CO[b]	2.124(2)	1.780(2)[a]	1.388(3)	178.9(2)[a]	92.02(9)[a]	-
SO_2	2.09 (2)	1.75 (2)[a]	1.36 (3)	178 (1)[a]	90.6 (6)	92.9(5)[a]
PPh_3	2.15 (1)	1.75 (2)[a]	1.42 (2)	178 (1)[a]	92.4 (4)	91.6(3)[a]
$PPh_2(OC(Me)(CHC(O)Me))$	2.18 (1)[c]	1.77 (1)[a]	1.54 [c,d]	177.2 [a,d]	92.8 [d]	94.3 [a,d]
$PhP(OC(CH_2)CHC(Me)O)^-$	[e]	1.77 [a]	[e]	[e]	[e]	[e]
$(C(O)Ph)^-$	2.17 (4)	1.78 (3)[a]	1.39 (8)	174(3)[a]	90 (1)[a]	88 (1)[a]
$N_2C(CO_2Me)_2$	2.139(7)	1.797(7)[a]	1.39 (1)	179.6 [a,d]	90.3(3)	94.8(3)[a]
$SC(C_6H_6(Me_2)_2-2,6)$	2.143(4)	1.777(3)[a]	1.385 [d]	180.7 [a,d]	89.1(1)	94.1(1)[a]
$C_2C(C_6H_{11})_2$	2.12 (1)	1.767(7)[a]	1.35 (2)	179.1(6)[a]	87.9(3)	90.9(3)[a]
$CCMe_2$	2.13 (2)	1.74 (1)	1.38 (2)[f]	178 (1)	87.7(7)	91.5(6)
CCHPh	2.16 (2)	1.80 (3)[a]	1.43 (3)	178 (2)[a]	89 (1)	92 (1)[a]
CMe_2	2.187(7)	1.793(5)[a]	1.417(9)	179.3 [a,d]	88.8(2)[e]	90.6(3)[a]
CFPh	2.148(7)	1.790(6)[a]	1.396 [d]	180.0 [a,d]	90.8(3)	91.9(3)[a]
C(OEt)Ph	2.17 (1)	1.80 (2)[a]	.42 (2)	176 (1)[a]	91.1(7)	34.1(7)[a]
$C(OMe)(C_6H_8(CHMe_2)(Me)-2,5$	2.15 (2)	1.80 (2)[a]	1.407 [d]	175.7 [a,d]	89.0(8)	9?.4(8)[a]
$C(CO_2Me)CHPPh_3$	2.158(5)	1.770(4)[a]	1.418(5)	177.5(3)[a]	91.7(2)	90.6(1)[a,g]
C(Ph)O- [h]	2.16 (2)	1.78 (2)[a]	1.411 [d]	178.6 [a,d]	89.2(9)[a]	95.4(9)[a]
$\eta^2C(O)CPh_2$	[e]	1.77 [a]	1.36	[e]	[e]	e,i

TABLE 6.2 (cont)

L	Mn-C ring[a]	Mn-CO	C-C(ring)[a]	Mn-C-O	OC-Mn-OC	OC-Mn-L
η^2-$CH_2CHC(O)Me$	2.137(8)	1.787(7)[a]	1.39(1)	177.1(6)[a]	88.6(4)	96.5(4)[a,j]
η^2-CH_2CPhCO_2Me	2.166 [c]	1.766 [a,d]	1.443 [d]	177.2 [a,d]	90.5 [a,d]	81,[d,k] 106[d,l]
η^2-$CHPhCHP(O)(OEt)_2$	2.121(8)	1.770(7)[a]	1.35(1)	176.9(6)[a]	87.6 [a,d]	95.7(2)[a,j]
η^2-C_8H_8	2.156(2)	1.787(2)[a]	1.410 [d]	178.7(2)[a]	88.8(1)	93.4 [a,j]
η^2-C_7H_8 [m]	*2.131(3)*	*1.773(2)*	*1.364(5)*	*178.1(2)*	*91.4(5)*	*95.1(5)*[j]
η^2-C_5H_6 [n]	2.143(9)	1.769(9)[a]	1.40(1)[a]	177.2(7)[a]	89.5(4)[a]	84,[d,k] 110[d,l]

a Average value
b Ref 59b
c Disordered C_5H_5 ring; bond lengths from highest occupancy (75%) atomic positions
d Bond data obtained from the Cambridge Crystallographic Data Base
e Bond data not available
f Ring C-C bonds not equal (C(2)-C(3): *1.34(2)*, C(3)-C(4): *1.45(2)*, *C(4)-C(4')*: *1.28(2)*Å)[69]
g OC-Mn-C (carbene) angles not equal (values: 85.5(1) and 95.7(1)°)[76]
h $[(\eta^5-C_5H_5)Mn(CO)_2C(Ph)]_2O$, av. values for two Mn fragments quoted.
i Two co-ordinated η^2-olefinic C-atoms not equidistant from Mn-atom (1.96(2) and 2.17(2)Å)[78]
j OC-Mn-A, A = midpoint of η^2 C-C double bond
k av. value of OC-Mn-C for CO and nearer η^2-C-atom
l av. value of OC-Mn-C for CO and farther η^2-C-atom
m Ref 83(b)
n $[(\eta^5-C_5H_5)Mn(CO)_2]_2(C_5H_6)$, av. values for the two Mn fragments quoted.

complexes are generally in the range 1.35 to 1.43Å, cf. av. value of 1.388(3)Å for $(\eta^5C_5H_5)Mn(CO)_3$.[59b] With one exception, the C-C bond lengths within one structure are all equal within experimental error. The exception, $(\eta^5C_5H_5)Mn(CO)_2(CCMe_2)$,[63] has an alternating pattern of C-C bond lengths (Fig. 6.3), indicative of some degree of C-C bond localization. The pattern is not, however, similar to that observed for $(\eta^5C_5H_5)Mn(CO)_3$, which also has non-equivalent ring C-C bonds (see Fig. 6.2). It is interesting, and perhaps significant, to note that the shortest C-C bond (C4-C4') in $(\eta^5C_5H_5)Mn(CO)_2(CCMe_2)$ corresponds to the C-C bond eclipsed by the vinylidene ligand. The non-equivalent ring C-C bond lengths could, however, be indicative of some unresolved disorder of the C_5-ring. A 25% C_5-ring disorder was observed for $(\eta^5C_5H_5)Mn(CO)_2[PPh_2(OC(Me)-(CHC(O)Me))]$.[53]

6.3.5 Mn-C-O bond angles

The Mn-C-O bond angles are in the range 174-179°, as expected.[19]

6.3.6 Packing, and Steric Factors

Crystal packing forces are probably responsible for (i) The overall conformation of the ligand tripod with respect to the cyclopentadienyl ring, although the electronic nature of the ligand L could govern whether L eclipses a ring C-atom or a ring C-C bond.

(ii) Angular deviations which destroy possible m molecular symmetry. For L = $CCMe_2$,[69] CMe_2,[11] $\eta^2C_7H_8$,[53] crystallographic m molecular symmetry is observed.

(iii) Small distortions and deviations from ideal geometry.

Steric factors could account for anomalous bond angle and bond length data. For example, for $(\eta^5C_5H_5)Mn(CO)_2[C(CO_2Me)CHPPh_3]$,[74] the OC-Mn-C carbene bond angles are 85.5(1) and 95.7(1)°, for CO(1) and CO(2) respectively cf. the ideal value of 90°, due to the bulky CO_2Me substituent directed towards the CO(2) ligand.

In the complex $(\eta^5C_5H_5)Mn(CO)_2[\eta^2C(O)CPh_2]$,[78]

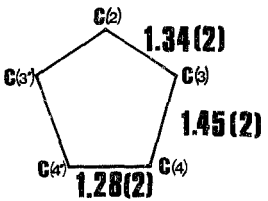


Figure 6.3 Ring C-C bond lengths (Å)[12] in $(\eta^5C_5H_5)Mn(CO)_2(COMe)$. (Atoms C(3) and C(4) are related to C(3') and C(4') by a crystallographic mirror plane through C(2) and the midpoint of the C(4)-C(4') bond.)

the two co-ordinated η^2-olefinic C-atoms (C1 and C2) are not equidistant from the Mn-atom (2.17(2) and 1.96(2)Å respectively), possibly due to steric interactions between the phenyl rings on C1 and the carbonyl groups. Further, the Mn-CO bond lengths differ (1.73 and 1.81Å).

6.4 Conclusion

The overall geometry of the $(\eta^5C_5H_5)Mn(CO)_2L$ complexes is similar to that of $(\eta^5C_5H_5)Mn(CO)_3$. Observed bond angle and bond length trends can be rationalized in electronic terms, and anomalies explained by the influence of steric factors and/or crystal packing forces.

VII. THE CRYSTAL AND MOLECULAR STRUCTURE OF $(\eta^5C_5H_5)Mn(CO)_2(CNBu^t)$

7.1 Introduction

An X-ray crystal study of $(\eta^5C_5H_5)Mn(CO)_2(CNBu^t)$, was undertaken as part of an investigation into the anomalous IR spectra exhibited by certain complexes of this type. It was hoped that the X-ray study of $(\eta^5C_5H_5)Mn(CO)_2(CNBu^t)$, in conjunction with that of $(\eta^5C_6H_5CO_2Me)Cr(CO)_2(CNBu^t)$ (ch.IV), might provide a structural explanation of the anomalous IR data of these complexes. This aspect will be discussed in ch. VIII.

$(\eta^5C_5H_5)Mn(CO)_2(CNBu^t)$ crystallizes in the orthohombric *non-centrosymmetric space group* $Pna2_1$, with four molecules in the unit cell. Fig. 7.2 shows a view of the unit cell, looking down the b-axis. The molecule is shown in Fig. 7.1, together with the numbering system used in the analysis.

Bond lengths and bond angles, and bond parameters involving hydrogen atoms are given in Tables 7.1, 7.2 and 7.3 respectively. Table 7.4 lists the deviations (Å) of the atoms from the mean plane through the cyclopentadienyl ring C-atoms (C(1)-C(5)).

7.2 Discussion of the Structure of $(\eta^5C_5H_5)Mn(CO)_2(CNBu^t)$

The structure of $(\eta^5C_5H_5)Mn(CO)_2(CNBu^t)$ will be discussed in terms of the structural features analysed for the related $(\eta^5C_5H_5)Mn(CO)_2L$ complexes (Table 6.2). The principal geometric characteristics of $(\eta^5C_5H_5)Mn(CO)_2(CNBu^t)$ are summarized in Table 7.5.

7.2.1 CO-Mn-CO and OC-Mn-CN angles

The complex has the "piano-stool" arrangement of ligands, with the C-Mn-C angles all close to 90°. The CO-Mn-CO angle is slightly smaller than the CO-Mn-CN angles, as expected[48] since $CNBu^t$ is a poorer π-acceptor than CO.[49] However, the difference (of 1°) is too slight to be significant.

7.2.2 Molecular conformation

In $(\eta^5C_5H_5)Mn(CO)_2(CNBu^t)$, the $CNBu^t$ ligand essentially eclipses a ring C-C bond (in projection, angle of eclipse C(4)-Mn-C(6) is 13.7°), but the disorder in the C5-ring (vide

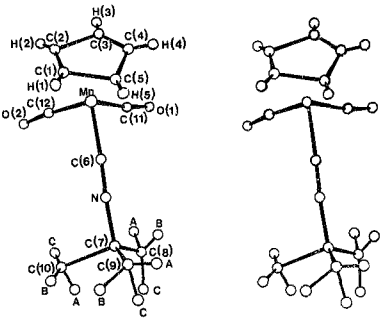


Figure 7.1. ORTEP[3] view of the $(\eta^5-C_5H_5)Mn(CO)_2(CNBu^t)$ molecule, showing the numbering system

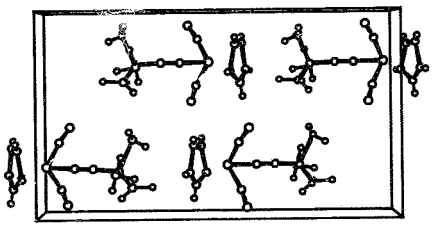


Figure 7.2: ORTEP[45] view of the unit cell of $(\eta^5C_5H_5)Mn(CO)_2(CNBu^t)$, looking down the b-axis

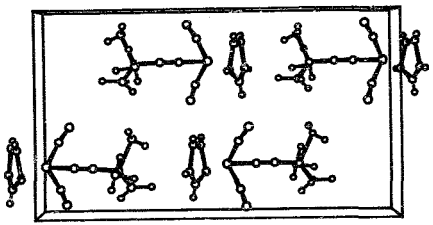


Figure 7.2: ORTEP[12] view of the unit cell of $(\eta^5-C_5H_5)Mn(CO)_2(CNBu^t)$, looking down the b-axis

TABLE 7.1 Bond lengths (Å) for (η^5-C_5H_5)Mn(CO)$_2$(CNBu^t)

Mn-C(1)	2.10(3)	C(1)-C(2)	1.55(5)
Mn-C(2)	2.09(2)	C(2)-C(3)	1.23(4)
Mn-C(3)	2.12(4)	C(3)-C(4)	1.39(5)
Mn-C(4)	2.17(2)	C(4)-C(5)	1.49(4)
Mn-C(5)	2.20(3)	C(5)-C(1)	1.27(5)
Mn-C(11)	1.82(3)	C(11)-O(1)	1.13(4)
Mn-C(12)	1.72(4)	C(12)-O(2)	1.20(5)
Mn-C(6)	1.85(2)	C(6)-N	1.17(2)
N-C(7)	1.48(2)	C(7)-C(9)	1.82(4)
C(7)-C(8)	1.30(5)	C(7)-C(10)	1.45(3)

TABLE 7.2 Bond angles (°) for (η^5-C_5H_5)Mn(CO)$_2$(CNBu^t)

C(2)-Mn-C(1)	43(1)	C(9)-C(7)-C(8)	107(2)
C(3)-Mn-C(1)	63(1)	C(10)-C(7)-C(8)	120(3)
C(3)-Mn-C(2)	34(1)	C(10)-C(7)-C(9)	110(2)
C(4)-Mn-C(1)	65(1)	C(11)-Mn-C(1)	137(2)
C(4)-Mn-C(2)	64(1)	C(11)-Mn-C(2)	98(1)
C(4)-Mn-C(3)	38(1)	C(11)-Mn-C(3)	96(2)
C(5)-Mn-C(1)	34(1)	C(11)-Mn-C(4)	122(1)
C(5)-Mn-C(2)	63(1)	C(11)-Mn-C(5)	158(1)
C(5)-Mn-C(3)	61(1)	C(12)-Mn-C(1)	90(2)
C(5)-Mn-C(4)	40(1)	C(12)-Mn-C(2)	113(2)
C(6)-Mn-C(1)	133(2)	C(12)-Mn-C(3)	147(2)
C(6)-Mn-C(2)	153(1)	C(12)-Mn-C(4)	147(1)
C(6)-Mn-C(3)	119(2)	C(12)-Mn-C(5)	107(1)
C(6)-Mn-C(4)	90(1)	C(2)-C(1)-Mn	68(2)
C(6)-Mn-C(5)	101(1)	C(5)-C(1)-Mn	77(2)
C(2)-C(1)-C(5)	105(3)	C(1)-C(2)-Mn	69(2)
C(1)-C(2)-C(3)	105(4)	C(3)-C(2)-Mn	75(2)
C(2)-C(3)-C(4)	118(4)	C(2)-C(3)-Mn	72(2)
C(3)-C(4)-C(5)	99(3)	C(4)-C(3)-Mn	73(2)
C(4)-C(5)-C(1)	112(3)	C(3)-C(4)-Mn	69(2)
C(8)-C(7)-N	108(3)	C(5)-C(4)-Mn	71(2)
C(9)-C(7)-N	101(3)	C(4)-C(5)-Mn	59(2)
C(10)-C(7)-N	109(2)	C(1)-C(5)-Mn	69(2)

TABLE 7.2 (cont.)

O(1)-C(11)-Mn	173(3)	C(11)-Mn-C(6)	91(2)
O(2)-C(12)-Mn	173(3)	C(12)-Mn-C(6)	93(2)
N-C(6)-Mn	177(2)	C(12)-Mn-C(11)	91(1)
C(7)-N-C(6)	172(2)		

TABLE 7.3 Bond parameters involving hydrogen atoms for $(\eta^5C_5H_5)Mn(CO)_2(CNBu^t)$

(a) Bond angles involving hydrogen atoms (°)

H(1)-C(1)-Mn	93(10)	H(1)-C(1)-C(2)	95(11)
H(2)-C(2)-Mn	110(10)	H(1)-C(1)-C(5)	151(13)
H(3)-C(3)-Mn	139(11)	H(2)-C(2)-C(1)	112(11)
H(4)-C(4)-Mn	138(7)	H(2)-C(2)-C(3)	143(11)
H(5)-C(5)-Mn	137(7)	H(3)-C(3)-C(2)	129(13)
H(8A)-C(8)-C(7)	102(17)	H(3)-C(3)-C(4)	110(12)
H(8B)-C(8)-C(7)	101(16)	H(4)-C(4)-C(3)	147(7)
H(8C)-C(8)-C(7)	119(10)	H(4)-C(4)-C(5)	108(7)
H(8A)-C(8)-H(8B)	137(23)	H(5)-C(5)-C(4)	94(7)
H(8B)-C(8)-H(8C)	84(21)	H(5)-C(5)-C(1)	151(7)
H(8C)-C(8)-H(8A)	115(18)	H(10A)-C(10)-C(7)	122(9)
H(9A)-C(9)-C(7)	87(21)	H(10B)-C(10)-C(7)	108(11)
H(9B)-C(9)-C(7)	106(13)	H(10C)-C(10)-C(7)	121(13)
H(9C)-C(9)-C(7)	94(9)	H(10A)-C(10)-H(10B)	78(13)
H(9A)-C(9)-H(9B)	107(25)	H(10B)-C(10)-H(10C)	83(15)
H(9B)-C(9)-H(9C)	155(17)	H(10C)-C(10)-H(10A)	117(15)
H(9C)-C(9)-H(9A)	89(19)		

(b) Bond lengths involving hydrogen atoms (Å)

C(1)-H(1)	0.9(1)	C(8)-H(8C)	1.3(2)
C(2)-H(2)	0.7(1)	C(9)-H(9A)	0.8(3)
C(3)-H(3)	0.8(1)	C(9)-H(9B)	1.0(3)
C(4)-H(4)	1.0(1)	C(9)-H(9C)	1.1(2)
C(5)-H(5)	1.1(1)	C(10)-H(10A)	1.2(2)
C(8)-H(8A)	1.0(3)	C(10)-H(10B)	1.0(2)
C(8)-H(8B)	0.8(2)	C(10)-H(10C)	0.9(2)

TABLE 7.4 Deviations (Å) of atoms from the plane defined by the 5 C-atoms (C(1)-C(5)) of the cyclopentadienyl ring[a] of $(\pi\text{-}C_5H_5)Mn(CO)_2(CNBu^t)$

Atom	Deviation from Plane (Å)
Mn	-1.7789
N	-3.5564
O(1)	-3.3044
O(2)	-3.4878
C(1)	-0.0340
C(2)	-0.0102
C(3)	0.0451
C(4)	-0.0565
C(5)	0.0557
H(1)	-0.3396
H(2)	-0.0876
H(3)	0.2305
H(4)	0.1922
H(5)	0.4329
C(6)	-2.8395
C(7)	-4.6073
C(8)	-5.4712
H(6A)	-6.3209
H(6B)	-4.9481
H(6C)	-5.8411
C(9)	-5.4473
H(9A)	-5.9892
H(9B)	-5.7743
H(9C)	-4.8344
C(10)	-3.9937
H(10A)	-3.9949
H(10B)	-4.7604
H(10C)	-3.6776
C(11)	-2.8159
C(12)	-2.7204

[a] Equation of the plane defined by atoms C(1)-C(5):
(17.7778)x + (-2.2175)y + (-0.0794)z = 8.6923

TABLE 7.5 Principal geometric characteristics (distances, Å, angles, °) of $(\eta^5C_5H_5)Mn(CO)_2(CNBu^t)$

Mn-Cp [a]	1.78
av. Mn-C ring	2.14(4)
av. Mn-CO	1.77(4)
Mn-CN	1.85(2)
av. C-C(ring) [b]	1.39(4)
av. Mn-C-O	173(3)
Mn-C-N	177(2)
C-N-C	172(2)
CO-Mn-CO	91(1)
av. CO-Mn-CN	92(2)

[a] *Co = centre* of gravity of C5-ring

[b] Ring C-C bonds not equivalent (see Fig. 7.3)

infra) precludes a detailed analysis of the conformation of the $Mn(CO)_2L$ "tripod" relative to the (C_5H_5) ring, as has been done for the $(\eta^5C_5H_5)Mn(CO)_3$ precursor[59b] (see section 6.2.2).

7.2.3. Mn-C bond lengths

The av. Mn-C *ring* bond length is 2.14(4)Å, *cf.* 2.124(2)Å for $(\eta^5C_5H_5)Mn(CO)_3$[59b]. The Mn-Cp distance is 1.779Å, *cf.* 1.766Å for $(\eta^5C_5H_5)Mn(CO)_3$[59b], and 1.790Å, 1.778(1)Å and 1.773(3)Å for the complexes $(\eta^5C_5H_5)Mn(CO)_2L$, L = $(C(CO_2Me)$-$CHPPh_3)$[78],$(\eta^2CH_2CHC(O)Me)$[75] and $(\eta^5C_7H_8)$[59b] respectively.

The av. Mn-CO distance is 1.77(4)Å *cf.* 1.780(2)Å and 1.75(2)Å for $(\eta^5C_5H_5)Mn(CO)_3$[59b] and $(\eta^5C_5H_5)Mn(CO)_2(PPh_3$[62] respectively. This trend is in the expected direction, since $CNBu^t$ is a poorer π-acceptor than CO, but a better σ-acceptor than PPh_3[42a]. However, with the small range (3σ), the M-CO bond distances are effectively equal within the limits of experimental error. Note that the Mn-CO bond lengths in $(\eta^5C_5H_5)Mn(CO)_2(CNBu^t)$ are not equal within error limits (1.82(3) and 1.72(4)Å for Mn-C(11) and Mn-C(12) respectively.) A similar effect was observed for $(\eta^5C_5H_5)Mn(CO)_2[\eta^2C(O)CPh_2]$[76] (see section 6.3.6.) The Mn-CN bond length is 1.85(2)Å.

7.2.4 Ring planarity and C-C bond lengths

As for $(\eta^5C_5H_5)Mn(CO)_3$[59b], the C5-ring in $(\eta^5C_5H_5)Mn(CO)_2(CNBu^t)$ is essentially planar (see Table 7.4). However, the ring C-C bond lengths are not equivalent (Fig. 7.3), indicative of some degree of disorder. A 25% disorder of the C5-ring was observed for $(\eta^5C_5H_5)Mn(CO)_2[PPh_2$-$(OC(Me)(CHC(O)Me))]$.[63] Unresolved C5-ring disorder could also account for the non-equivalent ring C-C bond lengths (Fig. 6.3.) in $(\eta^5C_5H_5)Mn(CO)_2(CCMe_2)$.[59] Non-equivalent ring C-C bond lengths could be a genuine electronic effect indicative of some degree of C-C bond localization, in accurately determined structures, eg. $(\eta^5C_5H_5)Mn(CO)_3$.[59b]

7.2.5 M-C-O and M-C-N bond angles

Both the Mn-C-O bond angles are 173(3)°. Near linearity (ca. 175°) is expected.[19] Crystal packing forces

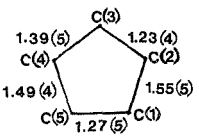


Figure 7.3 Ring C-C bond lengths (Å) in (η^5-C_5H_5)Mn(CO)$_2$(CNBu^t)

could also be responsible for deviations. The isonitrile ligand co-ordinates in a linear fashion, with the Mn-C-N bond angle 177(4)°.

7.2.6 Conformation of the CNBu^t ligand

The isonitrile ligand is slightly bent, with a C-N-C angle of 172(2)°. However, for terminal isonitrile ligands, a C-N-R angle >170° is considered linear.[11b] Note that the CNBu^t ligand bends inwards away from the ring, in contrast to the CNBu^t ligand in (η^5-$C_6H_5CO_2Me$)Cr(CO)$_2$(CNBu^t) (ch. IV), which bends outwards towards the arene ring.

7.2.7 Packing

As for (η^5-C_5H_5)Mn(CO)$_3$,[11b,11] the overall conformation, and in particular the orientation of the ligand tripod with respect to the (C_5H_5) ring, is probably determined largely by crystal packing forces. Short non-bonded intermolecular distances include C(11)....H(5):2.96Å, O(1)....H(5):2.41Å, O(1)....H(1): 2.61Å and O(1)....H(10C):2.86Å.

Small distortion due to close intramolecular non-bonded contacts could also be due to packing requirements eg. C(12)...C(1): 2.72Å and C(12)...H(1): 2.39Å.

7.3 Experimental

7.3.1 Data collection

The complex ($\eta^5C_5H_5$)Mn(CO)$_2$(CNBu^t) was prepared as described in ch. V. Crystals of ($\eta^5C_5H_5$)Mn(CO)$_2$(CNBu^t) were obtained from a dichloromethane solution as pale yellow needles. Preliminary investigation by standard Weissenberg photography established the space group as either the centrosymmetric Pnma or the non-centrosymmetric Pna2$_1$. Refined cell constants were obtained during data collection on a Phillips PW1100 four-circle diffractometer using graphite-monochromated MoKα radiation (λ = 0.7107Å) at room temperature (20°C). During data collection, the crystal deteriorated on long exposure to the X-ray beam, as was evidenced by the fall-off in intensity of certain standard reflections which were checked at intervals. The data were corrected for Lorentz and polarization effects, but absorption corrections were not made as the linear absorption coefficient was only 9.70 cm^{-1}. Crystal data and details of the structure analysis are summarized in Table 7.6.

7.3.2 Structure Solution and Refinement

Structure analysis and refinement were carried out using the program SHELX 82.[168] Initial co-ordinates for the manganese atom were derived from a Patterson synthesis, the other fifteen non-hydrogen atoms being located from difference Fourier syntheses. The basic structure was solved using the centrosymmetric Pnma, but refinement was only possible after transforming to the non-centrosymmetric Pna2$_1$. The fourteen hydrogen atoms were placed from subsequent difference Fourier syntheses. Positional parameters and anisotropic temperature factors for the non-hydrogen atoms were refined by full-matrix least squares analysis. The methyl hydrogens were assigned a common isotropic temperature factor, which refined to a value of 0.087(23)Å.

The cyclopentadienyl ring showed disorder, and in the initial stages was refined as a rigid pentagon. All restraints were removed in the final cycles. Least-squares refinement was considered complete when all positional shifts were less than 0.5σ. At this stage the conventional R was 0.0996. Unit weights were used. Scattering factors for Mn were taken from "International Tables for X-ray Crystallography,"[56b] and anomalous dispersion corrections for manganese were made.[56c] Final atomic coordinates and anisotropic temperature factors for the non-hydrogen atoms are given in Tables 7.7 and 7.8 respectively. A listing of the Structure Factors is to be found in Appendix D.

TABLE 7.6 Crystal data and details of structural analysis for $(\eta^5-C_5H_5)Mn(CO)_2(CNBu^t)$

Formula	$MnC_{12}H_{14}NO_2$
Mr	259.18
Crystal dimensions (mm)	0.60 x .05 x .09
Space Group	$Pna2_1$
a(Å)	19.123(9)
b(Å)	6.020(3)
c(Å)	10.942(5)
V(Å^3)	1259.65
Z	4
Dc (g cm^{-3})	1.37
F (000)	535.97
μ (cm^{-1})	9.70
λ(Å)	MoKα (0.7107)
Scan mode	ω/2θ
Range (°)	$3 \leq \theta \leq 25$
Scan width (°)	1.00
Scan speed (°s^{-1})	0.033
Range of hkl	+h, +k, +ℓ
Measured intensities	1049
Unique reflections	878
Internal consistency R-index	0.0000
Omitted reflections	112
Observed reflection criterion	$F>6(F)$
R (R = Rw)	0.0996

TABLE 7.7 Fractional atomic co-ordinates for $(\eta^5-C_5H_5)Mn(CO)_2(CNBu^t)$

Atom	x/a	y/b	z/c
Mn	0.4744(1)	0.6579(5)	0.7500(0)
N	0.341(1)	0.393(3)	0.745(4)
O(1)	0.423(1)	0.748(6)	0.553(2)
O(2)	0.416(2)	0.956(5)	0.935(3)
C(1)	0.469(3)	0.625(6)	0.845(4)
C(2)	0.530(1)	0.707(5)	0.712(2)
C(3)	0.562(2)	0.550(7)	0.648(4)
C(4)	0.534(1)	0.363(4)	0.706(3)
C(5)	0.548(2)	0.425(5)	0.835(3)
C(6)	0.394(1)	0.491(4)	0.748(5)
C(7)	0.270(1)	0.299(3)	0.737(3)
C(8)	0.235(2)	0.411(9)	0.655(3)
C(9)	0.235(3)	0.377(5)	0.885(4)
C(10)	0.275(1)	0.059(4)	0.728(3)
C(11)	0.439(2)	0.841(5)	0.633(3)
C(12)	0.443(2)	0.830(9)	0.864(3)
H(1)	0.566(8)	0.761(28)	0.878(15)
H(2)	0.588(7)	0.825(24)	0.710(12)
H(3)	0.573(8)	0.521(27)	0.578(13)
H(4)	0.527(7)	0.197(24)	0.702(11)
H(5)	0.548(7)	0.247(23)	0.868(12)
H(8A)	0.185(18)	0.350(48)	0.667(30)
H(8B)	0.264(12)	0.417(43)	0.000(23)
H(8C)	0.240(11)	0.620(40)	0.653(19)
H(9A)	0.192(18)	0.345(53)	0.853(31)
H(9B)	0.238(12)	0.536(44)	0.889(21)
H(9C)	0.238(11)	0.201(38)	0.923(18)
H(10A)	0.263(11)	-0.059(34)	0.814(20)
H(10B)	0.226(10)	-0.001(32)	0.704(17)
H(10C)	0.286(11,	-0.009(36)	0.665(20)

TABLE 7.8 Anisotropic thermal parameters ($Å^2$) for the non-hydrogen[a] atoms of $(\eta^5C_5H_5)Mn(CO)_2(CNBu^t)$

Atom	U_{11}	U_{22}	U_{33}	U_{23}	U_{13}	U_{12}
Mn	0.034(1)	0.071(2)	0.053(2)	0.007(4)	0.000(3)	-0.002(2)
N	0.05(1)	0.08(1)	0.08(1)	-0.02(2)	-0.02(2)	-0.01(1)
O(1)	0.04(1)	0.17(3)	0.05(1)	0.02(2)	0.01(1)	0.00(2)
O(2)	0.10(2)	0.09(2)	0.06(1)	-0.03(1)	-0.01(1)	0.04(2)
C(1)	0.13(3)	0.05(2)	0.07(2)	-0.03(2)	-0.08(2)	0.02(2)
C(2)	0.02(1)	0.05(2)	0.07(2)	-0.00(2)	-0.00(1)	0.01(1)
C(3)	0.10(3)	0.09(3)	0.07(3)	-0.04(3)	-0.01(2)	0.04(2)
C(4)	0.06(1)	0.02(1)	0.12(3)	0.03(1)	0.05(2)	0.01(1)
C(5)[b]	0.058(8)					
C(6)[b]	0.068(6)					
C(7)[b]	0.047(6)					
C(8)	0.05(1)	0.17(5)	0.05(2)	-0.00(2)	-0.01(1)	0.01(2)
C(9)	0.19(6)	0.07(2)	0.09(3)	-0.03(2)	0.09(4)	-0.09(3)
C(10)[b]	0.056(6)					
C(11)[b]	0.042(5)					
C(12)	0.05(2)	0.19(4)	0.04(1)	-0.01(2)	-0.02(1)	0.02(2)

[a] The ring H-atoms (H1 to H5) have isotropic temperature factor of 0.0001(38)$Å^2$; the methyl H-atoms (H8A-C, H9A-C, H10A-C) were assigned a common temperature factor which refined to 0.087(23)$Å^2$.

[b] Refined as an isotropic atom.

VIII. ANOMALOUS INFRA RED SPECTRA OF (η^6-ARENE)$Cr(CO)_2$(CNR) AND ($\eta^5C_5H_5$)$Mn(CO)_2$(CNR) COMPLEXES

8.1 Introduction - Anomalous IR data

As mentioned previously, certain complexes of the type (η^6-Arene)$Cr(CO)_2$(CNR) and ($\eta^5C_5H_5$)$Mn(CO)_2$(CNR) were found to give anomalous infra red(IR) spectra, both in solution and the solid state. (Chs. II and V respectively).

On the basis of group theory analysis, compounds of the above type are predicted to given infra red spectra with two ν(CO) bands and one ν(NC) absorption band. This is indeed observed for complexes ($\eta^5C_5H_5$)$Mn(CO)_2$(CNR) (R = $CH_2C_6H_5$, $C_6H_3Me_2$-2,6, Me). However, for R = Bu^t and C_6H_{11}, two ν(CO) and <u>two</u> ν(NC) bands are observed in both the solid state and in hexane solution (see Table 5.2). Further, all the ($\eta^5C_6H_5X$)$Cr(CO)_2$(CNR) (R = Bu^t, X = Me, H, Cℓ, CO_2Me; R = $C_6H_3Me_2$-2,6, X = Me, H) complexes studied also gave two ν(CO) and <u>two</u> ν(NC) bands both in the solid state and in $CH_2Cℓ_2$ or hexane solution (Table 2.1), with the exception of ($\eta^5C_6H_5CO_2Me$)$Cr(CO)_2$($CNC_6H_3Me_2$-2,6), which in solution (hexane, $CCℓ_4$, $CH_2Cℓ_2$, $CHCℓ_3$) gives two ν(CO) bands and only one ν(NC) band, as expected, but in the solid state (KBr), gives <u>three</u> ν(CO) bands and one ν(NC) band (Figure 8.1(a); see section 8.5). A typical example of the anomalous IR data is shown in Figure 8.1(b), the solid state spectrum of ($\eta^5C_6H_5CO_2Me$)$Cr(CO)_2$($CNBu^t$). [IR(KBr): ν(NC): 2090, 2060(sh); ν(CO): 1908, 1856, ν(COOMe): 1700 cm^{-1}.]

Anomalous IR data of this nature is also observed for the related complex ($\eta^5C_5H_5$)$Ru(CNBu^t)_2I$.[*] This complex is expected to give two ν(NC) IR adsorptions, but <u>three</u> ν(NC) bands are observed in the IR spectrum in both solution ($CH_2Cℓ_2$, benzene) and the solid state. [IR(KBr): ν(NC): 2130, 2098, 2060 cm^{-1}].

In the cases of the related complexes, ($\eta^5C_5H_5$)$Fe(CO)$-$[P(OMe)_3]X$ (X = Cℓ, Br, I)[**a] and ($\eta^5C_5H_4Me$)$Fe(CO)[P(OMe)_3]I$,[**b] the ν(CO) absorption band is resolved into two components in n-heptane solutions. The doubling of the number of ν(CO)

bands in these complexes has been ascribed to rotational isomerization,[88] arising from either restricted rotation about the M-P bond with the formation of eclipsed and staggered isomers, or restricted conformational rotation within the $P(OMe)_3$ ligand.

Similar effects of observing more than the anticipated number of infra red bands have been reported. For example, the complexes trans-$(\eta^5C_5H_5)Fe(CO)_2[C(O)CH = CHR]$ (R = Me, Ph)[88a] give three ν(CO) bands in the IR spectra, (hexane solution) instead of the expected two, and the related complexes $(\eta^5C_5H_5)Pt\ R_1\ R_2[C(O)Me]$($R_1$ = R_2 = Me,Et; R_1 = Me, R_2 = Et)[88b] have two ν(C(O)R) bands in the IR spectra (hexane or $CC\ell_4$), while only one ν(C(O)R) band is predicted. This splitting has been ascribed to conformational isomerization about the metal-acetyl bond.[88] In the former case the resolution of the bands due to the conformers is not complete, with only the high frequency band showing splitting.[88a] The possibility of more than two isomers co-existing in solution also cannot be excluded.[88a] No solid state IR data of these complexes has been reported, however.

In an attempt to formulate a rationalization of the anomalous IR data of the $(\eta^6$Arene$)Cr(CO)_2(CNR)$ and $(\eta^5C_5H_5)Mn(CO)_2(CNR)$ complexes, IR spectral and X-ray crystallographic structural studies of two representative compounds, $(\eta^6C_6H_5CO_2Me)Cr(CO)_2(CNBu^t)$ and $(\eta^5C_5H_5)Mn(CO)_2$-$CNBu^t$), were undertaken. Since the anomalous IR data persist both in solution and in the solid state, this fact must be taken into account by any proposed explanation of the effect.

8.2 IR spectral studies of $(\eta^6C_6H_5CO_2Me)Cr(CO)_2(CNBu^t)$ and $(\eta^5C_5H_5)Mn(CO)_2(CNBu^t)$ in different solvents

IR spectral studies of the complexes $(\eta^6C_6H_5CO_2Me)Cr(CO)_2$-$(CNBu^t)$ and $(\eta^5C_5H_5)Mn(CC)_2(CNBu^t)$ in solvents of different polarity (Table 8.1 and 8.2 respectively) revealed that the relative intensity of the lower frequency band increases with decreasing solvent polarity. This suggests the existence of conformers with different dipole moments. In the case of $(\eta^6C_6H_5CO_2Me)Cr(CO)_2(CNBu^t)$, this

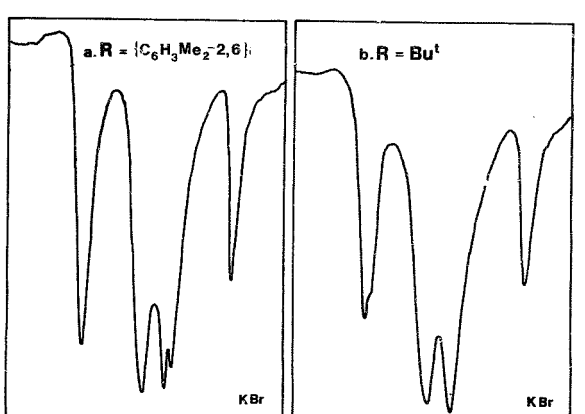


Figure 8.1 Solid state IR spectra (KBr) of (η^6-$C_6H_5CO_2Me$)$Cr(CO)_2$(CNR: (a) R = $C_6H_3Me_2$-2,6, (b) R = Bu^t

effect cannot be due to interaction of the RNC group with the arene-ring substituent, since $(\eta^6C_6H_6)Cr(CO)_2(CNBu^t)$ also has two ν(NC) stretching frequencies. Further, unless there is fortuitous overlap of two sets of CO stretching frequencies, the two different conformers must have the CO ligands in very similar environments. To test this hypothesis and to determine the nature of the different conformers, crystal structure determinations of the complexes $(\eta^6C_6H_5CO_2Me)Cr(CO)_2(CNBu^t)$ and $(\eta^5C_5H_5)Mn(CO)_2(CNBu^t)$, were undertaken. The full crystal and molecular structures of these two complexes are reported in chs. IV and VII respectively. ructural features which could have bearing on the -R effect will be discussed.

8.3 Structural data on $\eta^6C_6H_5CO_2Me)Cr(CO)_2(CNBu^t)$ and $(\eta^5C_5H_5)Mn(CO)_2(CNBu^t)$ from X-ray Crystallographic Studies

The $(\eta^6C_6H_5CO_2Me)Cr(CO)_2(CNBu^t)$ and $(\eta^5C_5H_5)Mn(CO)_2(CNBu^t)$ molecules are illustrated in Figures 8.2 and 8.3 respectively. In both cases, the structural feature of note is the non-linear isonitrile ligand (C-N-C angle of 166.8(4)° and 172(2)° respectively). Further, in the case of $(\eta^6C_6H_5CO_2Me)$-$Cr(CO)_2(CNBu^t)$, the isonitrile ligand bends towards the ring (Figure 8.2), while for $(\eta^5C_5H_5)Mn(CO)_2(CNBu^t)$, the isonitrile bends away from the ring (Figure 8.3). In both isonitrile structures the C-N-C plane of the isonitrile ligand is close to perpendicular to the mean plane of the respective carbocycle rings (11° for Cr, 4° for Mn) (Figure 8.4(c), (d)). It is thus possible that the observation of a non-linear RNC group could give rise to different conformers, two of which correspond to the structures shown in Figure 8.4(a) and (b). This could provide an explanation of the solution IR data. However, for both the Cr and Mn-structures, there is only one molecule in the asymmetric unit cell (Crystal data: $P\bar{1}$, Z = 2, and $Pna2_1$, Z = 4, respectively), of the conformations shown in Figure 8.4(a) and (b) respectively, and there is no evidence of disorder of the isonitrile ligand. Hence an alternative explanation is required to explain the solid state (KBr) IR data.

TABLE 8.1: IR spectral study of $[(\eta^6-C_6H_5CO_2Me)Cr(CO)_2(CNBu^t)]$ in different solvents[a]

Solvent	ν(CO)/cm^{-1}		ν(COOMe)/cm^{-1}	ν(NC)/cm^{-1}		Intensity Ratio A:B[b]
				A	B	
chloroform	1924 vs	1872 s	1708 m	2112 ms	2074 sh	2.5
dichloromethane	1920 vs	1868 s	1710 m	2100 ms	2060 sh	2.3
toluene	1922 vs	1865 s	1700 m	2106 m	2070 sh	-
tetrahydrofuran	1924 vs	1879 s	1718 m	2104 m	2076 sh	1.5
n-hexane	1960 vs	1880 s	1697 m	2100 m	2076 sh	1.9
benzene	1940 vs	1898 s	1720 m	2100 mw	2070 w	1.1
carbon tetrachloride	1930 vs	1884 s	1699 m	2112 m	2070 ms	0.8

[a] IR (KBr): ν(NC), 2090, 2060(sh); ν(CO), 1908, 1856; ν(COOMe), 1700 cm^{-1}.

[b] Estimated from peak areas (± 15%)

TABLE 8.2: IR spectral study of $(C_5H_5)Mn(CO)_2(CNBu^t)$ in different solvents[a]

Solvents	ν(CO)/cm^{-1}	ν(CN)/cm^{-1}		Ratio A:B[b]
		A	B	
THF	1941, 1881	2106	2074(sh)	2.9 : 1
$CHCl_3$	1942, 1882	2114	2082(sh)	2.2 : 1
CH_2Cl_2	1940, 1881	2116	2082(sh)	2.0 : 1
$C_6H_5CH_3$	1943, 1883	2110	2080	1.7 : 1
C_6H_6	1944, 1893	2108	2074	1.6 : 1
CCl_4	1948, 1897	2104	2073	1.4 : 1
C_6H_{12}	1952, 1905	2102	2070	1.2 : 1

[a] IR(KBr): ν(NC), 2118, 2072(sh); ν(CO), 1971, 1926 cm^{-1}

[b] Estimated from peak areas (± 15%)

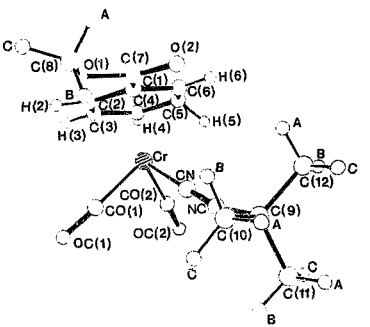


Figure 8.2 Sideways ORTEP [4] view of the $(\eta^6-C_6H_5CO_2Me)Cr(CO)_2(CNBu^t)$ molecule.

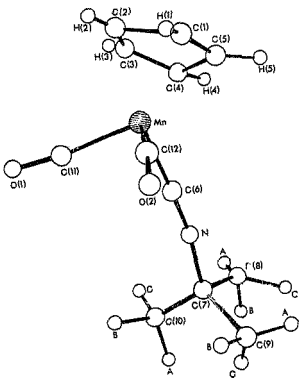
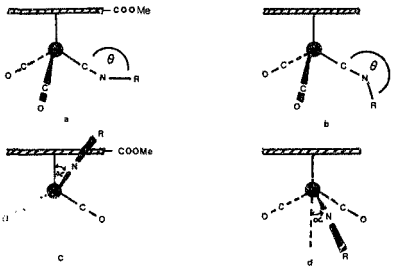


Figure 1 : Sideways ORTEP[45] view of the $(\eta^5C_5H_5)Mn(CO)_2(CNBu^t)$ molecule



(a) $(\eta^6\text{-}C_6H_5CO_2Me)Cr(CO)_2(CNBu^t)$ — $\theta = 166{\cdot}8(4)^\circ$

(b) $(\eta^5\text{-}C_5H_5)Mn(CO)_2(CNBu^t)$ — $\theta = 188(2)^\circ$

(c) $(\eta^6\text{-}C_6H_5CO_2Me)Cr(CO)_2(CNBu^t)$ — $\alpha = 11(1)^\circ$

(d) $(\eta^5\text{-}C_5H_5)Mn(CO)_2(CNBu^t)$ — $\alpha = 4(2)^\circ$

Figure 8.4 Diagram illustrating the conformation of the $CNBu^t$ ligand in $(\eta^6\text{-}C_6H_5CO_2Me)Cr(CO)_2(CNBu^t)$ ((a) and (c)) and $(\eta^5\text{-}C_5H_5)Mn(CO)_2(CNBu^t)$ ((b) and (d))

8.4 Structural data on $(\eta^5C_5H_5)Ru(CNBu^t)_2I$ from an X-ray Crystallographic study

As mentioned in section 8.1, $(\eta^5C_5H_5)Ru(CNBu^t)_2I$ gives three, instead of two ν(NC) adsorptions in the IR spectrum both in solid state and in solution. The X-ray crystal and molecular structure of this complex has been reported.[97] The compound crystallizes in the triclinic space group $P\bar{1}$ with Z = 4, ie. there are two molecules in the asymmetric unit. These two crystallographically independent molecules do not have the same ligand conformation with respect to the cyclopentadienyl ring. This suggests a possible explanation of the solid-state IR data. The two conformations probably arise from packing forces in the crystal. Further, there is the possibility of intermolecular interactions between the two different molecules.

Of significance is the finding that each molecule contains two different types of RNC groups, viz. one near-linear (C-N-C,175°(av.)), and one with a larger C-N-C bend (162°(av.)). In both molecules the bent isonitrile points *away from the ring*. This suggests the possibility of the existence of conformers (Figure 8.4(a) and (b)) to account for the *solution* IR data. Another possible explanation could be the lowering of the symmetry of the molecule by the bending of an isonitrile.

8.5 The solid state IR spectrum and crystal structure of $(\eta^6C_6H_5CO_2Me)Cr(CO)_2(CNC_6H_3Me_2\text{-}2,6)$

In hexane solution, the IR spectrum of the complex $(\eta^6C_6H_5CO_2Me)Cr(CO)_2(CNC_6H_3Me_2\text{-}2,6)$, unlike that of the other $(\eta^6Arene)Cr(CO)_2(CNR)$ derivatives studied, is as expected, viz. two ν(CO) bands and one ν(NC) band. However, in the solid state (KBr), three ν(CO) bands and one ν(NC) band is observed. (Figure 8.1(a):IR (KBr): ν(NC): 2070; ν(CO): 1904, 1855, 1840; ν(COOMe): 1715 cm^{-1}).

If, as suggested in sections 8.2-8.3, the observation of two ν(NC) IR bands for $(\pi^6C_6H_5CO_2Me)Cr(CO)_2(CNBu^t)$, arises due to the bent isonitrile ligand (conformers in solution, influence of crystal packing forces in solid state), the

observation of only one ν(NC) IR band (in both solution and solid state) for $(\eta^5C_6H_5CO_2Me)Cr(CO)_2(CNC_6H_3Me_2\text{-}2,6)$ suggests the isonitrile ligand should be linear in this complex. Hence a crystal structure determination of the compound was undertaken. Also, the observation of splitting of one of the ν(CO) bands in the solid state IR spectrum only was considered likely to be accountable in terms of crystal packing.

Standard Weissenberg and precession photography gave the monoclinic space group $P2_1/c$ (absences h0ℓ, ℓ = 2n + 1, and 0k0, k = 2n + 1), and the unit cell parameters were determined as a = 30.15(6)Å, b = 7.35(2)Å, c = 13.24(4)Å, β = 105°, V = 3560Å^3 with Z = 8. A full data set was collected, but attempts to solve the molecular structure, in $P2_1/c$, and other possible monoclinic space groups,* using heavy atom, and direct methods, were not successful.

However, as the X-ray photographs obtained showed no evidence of centering, it appears as if the asymmetric unit contains at least two (possibly four) molecules, with the possibility of intermolecular interactions, eg. between a carbonyl on one molecule and a group on a crystallographically independent molecule. Therein probably lies the explanation of the anomalous solid state IR spectrum.

8.6 Possible explanations for the anomalous IR data

8.6.1 Conformers in solution

(a) RNC bending

As expected in sections 8.2-8.4, the observation of ben[illegible]nitrile ligands in the three isonitrile derivatives studied crystallographically suggests the existence of conformers (eg. Figure 8.4(a) and (b)) could account for the anomalous IR solution data. The predominance of one or other conformer appears from the IR studies (section 8.2) to depend on the solvent polarity. It has been shown[93] for biphenylchromiumtricarbonyl that increased inductive electron withdrawal in chloroform than in benzene results from interaction of the strongly polar solvent with the electron-rich chromium centre.

* The condition 0k1, k = 2n+1 was also observed; hence it was thought that the compound might exhibit pseudo-orthorhombic symmetry.

(b) Tripodal rotation

Conformational isomers could also arise in solution due to the rotation of the L_3 tripod around the metal-ring axis. For the complexes examined, the barrier to such a rotation is predicted to be very small.[7]

This proposal receives a measure of support from recent low temperature C^{13} NMR studies on $(\pi\text{-}C_6Et_6)Cr(CO)_2(CS)$,[11a] in which the low temperature isomer was found to possess the same symmetry as the solid state structure. It has been claimed that this demonstrates that rotation resulting in isomers co-existing in solution is due to tripodal rotation around the Cr-Arene bond, which is slowed down at low temperatures. However, this claim has been disputed by other workers,[11b,c] who interpret the results in terms of restricted ethyl group rotation about the arene ring.

8.6.2 Solid state effects

(a) Crystal lattice effects

In solid state infra red spectra, an absorption band splitting may occur when the band corresponds to a degenerate vibration of the isolated molecule because the site symmetry of the molecule in the crystal lattice may be lower than that of the isolated molecule.[92,93]

With non-degenerate vibrations, the coupling together of vibrations of adjacent molecules can give rise to various combinations leading to band multiplicity.[93] A simple factor-group analysis often fails to predict the number of observed IR bands. This is a consequence of the vibrational unit cell appropriate to the groups, being of different effective symmetry to the crystallographic unit cell.[93]

(b) Packing effects

The crystal lattice is governed by the principle of dense packing[93] ie. the molecules pack together in such a way as to minimize the voids between adjacent molecules and so make the most economic use of space. As a result of the influence of crystal packing forces, interaction

between groups on adjacent molecules, or the same molecule may become possible owing to relatively short non-bonded distances. Hence the anomalous IR data could arise from short intermolecular or intramolecular non-bonded contacts (eg. O(2)...H(10C), 2.75Å, or O(2)...H(8A), 2.55Å respectively, in $(\eta^6C_6H_5CO_2Me)Cr(CO)_2(CNBu^t)$.)

8.6.3. Lowering of molecular symmetry by bent isonitrile

The anomalous IR data could also arise from a lowering of the molecular symmetry by the bent isonitrile ligand. (C-N-C in range 162-172°). It has been shown using *Ab Initio* MO Calculations[94] that for RNC ligands, as the C-N-C angle decreases, the π-acceptor character of the RNC ligand increases markedly. Hence a bent isonitrile reflects an enhanced degree of back-bonding $(M(3d)\rightarrow(C\equiv N)\pi^*.)$[95] Hence the degree of bending found for a particular isonitrile ligand could reflect electronic rather than steric factors.

8.7 Conclusion

From the foregoing analysis, the most likely rationalization of the anomalous IR data for the $(\eta^6\text{Arene})Cr(CO)_2(CNR)$ and $(\eta^5C_5H_5)Mn(CO)_2(CNR)$ complexes appears to be:-

(a) In solution, the existence of conformers with the RNC ligand bending towards (fig. 8.4(a)) or away from (Fig. 8.4(b)) the ring. The predominance of one or other conformer in a particular solvent depends on the solvent polarity. The results of the IR studies in solvents of varying polarities (section 8.2) favours conformers arising from RNC-bending (vide supra) rather than from tripodal rotation.

(b) In solid state, a lowering of the molecular symmetry due to the bending of the RNC ligand (one conformer only present in the crystal*) or intramolecular interactions between groups. Alternately, the phenomenon may be due to crystal lattice effects (see section 8.6.2.(a)).

* It is possible that there could be more than one conformer in the polycrystalline sample of $(\eta^6C_6H_5CO_2Me)Cr(CO)_2(CNBu^t)$, but the $(\eta^5C_5H_5)Mn(CO)_2(CNBut)$ sample consisted of single crystals.

IX. THE GEOMETRY OF $Fe(CO)_{5-n}(L)_n$ (n = 1,2) STRUCTURES, AND THE CRYSTAL AND MOLECULAR STRUCTURE OF $Fe(CO)_3(CNMe)_2$

9.1 Introduction

For penta co-ordinate transition metal complexes of the type $M(L)_5$, two basic geometries are possible, viz. the D_{3h} trigonal bipyramidal (tbp), and the C_{4v} square pyramidal (spy). The energy difference between the two geometries is very small,[96,97] with the trigonal pyramidal arrangement of five valence electron pairs being slightly more stable for d^0 and d^{10} transition metals, as well as for non-transition elements.[94]

However, according to *Gillespie's*[96] *valence-shell* electron-pair repulsion theory, for transition metal atoms with non-symmetrical d-configurations, the interaction of the valence-shell electron pairs with the non-bonding-d-shell as well as with each other, determines the overall geometry of the $M(L)_5$ complex. This additional interaction may result in the square pyramidal geometry becoming more stable than the trigonal bipyramidal structure.

On the basis of Molecular Orbital (MO) calculations, Elian and Hoffmann[98] have shown that for d^8 transition metals eg. Fe^0, complexes of the type $M(L)_5$ are predicted to adopt a trigonal bipyramidal structure. Hence $Fe(L)_5$ complexes would be expected to exhibit trigonal bipyramidal geometry.

The X-ray structure of iron pentacarbonyl, $Fe(CO)_5$, was first reported by Hanson[99a] in 1962, and redetermined the following year by Donohue and Caron.[99b] The geometry of the $Fe(CO)_5$ molecule is trigonal bipyramidal, with no significant distortions according to the redetermined structure.[99b] The OC-Fe-CO angles are all close to the ideal values *(ax OC-Fe-COax : 176(2)°, av. eq OC-Fe-COax 90(1)°, and* eq OC-Fe-COeq : 120(1)°[99b]). Within the limits of experimental error, the Fe-Cax and Fe-Ceq bond lengths are equal (av. Fe-CO : 1.79(2)Å[99b]).

However, from a more recent (1969) electron diffraction study[100] of $Fe(CO)_5$, the Fe-COax bonds (av. 1.806(5)Å) are significantly shorter than the Fe-COeq bonds (av. 1.833(4)Å).

From an analysis of electronic effects in tbp d^8 $M(L)_5$ complexes, Rossi and Hoffmann[101] have concluded that strong σ-donors will strengthen axial M-L bonds. A π-acceptor tends to counteract this σ-bonding effect, while a π-donor reinforces it. Hence for ligands that are good π-acceptors, the σ- and π-bonding effects oppose each other, although the σ-bonding effect seems to dominate, i.e. longer equatorial M-L bonds are found. This is indeed observed for $Fe(CO)_5$ (*vide supra*), *since carbonyls are good π-acceptors.*[93]

Using valence-shell electron-pair repulsion theory, Gillespie[96] reached the conclusion that the oblate ellipsoidal electron clouds of d^8 tbp $M(L)_5$ complexes favour axial bonds which are shorter than equatorial bonds. However, Gillespie pointed out that this difference in bond lengths is likely to be small.

When considering the overall geometry of $M(L)_5$ complexes, steric and electrostatic effects[101] as well as electronic factors must be taken into account. For complexes of the type $Fe(CO)_{5-n}(L)_n$ (n = 1-5), where ligand(s) L has been substituted for one or more carbonyls, steric factors may have an important influence on structure, especially if L is a bulky ligand.

9.2 The Geometry of $Fe(CO)_4L$ Structures

9.2.1. Axial versus Equatorial Site Preference of L

Given that d^8 complexes of the type $M(L)_5$ are expected to display tbp geometry[95,97] for complexes of the type $Fe(CO)_4L$, the relative stability of the axial (ax) or equatorial (eq) location of a ligand L vis-à-vis CO is dependent on electronic factors, such as the σ- and π-bonding characteristics of the ligand L relative to CO, as well as on steric considerations.[102] A ligand L which has large steric requirements might be driven by steric forces towards an equatorial position, where the number of 90° interactions with adjacent ligands is smaller.[103]

Based on electronic considerations, Rossi and Hoffmann[101] have predicted that both good σ-donors and good π-donors

prefer axial sites. With a ligand that is both a good σ-donor and a good π-acceptor, however, the trends oppose, and the site occupied by the ligand depends on the relative strength of the σ- and π-bonding effects. Nevertheless, based on a simple π-bonding model, strong π-acceptors tend to occupy equatorial sites, so that back-bonding may be optimized.[124] This results from the greater availability of metal d-orbitals of correct symmetry to form π-bonds with ligands in *equatorial versus axial sites.*[97] *Hence,* for $Fe(CO)_4L$ complexes, in the absence of overwhelming steric repulsion,[97] a ligand L that is a weaker π-acceptor *and/or a stronger* σ-donor than CO (*eg.* isonitriles,[93] phosphines,[93b,165] stibines,[165] arsines,[165] sulphides,[165] amines[167]) would be expected to occupy an axial position.

Table 9.1 lists complexes of the type $Fe(CO)_4L$ (excluding those complexes with olefinic ligands and complexes with bidentate ligands such as $Fe(CO)_4(AsC_6F_5)_2$[168] $[Fe(CO)_4(B_2H_{12})]^-$,[169] in which the iron atom is essentially hexa co-ordinate) for which X-ray Crystal and Molecular structures have been determined. All these complexes exhibit tbp geometry (C3v symmetry), with ligand L occupying an axial site, with the exception of L = $PFh(PFh_2)_2$,[130] which occupies an equatorial position. This exception is probably due to the predominance of steric factors with the bulky phosphine ligand.

9.2.2 Distortions to the tbp geometry

Geometric data for the ax-L-Fe(CO)$_4$ tbp structures of Table 9.1 are summarized in Table 9.2. In the majority of cases, the tbp geometry is slightly distorted, with a bending of the equatorial CO ligands towards the axial L substituent[169,118] (ie. axOC-Fe-COeq angles slightly greater than the ideal 90°, and L-Fe-COeq angles slightly less than 90°.)

A variety of possible reasons have been advanced to account for this phenomenon:-

1) Influence of crystal packing forces.[93a]

TABLE 9.1: *X*-Ray Crystal Structures of $Fe(CO)_4L$ Complexes[a]

Complex	Space Group, Z	Geometry[b]	Position of L[c]	Reference
$[HFe(CO)_4]^-$	$P2_1/c,4$	tbp	ax	111
$[NCFe(CO)_4]^-$	$P2_1/c,4$	tbp	ax	97
$(Me_3As)Fe(CO)_4$	R3,3 [d]	tbp	ax	112
$(Me_3Sb)Fe(CO)_4$	R3,3 [d]	tbp	ax	112
$(Ph_3Sb)Fe(CO)_4$	$P\bar{1},2$	tbp	ax	113
$(Ph_3P)Fe(CO)_4$	$P\bar{1},2$	tbp	ax	104
$(^tBu_3P)Fe(CO)_4$	$P2_12_12_1,4$	tbp	ax	114
$(Ph_2HP)Fe(CO)_4$	$P2_1/c,4$	tbp	ax	115
$(OC)_4Fe(PMe_2)_2Fe(CO)_4$	$P\bar{1},1$ [e]	tbp [f]	ax	
$[(Me_2N)_3P]Fe(CO)_4$	$P2_1/c,4$	tbp	ax	
$[n^1\text{-}PPh_2CH_2CH_2PPh_2]Fe(CO)_4$	$P2_1/c,4$	tbp	ax	1
$[(Me_2As)C(CF)_2CPPh_2]Fe(CO)_4$	$P2_1/c,4$	tbp	ax	116
$[(Me)NCH_2CH_2N(Me)PF]Fe(CO)_4$	$P2_1/c,4$	tbp	ax	120
$[(PPh_2)_2PhP]Fe(CO)_4$	$P\bar{1},2$	tbp	eq	110
$(C_5H_5N)Fe(CO)_4$	$P2_1/n,4$	tbp	ax	107
$[CHCHN(CH_2)_2N]Fe(CO)_4$	$P2_1/c,4$	tbp	ax	107
$[CH(CH)_3NN]Fe(CO)_4$	$P2_1/n,4$	tbp	ax	121
$[(CO_2Me)_2CCHPhCH_2NN]Fe(CO)_4$	$P2_1/c,4$	tbp	ax	122
$[PhCH(CH)_2N(Me)]Fe(CO)_4$	$P2_1/n,4$	tbp	ax	123
$(Ph_2C_3S)Fe(CO)_4$	$P\bar{1},2$	tbp	ax	124
$[CH_2S(CH_2)_3S]Fe(CO)_4$	$Pn2_1a,4$	tbp	ax	106

TABLE 9.1 (Cont.)

Complex	Space Group Z	Geometry[b]	Position of L[c]	Reference
$[(Me)\overline{N(CH)_2N(Me)C}]Fe(CO)_4$	C2/c,8	tbp	ax	125
$[\overline{O(C_6H_{10})_2OC}]Fe(CO)_4$	$P2_1/c$,4	tbp	ax	126
$[(H_7C_3)Fe(CO)_4]^-$	C2/c,8	tbp	ax	127
$[(Ce_3Si)Fe(CO)_4]^-$	$P2_1$,2	tbp	ax	128

[a] L not an olefin or bidentate ligand

[b] tbp = trigonal bipyramidal

[c] ax = axial, eq = equatorial

[d] molecule posseses crystallographic 3-fold symmetry

[e] asymmetric unit corresponds to $(Me_2P)Fe(CO)_4$ fragment

[f] co-ordination of Fe-atom

TABLE 9.2: Geometric data for ax-L-Fe(CO)$_4$ tbp structures
(Bond angles in degrees, bond lengths in Å)

L	L-Fe-COax	L-Fe-COeq[a]	axOC-Fe-OCeq[a]	eqOC-Fe-COeq[a]	Fe-C-O[a]	Fe-COax	Fe-COeq[a]
H^-	175(5)	81(5)	99.1(7)	117.6(8)	177.7(2)	1.72(2)	1.75(2)
CN^-	175.9(3)	87.4(3)	92.7(4)	119.8(4)	178.9(9)	1.723(8)	1.768(8)
$AsMe_3$[b]	180.0[c]	94.0[c]	86.0[c]	119.5[c]	167[c,d]	2.4(3)	1.73[c]
$SbMe_3$[b]	180.0[c]	88.4[c]	91.6[c]	119.9[c]	178[c,e]	1.81(9)	1.66[c]
$SbPh_3$	178.1(4)	88.3(2)	91.7(2)	119.9(2)	179(1)	1.765(4)	1.787(4)
PPh_3	178.3(1)	88.8(1)	91.2(2)	119.9(2)	178.5(4)	1.795(4)	1.795(4)
PBu^t_3[f]	175.7(1)	93.3(7)	87(1)	119.7(2)	173.2(4)[f]	1.788(4)	1.792(4)
$PHPh_2$	177.1(3)	89.2(2)	90.9(4)	120.0(2)	177.1(8)	1.781(8)	1.793(9)
PMe_2[g]	175.4(8)	89.1(6)	91(1)	120.0(9)	176(2)	1.78(1)	1.79(1)
$P(NMe_2)_3$	178.1(2)	91.1(2)	90.9(2)	120.0(2)	177.9(5)	1.793(6)	1.787(5)
$[\eta^1\text{-}PPh_2CH_2CH_2PPh_2]$	179.3(2)	91(2)	91.5(3)	120.0(3)	178.7(6)	1.771(6)	1.790(6)
$[(Me_2As)C(CF)_2CPPh_2]$	178.8(9)	89(4)	90.6(6)	120.0(6)	179(2)	1.74(2)	1.74(1)
$\{(Me)\overline{NCH_2CH_2N(Me)}PF\}$	175.4(2)	88.1(2)	91.0(3)	120.0(3)	178.7(6)	1.803(6)	1.76(6)
C_5H_5N	176.2(2)	89.5(2)	89.8(3)	120.0(3)	178.3(6)	1.772(7)	1.805(7)
$[\overline{CHCHN(CH_2)}N]$	175.8(2)	90.7(1)	89.4(2)	120.0(2)	177.8(4)	1.774(4)	1.810(4)
$[\overline{CH(CH)_3NN}]$	175.6(2)	89.8(2)	90.3(3)	120.0(3)	177.7(6)	1.765(7)	1.809(7)
$[\overline{(CO_2Me)_2CCHPhCH_2NN}]$	178.7(1)	90.7(1)	89.3(2)	120.0(2)	177.4(3)	1.773(4)	1.807(4)
$[PhCH(CH)_2N(Me)]$	174.5(2)	91.1(2)	89.1(3)	119.3(3)	176.5(6)	1.744(6)	1.790(6)
(Ph_2C_3S)	176.2[c]	89.0[c]	91.0[c]	120.0[c]	178.6[c]	1.758(4)	1.810(4)

TABLE 9.2 (Cont.)

L	L-Fe-COax	L-Fe-COeq[a]	axOC-Fe-OCeq[a]	eqOC-Fe-COeq[a]	Fe-C-O[a]	Fe-COax	Fe-COeq[a]
$[\overline{CH_2S(CH_2)_2}_3S]$	179.4(3)	89.9(3)	91.7(4)	120.0(5)	175.2(8)	1.789(9)	1.764(9)
$[(Me)\overline{N(CH)_2}_2N(Me)C]$	167.6(2)	90.8(2)	90.2(3)	120.0 [c]	176.3(5)	1.767(6)	1.789(8)
$[O\overline{(C_6H_{10})_2}OC]$	179.26(6)	88.85(7)	91.15(7)	119.96(7)	178.6(2)	1.795(2)	1.799(2)
$(C_3H_7)^-$	175.3(9)	83.9(8)	96.1(9)	118.9(9)	176(2)	1.74(2)	1.75(2)
$(SiCl_3)^-$	178(1)	86(1)	94(1)	119(1)	177(3)	1.77(3)	1.75(3)

[a] Average value

[b] 3-fold symmetry crystallographically imposed on molecule

[c] *Bond data obtained from the Cambridge Crystallographic Data Base*

[d] Fe-C-O(eq): 162.8°, Fe-C-O(ax): 180.0°

[e] Fe-C-O(eq): 176.8°, Fe-C-O(ax): 180.0°

[f] av. Fe-C-O(eq): 171.9(4)°, Fe-C-O(ax): 177.2(4)°

[g] $(OC)_4Fe(PMe_2)_2Fe(CO)_4$

2) Steric factors

a) Intramolecular interactions, especially repulsions between phenyl groups on L with equatorial carbonyls.[113,114,119]

b) Short intermolecular contacts.[113]

3) Electronic factors

i) Rehybridization of orbitals of Fe resulting in a decrease in repulsions between electron pairs of Fe and L, and a concomitant enhancement of overlap of filled Fe-orbitals with acceptor-orbitals of the equatorial CO ligands. The new hybrid orbitals occupied by non-bonding electrons would be pointing away from the axial position of the tbp occupied by CO.[129,130]

ii) An electron density donation from L σ_z orbitals to eqCO 2 π_y orbitals. A bending of eqCO ligands towards L would be expected to increase Fe-COeq orbital overlap.[131]

iii) Valence-shell electron-pair repulsions: An increase in the angle between multiple-bond character Fe-CO bonds, and the decrease in the angle between the single Fe-L bond and the Fe-COeq bonds would decrease repulsions between the bonding electrons and so stabilize the molecule[129] (applies to cases where the Fe-L bond is of single-bond character.)

9.2.3 Fe-CO bond length trends

In the parent complex, $Fe(CO)_5$, the Fe-COax bonds (av. 1.806(5)Å) are significantly shorter than the Fe-COeq bonds (av. 1.833(4)Å).[188] The electronic rationale for this effect of shorter *M-Lax bonds than M-Leq bonds in* d^8 tbp $M(L)_5$ complexes has been discussed in Section 9.1. However, for substituted complexes of the type ax-$LFe(CO)_4$, the effect of L on the Fe-CO bond lengths must be considered. The nature of this effect depends on the electronic properties of the ligand L relative to CO. The two axial ligands compete for the two Fe d_π orbitals.[117b,132] When L is a poorer π-acceptor than CO, metal back-bonding to

the axial CO will increase, resulting in a shorter Fe-COax bond.[116,117b] It has been shown from core electron-binding energies and valence-orbital ionization potentials[133] that for ax-$LFe(CO)_4$ complexes, where L is a poorer π-acceptor than CO, the Fe dx^2-y^2, dxy orbitals do not interact with the axial ligands, whereas the Fe dxz, dyz orbitals are destabilized by ca. 0.3ev (relative to $Fe(CO)_5$) because of the loss of the strongly back-bonding CO ligand.

The Fe-CO bond length data in Table 9.2 for ax-$LFe(CO)_4$ complexes shows two trends:-

1) The Fe-C bond lengths in the substituted complexes are generally shorter than those in $Fe(CO)_5$ itself. This trend is rationalized in terms of the replacement of one CC group by a poorer π-acceptor ligand L increasing the amount of π-bonding to the remaining four CO groups and thus shortening the Fe-CO bond lengths.[166]

2) For the majority of ax-$LFe(CO)_4$ complexes, the Fe-COax *bond length is shorter than the Fe-COeq* bond lengths. For ligands L which are poorer π-acceptors than CO, this is expected in terms of the axial trans-effect (vide supra).

In the case of eq-$[(PPh_2)_2PhP]Fe(CO)_4$, where no axial trans effect operates, the Fe-COeq and Fe-COax bond lengths are equal within experimental error (av. values of 178.0(6) and 178.8(6)[c] respectively[116]), but shorter than those found in $Fe(CO)_5$ (vide supra).

However, Cotton et al[166] have pointed out that caution must be exercized in interpreting Fe-CO bond length differences as significant, especially where the differences are small, as the data have generally not been corrected for thermal motion. For instance, a greater thermal motion in the axial carbonyl and correction for thermal motion, would lengthen the Fe-COax bond more than the Fe-COeq bonds.

9.2.4 Fe-C-O bond angles

In these $LFe(CO)_4$ complexes, the carbonyl ligands

co-ordinate in an essentially linear manner, with Fe-C-O bond angles generally in the range 175 - 179°. (Table 9.2). Kettle[19] has shown that ca. 5° deviations from linearity are expected for $M(CO)_n$ (n = 2-4) groups, due to different occupation of the two anti-bonding π^* orbitals on a carbonyl ligand. This applies to other ligands electronically similar to CO, eg. CN. (In $[(NC)Fe(CO)_4]^-$, the Fe-C-N bond angle is found to be 178.0(7)°[97]). The reason for the different Fe-C-O angles within the $Fe(CO)_4$ group must lie in crystal packing forces.[19]

The larger deviations from linearity of the *sqFe*-C-O bonds (av. Fe-C-O(eq): 171.9(4)°) than the axFe-C-O bond (*Fe-C-O(ax): 177.2(4)°*) *in* $(^tBu_3P)Fe(CO)_4$,[114] could be due to steric repulsions between the eq CO ligands and the ^tBu-*groups of the* bulky phosphine ligand (Tolman cone angle[81a] for $^tBu_3P$: 182°). A similar effect is observed with the bulky $AsMe_3$ and $SbMe_3$ ligands[112] (see footnotes d and e to Table 9.2). Deviations from ideal geometry could also be due to crystal packing forces.[98a]

9.3 The Geometry of $Fe(CO)_3(L)_2$ Structures

9.3.1 *Geometry* - tbp, distorted tbp, spy

For penta co-ordinate complexes, there are two basic geometry types viz. tbp and spy. *These two geometries may* differ little in energy,[98,87,125] and the actual arrangement may *lie somewhere between the two ideal* configurations.[126] As mentioned previously, for d^0 $M(L)_5$ complexes, a tbp *geometry is predicted on* electronic grounds.[98,101]

Table 9.3 lists complexes of the type $Fe(CO)_3(L)_2$ (excluding those complexes where $(L)_2$ = diene ligand,(eg. 1,2-bis(2|6'-di-isopropylphenyliminoethane[133]) which determines the substitution geometry) for which X-ray Crystal and Molecular structures have been determined. With the exception of the case where $(L)_2$ is the bidentate phosphine ligand $Ph_2PCH_2PPh_2$,[114] all the complexes have the expected tbp geometry.

The exception, the complex $Fe(CO)_3(Ph_2PCH_2PPh_2)$,[114] has a geometry intermediate between tbp and spy, and can be

viewed either as a distorted tbp with the P-atoms co-ordinating in *axial and equatorial sites, or as a distorted* spy in which both P-atoms occupy cis-basal sites. Regarding the structure as a severely distorted tbp, the axP-Fe-Peq angle is 73.5(1)Å, a significant deviation from the ideal 90°. This is a consequence of the steric strain inherent in the $Ph_2PCH_2PPh_2$ ligand itself. The distorted geometry is a consequence of the bidentate nature, and small bite size of the $Ph_2PCH_2PPh_2$ ligand.

The symmetrically substituted biphosphine complexes, diax-$[(R_3P)_2Fe(CO)_3]$ (R = OCH_3,[116] NMe_2[117]), have essentially undistorted tbp geometry. However, the complex diax-$\{[(3,5\text{-}Me_2C_6H_3O)_3P]Fe(CO)_3(CHO)\}$[117] has a slightly distorted tbp geometry, with av. OC-Fe-CHO angle of 86.3(2)° and av. OC-Fe-P angle of 93.3(1)°. This bending of the equatorial CO ligands towards the axial CHO^- group is probably a consequence of steric repulsions between the phenyl rings of the bulky phosphate ligand and the equatorial CO ligands. In ax-eq$[Me_3As(C_6H_4)AsMe_3]Fe(CO)_3$,[118] the equatorial CO ligands bend towards the ax-As atom (axAs-Fe-COeq: 89°, axOC-Fe-COeq: 92°). This is probably due to electronic factors[94] (see Section 9.2.2.)

9.3.2 Ligand site preferences - ax-ax, ax-eq, eq-eq

On the basis of symmetry and overlap arguments, Rossi and Hoffmann[101] have shown that, for d^8 tbp $M(L)_5$ complexes, the stronger σ-donor ligand would preferentially occupy an axial site, while the stronger π-acceptor ligand would be found in an equatorial position. Hence a ligand L that is a stronger σ-donor, and/or weaker π-acceptor, would be expected on electronic grounds to occupy an axial site in tbp $Fe(CO)_3(L)_2$ complexes.

In Table 9.3, the sites occupied by the ligands L and L' in the complexes $Fe(CO)_3LL'$ are given. For diphosphine derivatives (L = L' = $P(OCH)_3$,[116] $P(NMe)_3$[117]), the phosphine ligands, which are weaker π-acceptors than CO,[93a] occupy the two axial sites, with the more strongly π-accepting carbonyls in the equatorial positions, where

TABLE 9.3: X-Ray Crystal Structures of $Fe(CO)_3LL'$ Structures

Ligand L	Ligand L'	Geometry[a]	Site occupied by ligand[b] L	L'	Space Group, Z	Reference
$P(OCH_3)_3$	$P(OCH_3)_3$	tbp	ax	ax	C2/c, 4	136
$P(NMe_2)_3$	$P(NMe_2)_3$	tbp	ax	ax	$P2_1/c$,4	117
$(3,5\text{-}Me_2C_6H_3O)_3P$	$(CHO)^-$	tbp	ax	ax	C2/c,8	137
$Me_3As(C_6H_4)AsMe_3$ [c]			ax	eq	Pnma,4 [d]	138
PPh_3	cis-$[CH_3CH_2OC(O)C]_2$	tbp	ax	eq	$P\bar{1}$,2	139
PPh_3	trans-$[CH_3CH_2OC(O)C]_2$	tbp	eq	eq	C2/c,8	139
PPh_3	CH_2CHCO_2Me	tbp	ax	eq	$P\bar{1}$,2	140
$Ph_2PCH_2PPh_2$ [c]		tbp	ax	eq	$P\bar{1}$,2	134
		/spy [e]	bs	bs		

[a] tbp = trigonal bipyramidal, spy = square pyramidal

[b] In tbp geometry, ax = axial, eq = equatorial
In spy geometry, ap = apical, bs = basal

[c] Bidentate ligand

[d] $(Me_3As(C_6H_4)AsMe_3)Fe(CO)_3$ molecule posseses crystallographic mirror (m) symmetry

[e] Geometry intermediate between tbp and spy.

TABLE 9.4 Geometric data for $Fe(CO)_3LL'$ structures
(Bond angles in degrees, bond lengths in Å)

Complex	Fe-COax	Fe-COeq	P-C-O[a]
diax[$(CH_3O)_3P]_2Fe(CO)_3$	~	1.761(6)[a]	179.4(4)
diax[$(Me_2N)_3P]_2Fe(CO)_3$	~	1.758(3)[a]	177.6(3)
diax[(3,5-$Me_2C_6H_3O)_3P$]$Fe(CO)_3(CHO)^-$	~	1.760(5)[a]	177.1[b]
ax-eq($Me_3As(C_6H_4$)$AsMe_3$)$Fe(CO)_3$	1.81	1.68	174.0[b,c]
ax-eq(Ph_3P)(cis-[$CH_3CH_2OC(O)C]_2Fe(CO)_3$	1.796(6)	1.786(6)[a]	175.2(5)
eq-eq(Ph_3P)(trans-[$CH_3CH_2OC(O)C]_2$)$Fe(CO)_3$	1.803(5)[a]	1.766(5)	176.0(5)
ax-eq(Ph_3P)(CH_2CHCO_2Me)$Fe(CO)_3$	1.784(2)	1.782(2)[a]	176.6(2)
ax-eq(Ph_2PCH_2 $\cdot\cdot_2$)$Fe(CO)_3$	1.74(1)	1.77(1)[a]	177(1)

[a] average value

[b] Bond data obtained from the Cambridge Crystallographic Data Base

[c] Fe-C-O(eq): 171.6°, Fe-C-O(ax): 178.9°

[d] Regarded as distorted tbp

backbonding to the metal atom can be optimized.[104] Diaxial substitution is also observed for the phosphite-formyl complex, $[(3,5\text{-}Me_2C_6H_3O)_3P]Fe(CO)_3(CHO)^-$.[137]

The bidentate arsine ligand, $(L)_2 = Me_3As(C_6H_4)\text{-}AsMe_3$,[138] co-ordinates to the Fe-atom in an ax-eq fashion. However, this co-ordination geometry is dictated by the steric restrains inherent in the bidentate ligand, reflected also in the axAs-Fe-Aseq angle of 84°. Hence only one As-atom is able to occupy the electronically favoured axial position. The subjugation of electronic factors to the spatial limitations of bidentate ligands is also demonstrated by the bidentate phosphine ligand, $(L)_2 = Ph_2PCH_2PPh_2$,[124] where P-atoms again co-ordinate ax-eq in a distorted tbp. The severe distortions to the geometry, with an axP-Fe-Peq angle of only 73.5(1)Å, reflect the steric strain of this bidentate ligand.

The pair of related phosphine-olefin complexes, $L = PPh_3$, $L' =$ <u>cis</u> or <u>trans</u> isomer of $CH_3CH_2OC{=}CCOCH_2CH_3$,[139] provides an illustration of steric vs electronic control of the ligand site preference in tbp $Fe(CO)_3LL'$ complexes. In accordance with the electronic predictions of Rossi and Hoffmann,[101] the olefinic ligand should occupy an equatorial site with the carbon-carbon double bond approximately in the equatorial plane, as such a ligand arrangement provides for optimum π-backbonding interaction. This mode of co-ordination is indeed found for both the above isomeric olefin ligands.[139]

Further, PR_3, being a stronger σ-donor and weaker π-acceptor[12a,144] than CO, should on electronic grounds[101] occupy an axial site. In the case of $Fe(CO)_3(PPh_3)(\underline{cis}\text{-}[CH_3CH_2OC(O)C]_2)$, the phosphine ligand does indeed occupy the electronically favoured axial position.[139] However, in the case of the $Fe(CO)_3(PPh_3)(\underline{trans}\text{-}[CH_3CH_2OC(O)C]_2)$ complex, the phosphine co-ordinates in the electronically less favoured equatorial site.[139] This unexpected equatorial disposition of the phosphine ligand has been ascribed to the steric hinderance caused by the <u>trans</u>-substituents of the olefin at the axial sites of the trigonal bipyramid.[139] The bulky PPh_3 ligand (Tolman cone

angle[85] for PPh_3: 145°) thus prefers to co-ordinate at an electronically less favoured equatorial site. In this instance, steric effects dominate the electronic site preference in determining the final ligand arrangement. Further, in both the $Fe(CO)_3(PPh_3)$(olefin) complexes, the olefin substituents are directed towards the other side of the molecule away from the bulky PPh_3 ligand, in order to minimize steric repulsions in the compounds.[139]

In the complex $Fe(CO)_3(PPh_3)(CH_2{=}CHCO_2Me)$,[140] the phosphine ligand occupies an axial site, while the olefin co-ordinates equatorially, as expected on electronic grounds.[101,139] The co-ordination plane of the olefinic ligand is tilted by 11.2° from the equatorial plane of the iron atom, and the carbomethoxy group is directed away from the triphenyl phosphine ligand, a reflection of the influence of steric factors on structure.

9.3.3 Fe-CO bond length trends

Substitution of an axial CO by a poorer π-accepting ligand in $Fe(CO)_5$, results in a shortening of the Fe-CO bonds in $Fe(CO)_4L$ relative to $Fe(CO)_5$,[106] and a greater shortening of the axial Fe-CO bond trans to L than of the Fe-COeq bonds[117b] (axial trans effect). As would thus be anticipated, upon replacement of one CO ligand by a strongly σ-donating/weakly π-accepting ligand, such as PR_3, additional CO replacement becomes more difficult.[134] However, this second substitution, once achieved, would be expected to result in a further shortening of the remaining Fe-COeq bonds.[117b] This is indeed observed for the diax complexes $Fe(CO)_3LL'$ (L = L' = $P(OCH_3)_3$,[138] $P(NMe_3)_3$;[117] L = $P(OC_6H_3Me_2\text{-}3,5)_3$, L' = CHO^-[137]) (see Table 9.4).

Rossi and Hoffmann[86] have evaluated the relative strength of axial and equatorial bonds in d^8 tbp complexes. Their conclusions were that M-L σ-bonding results in stronger axial bonds, π-donation will weaken metal-ligand bonds, but greater weakening of the equatorial bonds is expected, while π-acceptor ligands strengthen metal-ligand bonding, especially when the ligand occupies an equatorial site. Hence if ligands are π-donors, σ-and π- bonding

effects co-operate, resulting in strong axial and weak equatorial bonds. However, for good π-acceptors, the σ- and π-bonding effects oppose each other, although the σ-effect seems to dominate, with longer equatorial bonds found. As expected, these conclusions parallel the site preference arguments.

Table 9.4 gives Fe-CO bond length data for the $Fe(CO)_3LL'$ complexes. For the complex ax-eq($Me_2As(C_6H_4)$-$AsMe_2$)$Fe(CO)_3$,[138] the short Fe-COeq bond of 1.68Å reflects the increased back-bonding to the two remaining carbonyl ligands on equatorial substitution of a *weakly π-accepting arsine* ligand. A similar shortening of the sole remaining Fe-COeq bond (1.766(5)Å) *is observed in the complex* eq-eq(Ph_3P)-[trans-$(CH_3CH_2OC(O)C)_2$]$Fe(CO)_3$,[139] where the weakly π-*accepting phosphine* ligand occupies an equatorial site. In the related complex, ax-eq(Ph_3P)[cis-$(CH_3CH_2OC(O)C)_2$]-$Fe(CO)_3$,[139] the Fe-COax bond (1.795(6)Å) would be expected to be similar to that in the mono-substituted ax-(Ph_3P)-$Fe(CO)_4$[134] (1.795(4)Å). The shorter Fe-COeq than Fe-COax bonds in both these olefinic complexes, reflects the stronger bonding of the equatorial carbonyls to Fe, owing to the equatorial substitution of an olefinic ligand, which is generally a poorer π-acceptor than CO.[139] The Fe-COax (1.784(2)Å) and Fe-COeq (1.780(2) and 1.783(2)Å) bond lengths in the related complex, ax-eq(Ph_3P)CH_2CHCO_2Me)$Fe(CO)_3$,[146] are, however, equal within experimental error.

9.3.4 Fe-C-O bond angles

The Fe-C-O bond angles for the $Fe(CO)_3L_2$ complexes are given in Table 9.4. In accordance with Kettle's[28] predictions of near-linearity of M-C-O bonds for $M(CO)_3$ fragments, the Fe-C-O bond angles are in the range 175-179°. Variations of Fe-C-O angles within an $Fe(CO)_3$ group are ascribed to the influence of crystal packing forces.[9] Crystal packing forces could also account for *minor deviations from* ideal tbp geometry. Note that for ax-eq($Me_2As(C_6H_4)AsMe_2$)-$Fe(CO)_3$ [28] *the axFe-C-O bond angle is essentially* linear (178.9°), but the eqFe-C-O bond angle is only 171.6°. This *deviation from linearity* probably arises from steric

repulsions between the eq carbonyls and the bulky bidentate arsine ligand.

9.4 The Crystal and Molecular Structure of $Fe(CO)_2(CNMe)_2$

9.4.1 Anomalous Infra Red Data

On the basis of the electronic predictions of Rossi and Hoffmann,[161] the diisonitrile complex $Fe(CO)_3(CNR)_2$ would be expected to have tbp geometry, with the isonitrile ligands, being stronger σ-donors, but weaker π-acceptors than CO,[43] occupying the axial sites. Such a diax-$(RNC)_2$-$Fe(CO)_3$ tbp geometry would have D_{3h} molecular symmetry.[161]

The infra red spectrum of this ligand arrangement is predicted from group theory analysis to give one ν(CN) and one ν(CO) stretching absorption.[161] However, complexes of the type $Fe(CO)_3(CNR)_2$ (R = Me,[161-2] C_6H_{11},[162] Bu^t,[161-2] CH_2Ph,[162] Ph,[162] $C_6H_3Me_2$-2,6,[162] $C_6H_2Me_3$-2,4,6,[162] C_2H_5[161]) typically give one ν(CN) and two ν(CO) adsorption in various solvents ($CHCl_3$,[161-2] CS,[161] CCl_4[161]). For example, the compound $Fe(CO)_3(CNMe)_2$ gave one ν(CN) and more than one ν(CO) adsorptions in both solution and the solid state. [IR($CHCl_3$ solution),[162] ν(CN): 2160 cm^{-1}, ν(CO): 2000, 1922 cm^{-1}; IR(KBr), ν(CN): 2182(s) cm^{-1}; ν(CO): 2026(w), 1935(sh), 1919(s), 1897(s), 1878(sh) cm^{-1} (s = strong, w = weak, sh = shoulder)].

A similar phenomenon of anomalous IR data has been observed for the bisphosphite complex diax-$[(Me_3O)_3P]_2Fe(CO)_3$.[162a] Bisphosphine complexes of the type $Fe(CO)_3(PR_3)_2$ would also be predicted to give only one ν(CO) IR absorption. This is observed for $Fe(CO)_3(PR_3)_2$ (R = Ph,[161,162a] C_2H_5[162]) complexes. (Note that the diisonitrile complex $Fe(CO)_3(CNC_2H_5)_2$ (in n-hexadecane, $C_{16}H_{34}$[162b]) has been reported to give only one ν(CO) absorption also, in contrast to the results of other studies[161-2] (vide supra) on this and related complexes). However, the complex $Fe(CO)_3(P(OMe)_3)_2$ gives three ν(CO) adsorptions: the E' band splits into two bands, and there is also a third band assigned as A_1',[163] which is not expected to be infra red active in the D_{3h} symmetry.[161] A crystal structure determination of the $Fe(CO)_3\{P(OMe)_3\}_2$ complex has been performed.[114] The geometry is tbp with the

phosphite ligands in axial sites. The anomalous IR data has been ascribed to a lowering of the symmetry of the molecule from D_{3h} due to internal asymmetry of the $P(OMe)_3$ ligands.[161] The three P-O bonds of $P(OMe)_3$ are not equivalent, probably due to an asymmetrical configuration of the three $O-CH_3$ groups. A feeble activation of the A_1' band results from the vibration of one of the CO groups in $Fe(CO)_3(P(OMe)_3)_2$ being different from that of the other two, owing to interaction of one CO with a phosphite ligand.[161b]

A crystal structure determination of the complex $Fe(CO)_3(CNMe)_2$ was thus undertaken in order to determine whether the anomalous IR data (vide supra) could be ascribed to a deviation from idealized D_{3h} symmetry, due to possible non-linearity (the result of electronic or steric effects) of the C-N-C unit bound to Fe, which could allow the A_1' band to gain a little intensity.[161]

The precedent for the above proposition was the X-ray molecular structure of the penta-isonitrile complex, $Fe(CNBu^t)_5$,[95] which shows marked deviations from D_{3h} symmetry of idealized tbp geometry, with substantial bending of the isonitrile ligands at the N-atoms (mean C-N-C angle 134(2)°). This non-linearity of the isonitrile ligands has been attributed to extensive back-bonding of Fe(3d) electrons to the $(^{\sim}sN)\pi^*$ antibonding orbitals.[95] In addition, the small size of the methylisonitrile ligand ("fan-shaped" angle[44] for MeNC: 52°(wideness), 52° (thickness)) further limits the possibility that the anomalous IR data results from steric effects, eg. unexpected substitution geometry![39]

9.4.2. Discussion of the Structure

The geometry of the $Fe(CO)_3(CNMe)_2$ molecule is illustrated in Figure 9.1, which also shows the numbering scheme used in the analysis. $Fe(CO)_3(CNMe)_2$ crystallizes in the monoclinic space group $P2_1/c$, with $Z = 4$. A view of the unit cell, looking down the b-axis, is shown in Figure 9.2. Bond lengths and bond angles are given in Tables 9.5 and 9.6 respectively.

As predicted,[161] the geometry of the $Fe(CO)_3(CNMe)_2$ complex is tbp, with the methylisonitrile ligands in axial

positions. No distortions to the tbp geometry are apparent. The C-Fe-C angles are close to the ideal values (mean OC-Fe-CN: 90.0(3)°, mean OC-Fe-CO: 120.0(4)°, and NC-Fe-CN: 177.1(3)°). Further, the CO and CNMe ligands are linearly co-ordinated to the central Fe atom. The slight deviations from linearity are in accordance with Kettle's [39] predictions for $M(CR)_n$ ($R = O, N$, $n = 2,3$) units (mean Fe-C-O and Fe-C-N angles 178.6(8) and 177.5(6)° respectively). The isonitrile ligands (mean C-N-C: 177.2(9)°) are also linear.[41b]

Hence the anomalous IR data cannot be ascribed to a lowering of the idealized D_{3h} symmetry due to non-linearity of the isonitrile ligands. However, the D_{3h} symmetry could conceivably be lowered due to an internal asymmetry in the isonitrile ligands, similar to that observed for the phosphite ligands of diax[$Fe(CO)_3(P(OMe)_3)_2$].[134, 143] For the $CNCH_3$ ligand, the uncertainty in the positions of the hydrogen atoms does not allow for a meaningful analysis of their relative orientations. Other explanations could account for the anomalous IR data. For example, Cotton and Parish [41] have proposed that the second weak $\nu(CO)$ band could be a combination or overtone band which has gained intensity by Fermi resonance with the strong *fundamental*.

The Fe-CO bond lengths in diax[$Fe(CO)_3(CNMe)_2$] (av. 1.785(8)Å) are shorter than those in the parent carbonyl, $Fe(CO)_5$ (av. Fe-COax: 1.806(5)Å and av. Fe-COeq: 1.833(4)Å [100]), but slightly longer than the Fe-CO bonds in diax[$(Me_3N)_3P]_2Fe(CO)_3$ [117] and diax[$(CH_3O)_3P]_2Fe(CO)_3$ [139] (av. values of 1.759(3) and 1.761(6)Å respectively). These trends are understandable in terms of the electronic nature of isonitrile ligands, which are better π-acceptors than phosphines, but poorer π-acceptors than CO.[39a]

The Fe-CNR bond length found in the only other structure of the type $Fe(CO)_{5-n}(CNR)_n$ ($n = 1-5$), $Fe(CNBu^t)_5$[39] (av. 1.824(8)Å), is much shorter than the mean Fe-CNMe distance of 1.867(8)Å in $Fe(CO)_3(CNMe)_2$, consistent with the increased electron density on the Fe atom in the $Fe(CNBu^t)_5$ complex. In the latter structure, however, the isonitrile ligands deviate markedly from linearity, indicative of *extensive back-bonding*.[39]

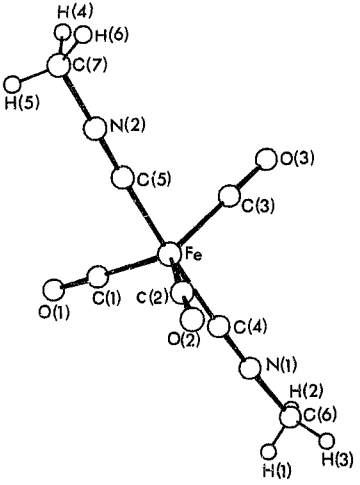


Figure 9.1: An ORTEP[13] view of the $Fe(CO)_3(CNMe)_2$ molecule, showing the numbering system used.

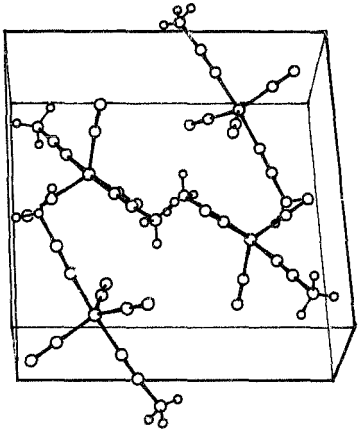


Figure 9.2: An ORTEP[43] view of the unit cell of $Fe(CO)_3(CNMe)_2$, looking down the b-axis.

TABLE 9.5: Bond lengths (Å) for $Fe(CO)_3(CNMe)_2$

Fe-C(1)	1.775(8)	C(1)-O(1)	1.150(9)
Fe-C(2)	1.790(8)	C(2)-O(2)	1.138(8)
Fe-C(3)	1.791(9)	C(3)-O(3)	1.144(9)
Fe-C(4)	1.873(8)	C(4)-N(1)	1.148(8)
Fe-C(5)	1.860(8)	C(5)-N(2)	1.150(8)
N(1)-C(6)	1.416(10)	N(2)-C(7)	1.430(11)
C(6)-H(1)	0.83(6)	C(7)-H(4)	0.98(11)
C(6)-H(2)	0.89(9)	C(7)-H(5)	0.93(13)
C(6)-H(3)	1.05(12)	C(7)-H(6)	1.04(12)

TABLE 9.6: Bond angles (°) for $Fe(CO)_3(CNMe)_2$

Fe-C(1)-O(1)	178.4(8)	C(4)-N(1)-C(6)	176.3(8)
Fe-C(2)-O(2)	178.3(7)	C(5)-N(2)-C(7)	178.1(9)
Fe-C(3)-O(3)	179.2(8)	N(1)-C(6)-H(1)	108(5)
Fe-C(4)-N(1)	178.0(6)	N(1)-C(6)-H(2)	109(6)
Fe-C(5)-N(2)	176.9(6)	N(1)-C(6)-H(3)	117(6)
C(1)-Fe-C(4)	90.7(3)	N(2)-C(7)-H(4)	103(6)
C(2)-Fe-C(4)	89.5(3)	N(2)-C(7)-H(5)	100(8)
C(3)-Fe-C(4)	89.1(3)	N(2)-C(7)-H(6)	118(7)
C(1)-Fe-C(5)	92.2(3)	H(1)-C(6)-H(2)	93(7)
C(2)-Fe-C(5)	89.2(3)	H(1)-C(6)-H(3)	93(8)
C(3)-Fe-C(5)	89.5(3)	H(2)-C(6)-H(3)	129(8)
C(4)-Fe-C(5)	177.1(3)	H(4)-C(7)-H(5)	114(10)
C(1)-Fe-C(2)	119.6(4)	H(4)-C(7)-H(6)	102(9)
C(1)-Fe-C(3)	118.2(4)	H(5)-C(7)-H(6)	119(10)
C(2)-Fe-C(3)	122.2(4)		

9.5 EXPERIMENTAL

9.5.1 Data collection

The compound $Fe(CO)_3(CNMe)_2$ was obtained from the $CoCl_2.2H_2O$ catalysed reaction between $Fe(CO)_5$ and MeNC.[1,2] Since the compound was both air and light sensitive, yellow crystals were grown under nitrogen in the dark from a benzene-hexane solution at 20°C.

Preliminary investigations by standard Weissenberg and precession photography established the monoclinic space group $P2_1/c$ from the absences $h0\ell$, $\ell = 2n + 1$, and $0k0$, $k = 2n + 1$. *Refined cell constants* were obtained during data collection on a Philips PW1100 four-circle diffractometer, using graphite monochromated MoKα radiation ($\lambda = 0.7107\text{Å}$) at room temperature (20°C). Lorentz and polarization corrections were applied, but corrections for absorption were omitted as the linear absorption coefficient is only 16.32 cm^{-1}. No special precautions were taken during data collection, and crystal deterioration was not observed. Crystal data and details of the structure analysis are summarized in Table 9.7.

9.5.2 Structure Solution and Refinement

Structure analysis and refinement were carried out using the program SHELX82[3a]. Initial co-ordinates for the iron atom were derived from a Patterson synthesis and difference Fourier syntheses yielded positions, first for all 13 non-hydrogen atoms, and after least-squares refinement of these, also for the 6 hydrogen atoms. Positional parameters for all atoms, and anisotropic temperature factors for non-hydrogen atoms, were refined by *full-matrix least-squares analyses*. Least-squares refinement was considered complete when all parameter shifts were less than 0.5σ. At this stage, the conventional $R = 0.0680$. Unit weights were used. Scattering factors for Fe(0) were taken from "International Tables for X-ray Crystallography,"[3b] and anomalous dispersion corrections[3c] for iron were made.

Fractional atomic co-ordinates of all atoms, and anisotropic thermal parameters for the non-hydrogen atoms, are given in Tables 9.8 and 9.9 respectively. A listing of the Structure Factors is to be found in Appendix D.

TABLE 9.7: Crystal data and details of structural analysis for $Fe(CO)_3(CNMe)_2$

Formula	$FeC_7H_6N_2O_3$
Mr	221.99
Crystal dimensions (mm)	0.19 x 0.19 x 0.14
Space Group	$P2_1/c$ (No. 14)
a (Å)	12.451(6)
b (Å)	6.564(3)
c (Å)	12.087(6)
β (°)	92.45(3)
U (Å^3)	986.95
Z	4
F(000)	447.96
Dc (gcm^{-3})	1.49
μ (cm^{-1})	16.32
λ (Å)	MoKα (0.7107)
Scan mode	$\omega/2\theta$
Range (°)	$3 \leq \theta \leq 23$
Scan width (°)	1.60
Scan speed (° sec^{-1})	0.053
Range of hkℓ	$\pm h$, $+k$, $+\ell$
Measured intensities	1517
Unique reflections	1335
Internal consistency R-index	0.0000
R (R = Rw)	0.0680

TABLE 9.8(a): Fractional atomic co-ordinates for the non-hydrogen atoms of $Fe(CO)_3(CNMe)_2$

Atom	x/a	y/b	z/c
Fe	0.2457(1)	0.3155(2)	0.5729(1)
N(1)	0.3692(5)	0.0696(10)	0.4097(5)
N(2)	0.1393(5)	0.5622(10)	0.7472(5)
O(1)	0.0518(5)	0.3058(11)	0.4276(5)
O(2)	0.2863(6)	-0.0062(10)	0.7371(5)
O(3)	0.3977(5)	0.6515(10)	0.5450(6)
C(1)	0.1278(7)	0.3069(12)	0.4852(6)
C(2)	0.2693(6)	0.1199(11)	0.6743(6)
C(3)	0.3384(7)	0.5203(13)	0.5550(7)
C(4)	0.3206(5)	0.1614(11)	0.4710(5)
C(5)	0.1776(5)	0.4692(11)	0.6785(6)
C(6)	0.4352(8)	-0.0411(19)	0.3385(8)
C(7)	0.899(11)	0.6818(20)	0.8298(10)

TABLE 9.8(b): Fractional atomic co-ordinates and isotropic temperature factors for the hydrogen atoms of $Fe(CO)_3(CNMe)_2$

Atom	x/a	y/b	c/z	U(Å²)
H(1)	0.399(5)	-0.137(10)	0.311(5)	0.05(2)
H(2)	0.438(7)	0.025(14)	0.274(8)	0.09(3)
H(3)	0.492(9)	-0.139(20)	0.376(9)	0.16(5)
H(4)	0.091(8)	0.820(18)	0.799(8)	0.12(4)
H(5)	0.022(10)	0.621(21)	0.829(10)	0.16(6)
H(6)	0.132(9)	0.702(19)	0.905(10)	0.16(5)

TABLE 9.9: Anisotropic temperature factors ($Å^2$) for the non-hydrogen atoms of $Fe(CO)_3(CNMe)_2$

Atom	U11	U22	U33	U23	U13	U12
Fe	0.0457(6)	0.0461(6)	0.0469(6)	-0.006(5)	0.0050(4)	0.0026(5)
N(1)	0.060(4)	0.066(4)	0.047(3)	-0.006(3)	0.005(3)	0.014(3)
N(2)	0.060(4)	0.062(4)	0.059(4)	-0.008(3)	0.009(3)	0.003(3)
O(1)	0.069(4)	0.117(6)	0.086(4)	-0.021(4)	-0.027(3)	0.024(4)
O(2)	0.069(4)	0.069(4)	0.082(4)	0.026(4)	0.025(4)	0.023(4)
O(3)	0.120(5)	0.073(4)	0.115(5)	-0.003(4)	0.039(4)	-0.038(4)
C(1)	0.069(5)	0.056(5)	0.056(4)	-0.002(4)	0.006(4)	0.008(4)
C(2)	0.065(5)	0.045(4)	0.055(4)	0.003(4)	0.015(4)	0.004(4)
C(3)	0.069(5)	0.056(5)	0.068(5)	-0.004(4)	0.016(4)	-0.003(4)
C(4)	0.044(4)	0.060(5)	0.040(4)	0.008(3)	-0.006(3)	-0.004(3)
C(5)	0.046(4)	0.051(4)	0.061(4)	-0.001(4)	-0.003(3)	0.001(3)
C(6)	0.071(6)	0.087(7)	0.050(5)	-0.015(5)	0.010(4)	0.018(6)
C(7)	0.098(8)	0.079(8)	0.085(7)	-0.014(6)	0.025(6)	0.028(7)

X. Derivatives of dirhenium decacarbonyl - a Survey of the Literature

10.1 Introduction

Since the preparation of dirhenium decacarbonyl, $Re_2(CO)_{10}$ by Hieber and Fuchs[145] in 1941, and that of dimanganese decacarbonyl, $Mn_2(CO)_{10}$, by Brimm, Lynch and Sesny[146] in 1954, these two metal carbonyl dimers have been extensively investigated. Studies of these molecules have been carried out by IR spectroscopy[146] (in the solid, in solution, and in the gas phase[148a]), Raman spectroscopy,[147] single-crystal Raman spectroscopy,[148] high-pressure solid state Raman spectroscopy,[149] IR and Raman spectroscopy on ^{13}CO enriched samples,[150] polarized IR, and visible and near ultra violet (UV) spectroscopy,[151] ^{17}O NMR spectroscopy ($Mn_2(CO)_{10}$),[152] electron spin resonance (ESR) spectroscopy,[153] mass spectroscopy (MS),[154] gas phase electron diffraction[155a-b] and single-crystal X-ray diffraction at room temperature,[157-8] and at 74K ($Mn_2(CO)_{10}$).[159]

An enormous chemistry of $M_2(CO)_{10}$ (M = Re, Mn) has been reported.[160] Notwithstanding the substantial numbers of chemical reactions that have been carried out on the $M_2(CO)_{10}$ dimers, no significant attempt has been made in the Literature to ascertain factors responsible for the stereochemistry of the products from the reaction of $M_2(CO)_{10}$ with ligand L.

A review of the reaction of $Re_2(CO)_{10}$ with ligands L, in which the products have the stoichiometry $Re_2(CO)_{10-n}(L)_n$ (n = 1-10) and the rhenium-rhenium bond remains intact, has thus been undertaken. In particular, emphasis is placed on a description of the stereochemistry of the resulting $Re_2(CO)_{10-n}(L)_n$ products.

The metal-metal bond in the $Re_2(CO)_{10}$ (or $Mn_2(CO)_{10}$) dimer may be cleaved by photolysis (eg. flash photolysis has been employed in kinetic studies of the homolysis of $M_2(CO)_{10}$ (M = Re, Mn), to give $M(CO)_5$ radicals[161]), or by chemical methods[162] such as the action of sodium metal, or of halogens. The latter methods have led to the synthesis

of a wide range of monometallic complexes, and for example, the area of rhenium pentacarbonyl chemistry has been the subject of extensive investigation in its own right. Reactions leading to monomeric rhenium species will however not be discussed here. (See Ref. 160 for a comprehensive review of this area of rhenium carbonyl chemistry.)

The review has been restricted to $Re_2(CO)_{10}$ derivatives. The metal-metal bond in $Re_2(CO)_{10}$ is stronger than that in $Mn_2(CO)_{10}$ (D(Re-Re): 128 kJ mol^{-1}, cf. D(Mn-Mn): 67 kJ mol^{-1};[161] although controversy surrounds the exact values of D(M-M) (see ch. XII), there is no dispute regarding the relative order, viz. D(Re-Re) > D(Mn-Mn)), and hence the possibility of metal-metal bond cleavage during reaction with L is less probable. On occasion, reference to $Mn_2(CO)_{10-n}(L)_n$ derivatives will, however, be made.

Further, $Re_2(CO)_{10}$ may also undergo reactions with itself, in the presence of ligand,[164] or with other metal carbonyl complexes, resulting in the formation of higher rhenium or mixed-metal clusters.[140] Such reactions, as well as those of the higher rhenium carbonyl clusters (some of which yield dimeric rhenium products,[143] often through decomposition reactions), as well as reactions of monomeric rhenium species which yield dimeric rhenium products,[165] will not be considered here.

Despite the tremendous growth in recent years in the use of single crystal X-ray diffraction methods in product characterization, relatively few X-ray crystal structures have been reported of dirhenium carbonyl complexes. This is due in part to the relatively few system studies reported in this area of rhenium carbonyl chemistry, owing to the synthetic difficulties often encountered (vide infra). In discussing the dirhenium carbonyl derivatives, emphasis will be placed on those complexes for which an X-ray crystal and molecular structure has been reported, and a discussion of the salient structural features of these complexes, as well as those of crystallographically studied dirhenium carbonyl complexes prepared by reaction of higher nuclear rhenium clusters,[143] or of rhenium monomers,[166] will be

given in ch. XIII.

The reactions of interest are usually simple carbonyl substitution reactions, in which one or more carbonyl (CO) ligands are replaced by donor *ligand(s)* L, viz.

$$Re_2(CO)_{10} + nL \rightarrow Re_2(CO)_{10-n}(L)_n + nCO \qquad (10.1)$$

Such reactions generally involve photochemical techniques, although there are examples of thermal reactions of $Re_2(CO)_{10}$ with L, or of *photochemically* prepared $Re_2(CO)_{10-n}(L)_n$ derivatives reacting with a ligand L'.[167-171] Such examples are relatively few, possibly due to difficulty often encountered *in effecting simple* carbonyl substitution reactions under mild thermal conditions (ΔH for CO dissociation, D(Re-CO) is calculated to be 195 kJ mol^{-1}[172]).

Trimethylamine-N-oxide induced reactions of $Re_2(CO)_{10}$ with L have been employed to circumvent this problem.[167,173-175] In this method, CO is oxidized to CO_2 under low temperature conditions, viz.

$$Re_2(CO)_{10} + nMe_3NO + nL \rightarrow Re_2(CO)_{10-n}(L)_n + nMe_3N + nCO_2 \qquad (10.2)$$

There have also been studies conducted in which CO ligands are converted into other ligand while attached to the metal. For instance, the anionic formyl complex $Li^+\{Re_2(CO)_9CHO\}^-$ *has been prepared* by the reaction of $LiEt_3BH$ with $Re_2(CO)_{10}$,[176] and the reaction of $Re_2(CO)_{10}$ with LiR in ether, and subsequent alkylation with $[R_3O]\{BF_4\}/H_2O$ yields the carbene *complex* $Re_2(CO)_9[C(OR')R]$.[177-8]

The $Re_2(CO)_{10}/L$ systems that have been reported in the literature will be discussed under ligand type L.

10.2 Reactions of $Re_2(CO)_{10}$ with phosphines (and arsines)

The reaction of $Re_2(CO)_{10}$ with phosphine ligand (eqn. 10.3) has received considerable attention.

$$Re_2(CO)_{10} + nPR_3 \rightarrow Re_2(CO)_{10-n}(PR_3)_n + nCO \; (n = 1,2) \qquad (10.3)$$

Uncertainty as to the mechanism of this reaction has *resulted in extensive* kinetic studies by several groups. Kinetic and mechanistic studies on this system will be

discussed in ch XV. The various synthetic methods employed to bring about reaction (10.3) are described below.

10.2.1 Thermal reactions

The reaction between $Re_2(CO)_{10}$ and a large excess of phosphine, PR_3 (PR_3 = PPh_3,[179-182] PEt_2Ph,[180] a $PMePh_2$,[164] $P(OPh)_3$,[183] $P(OC_6H_4Me\text{-}o)_3$,[165] $P(OC_6H_4Cl\text{-}p)_3$,[165] $P(C_6H_4Me\text{-}p)_3$,[165] $P(C_6H_{11})_3$[184]), in refluxing xylene gives $Re_2(CO)_8(PR_3)_2$. Long reaction times (15 to 50 h) are required, and product yields are generally poor (<30%), although some workers have reported good yields (75%) for PPh_3.[181] In most cases, the reaction yields more than one product, eg. mer-trans-$HRe(CO)_3(PR_3)_2$[180a,182,187] (PR_3 = Ph_3, $P(C_6H_4Me\text{-}p)_3$,[185] $P(C_6H_{11})_3$,[183] $P(OC_6H_4Me\text{-}o)_3$[187] (the latter originally incorretly identified as the metalated complex $[Re(CO)_3(PR_3)(PR_2\text{-}H)]$[185]). In the case of PR_3 = $P(C_6H_4Me\text{-}o)_3$,[185] only the metalated product $Re(CO)_4(PR_2\text{-}H)$ was obtained. The reaction with $P(OEt)_3$[185] yielded a mixture of seven products which were not characterized. With PR_3 = $P(OPh)_3$,[185] a trisubstituted product, $Re_2(CO)_7[P(OPh)_3]$ was also obtained. Chromatography is necessary to separate the products.[182-186]

The reaction between $Re_2(CO)_{10}$ and PMe_2Ph[183] in refluxing petroleum ether (80-100°C, 96 h) yielded $Re_2(CO)_8(PMe_2Ph)_2$ (46%), together with some $HRe(CO)_3(PMe_2Ph)_2$. If the reaction is conducted in n-hexane, and stopped after 5 h, $Re_2(CO)_9(PMe_2Ph)$ is obtained.[184]

The monosubstituted $Re_2(CO)_9(PPh_3)$ has been obtained (36%) from $Re_2(CO)_8(PPh_3)_2$ by passing a stream of CO through a solution of $Re_2(CO)_8(PPh_3)_2$ at 130°C for 30 h.[181] $Re_2(CO)_9(PPh_3)$ has also been obtained as the major product from the 1:1 reaction of $Re_2(CO)_{10}$ with PPh_3 in refluxing xylene.[168b]

Tetrasubstituted $[Re(CO)_3(PPh_3)_2]_2$ has been obtained from the reaction of $Re_2(CO)_{10}$ and PPh_3 (1:5 ratio) in refluxing xylene.[168b] However, in solution this product appears to exist as the monomeric $HRe(CO)_3(PPh_3)_2$.[185b,188] Heating $Re_2(CO)_{10}$ with the bidentate phosphine ligand, $Ph_2PCH_2CH_2PPh_2$ (1:4 ratio), in a sealed evacuated tube (240°C, 2 h) gave the tetrasubstituted complex, cis-

$[Re(CO)_3(Ph_2PCH_2CH_2PPh_2)_2]_2$ (20%).[186b]

10.2.2 Photochemical reactions

UV-irradiation of $Re_2(CO)_{10}$ and PR_3 in petroleum ether (PR_3 = PPh_3, PEt_2Ph[188a]) or cyclohexane (PR_3 = PPh_3[177b]) gave $Re_2(CO)_8(PR_3)_2$ in good yield (70-85%).

The photochemical reaction in cyclohexane between $Re_2(CO)_{10}$ and $PMePh_2$[184] (2:1 ratio) after 12 h of UV-irradiation, yielded $Re_2(CO)_8(PMePh_2)$ (4%), $Re_2(CO)_8(PMePh_2)_2$ (7%), two isomers of $Re_2(CO)_7(PMePh_2)_3$ (combined yield 10%) and a trace amount of $Re_4(CO)_{16}(PMePh_2)_6$. When a 1:1 ratio between $Re_2(CO)_{10}$ and phosphine was used, only the two isomers of $Re_2(CO)_7(PMePh_2)_3$ (combined yield 22%) (and some $HRe(CO)_3(PMePh_2)_2$)was obtained.[184]

Irradiation of $Re_2(CO)_{10}$ and PMe_2Ph[183] (1:2 ratio) in petroleum ether (60-80°C) for 6 h gave $Re_2(CO)_8(PMe_2Ph)_2$ (4%), and an isomer of $Re_2(CO)_7(PMe_2Ph)_3$ (13%), as well as trace amounts of $HRe(CO)_3(PMe_2Ph)_2$ and isomers of $Re(CO)_3(PMe_2Ph)_2Cl$. The same reaction in cyclohexane after 3 h yielded only $Re_2(CO)_7(PMe_2Ph)_3$ (13%) and a trace of an isomer of $Re(CO)_3(PMe_2Ph)_2Cl$.[183] (The chlorine compounds arise from the addition of chlorinated solvents to the crude reaction mixtures). The products were separated by chromatography.

The bisphosphine complex $Re_2(CO)_8(PHPh_2)_2$[185] was obtained from the 10 h photochemical reaction between $Re_2(CO)_{10}$ and $PHPh_2$ (1:2 ratio) in benzene solution.

The photochemical reaction under vacuum of $Re_2(CO)_{10}$ with a 5-fold excess of PPh_3, at 60°C,[186] yielded three isomers of $Re_2(CO)_7(PPh_3)_3$, assigned on the basis of ^{13}PNMR spectra as 1-ax,2,2-transdieq-$Re_2(CO)_2$-$(PPh_3)_3$ (35%), 1-eq,2,2-axeq-$Re_2(CO)_7(PPh_3)_3$ (15%), and 1-eq,2,2-transdieq-$Re_2(CO)_7(PPh_3)_3$ (5%), as well as $Re_2(CO)_8(PPh_3)_2$ (40%), and a trace amount of a rhenium compound tentatively identified as $Re_2(CO)_6(PPh_3)_4$.

High temperature ultraviolet methods yielded $M_2(CO)_{10-n}(PF_3)_n$ (M = Mn, Re; n = 1-4) species as unresolved mixtures of isomers.[150]

There has been one report of a reaction of $Re_2(CO)_{10}$ with an arsine. A 6 h UV-irradiation of $Re_2(CO)_{10}$ and $AsMe_2Ph$ (1:2 ratio[82]) in petroleum ether (40-60°C) yielded the bisarsine complex $Re_2(CO)_8(AsMe_2Ph)_2$ (9%).

10.2.3 Amine-oxide assisted reactions

An amine-oxide assisted reaction between $Re_2(CO)_{10}$ and PPh_3 has been employed in the synthesis under mild conditions (20°C, 2 h) of $Re_2(CO)_9(PPh_3)$ and $Re_2(CO)_8(PPh_3)_2$.[171]

viz. $$Re_2(CO)_{10} + nEt_3NC + nPPh_3 \rightarrow Re_2(CO)_{10-n}(PPh_3)n + nEt_3N + n(CO)_2 \qquad (10.4)$$

10.2.4. Comment on product formulations

From the above it can be seen that synthetic studies of the seemingly simple thermal and photochemical routes yield a wide range of dimeric and monomeric rhenium-phosphine complexes. However, as product characterization has relied almost entirely on IR spectroscopy, product formulation, and assignment of geometric isomers, may in certain cases be subject to question, especially in the absence of any X-ray crystallographic studies of $Re_2(CO)_{10-n}(PR_3)_n$ complexes. Notwithstanding the uncertainty, the data suggest that in the majority of cases monosubstitution is axial, and disubstitution diaxial. This aspect will be discussed in ch XV.

10.3 The reaction of $Re_2(CO)_{10}$ with ^{13}CO

The use of acetonitrile as a donor solvent in the reactions of $M_2(CO)_{10}$ (M = Re, Mn) and Me_3NO results in the complex $M_2(CO)_9(NCMe)$, from which the MeCN ligand can readily be displaced under mild thermal conditions. This method has been used in the synthesis of high purity ^{13}CO-labelled $Re_2(CO)_9(^{13}CO)$,[191] viz.

$$Re_2(CO)_{10} + Me_3NO + MeCN \rightarrow Re_2(CO)_9(NCMe) + Me_3N + CO_2 \qquad (10.5)$$

$$Re_2(CO)_9(NCMe) + {}^{13}C \rightarrow Re_2(CO)_9(^{13}CO) + MeCN \qquad (10.6)$$

Sunlight irradiation of a hexane solution of

$Mn_2(CO)_{10}$ in contact with ^{13}CO-rich (22.5%) carbon monoxide for several hours resulted in a threefold enrichment of the natural ^{13}CO content of the $Mn_2(CO)_{10}$ dimer.[154b] However, this method is unsatisfactory, as both $Mn_2(CO)_{10}$ and $Re_2(CO)_{10}$ exchange CO very slowly.[154c]

Indirect methods have also been employed in the preparation of ^{13}C-enriched samples of $M_2(CO)_{10}$, for example, the reaction of a ^{13}CO-enriched $M(CO)_5X$ (M = Re, X = Cℓ; M = Mn, X = Br) sample with $NaM(CO)_5$.[154c] (Both $M(CO)_5X$ and $NaM(CO)_5$ were themselves prepared from the $M_2(CO)_{10}$ dimer, by cleavage with halogen X or sodium amalgam respectively). Isotopically labelled $Re_2(CO)_{10}$ has also been prepared by reacting $HRe_3(CO)_{14}$ with carbon monoxide (50% ^{13}CO-enriched) under vacuum, to give $HRe(CO)_5$ and $Re_2(CO)_{10}$.[154a]

Only the amine-oxide assisted reaction between $Re_2(CO)_{10}$ and ^{13}CO *results in the production of high* purity $Re_2(CO)_9(^{13}CO)$, suitable for synthetic purposes (as opposed to use in IR and Raman spectroscopic studies[154e]). This reaction highlights the synthetic utility of the amine-oxide-induced route. This method has not been investigated (prior to this work) with ligands such as isonitriles and arsines, the reported reactions of $Re_2(CO)_{10}$ with these ligands being entirely photochemical (*see* sections 10.4 and 10.2.(b) respectively).

10.4 Photochemical reaction of $Re_2(CO)_{10}$ with isonitriles

Methylisonitrile (MeNC) derivatives, $M_2(CO)_{10-n}(CNMe)_n$ (M = Re, n = 1; M = Mn, n = 1,3,4), have been prepared by the photochemical reaction of $M_2(CO)_{10}$ with MeNC.[152] These complexes have been studied by Raman spectroscopy, and have been reported to be isostructural[152b] with the parent $M_2(CO)_{10}$ compounds,[154] but the crystal and molecular structures *have not been reported, presumably* due to the disorder problems encountered.[152b]

10.5 Amine-oxide assisted reaction of $Re_2(CO)_{10}$ with nitriles

The complexes $Re_2(CO)_{10-n}(NCR)_n$ (n = 1,2; R = Me, Et, Pr^n, Pr^i) were prepared via the amine-oxide assisted reaction

of $Re_2(CO)_{10}$ with RCN.[174]

viz. $Re_2(CO)_{10} + n\ Et_3NO + nRCN \rightarrow Re_2(CO)_{10-n}(NCR)_n + nEt_3N + nCO_2$ (10.7)

The complexes $Re_2(CO)_9(NCMe)$[173] and $Re_2(CO)_8(NCMe)_2$[175] have also been obtained from the amine-oxide assisted reaction of $Re_2(CO)_{10}$ in acetonitrile, in the absence of added donor ligand. (See also Section 10.10.1).

10.6 Photochemical reactions of $Re_2(CO)_{10}$ with olefins

The photochemical-induced reaction of $Re_2(CO)_{10}$ and olefins has been studied for several different olefins.[148-71,193-5] The major disadvantage is that the photochemical reaction usually results in a complex mixture of products, which often requires sophisticated methods such as high-pressure liquid chromatography (HPLC[196]) to effect separation. In addition to the octacarbonyl-μ-olefinyl-μ-hydrido-dirhenium complexes (Fig. 10.1(a)), olefinic rhenium monomers, di-rhenium complexes in which the Re-Re bond has been cleaved, with the olefin bridging the two Re atoms, or with the two metals joined through an olefinic residue, and even tri-*rhenium olefinic complexes, are* usually formed, in lesser or greater proportions. In some cases, monomeric and Re-Re bond cleaved dimeric products are formed exclusively from the reaction. Even in favourable cases, usually more than one octacarbonyl-μ-olefinyl-μ-hydrido-dirhenium complex is formed, due to cleavage, rearrangement or isomerization of the olefin ligand itself. In some instances, the simple substitution product, enneacarbonyl-η-olefin-dirhenium (Fig. 10.1(b)), can also be isolated.[193]

10.6.1. The photochemical reaction of $Re_2(CO)_{10}$ with olefins in hexane solution

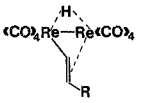
The photochemical reaction in hexane between $Re_2(CO)_{10}$ and a variety of acyclic and cyclic olefins with one to four C=C bonds has been studied.[193] Table 10.1 lists the olefin derivatives of dirhenium carbonyl dimer in which the rhenium-rhenium bond remains intact. The structures of these products are shown in Fig. 10.2.

With ethylene(I), styrol(II), 1,3-cyclopentadiene(III), 1,3-cyclohexadiene(IV), 1,3,5,7-cyclooctatetraen(V) and 6,6-dimethylfulven(VI), the main products were octacarbonyl-μ-olefinyl-μ-hydrido-dirhenium(I) complexes (Fig. 10.2, I-V-(A,B),(VIA)), isomerism of the olefin ligands being observed. With ethylene, octacarbonyl-μ-η-1,3-butadienedirhenium(0) (Fig. 10.2(IC)) was also obtained. In the cases of ethylene, 1,3,5,7-cyclooctatetraen and 6,6-dimethylfulven, ennea-carbonyl-μ-olefin-dirhenium was also observed (Fig. 10.2(ID), (VC) and (VIB) respectively). For ethylene, additionrl vinyl-bridged trinuclear complexes resulted. The only dinuclear products obtained from the reactions of $Re_2(CO)_{10}$ with cyclohexane and with 1,3,5-cycloheptatriene, were metal-metal bond cleaved octacarbonyl-μ-olefinyl-μ-hydrido-dirhenium complexes. In the case of the latter olefin, η-cycloheptadienylrhenium tricarbonyl side products were also obtained.

10.6.2. The photochemical reactions of $Re_2(CO)_{10}$ with 1,3-butadiene

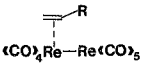
In tetrahydrofuran (THF) solution photolysis of $Re_2(CO)_{10}$ and 1,3-butadiene or cyclooctatetraene,[194] yielded the olefinic complexes, $(CO)_4Re\text{-}\mu(O{:}\eta^2C_4H_5)Re(CO)_4$ (Fig. 10.3, (VIIA)) and $(CO)_4Re\text{-}\mu(\eta^2{:}\eta^2C_4H_6)Re(CO)_4$ (Fig. 10.3(VIIB)). The latter complex has also been obtained from the photolysis of $Re_2(CO)_{10}$ with 1,3-butadiene in pentane solution.[193] The structure of this dimer (VIIB) has been determined oy X-ray crystallography[198] (see ch XIII). In these reactions, trinuclear, and metal-metal bond-cleaved dinuclear rhenium compounds were also obtained.[194-6]

The photochemical reaction between $Re_2(CO)_{10}$ and 1,3-butadiene in hexane[194] has been reported to yield, in addition to Re-Re bond-cleaved dinuclear olefinic complexes, at a temperature of 240 K, the dimeric complex octacarbonyl-μ-[1,2-η-1-σ-(1,3-butadien-1-yl)]-μ-hydrido-dirhenium (Fig. 10.3(VIID)). (VIID) rearranges in solution to octacarbonyl-μ-η-1,3-butadienedirhenium(0), $(CO)_4Re\text{-}\mu(\eta^2{:}\eta^2C_6H_4)Re(CO)_4$ (Fig. 10.3 (VIIB)), the product mentioned



a

(a) octacarbonyl-μ-olefinyl-μ-hydrido-dirhenium



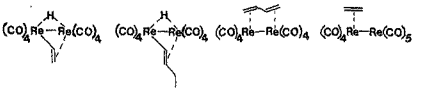
b

(b) enneacarbonyl-η-olefin-dirhenium

Figure 10.1: Possible Re-Re bonded dimeric olefin derivatives of $Re_2(CO)_{10}$ (olefin = )

TABLE 10.1: Re-Re bonded dimeric products from the photochemical reaction of $Re_2(CO)_{10}$ and olefins in hexane solution [93]

Olefin	Re-Re bonded dimeric product(s)
(I) ethylene	(IA) octacarbonyl-μ-hydrido-μ-(1-2-η-1-σ-vinyl)-dirhenium
	(IB) μ-[1-2-η-1-σ-(1-buten-1-yℓ)]-octacarbonyl-μ-hydrido-dirhenium
	(IC) μ-1-2:3-4-η-(1,3 butadiene)-octacarbonyl-dirhenium
	(ID) enneacarbonyl-η-ethylen-dirhenium
(II) styrol	(IIA) octacarbonyl-μ-hydrido-μ-[1-2-η-2-σ-(E-styryl)]-dirhenium
	(IIB) octacarbonyl-μ-hydrido-μ-[1-2-η-2-σ-(Z-styryl)]-dirhenium
(III) 1,3-cyclopentadiene	(IIIA) octacarbonyl-μ-[1-2-η-1-σ-(1,3-cyclopentadien-1-yℓ)]-μ-hydrido-dirhenium
	(IIIB) octacarbonyl-μ-[1-2-η-2-σ-(1,3-cyclopentadien-2-yℓ)]-μ-hydrido-dirhenium
(IV) 1,3-cyclohexadiene	(IVA) octacarbonyl-μ-[1-2-η-1-σ-(1,3-cyclohexadien-1-yℓ)]-μ-hydrido-dirhenium
	(IVB) octacarbonyl-μ-[1-2-η-2-σ-(1,3-cyclohexadien-2-yℓ)]-μ-hydrido-dirhenium
(V) 1,3,5,7-cyclooctatetraen	(VA) octacarbonyl-μ-[1-2-η-1-σ-(1,3,5,7-cyclooctatetraen-1-yℓ)]-μ-hydrido-dirhenium
	(VB) μ-[7-8-η-7-σ-(bicyclo-[4-2-0]octa-2,4,7-trien-7-yℓ)]octacarbonyl-μ-hydrido-dirhenium
	(VC) enneacarbonyl-η^2-1,3,5,7-cyclooctatetraen-dirhenium
(VI) 6,6-dimethylfulven	(VIA) octacarbonyl-μ-[1-2-η-2-σ-(6,6-dimethylfulven-2-yℓ)]-μ-hydrido-dirhenium
	(VIB) enneacarbonyl-1-2-η-(6,6-dimethylfulven)-dirhenium



IA IB IC ID

(I) ethylene



IIA IIB

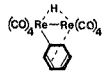
(II) styrol



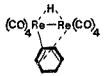
IIIA IIIB

(III) 1,3-cyclopentadiene

Figure 10.2: Re-Re bonded dimeric products from the photochemical reaction of $Re_2(CO)_{10}$ with olefins in hexane solution

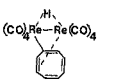


IVA

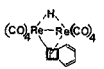


IVB

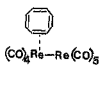
(IV) 1,3-cyclohexadiene 



VA

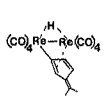


VB

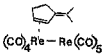


VC

(V) 1,3,5,7-cyclooctatetraen 



VIA



VIB

(VI) 6,6-dimethylfulven 

Figure 10.2: (contd.)

previously as obtained from the photochemical reaction of $Re_2(CO)_{10}$ and 1,3-butadiene in THF,[194] or in pentane solution,[195] and from that of $Re_2(CO)_{10}$ and ethylene in hexane solution (Fig. 10.2.(IC)[193]).

At a reaction temperature of 188K, however, the photochemical reaction between $Re_2(CO)_{10}$ and 1,3-butadiene in hexane[196] yielded, apart from the above Re-Re bond cleaved dimeric side products, in addition to the product (VII3), $(CO)_3Re(\eta\text{-}1,3\text{-butadiene})Re(CO)_5$ (Fig. 10.3(VIIC)) in comparable amounts.

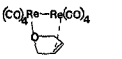
10.6.3 The photochemical reaction of $Re_2(CO)_{10}$ with 1,3,5-cycloheptatriene

Photolysis of $Re_2(CO)_{10}$ and excess 1,3,5-cycloheptatriene in petroleum ether (60-80°C)[197] yielded two Re-Re bonded dimeric products (Fig. 10.4), $(C_7H_8)Re_2(CO)_7$ (VIIIA) and $(C_7H_8)Re_2(CO)_6$ (VIIIB) (the structures of which have been deduced from FT ^1H NMR spectra), as well as monomeric and tetra-nuclear rhenium sideproducts. This is in contrast to the photochemical reaction of $Re_2(CO)_{10}$ with this olefin in hexane solution,[193] which gave only Re-Re bond-cleaved dimeric and η-cycloheptadienyl rhenium tricarbonyl monomeric products.

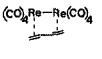
10.6.4 The photochemical reactions of $Re_2(CO)_{10}$ with 1-alkenes and 2-alkenes and further reactions of the products

Photolysis of a hexane[171] or toluene[176-1] solution of $Re_2(CO)_{10}$ in the presence of excess 1-alkene ((A) propylene,[169-71] (B) 1-butene[176-1] or (C) 1-hexene[176-1]) resulted in the formation of $(\mu\text{-}H)Re_2(CO)_8(\mu\text{-}(\eta^2\text{-}CH = CHR))$ (Fig. 10.5: R = Me (IXA1), Et (IXB1) or Bu^n (IXC) in high yields.[169-71] Mention has been made[171] of an X-ray crystal structure investigation of $(\mu\text{-}H)Re_2(CO)_8(\mu\text{-}\eta^2\text{-}CH = CHMe)$ (IXA), revealing an Re-Re bond length of ca. 3.20Å, but the full structure has not been reported to date.

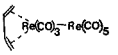
The photolysis in toluene of $Re_2(CO)_{10}$ with (A) or (B) also yields, in addition to the trans-isomers (IXA1) or (IXB1), the cis-isomers (IXA2) or (IXB2).[179] In the case of



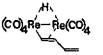
VIIA



VIIB

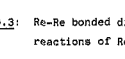


VIIC

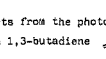


VIID

Figure 10.3: Re-Re bonded dimeric products from the photochemical reactions of $Re_2(CO)_{10}$ with 1,3-butadiene

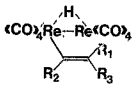


VIIIA



VIIIB

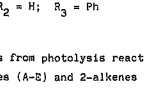
Figure 10.4: Re-Re bonded dimeric products from the photochemical reaction of $Re_2(CO)_{10}$ with 1,3,5-cycloheptatriene 



IX

(IXA1) $R_1 = R_2 = H$; $R_3 = Me$
(IXA2) $R_2 = R_3 = H$; $R_1 = Me$
(IXB1) $R_1 = R_2 = H$; $R_3 = Et$
(IXB2) $R_2 = R_3 = H$; $R_1 = Et$
(IXC) $R_1 = R_2 = H$; $R_3 = Bu^n$
(IXD) $R_1 = R_2 = R_3 = H$
(IXE) $R_1 = R_3 = H$; $R_2 = Et$
(IXF) $R_1 = H$; $R_2 = R_3 = Me$
(IXG) $R_1 = R_2 = H$; $R_3 = O\text{-}Bu^n$
(IXH) $R_1 = R_2 = H$; $R_3 = Ph$

Figure 10.5: Products from photolysis reactions of $Re_2(CO)_{10}$ with 1-alkenes (A-E) and 2-alkenes (F)



X

Figure 10.6: Dipolar addition product, $(\mu\text{-}H)(\mu\text{-}CH{=}CH_2)Re_2(CO)_8(PMe_3)$

(B), a further isomer, (IXE),[176] is also obtained. The cis-products, (IXA2) and (IXB2), isomerize spontaneously to the trans-products, (IXA1) and (IXB1).[175]

Photolysis of $Re_2(CO)_{10}$ with ethylene[173-1] yields, in addition to (IXD), $(\mu\text{-H})Re_2(CO)_8(\mu\text{-}(\eta^2\text{-CH=CH}_2))$, (IXB) and (IXE), $(\mu\text{-H})Re_2(CO)_8(\mu\text{-}(\eta^2\text{-EtC} = CH_2))$, formed from subsequent photochemical reactions of (IXD).

related study of internal olefins,[173-1] the photolysis of $Re_2(CO)_{10}$ with cis-2-butene resulted in the production, in low yield, of $(\mu\text{-H})Re_2(CO)_8(\mu\text{-}(\eta^2\text{-MeC} = CHMe))$, (IXF). Extended photolysis resulted in isomerization of (IXF) to (IXB). This later complex (IXB) was the only organometallic product to be obtained from the photolysis of $Re_2(CO)_{10}$ with trans-2-butene,[173-1] and probably resulted from the observed[176-1] slow isomerization of trans-2-butene to 1-butene during reaction.

Compounds (IXA-C) all react with ethylene at 25°C,[171] to give (IXD). Similarly, (IXD) undergoes alkene-exchange with 1-hexene[171] to give (IXC). Treatment of a heptane solution of (IXC) with excess vinyl-n-butyl ether[170] gives (IXG), $(\mu\text{-H})(\mu\text{-trans-CH=CHO-Bu}^n)Re_2(CO)_8$. Dissolution of (IXD) in neat styrene[170] yields (IXH), $(\mu\text{-H})(\mu\text{-trans CH = CHPh})\text{-}Re_2(CO)_8$ in quantitative yield (5-6 h). Compounds (IXA-F) react with excess olefin at room temperature to give the alkenyl-exchanged (μ-hydrido)(μ-alkenyl)dirhenium-octacarbonyl complex.[173]

Compounds (IXA)-(IXH) all react with excess py[173-1] in the dark to yield free olefin and 1,2-eq,eq-$Re_2(CO)_8(py)_2$. Room temperature reactions of (IXA)-(IXF) with CO[173-1] result in the formation of $Re_2(CO)_{10}$, with liberation of olefin. However, the photolysis of (IXB1) in the presence of py[171] yields $(\mu\text{-H})Re_2(CO)_7(\mu\text{-}(\eta^2\text{-CH = CH Et}))py$ as the major product.

A toluene solution of (IXD) reacts with H_2 (1 atm)[170] over 3 days to initially generate $H_2Re_2(CO)_8$, which is subsequently slowly converted to $H_2Re_3(CO)_{12}$. The reaction of (IXB1) with H_2 is similar.

Dissolution of (IXC) in neat acetonitrile (MeCN)[179] results in complete conversion to 1,2-eq,eq-$Re_2(CO)_8(NCMe)_2$ (5 h, room temperature). The major product of the reaction in toluene solution of (IXD) with H_2S[179] (1 atm, 6 h), is $Re_2(CO)_8(SH)_2$. (IXB1) reacts with excess acrylonitrile[179] in toluene solution to yield $Re_2(CO)_8(NCCH=CH_2)_2$.

Compounds (IXA)-(IXH) all react with excess PPh_3[178] in hexane at 25°C to give free olefin and 1,2-ax,eq-$Re_2(CO)_8(PPh_3)_2$, which isomerizes to 1,2-diax-$Re_2(CO)_8(PPh_3)_2$. The reaction of (IXD) with PBu^n_3 follows the same pattern.[178] However, the reaction of (IXD) with $P(OR)_3$ (R = Me, Ph) yields 1,2-eq,eq-$Re_2(CO)_8(P(OR)_3)_2$, which is stable to isomerization.[178] Treatment of (IXD) with excess PMe_3[178] in hexane or toluene solution rapidly generates the dipolar addition product $(\mu\text{-H})(\mu\text{-CH}=CH_2)Re_2(CO)_8(PMe_3)$ (X) (Fig. 10.6). This product (X) slowly decomposes in toluene solution to give 1,2-eq,eq-$Re_2(CO)_8(PMe_3)_2$, which is stable to isomerization.[178] Reaction of (IXA1) with excess PMe_3 in hexane at room temperature gives only 1,2-eq,eq-$Re_2(CO)_8(PMe_3)_2$ in near-quantitative yield (2-3 h). These bisphosphine dirhenium octacarbonyl products are of importance, as they are rare examples of equatorially substituted phosphine derivatives of $Re_2(CO)_{10}$. The geometry of phosphine substitution in $Re_2(CO)_{10-n}(PR_3)_n$ (n = 1-4) complexes will be discussed in ch. XV.

Similarly, (IXC) reacts with a variety of bidentate phosphino-ligands L-L (L-L = bis(diphenylphosphino)methane (dppm),[176,198] *bis(dimethylphosphino)methane(dmpm)*,[198] bis-(dimethylphosphino)ethane(dmpe)[198] and bis(diphenylphosphino)-ethane(dppe)[198]) to give the bridging ligand substituted dirhenium octacarbonyl compounds, 1,2-eq,eq-$Re_2(CO)_8(\mu\text{-L-L})$, in high yields (90%).

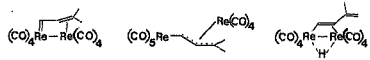
The major products of the photochemical reaction of 1,2-eq,eq-$Re_2(CO)_8(\mu\text{-L-L})$ (L-L = dppm, dmpm) with H_2O or MeOH are $(\mu\text{-H})(\mu\text{-OH})Re_2(CO)_6(\mu\text{-L-L})$ and $(\mu\text{-OR})_2Re_2(CO)_6(\mu\text{-L-L})$ (R = H or Me).[198] The structure of $(\mu\text{-H})(\mu\text{-OH})Re_2(CO)_6(\mu\text{-dppm})$ has been determined by X-ray crystallography[198] (see ch. XIII).

Reactions of $(\mu\text{-H})(\mu\text{-OR})Re_2(CO)_6(\mu\text{-L-L})$ and $(\mu\text{-OR})_2Re_2(CO)_6$-$(\mu\text{-L-L})$ with dry HCℓ lead to the formation of $(\mu\text{-H})(\mu\text{-C}\ell)$-$Re_2(CO)_6(\mu\text{-L-L})$ and $(\mu\text{-C}\ell)_2Re_2(CO)_6(\mu\text{-L-L})$ respectively.[198]

Treatment of a solution of (IXB1) with an excess of 3,3-dimethylcyclopropene [199] at room temperature leads to the formation (2 days, 80%) of dirhenium-octacarbonyl-(μ-carbene) complex, $Re_2(CO)_8(\mu\text{-}(\eta^1,\eta^3\text{-CH.CH.CMe}_2))$ (XIA) (Fig. 10.7), the structure of which has been determined by X-ray crystallography (see ch. XIII). Reaction of (XIA) with CO (100 atm, room temperature) leads to metal-metal bond cleavage and formation of $Re_2(CO)_9(\mu\text{-}(\eta^1,\eta^3\text{-CH.CH.CMe}_2)$ (XIB), which is unusual in that it contains a μ-carbene system not supported by a metal-metal bond.[199] On irradiation of (XIB) (2 h, room temperature), the η^1,η^2-butadienyl hydride, $(\mu\text{-H})Re_2(CO)_8$-$(\mu\text{-CH=CH.CMe=CH}_2)$ (XIC) results.[199]

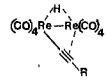
Treatment of (IXA1)[169] or (IXB1)[171] with excess phenylacetylene at room temperature gives the μ-hydrido-μ-alkynyl-octacarbonyl-dirhenium complex, $(\mu\text{-H})Re_2(CO)_8(\mu^2\text{-C}\equiv\text{CPh})$ (XIIA) (Fig. 10.8) as the major product (85%, 5-10 h). Similarly, reaction of (IXA1) with (p-methoxyphenyl) acetylene yields $(\mu\text{-H})Re_2(CO)_8(\mu\text{-p-C}\equiv\text{CC}_6\text{H}_4\text{OMe})$ (XIIB) (Fig. 10.8). Treatment of a hexane solution of (XIIA) with excess py[169] yields a single isomer of $(\mu\text{-H})(\mu\text{-C}\equiv\text{CPh})Re_2(CO)_7(py)$, in near quantitative yield (1-2 h, room temperature). This mono-substituted compound reacts slowly with excess py[169] to yield a single isomer of a disubstituted species, $(\mu\text{-H})$-$(\mu\text{-C}\equiv\text{CPh})Re_2(CO)_6(py)_2$. (XIIB) also undergoes CO substitution by py,[169] yielding $(\mu\text{-H})(\mu\text{-p-C}\equiv\text{CC}_6\text{H}_4\text{OMe})Re_2(CO)_7(py)$.

Treatment of a $CH_2C\ell_2$ or hexane solution of (XIIA) with excess PPh_3[169] results in essentially quantitative production of the disubstituted complex, $(\mu\text{-H})(\mu\text{-C}\equiv\text{CPh})Re_2$-$(CO)_6(PPh_3)_2$ (2 h). During monitoring of the reaction (in $CD_2C\ell_2$) by ^1H NMR spectroscopy, the monosubstituted complex, $(\mu\text{-H})(\mu\text{-C}\equiv\text{CPh})Re_2(CO)_7(PPh_3)$, was observed as the initial product. The reaction of(XIIA) with PBu^t_3 is analogous.[169] However, treatment of a hexane solution of (XIIA) with excess PMe_3 results in the immediate formation of a dipolar addition product, $(\mu\text{-H})(\mu\text{-C}\equiv\text{CPh})Re_2(CO)_8(PMe_3)$ (Fig. 10.9(XIIIA) or (XIIIB)).



XIA XIB XIC

Figure 10.7: Dirhenium carbonyl (μ-carbene) derivatives



XII

(A) R = Ph

(B) R = C_6H_4OMe-p

Figure 10.8: Products of reaction of (μ-H)(μ-trans-CH = CHMe)Re_2-$(CO)_8$ with acetylene



XIIIA XIIIB

Figure 10.9: Possible dipolar addition products, (μ-H)(μ-CsCPh)Re_2-$(CO)_8(PMe_3)$

10.7 Photochemical reaction of $Re_2(CO)_{10}$ with R_2SiH_2

The first report of a dirhenium carbonyl derivative with a bridging SiR_2 ligand was the formation of the complex $Re_2(CO)_8H_2(\mu\text{-}SiPh_2)$ in the photochemical reaction of $Re_2(CO)_{10}$ and Ph_2SiH_2 in benzene solution.[219a] The X-ray crystal structure of this complex has been determined.[219b] The crystal structures of the related derivatives, $Re_2(CO)_7H_2(\mu\text{-}SiEt_2)_2$[242] and $Re_2(CO)_6H_4(\mu\text{-}SiEt_2)_2$,[151] have also since been reported. No details of the synthesis of these compounds were given, but presumedly the method was similar to that for the synthesis of $Re_2(CO)_8H_2(\mu\text{-}SiPh_2)$[219a] (vide supra). The molecular structures of these three complexes will be considered in ch. XIII.

The room temperature reaction of $Re_2(CO)_8H_2(\mu\text{-}SiPh_2)$ with silicic acid in chloroform solution resulted in the formation of the dihydride derivative, $Re_2(CO)_8(\mu\text{-}H)_2$,[293] the structure of which has been determined by X-ray crystallography (see ch. XIII).

10.8 The photochemical reaction of $Re_2(CO)_{10}$ with H_2

UV-irradiation of $Re_2(CO)_{10}$ with H_2 in THF gives $Re_2(CO)_8(\mu\text{-}H)_2$, together with monomeric and trimeric rhenium products.[294] This complex has also been obtained from UV-irradiation of $Re_3(CO)_{12}H_3$,[295] from the thermal reaction of $Re_2(CO)_8H_2(\mu\text{-}SiPh_2)$ with $SiO_2.nH_2O$[293] (vide supra), and from the thermal reaction of $(\mu\text{-}H)(\mu\text{-}CHCH_2)Re_2(CO)_8$ with H_2[170] (see section 10.6.4).

10.9 Photochemical reaction of $Re_2(CO)_{10}$ with water

$Re_2(CO)_{10}$ is stable towards water even under drastic conditions;[144] it is also not attacked by dilute acids or bases.[144] A "base reaction" can only be achieved with methanolic potassium hydroxide, whereupon a dinuclear complex $K[Re_2(CO)_8O_2H]$ is formed.[288]

The photolysis of $Re_2(CO)_{10}$ in wet THF leads to the formation of eq-$Re_2(CO)_9(OH_2)$.[175] This product has been shown[175] to be formed via primary photochemical homolysis of the Re-Re bond, followed by thermal substitution of the $Re(CO)_5$· radical by H_2O, and then recombination with $Re(CO)_5$·,

to give $Re_2(CO)_9(OH_2)$.

Under 366nm irradiation, $Re_2(CO)_9(OH_2)$ decomposes via the proposed unstable intermediate $Re_2(CO)_8(OH_2)_2$, which looses H_2O and undergoes oxidative addition to an *O-H* bond to form $(\mu\text{-}H)Re_2(CO)_8(\mu\text{-}OH)$, which decomposes to $HRe(CO)_5$ and $Re_4(CO)_{12}(OH)_4$, the observed decomposition products.[175]

In THF solution, the co-ordinated water in eq-$Re_2(CO)_9(OH_2)$ is readily displaced by stronger nucleophilic ligands, e.g. CO, MeCN, PPh_3, to give $Re_2(CO)_{10}$, eq-$Re_2(CO)_9(NCMe)$ and ax-$Re_2(CO)_9PPh_3$ respectively.[175] Hence eq-$Re_2(CO)_9(OH_2)$ can be regarded as *a lightly stabilized form of the co-ordinately unsaturated* $Re_2(CO)_9$.[175] However, in non-coordinating solvents (e.g. toluene), only rhenium cluster compounds are obtained.[175] The role of the THF is probably to stabilize the $Re_2(CO)_9$ intermediate.

Under photolytic conditions, $Re_2(CO)_{10}$ reacts with H_2O in aqueous ether, yielding initially $Re_3(CO)_{12}H_3$ and $Re_4(CO)_{12}(OH)_4$, and after extended irradiation, exclusively $Re_4(CO)_{12}(OH)_4$.[267]

Irradiation of $Re_2(CO)_8$ (1,10-phenanthroline) (indirectly prepared[266]) in wet THF yields $Re_2(CO)_{10}$ and $Re_2(CO)_6$(1,10-phenanthroline)$_2$.[175] However, only $Re_4(CO)_{14}(OH)_4$ and some eq-$Re_2(CO)_9(NCMe)$ *are formed from the reaction of dieq-*$Re_2(CO)_8(NCMe)_2$ with H_2O in refluxing THF.[175] The unstable $Re_2(CO)_6(OH_2)_2$ may be formed as an intermediate in the reaction of $(\mu\text{-}H)(\mu\text{-}CHCH_2)Re_2(CO)_8$ with H_2O (wet THF), which eventually yields $Re_4(CO)_{12}(OH)_4$.[175]

10.10 N-donor ligand derivatives of $Re_2(CO)_{10}$

10.10.1 Trimethylamine-N-oxide-induced reactions of $Re_2(CO)_{10}$ with N-donor ligands

The thermal reactions of $Re_2(CO)_{10}$ with trimethyl-amine-N-oxide, Me_3NO, in the presence of N-donor ligands L lead to substituted derivatives, $Re_2(CO)_{10-n}(L)_n$ (n = 1,2), according to eqn. (10.8).

$$Re_2(CO)_{10} + nMe_3NO + nL \rightarrow Re_2(CO)_{10-n}(L)_n + nMe_3N + nCO_2 \qquad (10.8)$$

The reaction is usually performed in acetonitrile

(MeCN) solvent, and in the absence of added donor ligand L, acetonitrile derivatives, eq-$Re_2(CO)_9(NCMe)$[173] and dieq-$Re_2(CO)_8(NCMe)_2$[173] are formed (see also section 10.5).

In the presence of *N-donor ligand L, the reaction* results in the formation of substituted derivatives $Re_2(CO)_{10-n}(L)_n$ (n = 1,2). This method has been employed in the synthesis of the complexes eq-$Re_2(CO)_9L$ (L = py,[173] 2-Mepy.[173] $MeNH_2$,[167] $EtNH_2$[167]) and dieq-$Re_2(CO)_8(py)_2$.[173] These derivatives have been shown to undergo photolysis reactions[167] resulting in the formation of new dirhenium *carbonyl complexes* (*vide infra*).

10.10.2 Photolytic reactions of $Re_2(CO)_{10-n}L_n$ (n = 1,2, L = N-donor ligand)

Photolysis of solutions of mono- and di-substituted N-donor ligand derivatives of dirhenium carbonyl results in the formation of new di- and tri-substituted dimers. The photolysis reaction in THF solution of eq-$Re_2(CO)_9(NCMe)$ and of eq-$Re_2(CO)_9(py)$ or 1,2-*dieq-*$Re_2(CO)_8(py)_2$, yields the products 1,2-dieq-$Re_2(CO)_8(NCMe)_2$ and 1,1-$(\mu\text{-H})Re_2(CO)_7(py)(NC_5H_4)$ respectively.[167] Photolysis of eq-$Re_2(CO)_9(RNH_2)$ (R = Me, Et) in heptane yields 1,1-$Re_2(CO)_8(RNH_2)_2$.[167] In these reactions, other photolysis products usually include $Re_2(CO)_{10}$, monomeric rhenium carbonyl derivatives, and rhenium carbonyl cluster compounds.[167]

10.10.3 *Preparation of* $(\mu\text{-H})Re_2(CO)_8(\mu\text{-}NC_5H_4)$, and subsequent reactions with donor ligands

The compound $(\mu\text{-H})Re_2(CO)_8(\mu\text{-}NC_5H_4)$ is formed by heating 1,2-dieq-$Re_2(CO)_8(py)_2$ in refluxing benzene.[167] This complex has been characterized by X-ray crystallography[188] (see ch. XIII), and itself undergoes further CO-substitution reactions with other donor ligand .[167-8]

(a) *Thermal reactions with ligand L*

In benzene solution, $(\mu\text{-H})Re_2(CO)_8(\mu\text{-}NC_5H_4)$ reacts slowly with py to give 1,1-$(\mu\text{-H})Re_2(CO)_7(py)(NC_5H_4)$,[167] and with PPh_3 to yield $(\mu\text{-H})Re_2(CO)_7(\mu\text{-}NC_5H_4)(PPh_3)$ and $(\mu\text{-H})Re(CO)_8(\mu\text{-}NC_5H_4)(PPh_3)_2$.[166] Refluxing $(\mu\text{-H})Re_2(CO)_8(\mu\text{-}NC_5H_4)$ in acetonitrile solution gave $(\mu\text{-H})Re_2(CO)_7(\mu\text{-}NC_5H_4)(NCMe)$,[166]

the structure of which has been determined by X-ray crystallography[188] (see ch. XIII). All these thermal substitution reactions required very long reaction times (10-20 h).

(b) Reaction with Me_3NO in the presence of ligand L

When a solution of $(\mu\text{-H})Re_2(CO)_8(\mu\text{-}NC_5H_4)$ was treated with Me_3NO, in the presence of donor ligand L (L = py, PPh_3),[166] *mono- and disubstitution of CO resulted. Initially formed* was the complex $(\mu\text{-H})Re_2(CO)_7(\mu\text{-}NC_5H_4)(L)$, which over a 24 h period slowly converted to $(\mu\text{-H})Re_2(CO)_6(\mu\text{-}NC_5H_4)(L)_2$.[166] With L = 1-octene,[166] however, only the mono-substituted complex $(\mu\text{-H})Re_2(CO)_7(\mu\text{-}NC_5H_4)$(η²-1-octene) resulted, which did not undergo further reaction to the di-substituted product at room temperature.

(c) Photochemical reactions with ligand L

Photolysis of toluene solutions of $(\mu\text{-H})Re_2(CO)_8(\mu\text{-}NC_5H_4)$ and L (L = py, PPh_3)[166] resulted in the formation of mono-substituted $(\mu\text{-H})Re_2(CO)_7(\mu\text{-}NC_5H_4)(L)$, which over a period of 10-15 h was converted to di-substituted $(\mu\text{-H})Re_2(CO)_6(\mu\text{-}NC_5H_4)(L)_2$. *After a further* 10-15 *h* photolysis, tri-substituted $(\mu\text{-H})Re_2(CO)_5(\mu\text{-}NC_5H_4)(L)_3$ could be obtained. However, with L = $P(OPh)_3$, 1-octene,[166] only mono-substituted products, $(\mu\text{-H})Re_2(CO)_7(\mu\text{-}NC_5H_4)(L)$, could be isolated even after prolonged periods of photolysis.

10.10.4 Preparation of bis-N-donor-ligand derivatives of $Re_2(CO)_{10}$

Although $Mn_2(CO)_8$ (1,10-*phenanthroline*) *is synthesised* by the photolysis reaction of $Mn_2(CO)_{10}$ and 1,10-phenanthroline,[218-9] the synthesis of the rhenium analogue, $Re_2(CO)_8(L_2)$ ((L_2) = 1,10-phenanthroline, 2,2'-biquinoline, 2,2'-bipy and 4,7-diphenyl-1,10-phenanthroline), was achieved by airless addition (in the dark) of a THF solution of $NaRe(CO)_5$ to a deoxygenated $C\ell Re(CO)_3(L_2)$ solution.[218] The displacement of $C\ell^-$ by $Re(CO)_5^-$ occurs rapidly at 298 K to yield a highly coloured solution of $Re_2(CO)_8(L_2)$, and NaCℓ precipitate.

Irradiation of $Re_2(CO)_8$(1,10-phenanthroline) in wet THF yields $Re_2(CO)_{10}$ and $Re_2(CO)_6$(1,10-phenanthroline)$_2$.[173]

(eqn. 10.9(a)). This latter complex has also been obtained from the photolysis of $(OC)_5MnRe(CO)_3$(1,10-phenanthroline) in THF[218] (eqn. 10.9(b)).

$$2(OC)_5MRe(CO)_3(1,10\text{phenanthroline}) \xrightarrow{h\nu} M_2(CO)_{10} + Re_2(CO)_8(1,10\text{phenanthroline})_2$$

(a) M = Re; (b) M = Mn (10.9)

10.11 Dirhenium carbonyl carbene complexes

Reaction of $Re_2(CO)_{10}$ with LiR in ether, (to give $Re_2(CO)_9[C(OLi)R]$)[177a], and subsequent alkylation with $[R'_3O][BF_4]/H_2O$ yields the carbene complex eq-$Re_2(CO)_9[C(OR')R]$ (R = Me,[177a] Ph,[177] C_6H_4Me-p,[177b] R' = Me; R = $SiPh_3$, R' = Me[177a] Et[178]). Similarly, the reaction of $Re_2(CO)_{10}$ with $LiSiPh_3$ in THF, followed by treatment with $MeFSO_3$ gives eq-$Re_2(CO)_9[C(OMe)SiPh_3]$ or eq-$Re_2(CO)_9[C(OC_6H_8OMe)$-$SiPh_3]$, depending on the reaction conditions.[178a] In addition, the reaction of $Re_2(CO)_{10}$ with excess $LiSiPh_3$ and subsequent alkylation with $[Et_3O][BF_4]/H_2O$ yields not only eq-$Re_2(CO)_9[C(OEt)SiPh_3]$,[178a-c] but 1,2-ax,eq-$Re_2(CO)_8$-$[C(OEt)SiPh_3]$[178b,c] and dirhenium products characterized by X-ray crystallography[178c] (see ch. XIII) as $(CO)_4Re[\mu$-$C(SiPh_3)$-$CO(OEt)]Fe(CO)_3[C(OEt)SiPh_3]$ and $Re_2(CO)_8[\mu$-$C(SiPh_3)CO](\mu$-$H)$. The structures of eq-$Re_2(CO)_9[C(OR')SiPh_3]$ (R = Me,[253] Et[178a,253]) and 1,2-ax,eq-$Re_2(CO)_8[C(OEt)SiPh_3]$[253] have also been determined crystallographically (see ch. XIII). Further treatment of the carbene complex eq-$Re_2(CO)_9[C(OMe)R]$ (R = Ph, C_6H_4Me-p) with LiR /ether, followed by $[Me_3O][BF_4]$-$/H_2O$, yields the μ-methylidine complex $Re_2(CO)_8[\mu$-$C(OMe)R]_2$[177b]. The molecular structure of one such complex, $Re_2(CO)_8[\mu$-C-$(OMe)C_6H_4Me$-p$]_2$, has been determined by X-ray crystallography[177b] (see ch. XIII).

The isomeric carbene complex, ax-$Re_2(CO)_9[C(OR')SiPh_3]$ (R' = Me, Et), can be obtained by reaction of eq-$Re_2(CO)_9$-$[C(OR')SiPh_3]$ with Ag_2X_2 (X = Cl, Br) to give $[ax$-$Re_2(CO)_9$-$(CSiPh_3)]^+[AlX_4]^-$, which is then treated with alcohol, R'OH.[178a] The isomers, ax-or-eq-$Re_2(CO)_9[C\ OMe)SiPh_3]$, react with dialkylamine, HNR'_2 (R' = Me, Et) in pentane to

form ax- or eq-$[Re_2(CO)_9C(NR''_2)SiPh_3]$ respectively.[176a] Treatment of the ax- or-eq-isomers of $Re_2(CO)_9[C(OEt)SiPh_3]$ with $Li(C_6H_4Me)$ and subsequent alkylation with $[Et_3O][BF_4]$ yields the two isomers of 1,2-ax,eq-$Re_2(CO)_8[C(OEt)SiPh_3][C(OEt)C_6H_4Me]$[176b] (see Fig. 10.10 (XIVA) and (XIVB)).

The reaction of the cationic silyl carbyne complexes of dirhenium carbonyl, $[ax\text{-}Re_2(CO)_9(CSiPh_3)]^+[AlX_4]^-$ (X = Cl, Br) with alcohols, R''OH (R'' = Me, Et, Pr^i, Bu^t), has also been reported to yield alkoxy-carbene complexes, $ax\text{-}Re_2(CO)_9[C(OR'')SiPh_3]$ and $eq\text{-}Re_2(CO)_9[C(OR'')H]$.[211] *Halogen-silylcarbene complexes*, $ax\text{-}Re_2(CO)_9[C(X)SiPh_3]$ (X = Cl, Br), can be isolated as intermediates.[211] Reaction of $[ax\text{-}Re_2(CO)_9(CSiPh_3)]^+[AlBr_4]^-$ with dimethylamine, $HNMe_2$, gives $ax\text{-}Re_2(CO)_9[C(NMe)SiPh_3]$, and $eq\text{-}Re_2(CO)_9[C(NMe)H]$.[211] The latter compound can also be obtained by treating $eq\text{-}Re_2(CO)_9[C(OMe)H]$ with $HNMe_2$.[211] The X-ray crystal structure of $eq\text{-}Re_2(CO)_9[C(OMe)H]$ has been reported[211] (see ch. XIII).

10.12 Thermal reaction of $Re_2(CO)_{10}$ with acetylenes

The reaction of $Re_2(CO)_{10}$ with PhCCPh at 190°C gives $[Re_2(CO)_7(PhCCPh_2)]$, $[Re_2(CO)_6(PhCCPh)_3]$, and $[Re_2(CO)_4(PhCCPh)_4]$.[212] This latter complex reacts instantaneously with excess of isonitrile RNC (R = Bu^t, Bu^n, p-$MeOC_6H_4$ or p-$MeC_6H_4SO_2CH_2$) to give $[Re_2(CO)_4(PhCCPh)_3(CNR)_2]$.[212] An X-ray crystal structure analysis of one such isonitrile derivative, $[Re_2(CO)_4(PhCCPh)_3(CNCH_2SO_2C_6H_4Me\text{-}p)_2]$, has been performed[212] (see ch. XIII).

Complexes of the type μ-hydrido-μ-alkynyl-dirhenium-octacarbonyl are obtained from the reaction of μ-hydrido-μ-olefinyl *dirhenium octacarbonyl with acetylenes*[164] *(see* section 10.6.4).

10.13 Formation of $[cis\text{-}Re_2(CO)_9(CHO)]^-$ from $Re_2(CO)_{10}$

The anionic formyl complex of dirhenium carbonyl, $Li^+[cis\text{-}Re_2(CO)_9(CHO)]^-$ was prepared by the reaction of $LiEt_3BH$ with $Re_2(CO)_{10}$ in THF solution.[176] Analogous products were obtained for $Mn_2(CO)_{10}$ and for the *mixed-metal* decacarbonyl dimer, $ReMn(CO)_{10}$.[176]

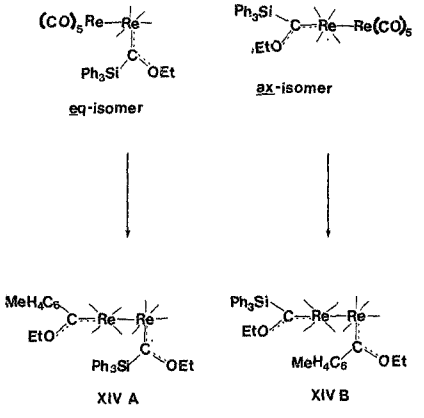


Figure 10.10: The two isomers of 1,2-ax,eq-$Re_2(CO)_8[C(OEt)SiPh_3]$-$[C(OEt)C_6H_4Me]$, (XIVA) and (XIVB)

Treatment of the eq- or ax- isomers of $Re_2(CO)_9$-$[C(OEt)SiPh_3]$ with $Li(C_6H_4Me)$ and subsequent alkylation with $[Et_3O][BF_4]$ yields the two isomers of 1,2-ax,eq-$Re_2(CO)_8[C(OEt)SiPh][C(OEt)C_6H_4Me]$, (XIVA) and (XIVB) respectively.[113b]

In the tranformylation reaction[213] of $Et_4N^+[trans\text{-}[(PhO)_3P](CO)_3FeCHO]^-$ with $Re_2(CO)_{10}$ in THF, $Et_4N^+[cis\text{-}Re_2(CO)_9(CHO)]^-$ was formed (82% yield as determined by ^1H NMR integration) together with a co-product, $(CO)_4Fe\text{-}[P(OPh)_3]$.

$Et_4N^+[cis\text{-}Re_2(CO)_9(CHO)]^-$ was also synthesized (32% yield) by the reaction of $K^+HB(O\text{-}Pr^i)_3^-$ with $Re_2(CO)_{10}$ in THF at 0°C, followed by aqueous basic workup and cation exchange with $Et_4N^+Br^-$.[213]

10.14 Formation of $Et_4N^+[cis\text{-}Re_2(CO)_9H]^-$ from $Re_2(CO)_{10}$

The reaction of $K^+HB(O\text{-}Pr^i)_3^-$ with $Re_2(CO)_{10}$ under fluorescent laboratory lighting (45-50°C, 3 h), followed by aqueous basic workup and cation exchange with $Et_4N^+Br^-$ gave the hydrido anion $Et_4N^+[cis\text{-}Re_2(CO)_9H]^-$.[213] This metal hydride can also be obtained from the photolysis of a THF solution of $Et_4N^+[cis\text{-}Re_2(CO)_9(CHO)]^-$.[213]

$Et_4N^+[HRe_2(CO)_9]^-$ has also been detected, though not isolated, in the *TEABH* reduction of $Re_2(CO)_{10}$ in MeCN[214] (see section 10.15).

10.15 Quaternary Ammonium Borohydride reductions of $Re_2(CO)_{10}$

Quaternary ammonium borohydrides, used in single phase or phase transfer reactions, are highly effective reagents for preparing metal carbonyl anions from metal carbonyls.[214]

The tetraethylammonium borohydride (TEABH) reduction of $Re_2(CO)_{10}$ in MeCN (80°C, 1 h) yielded the hydrido anion $Et_4N^+[HRe_2(CO)_9]^-$.[214] On stirring the crude product from this reaction with CH_2Cl_2 (room temperature, 1½ h), the chloro anion, $Et_4N^+[Re_2(CO)_9Cl]^-$ (39%) was formed.[214] This product was also obtained in high yield (89%) from the TEABH reduction of $Re_2(CO)_{10}$ in CH_2Cl_2 (room temperature, 2 h).[214]

10.16 Conclusion

From the foregoing review of reactions of $Re_2(CO)_{10}$ with ligand(s) L to give dimeric products $Re_2(CO)_{10-n}(L)_n$ (n = 1-4) in which the Re-Re bond remains intact, several points become apparent.

(i) The use of synthetic methods involving the direct reaction of the $Re_2(CO)_{10}$ dimer give products $Re_2(CO)_{10-n}(L)_n$,

where $n \leq 4$, (except for the acetylene complex $[Re_2(CO)_4(PhCCPh)_4]$ and the isonitrile dervatives, $[Re_2(CO)_4(PhCCPh)_3(CNR)_2]$ (see section 10.12). In the majority of reactions, only mono- and di-substituted products, $Re_2(CO)_{10-n}(L)_n$ ($n = 1$-2), result. In a few instances tri- and tetra-substituted complexes, $Re_2(CO)_{10-n}(L)_n$ ($n = 3,4$), have been prepared, but generally forcing reaction conditions are required. This limitation must be synthetic, and not steric in origin, since the decaphosphite dirhenium complex, $Re_2[P(OMe)_3]_{10}$, has been prepared by indirect methods.[215] [Tolman cone angle[85] for $P(OMe)_3$: 107°].

(ii) Apart from routine characterization, there has been very little comment on the position of ligand attack in $Re_2(CO)_{10}$, and the resultant stereochemistry of the $Re_2(CO)_{10-n}(L)_n$ ($n = 1$-4) complexes. Even where X-ray crystal structures of the product have been undertaken, little attempt has been made to rationalize the observed structure in terms of electronic and steric factors. The structures of $Re_2(CO)_{10-n}(L)_n$ ($n = 1$-4) complexes which have been determined by X-ray crystallographic techniques will be discussed in ch. XIII, and an attempt made to rationalize structural trends apparent, as well as any exceptions, in terms of underlying electronic and steric factors.

(iii) There have been no comprehensive systematic studies (chemical, structural, mechanistic) on $Re_2(CO)_{10}/L$ systems, apart from the kinetic-mechanistic studies on the $Re_2(CO)_{10}/PR_3$ system, which will be discussed in ch XV. Such a study was thus undertaken on the $Re_2(CO)_{10}/RNC$ system, which has received very little prior attention (see section 10.4). The results of this chemical and structural study will be presented in chs. XI and XIV respectively.

XI. CATALYTIC SYNTHESIS AND CHARACTERIZATION OF ISONITRILE DERIVATIVES OF DIRHENIUM DECACARBONYL

11.1 Introduction

Facile synthetic routes are continually being sought to substituted metal carbonyl complexes. Until recently, photochemical or (vigorous) thermal techniques have been employed to achieve substitution of CO by a ligand L, as shown in eqn. (11.1).

$$M(CO)_n + L \longrightarrow M(CO)_{n-1}(L) + CO \qquad (11.1)$$

With compounds containing a metal-metal bond, bond cleavage may occur, resulting in unwanted by-products, separation problems, and reduced yields.

The only report to date of the reaction between $Re_2(CO)_{10}$ and isonitriles has been a mention of the synthesis (and a Raman study) of the complex $Re_2(CO)_9(CNMe)$,[192b] which was *synthesized by photochemical methods.*[192a] However, the analogous reaction of $Mn_2(CO)_{10}$ with isonitrile ligands (RNC) has received more attention. The derivatives $Mn_2(CO)_{10-n}(CNR)_n$ (R = Me[192,214] or Bu^t,[214] n = 1-4) have been synthesized by thermal[214] (refluxing toluene) and/or photochemical methods.[214,192] *Indirect methods have also* been employed in the synthesis of these complexes. For instance, a series of complexes, $Mn_2(CO)_{10-n}(CNR)_n$ (n = 1,2,4,5; R = Me, Ph, p-CℓC$_6$H$_4$), was prepared by nucleophilic attack of $Mn(CO)_5^-$ on $Mn(CO)_{5-n}(CNR)_nX$ (X = Cℓ, Br, CN).[217] The complex $Mn_2(CO)_{10-n}(CNPh)_n$(n = 1,2) has been obtained in low yield from the reaction of $RMn(CO)_5$ (*R = Me, Ph*) with PhNC in THF.[218] In a systematic study by Behrens et al.,[219] the complexes $Mn_2(CO)_9(CNR)$ (R = Et, $SiMe_3$, $GeMe_3$, $SnMe_3$, PPh_2, COMe) were prepared by reaction of $Na[Mn_2(CO)_9CN]$ with Et_3OBF_4 or RCℓ.

Recently, Albers and Coville[426] have reported that Pd/C or Pd/$CaCO_3$ catalyses the reaction *between* $Mn_2(CO)_{10}$ *and* isonitriles, to give $Mn_2(CO)_{10-n}(CNR)_n$ (n = 1-3, R = Bu^t, $C_6H_5CH_2$, C_6H_{11}, Me; n = 1-4, R = $C_6H_3Me_2$-2,6). As a logical extension of this study, an investigation of the

transition metal catalysed thermal reaction between $Re_2(CO)_{10}$ and isonitrile ligands was undertaken.

What studies there have been of the properties of $M_2(CO)_{10-n}(CNR)_n$ (M = Mn, n = 1-4; M = Re, n = 1, R = Me) have employed Raman,[192b] IR[226] and ^1H NMR[192a,216,226] spectroscopy. No X-ray crystal structures of $M_2(CO)_{10-n}(CNR)_n$ compounds have been reported prior to this work. Hence a systematic study was undertaken of the $Re_2(CO)_{10}$/RNC system, in order to obtain chemical, mechanistic and structural information. Techniques employed in this investigation include IR, Raman, ^1H NMR and mass spectroscopy, and X-ray crystal X-ray diffraction (ch. XIV).

11.2 *Catalyst Testing*

In sunlight, the thermal reaction (11.2) in benzene at 55°C *between* $Re_2(CO)_{10}$ and Bu^tNC (1:1 ratio)

$$Re_2(CO)_{10} + Bu^tNC \longrightarrow Re_2(CO)_9(CNBu^t) + CO \qquad (11.2)$$

yields predominately $Re_2(CO)_9(CNBu^t)$ *(210 min). However, in* the dark (complete exclusion of all light) or in artificial laboratory light (no sunlight), no reaction occurs between $Re_2(CO)_{10}$ and Bu^tNC at 55°C (210 min). If after several hours of no reaction in the dark, the reaction vessel was exposed to sunlight, the reaction to $Re_2(CO)_9(CNBu^t)$ proceeded at the above rate. Hence the thermal reaction *between* $Re_2(CO)_{10}$ *and* Bu^tNC is dependent on sunlight. No attempts have been made to elucidate the mechanism of this thermal unc[illegible]ed reaction, but sunlight-initiated fission of the Re-Re or of a Re-CO bond could be implicated.[221]

Reaction (11.2) between $Re_2(CO)_{10}$ and Bu^tNC (1:1 ratio) in benzene at 55°C was used to screen *potential catalysts* (Table 11.1). Where catalysis was observed, the reaction time was taken as the complete conversion of $Re_2(CO)_{10}$ to $Re_2(CO)_9(CNBu^t)$ (as detected by TLC). Pd-metal, PdO and supported Pd-species were found to be exceptionally active catalysts, with reaction times ranging from less than 1 min for PdO and $Pd/CaCO_3$, to ca. 1 h for Pd-metal, and 2 h for *Pd/C (5% Pd).* (*The supports,* $CaCO_3$ and activated carbon, were found to be inactive). The corresponding Pt-species

were much less active (e.g. $Pt/A\ell_2O_3$(5% Pt): 70 min, cf. $Pd/A\ell_2O_3$(5% Pd): 5 min), or inactive (no catalysis with PtO_2, Pt/C (5 or 10% Pt)). Other activated carbon-supported species (5% Rh, Ru, Re) were also inactive, as were the transition metal salts investigated (e.g. $CoC\ell_2 \cdot 2H_2O$, which is known to catalyse the reaction between $Fe(CO)_5$ and isonitriles[142]).

The iron carbonyl dimer, $[(\eta^5C_5H_5)Fe(CO)_2]_2$, was tested for its catalytic ability, since this dimer has been found to be an active catalyst for related carbonyl substitution reactions, when used alone[20-1] or in combination with a co-catalyst such as PdO.[22] However, it was found that with $[(\eta^5C_5H_5)Fe(CO)_2]_2$ (4 mg) and PdO (4 mg), the reaction time was 1 min, the same as that for PdO (4 mg) alone, while that for $[(\eta^5C_5H_5)Fe(CO)_2]_2$ (4 mg) alone was 40 min. Hence in the case of this reaction, PdO would seem to be the active catalyst.

When catalysis was observed with a given species, the reaction proceeded at the same rate irrespective of whether the catalytic reaction was conducted in sunlight, in artificial light only, or in the dark. If, in the instance of the blank reaction in the dark, after several hours during which no reaction was observed, catalyst was added to the solution of $Re_2(CO)_{10}$ and Bu^tNC, the reaction to $Re_2(CO)_9(CNBu^t)$ proceeded at the normal rate for that catalyst. Hence the catalysed reaction is not dependent on sunlight, as in the blank reaction.

It was thought that a reducing agent such as $LiA\ell H_4$ might catalyze reaction (11.2). However, when a few mgs of $LiA\ell H_4$ were added to a solution of $Re_2(CO)_{10}$ and Bu^tNC in the dark, no reaction was observed (55°C, 2 h). It was thought traces of oxygen in the solution could be responsible for this lack of reaction. Further, erratic results initially obtained with some Pt-species (e.g. Pt/C, PtO_2) suggested that Pt might play a role in removing traces of oxygen from the solution. Hence the combination of Pt/C and $LiA\ell H_4$ was investigated as a potential catalyst for reaction (11.2).

It was found that if a small amount of $LiA\ell H_4$ was added to a reaction mixture of $Re_2(CO)_{10}$ (0.2 mmol), Bu^tNC (0.22 mmol)

TABLE 11.1: Effect of potential catalysts on the reaction

$$Re_2(CO)_{10} + Bu^tNC \longrightarrow Re_2(CO)_9(CNBu^t) + CO \qquad (11.2)$$

Potential catalyst[a]	Reaction time (min)
-	210[b]
PdO	<1
PtO_2	nc[c]
Pd(0)	50
Pd-impregnated polymer (~40 mesh)	105
Pd/C (10%)	105
Pd/C (5%)	120
Pt/C (10%)	nc[c]
Pt/C (5%)	nc[c]
Rh/C (5%)	nc[c]
Ru/C (5%)	nc[c]
Re/C (5%)	nc[c]
$Pd/CaCO_3$ (10%)	<1
$Pd/BaCO_3$ (5%)	6
$Pd/BaSO_4$ (5%)	130
Pd/Al_2O_3 (5%)	5
Pt/Al_2O_3 (5%)	70
Activated carbon, "Bergswerksverband"	nc[c]
$CaCO_3$	nc[c]
Platinous Bromide	nc[c]
Potassium tetrachloroplatinate(II)	nc[c]
$CoCl_2 \cdot 2H_2O$	nc[c]
$IrCl_3 \cdot nH_2O$	nc[c]
Zn(0)	nc[c]
$[(\eta^5C_5H_5)Fe(CO)_2]_2$	40

[a] Sources of chemicals used in this study given in Appendix A

[b] In sunlight; no reaction in the dark

[c] No catalysis

and Pt/C (5% Pt; 1mg) in benzene, which had been heated at 55°C for 4 h in the dark (with no reaction being observed), reaction to $Re_2(CO)_9(CNBu^t)$ was complete in less than 15 mins (the time depending on the amount of $LiAlH_4$ added). On addition of a further equivalent of Bu^tNC, the reaction to $Re_2(CO)_8(CNBu^t)_2$ was complete in less than 5 mins. However, if Pt/C and $LiAlH_4$ were added together to a solution of $Re_2(CO)_{10}$ and Bu^tNC (in the dark) with no pre-heating, no reaction was observed (for several hours). If more $LiAlH_4$ was then added after a few hours, a sluggish reaction was observed which proceeded very slowly over a period of several hours. If a solution of $Re_2(CO)_{10}$, Bu^tNC and Pt/C was heated at 55°C for 4 h (in the dark), oxygen bubbled through the solution, and $LiAlH_4$ then added, no reaction was observed (for several hours). If more $LiAlH_4$ was added after 2 h, a sluggish reaction was observed (cf. above). (The addition of oxygen has no effect on the reaction rate of the thermal uncatalysed reaction (in sunlight)). Hence the role of Pt/C in the Pt/C ~ $LiAlH_4$ catalytic system appears to be the removal from the solution of traces of O_2, which if present presumably prevent the catalysis of the reaction by $LiAlH_4$ by oxidizing the active catalytic species. No attempts have been made to further elucidate the mechanism by which the $LiAlH_4$-catalysed reaction operates. Other reducing agents such as zinc-metal do not catalyse reaction (11.2), hence the $LiAlH_4$-catalysed reaction could involve a mechanism involving the formation of hydride species.

On the basis of the results of the catalyst testing study (Table 11.1), PdO was selected as the catalyst to be used in the synthesis of $Re_2(CO)_{10-n}(CNR)_n$ derivatives (*vide infra*).

11.3 PdO-catalysed reaction of $Re_2(CO)_{10}$ with isonitriles

Using PdO as catalyst, a series of isonitrile derivatives, $Re_2(CO)_{10-n}(CNR)_n$ (n = 1-3, R = Bu^t, $C_6H_5CH_2$, C_6H_{11}; n = 1-4, R = 2,6-$Me_2C_6H_3$, Me), were prepared (reaction (11.3)) in generally high isolated yields, under moderate reaction conditions (Table 11.2).

$$Re_2(CO)_{10} + nRNC \longrightarrow Re_2(CO)_{10-n}(CNR)_n + nCO \qquad (11.3)$$

The power of this catalytic method is seen when comparing the reaction times at 55°C for the uncatalysed and the PdO-catalysed reaction (11.4)

$$Re_2(CO)_{10} + RNC \longrightarrow Re_2(CO)_9(CNR) + CO \qquad (11.4)$$

There is a substantial improvement in all cases (Table 11.3).

Owing to the facile nature of the PdO-catalysed synthesis of $Re_2(CO)_{10-n}(CNR)_n$ (n = 1,2), some $Re_2(CO)_{10(n+1)}(CNR)_{(n+1)}$ is also generally formed, accounting for the less than quantitative yield obtained. The products are readily purified by column chromatography.

For $Re_2(CO)_{10-n}(CNR)_n$ (n = 1,2) derivatives, reaction times are of the order of 1 to 5 min, but the synthesis of $Re_2(CO)_7(CNR)_3$ requires longer times (ca. 45 min). Tetra-substitution to give $Re_2(CO)_6(CNR)_4$ could only be achieved in poor yields (20-40%) for R = Ms and 2,6-$Me_2C_6H_3$; the other isonitriles gave no tetra-substituted product after 3 h reaction. This could reflect the better π-acceptor ability of aromatic (2,6-$Me_2C_6H_3NC$) than of aliphatic isonitrile ligands.[92b] In the case of MeNC, this could be due to the small size of the MeNC ligand[44] and its electronic similarity to CO.[92b] Higher substitution could not be achieved for any of the isonitriles even after 24 h, except possibly for RNC = $CNC_6H_3Me_2$-2,6. In this case a maroon solid was obtained with a complex ^1H NMR spectrum and IR ($CHCl_3$): 2085(sh), 2060(s), 1995(sh), 1975(ms), 1835(sh), 1890(m) cm^{-1}, but the elemental analysis of this compound did not correspond to that calculated for $Re_2(CO)_5(CNC_6H_3Me_2$-2,6$)_5$, and its identity was not pursued. Hence the limit for this catalytic synthetic method, involving <u>direct</u> substitution of RNC on $Re_2(CO)_{10}$, is reached at the tetra-substituted step.

The reasons for this are thought to be electronic rather than steric, since $Re_2[P(OMe)_3]_{10}$ (Tolman cone angle[93] for $P(OMe)_3$: 107°) is known[215] (prepared by indirect methods). An X-ray crystal structure determination of the tetra-substituted $Re_2(CO)_6(CNC_6H_3Me_2$-2,6$)_4$ (ch. XIV) has shown that there are two <u>cis</u>-equatorial isonitrile ligands on each Re-atom. Since isonitriles are weaker π-acceptors than

TABLE 11.2: Reaction conditions and product yields for the PdO catalysed syntheses of the complexes $Re_2(CO)_{10-n}(CNR)_n$

R	n	T(°C)	t(min)	Isolated yield (%)
Bu^t	1	55	1	98
	2	55	5	80
	3	55	45	80
$C_6H_5CH_2$	1	55	1	75
	2	80	5	75
	3	80	45	85
C_6H_{11}	1	55	1	80
	2	110	15	70
	3	110	60	75
$2,6\text{-}Me_2C_6H_3$	1	55	5	70
	2	80	20	70
	3	110	40	98
	4	110	150	40
Me	1	55	10	80
	2	110	15	80
	3	110	30	80
	4	110	150	20

TABLE 11.3: Reaction times at 55°C for the uncatalysed and PdO-catalysed reaction

$$Re_2(CO)_{10} + RNC \longrightarrow Re_2(CO)_9(CNR) + CO \qquad (11.4)$$

R	Reaction Time (min) Uncatalysed[a]	PdO catalysed
Bu^t	210	<1
$C_6H_5CH_2$	360 [b]	<1
C_6H_{11}	180	<1
$2,6\text{-}Me_2C_6H_3$	360 [b]	5
Me	120	10

[a] Under laboratory light conditions

[b] Reaction incomplete

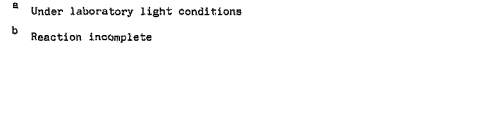


Figure 11.1: Synthetic routes to the mixed-isocitrile derivative, $Re_2(CO)_8(CNBu^t)(CNC_6H_3Me_2\text{-}2,6)$ (T = 55°C).

carbonyls,[93] the CO-group trans to an isonitrile ligand is less labile than that trans to another carbonyl ligand.[192] A fifth isonitrile ligand would have to go trans to another isonitrile, or trans to the Re-Re bond, both electronically unfavourable situations.[122,139] However, it is possible to prepare such complexes by means of indirect methods, e.g. $Mn_2(CO)_5(CNR)_5$ (R = Me, Ph, p-$C\ell C_6H_4$) has been prepared by nucleophilic attack of $Mn(CO)_5^-$ on $Mn(CNR)_5X$ (X = Cℓ, Br, CN).[217]

Since the catalytic reaction of $Re_2(CO)_{10}$ with RNC proceeds in a quantitative and stepwise manner, the degree of isonitrile substitution can be controlled by the number of equivalents of RNC added. Hence it is possible to prepare mixed isonitrile derivatives by adding one equivalent of RNC, and on complete conversion of $Re_2(CO)_{10}$ to $Re_2(CO)_9(CNR)$, a second equivalent of a different isonitrile, R'NC, to give the mixed-isonitrile derivative, $Re_2(CO)_8(CNR)(CNR')$, e.g. $Re_2(CO)_8(CNBu^t)(CNC_6H_3Me_2\text{-}2,6)$. The order in which the RNC and R'NC ligands are added in the mixed reaction is not of consequence, the same product being obtained in either case (see Fig. 11.1).

Satisfactory elemental analyses have been obtained for all the $Re_2(CO)_{10-n}(CNR)_n$ (n = 1-4) complexes. (Table 11.4). These complexes have been characterized by IR (Table 11.5) and ^1H NMR (Table 11.6) spectroscopy (vide infra), and an X-ray crystallographic study of a series of representative complexes has been undertaken (ch. XIV).

11.4 Characterization of the dirhenium carbonyl isonitrile derivatives

11.4.1. Infra Red Spectroscopy

IR data for the $Re_2(CO)_{10-n}(CNR)_n$ (n = 1-4) complexes are given in Table 11.5. These compounds have complex IR spectra.

In the case of the mono-substituted $M_2(CO)_9(L)$ (M = Re, Mn) complex, ax-$M_2(CO)_9(L)$ (point group C4v) is predicted to have 5 ν(CO) IR bands, while eq-$M_2(CO)_9(L)$ (point group Cs) should have 9 ν(CO) IR bands. However, many

TABLE 11.4: Analytical data for the $Re_2(CO)_{10-n}(CNR)_n$ (n = 1-4) complexes

Complex	Colour	mp(°C)	Elemental analysis (%)[a] C	H	N
$Re_2(CO)_9(CNBu^t)$	white	104-106	23.6(23.8)	1.2(1.3)	1.9(2.0)
$Re_2(CO)_9(CNCH_2C_6H_5)$	yellow	66-67	27.9(27.5)	0.98(0.95)	2.0(1.9)
$Re_2(CO)_9(CNC_6H_{11})$	white	60-61	26.4(26.2)	1.4(1.5)	2.0(1.9)
$Re_2(CO)_9(CNC_6H_3Me_2\text{-}2,6)$	cream	108-110	28.4(28.6)	1.2(1.2)	1.9(1.9)
$Re_2(CO)_9(CNMe)$	yellow	104-106	20.1(19.9)	[illegible]	[illegible]
$Re_2(CO)_8(CNBu^t)_2$	white	94-97	28.6(28.3)	2.3(2.[illegible]	[illegible]
$Re_2(CO)_8(CNCH_2C_6H_5)_2$	yel	73-75	34.9(35.4)	1.7(1.7)	3.5(3.4)
$Re_2(CO)_8(CNC_6H_{11})_2$	yel	42-44	32.6(32.4)	2.7(2.7)	3.4(3.4)
$Re_2(CO)_8(CNC_6H_3Me_2\text{-}2,6)_2$	yello	173-174	36.2(36.4)	1.9(2.1)	3.3(3.3)
$Re_2(CO)_8(CNMe)_2$	yellow	121-124	21.6(21.2)	0.92(0.89)	4.3(4.1)
$Re_2(CO)_8(CNBu^t)(CNC_6H_3Me_2\text{-}2,6)$	yellow	106-108	32.4(32.6)	2.2(2.2)	3.5(3.5)
$Re_2(CO)_7(CNBu^t)_3$	white	150-152	33.5(32.3)	3.5(3.3)	5.2(5.1)
$Re_2(CO)_7(CNCH_2C_6H_5)_3$	yellow	115-116	40.3(40.5)	2.3(2.3)	4.6(4.6)
$Re_2(CO)_7(CNC_6H_{11})_3$	yellow	44-46	38.4(37.5)	3.7(3.7)	4.7(4.7)
$Re_2(CO)_7(CNC_6H_3Me_2\text{-}2,6)_3$	yellow	164-166	[illegible](42.3)	4.1(4.4)	2.8(3.1)
$Re_2(CO)_7(CNMe)_3$	yellow	143-144	22.5(22.6)	1.2(1.3)	5.9(6.0)
$Re_2(CO)_6(CNC_6H_3Me_2\text{-}2,6)_4$	yellow	201-202	42.2(42.4)	3.4(3.4)	5.3(5.3)
$Re_2(CO)_6(CNMe)_4$	yellow	201-204	24.3(23.9)	1.5(1.7)	7.8(8.0)

[a] Found, calculated in parentheses

TABLE 11.5: Infra Red data of the complexes $Re_2(CO)_{10-n}(CNR)_n$ (n = 1-4)

Complex	ν(NC)(cm^{-1})[c]	ν(CO) (cm^{-1})[c]							
$Re_2(CO)_9(CNBu^t)$[a]	2173(m)	2101(m)		2050(m)	2018(sh)	1996(vs)	1979(w)	1970(m)	1952(s)
$Re_2(CO)_9(CNCH_2C_6H_5)$[a]	2180(m)	2100(m)		2050(m)	2018(sh)	1997(vs)		1971(m)	1954(s)
$Re_2(CO)_9(CNC_6H_{11})$[a]	2180(m)	2102(m)	2076(w)	2050(m)	2018(m)	1997(vs)		1970(m)	1952(s)
$Re_2(CO)_9(CNC_6H_3Me_2\text{-}2,6)$[a]	2148(m)	2090(m)		2048(m)	2019(sh)	2000(vs)		1974(m)	1955(s)
$Re_2(CO)_9(CNMe)$[a]	2197(m)	2105(m)	2076(w)	2053(m)	2019(m)	1998(vs)		1972(m)	1955(s)
$Re_2(CO)_8(CNBu^t)_2$[a]	2154(m)	2060(w)	2029(m)	1978(vs)	1945(sh)	1935(s)			
$Re_2(CO)_8(CNCH_2C_6H_5)_2$[a]	2164(m)	2066(w)	2031(m)	1982(vs)		1939(s)			
$Re_2(CO)_8(CNC_6H_{11})_2$[a]	2160(m)	2064(m)	2028(s)	1979(vs)	1945(sh)	1922(w)			
$Re_2(CO)_8(CNC_6H_3Me_2\text{-}2,6)_2$[a]	2166(m),2124(m)	2055(m)	2027(s)	1984(vs)	1949(sh)	1940(m)			
$Re_2(CO)_8(CNMe)_2$[b]	2190(m)	2072(w)	2032(m)	1980(vs)	1947(sh)	1922(m)			
$Re_2(CO)_8(CNBu^t)(CNC_6H_3Me_2\text{-}2,6)$[a]	2170(w),2136(m)	2059(m)	2030(s)	1982(vs)		1939(s)			
$Re_2(CO)_7(CNBu^t)_3$[a]	2154(m),2140(sh)		2030(w)	1987(vs)	1967(vs)	1924(w)	1910(s)		
$Re_2(CO)_7(CNCH_2C_6H_5)_3$[b]	2160(m)		2039(m)	1992(vs)	1963(vs)		1900(s)		
$Re_2(CO)_7(CNC_6H_{11})_3$[a]	2156(m),2138(sh)		2032(m)	1990(vs)	1960(vs)	1927(m)	1912(s)		
$Re_2(CO)_7(CNC_6H_3Me_2\text{-}2,6)_3$[b]	2122(m),2105(sh)	2060(w)	2033(m)	1990(vs)	1968(vs)	1929(sh)	1908(m)		
$Re_2(CO)_7(CNMe)_3$[b]	2180(m)	2040(w)	2032(sh)	1980(vs)	1959(vs)	1919(sh)	1898(m)		
$Re_2(CO)_6(CNC_6H_3Me_2\text{-}2,6)_4$[b]	2112(s),2095(sh)	1978(vs)	1944(m)	1891(m)					
$Re_2(CO)_6(CNMe)_4$[b]	2168(m)	1971(vs)	1928(m)	1880(m)					

[a] Recorded in hexane

[b] Recorded in chloroform

[c] sh = shoulder, w = weak, m = medium, s = strong, vs = very strong

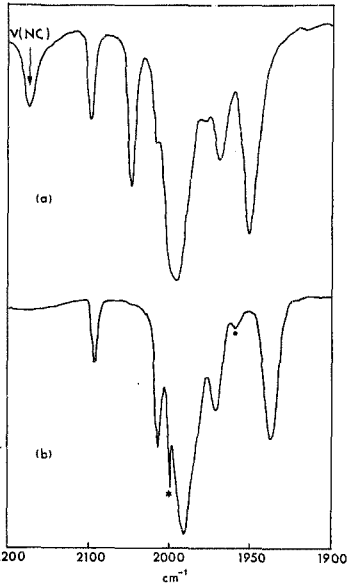


Figure 11.2: IR spectra (recorded in hexane, at X5 expansion) of (a) eq-$Re_2(CO)_9(CNBu^t)$, and (b) ax-$Mn_2(CO)_9(PMe_2Ph)$

* 'peak' due to monochromator change at 2000cm^{-1}

• weak band due to the presence of the ^{13}C-isotope

eq-$M_2(CO)_9(L)$ complexes reported in the literature[222] have fewer ν(CO) IR bands - *usually 6, owing to band overlap.* Axial complexes such as ax-$Mn_2(CO)_9(PR_3)$,[222-3] do have 5 ν(CO) IR bands, but there is also a weak band due to the presence *of the* ^{13}C *isotope (e.g.* ax-$Mn_2(CO)_9(PhMe_2Ph)$, IR(hexane), ν(CO): 2094(m), 2015(s), 1981(vs), 1971(ms), 1959(w) – (^{13}C peak), 1937(s) cm^{-1}). Hence the two isomers may both have IR spectra with the same number (6) of ν(CO) bands, the difference being in the relative intensities of the bands. The $Re_2(CO)_9$-(CNR) complexes are found to have one ν(CN) and 6 or 7 ν(CO) bands, not inconsistent with an eq-$Re_2(CO)_9(CNR)$ geometry. The complex $Re_2(CO)_9(CNBu^t)$ has been shown by X-ray crystallography to have the Bu^tNC ligand in the equatorial position (ch. XIV). Fig. 11.2 shows the IR spectra (ν(CO) region) of (a) eq-$Re_2(CO)_9(CNBu^t)$ and (b) ax-$Mn_2(CO)_9(PMe_2Ph)$[223] (substitution geometry established by X-ray crystallography[224]). The intensity patterns (ν(CO) bands) are superficially similar ((a) m,m-s,sh,vs,m-s,s; (b) m,s,vs,m-s,w,s). *However,* with the knowledge of which pattern corresponds to which structure, these two spectra, backed up as they are by X-ray *crystal structures,* could be used as reference spectra for the assignment of substitution geometry for $M_2(CO)_9(L)$ complexes.

For di-substituted $M_2(CO)_8(L)_2$ complexes, there are three possible geometry-types, viz. diax, ax,eq and dieq. Di-axial is ruled out for $Re_2(CO)_8(CNR)_2$ derivatives, because for this geometry (point group D4d) 2 ν(CO) IR bands are predicted, as is indeed observed for diax-$Mn_2(CO)_8(PR_3)_2$ complexes[223]The $Re_2(CO)_8(CNR)_2$ complexes have complex IR spectra with 4 or 5 ν(CO) bands. For ax,eq, and for dieq geometry, the two ligands may be on the same ($(CO)_5M$-$M(CO)_3$-$(L)_2$) or different ($(L)(CO)_4Re$-$Re(CO)_4(L)$) metal atoms. However, 8 ν(CO) IR bands are expected for all four cases (assuming staggered conformations). Fewer bands (usually 6) are generally exhibited by ax,eq-$M_2(CO)_8(L)_2$ complexes,[222] owing to band overlap. It is thus impossible to determine the substitution geometry from the IR spectrum, without a *prior knowledge of the intensity patterns characteristic of*

all the possible isomers. Further, the possibility of the product being a mixture of different geometric isomers (vide infra) cannot be excluded on the basis of IR data alone, although ^{1}H NMR is useful in this regard (see section 11.4.2).

X-ray crystallographic studies (ch. XIV) have shown the substitution of both $Re_2(CO)_8(CNC_6H_4Me_2\text{-}2,6)_2$ and $Mn_2(CO)_8(CNBu^t)_2$ to be diequatorial. However, in the former complex, the two isonitrile ligands are on different rhenium atoms, ie. 1,2-cis-dieq-$Re_2(CO)_8(CNC_6H_4Me_2\text{-}2,6)_2$ [FTIR(hexane), ν(NC): 2150(m), 2122(sh); ν(CO): 2053(m), 2028(s), 1985(vs), 1952(m), 1943(s) cm^{-1}], while the latter complex has both isonitrile ligands on the same manganese atom, ie 1,1-cis-dieq-$Mn_2(CO)_8(CNBu^t)_2$ [FTIR(hexane), ν(NC): 2174(w), 2154(w); ν(CO): 2055(m), 1999(vs), 1972(vs), 1963(w), 1952(m), 1935(m) cm^{-1}]. The 1,2-dieq-$Mn_2(CO)_8(CNBu^t)_2$ isomer is however also known [FTIR(hexane), ν(NC): 2144(w); ν(CO): 2049(w), 2006(s), 1977(vs), 1943(sh), 1939(w) cm^{-1}][225] (see section 11.4.2.) and 1,1-cis-dieq-$Re_2(CO)_8(CNBu^t)_2$ has been prepared indirectly [FTIR(hexane), ν(NC): 2183(m), 2157(w); ν(CO): 2065(m), 2032(s), 1987(vs), 1952(m), 1935(s) cm^{-1}].[224]

It is interesting to note that the IR spectrum of a polycrystalline sample of $Mn_2(CO)_8(CNBu^t)_2$ [IR(hexane), ν(NC): 2172(w), 2152(m); ν(CO): 2057(m), 1996(m), 1976(vs), 1949(w), 1936(m) cm^{-1}][224] is clearly a supposition of the above two spectrum types, indicative of the presence of both isomers, viz. 1,2-dieq-$Mn_2(CO)_8(CNBu^t)_2$ and 1,1-cis-dieq-$Mn_2(CO)_8(CNBu^t)_2$, the former predominating. The other $Mn_2(CO)_8(CNR)_2$ complexes reported have similar spectra.[224] The ^{1}H NMR spectra of these $Mn_2(CO)_8(CNR)_2$ complexes also provide evidence for the presence of two isomers, in contrast to the $Re_2(CO)_8(CNR)_2$ complexes (see section 11.4.2).

The FTIR spectra (hexane) of single-crystal samples of 1,2-dieq-$Re_2(CO)_8(CNC_6H_4Me_2\text{-}2,6)_2$ and 1,1-cis-dieq-$Mn_2(CO)_8(CNBu^t)_2$ are shown (ν(CO) region) in Fig. 11.3(a) and (b) respectively. In both cases there are 6 ν(CO) bands, but the relative intensities of the bands differ significantly. Hence IR spectra could be used to assign the substitution

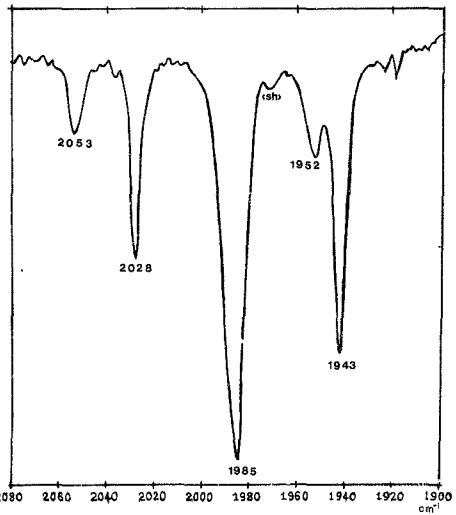


Figure 11.3(a): FTIR spectrum of 1,2-dieq-$Re_2(CO)_8(CNC_6H_3Me_2\text{-}2,6)_2$ (recorded in hexane)

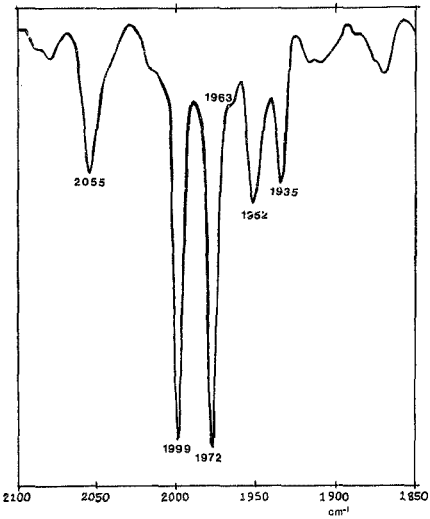


Figure 11.3(b): FTIR spectrum of 1,1-cis-dieq-$Mn_2(CO)_8(CNBu^t)_2$ (recorded in hexane)

geometry of such complexes. (This aspect of establishing a correlation between IR spectral data and substitution geometry for $M_2(CO)_8(L)_2$ complexes will be further elaborated in ch. XV). All the $Re_2(CO)_8(CNR)_2$ complexes prepared have IR spectra similar to that of 1,2-di-eq-$Re_2(CO)_8(CNC_6H_3Me_2\text{-}2,6)_2$. The $Re_2(CO)_8(CNR)_2$ complexes all have one ν(NC) IR band, with the exception of $Re_2(CO)_8(CNC_6H_3Me_2\text{-}2,6)_2$, which has two. As expected, the mixed isonitrile derivative, $Re_2(CO)_8(CNBu^t)(CNC_6H_3Me_2\text{-}2,6)$, has two ν(NC) absorptions.

For $M_2(CO)_7(CNR)_3$ complexes, 7 ν(CO) IR bands are predicted for the most likely geometries with all three RNC ligands equatorially substituted (axial substitution is electronically disfavoured,[139] and no ax-$M_2(CO)_{10-n}(CNR)_n$ (n = 1,2) isomers are known). The $Re_2(CO)_7(CNR)_3$ complexes have 4 to 6 ν(CO), and 1 or 2 ν(NC) bands in their IR spectra. The structure of $Re_2(CO)_7(CNMe)_3$ has been determined by X-ray crystallography (ch XIV), and was found to be a 1-eq,1,2-cis-dieq-isomer. Different conformations are possible in solution, but probably not isolable. The conformation observed in the crystal could be largely determined by crystal packing forces (see ch. XIV).

The IR spectrum of an all-equatorially substituted $M_2(CO)_6(CNR)_4$ compound is expected to have 6 ν(CO) bands for both the staggered and eclipsed forms. The $Re_2(CO)_6(CNR)_4$ (R = $C_6H_3Me_2$-2,6; Me) complexes have 3 or 4 ν(CO) bands, and 1 (R = Me) or 2 (R = $C_6H_3Me_2$-2,6) ν(NC) bands. The complex $Re_2(CO)_6(CNC_6H_3Me_2\text{-}2,6)_4$ has been shown crystallographically (ch. XIV) to have a staggered geometry, with two isonitrile ligands occupying cis-equatorial positions on each rhenium atom. [FTIR (benzene), ν(NC): 2109(m), 2089(m); ν(CO): 1978(vs), 1942(m), 1929(w), 1899(m) cm^{-1}]. The analogous $Mn_2(CO)_6(CN\,C_6H_3Me_2\text{-}2,6)_4$, however, has 1 ν(NC) and 5 ν(CO) bands.[226]

From the above discussion it is apparent that the number of ν(CO) bands observed in an IR spectrum of a metal carbonyl complex of the type $M_2(CO)_{10-n}(L)_n$ (n = 1-4) is often less than the number predicted by the application of Group Theory,

due to possible band overlap. Further, Group Theory often predicts the same number of bands for alternate geometries. Hence IR data alone is not sufficient for an unambiguous assignment of substitution geometry. However, used in conjunction with X-ray crystallography for selected complexes, it is possible to establish a correlation between IR spectral data (intensity patterns) and substitution geometry, as was illustrated in the case of the two possible isomers of dieq-$M_2(CO)_8(CNR)_2$ (M = Re, Mn). This correlation is extended to other isomers of $M_2(CO)_8(L)_2$ in ch. XV. (Section 15B).

11.4.2 Proton Nuclear Magnetic Resonance Spectroscopy

The ^1H NMR spectra of the $Re_2(CO)_{10-n}(CNR)_n$ (n = 1-4) complexes are given in Table 11.6. The monosubstituted $Re_2(CO)_9(CNR)$, disubstituted $Re_2(CO)_8(CNR)_2$ (with the exception of R = Me, vide infra) and tetra-substituted $Re_2(CO)_6(CNR)_4$ complexes give the expected ^1H NMR spectra (single $\delta(CH_x)$ (x = 2,3) resonances). The simple spectrum observed for $Re_2(CO)_6(CNC_6H_3Me_2\text{-}2,4)_4$ is in contrast to the complex spectrum reported for the analogous $Mn_2(CO)_6(CNC_6H_3Me_2\text{-}2,6)_4$.[220] The signal for the CH_2 or CH_3 protons of the trisubstituted $Re_2(CO)_7(CNR)_3$ complexes consists of two resonances in a 1:2 ratio. This was also observed for the $Mn_2(CO)_7(CNR)_3$ complexes.[219] The three isonitriles are expected to arrange themselves in equatorial positions around the dimer in a 2:1 ratio, as indicated in Fig. 11.5. Such a structure (C) is found in the solid state for $Re_2(CO)_7(CNMe)_3$ (ch. XIV).

The ^1H NMR spectra for the $Re_2(CO)_{10-n}(CNR)_n$ (n = 1-4) complexes show a trend of the CH_x (x = 2,3) resonance to lower field with increasing n (Fig. 11.4). The trend to lower field is expected (consequence of increased electron density on the metal[192b]), but the remarkable feature is the linear shift with similar slopes for all the isonitriles studied. This provides strong evidence for the dimer being treated as a single unit and not as two poorly interacting halves.

An interesting observation in the case of $Re_2(CO)_{10-n}$-

$(CNCH_2C_6H_5)_n$ (n = 1-3) is that the C_6H_5-signal, which is a complex multiplet for mono-and di-substituted derivatives, becomes a sharp singlet for $Re_2(CO)_7(CNCH_2C_6H_5)_3$. For the $Re_2(CO)_{10-n}(CNC_6H_3Me_2\text{-}2,6)_n$ (n = 1-4) derivatives, there are only two C_6H_3-resonances when n= 4, as opposed to the three for n = 1,2,3.

In the case of the disubstituted derivatives, $Re_2(CO)_8(CNR)_2$, the ^1H NMR spectra are as expected for R = Bu^t, $C_6H_5CH_2$, C_6H_{11}, $2,6\text{-}Me_2C_6H_3$ (ie. a single resonance for CH_x (x = 2,3), but for R = Me, the CH_3-group has two resonances in a ca. 1:5 ratio. This phenomenon is observed for the CH_2 or CH_3 protons of all the related $Mn_2(CO)_8(CNR)_2$ (R = Bu^t, $C_6H_5CH_2$, C_6H_{11}, $2,6\text{-}Me_2C_6H_3$ and Me) complexes.[228] This suggests that two isomers are present in solution. For $Mn_2(CO)_8(CNBu^t)_2$, these isomers have been shown to be 1,1-cis-dieq-$Mn_2(CO)_8(CNBu^t)$ (Fig. 11.6(A)) and 1,2-dieq-$Mn_2(CO)_8(CNBu^t)_2$ (Fig. 11.6(B)), with the latter predominating (see section 11.5.2). There also appear to be two isomers in solution for the mixed isonitrile derivative, $Re_2(CO)_8(CNBu^t)(CNC_6H_3Me_2\text{-}2,6)$.

11.4.3 Raman Spectroscopy[226]

Raman studies were undertaken[226] on the $Re_2(CO)_{10-n}(CNR)_n$ (n = 1-3, R = Bu^t, $C_6H_5CH_2$; n = 1-4, R = $2,6\text{-}Me_2C_6H_3$, Me) complexes. For $Re_2(CO)_{10-n}(CNR)_n$, as the value of n increases, the peak frequencies in the CO-stretching region decrease regularly, while the peak frequencies in the M-C-O bending region increase. However, this usual behaviour of the CO-stretching and M-C-O bending modes is not followed by that of the main peak at ca. 120 cm^{-1}, assigned to the C-Re-C bending mode. As a function of n, this peak frequency increases (n = 0-2), reaches a maximum at n = 2, then decreases (n = 3,4; R = Bu^t, $C_6H_5CH_2$, $2,6\text{-}Me_2C_6H_3$). This effect can be explained by a decrement of the force constant of the Re-C bond, then by an increment of the force constant, due to the increasing steric hinderance effect induced by multiple substitution of bulky isonitrile groups [e.g. "fan-shaped" angles[44] (wideness, thickness) for

TABLE 11.6: ^{1}H NMR data of the complexes $Re_2(CO)_{10-n}(CNR)_n$ (n = 1-4)

R	n	δ/ppm[a] C_6H_n	CH_3	or CH_2
Bu^t	1	-	0.75	
	2	-	0.87	
	3		1.02,0.98[b]	
$C_6H_5CH_2$	1	6.74-6.99[c]		3.77
	2	6.82-7.00[c]		3.87
	3	6.95		4.05,4.00[b]
C_6H_{11}	1	1.26-1.05[c],0.97-0.82[c]	-	
	2	1.26,1.09[c],0.90,0.85[c]	-	
	3	1.40[c],0.93,0.89[c]	-	
$2,6\text{-}Me_2C_6H_3$	1	6.69,6.63,6.58	2.00	
	2	6.68,6.63,6.58	2.10	
	3	6.67,6.64,6.59	2.23,2.18[b]	
	4	6.64,6.60	2.34	
Me	1	-	1.94	
	2	-	2.16,2.10[d]	
	3	-	2.31,2.25[b]	
	4	-	2.45	
$Re_2(CO)_8(CNBu^t)$-$(CNC_6H_3Me_2\text{-}2,6)$		6.69,6.64,6.60[c]	0.86;2.14,2.10[d]	(Bu^t)(C_6H_3-Me_2-2,6)

[a] Recorded in C_6D_6, relative to TMS

[b] Ratio 1:2

[c] Multiplet

[d] Ratio 1:5

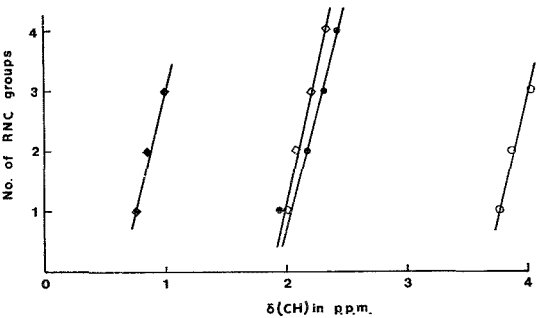


Figure 11.4: Plot of $\delta(CH_x)$ (x = 2,3) vs n(RNC) for the $Re_2(CO)_{10-n}(CNR)_n$ (n = 1-4) complexes (◆= Bu^tNC, ◇= $2,6\text{-}Me_2C_6H_3NC$, ● = MeNC and ○ = $C_6H_5CH_2NC$)

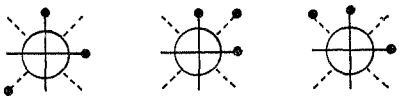


Figure 11.5: Newman projection of possible cis-equatorial conformational isomers of $M_2(CO)_7(CNR)_3$ (M = Re, Mn), as viewed down the M-M bond (• = RNC)

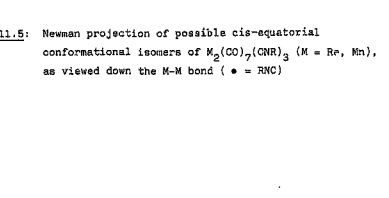


Figure 11.6: Isomers of $Mn_2(CO)_8(CNBu^t)_2$
(A) 1,1-cis-dieq, and (B) 1,2-dieq

Bu^tNC and 2,6-$Me_2C_6H_3NC$ respectively: 70°, 68°; 106°, 53°] and the capacity of the isonitriles to bend.

In the UV spectra[226] of the $Re_2(CO)_{10-n}(CNR)_n$ complexes, the $\sigma\rightarrow\sigma^*$ band of the Re-Re bond undergoes a red shift as a function of increasing n, indicative of an increase in electron density on the metal atoms, a result of replacing CO ligands with the poorer π-acceptor RNC ligands.[41] However, the intensity of this band remains relatively constant, indicating that increasing degree of isonitrile substitution does not cause any significant deformations of the complex in solution. This has been supported by X-ray data (see ch.XIV).

11.4.4 Mass Spectroscopy

(a) Mass spectrum of $Re_2(CO)_9(CNBu^t)$

The mass spectral data for $Re_2(CO)_9(CNBu^t)$ is given in Table 11.7. Since there are two naturally occuring isotopes of rhenium, $^{185}_{75}Re$ and $^{187}_{75}Re$, with natural abundances of 37.5% and 62.5% respectively, for monomeric fragments, two peaks occur in the mass spectrum, with the ratio ca. 1:1.67, corresponding to the two isotopes. For dimeric fragments, three peaks occur, corresponding to the possible isotope combinations $(^{185}Re)_2$, $(^{185}Re^{187}Re)$, $(^{187}Re)_2$, in the ratio ca.1:3.36:2.79. Where peak overlap occurs for two different fragments, the ideal isotope ratio will be disturbed.

Figs. 11.7(a) and 11.7(b) respectively show the dimeric (where Re_2 unit remains intact) and monomeric (Re fragment) fragmentation paths for $Re_2(CO)_9(CNBu^t)$. Obviously cross-over from the dimeric to the monomeric paths is possible at any stage. The fragmentation pattern is as expected. (Note that the Bu^t group is lost before the CN fragment, which is the last to be lost. This behaviour is typical for the $CNBu^t$ ligand, and reflects the stability of the Me_3C^+ ion.[77]) No one path appears to predominate. It is not possible to deduce from the MS data whether the Bu^tNC substitution is axial or equatorial.

TABLE 11.7: Mass spectral data for $Re_2(CO)_9(CNBu^t)$

m/z[a,b]	Relative intensities(%)	Fragment
185,187	1, 2	Re^+
211,213	<1, 1	$Re(CN)^+$
212,214	<1,<1	$Re(CNH)^+$
213,215	1,<1	$Re(CO)^+$
241,243	1,<1	$Re(CO)_2^+$
268,270	1, 2	$Re(CNBu^t)^+$
269,271	2, 3	$Re(CO)_3^+$
296,298	8, 13	$Re(CO)(CNBu^t)^+$
297,299	<1, 3	$Re(CO)_4^+$
324,326	61, 100	$Re(CO)_2(CNBu^t)^+$
325,327	4, 6	$Re(CO)_5^+$
352,354	2, 4	$Re(CO)_3(CNBu^t)^+$
370,372,374	4, 13, 11	Re_2^+
380,382	11, 18	$Re(CO)_4(CNBu^t)^+$
396,398,400	10, 29, 25	$Re_2(CN)^+$
397,399,401	5, 16, 12	$Re_2(CNH)^+$
398,400,402	29, 25, 2	$Re_2(CO)^+$
426,428,430	8, 20, 16	$Re_2(CO)_2^+$
453,455,457	18, 21, 16	$Re_2(CNBu^t)^+$
454,456,458	8, 23, 20	$Re_2(CO)_3^+$
481,483,485	3, 13, 11	$Re_2(CO)(CNBu^t)^+$
482,484,486	11, 29, 23	$Re_2(CO)_4^+$
509,511,513	5, 16, 15	$Re_2(CO)_2(CNBu^t)^+$
510,512,514	13, 36, 11	$Re_2(CO)_5^+$
537,539,541	3, 15, 15	$Re_2(CO)_3(CNBu^t)^+$
538,540,542	13, 34, 11	$Re_2(CO)_6^+$
565,567,569	3, 13, 13	$Re_2(CO)_4(CNBu^t)^+$
566,568,570	16, 47, 41	$Re_2(CO)_7^+$
593,595,597	28, 84, 70	$Re_2(CO)_5(CNBu^t)^+$
594,596,598	11, 17, 8	$Re_2(CO)_8^+$
621,623,625	3, 8, 6	$Re_2(CO)_6(CNBu^t)^+$

TABLE 11.7: Mass spectral data for $Re_2(CO)_9(CNBu^t)$ (Contd)

m/z	Relative intensities(%)	Fragment
622,624,626	2, 3, 1	$Re_2(CO)_9^+$
649,651,653	2, 6, 4	$Re_2(CO)_7(CNBu^t)^+$
677,679,681	1, 2, 2	$Re_2(CO)_8(CNBu^t)^+$
705,707,709	11, 36, 31	$Re_2(CO)_9(CNBu^t)^+$

[a] Fragments with m/z <185 are not reported.

[b] For monomeric fragments, ^{185}Re, ^{187}Re, and for dimeric fragments $(^{185}Re)_2$, $(^{185}Re\ ^{187}Re)$, $(^{187}Re)_2$

FIGURE 11.7(a): Dimeric fragmentation pattern for $Re_2(CO)_9(CNBu^t)$

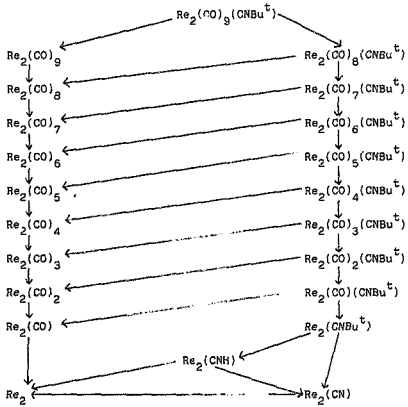
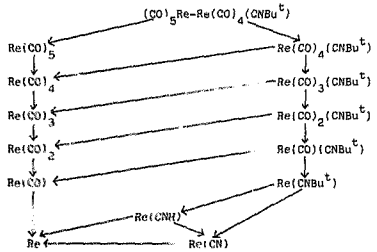


FIGURE 11.7(b): Monomeric fragmentation pattern for $Re_2(CO)_9(CNBu^t)$



(b) Mass spectrum of $Mn_2(CO)_8(CNBu^t)_2$

Mass spectra were recorded of (I) a polycrystalline sample of $Mn_2(CO)_8(CNBu^t)_2$, containing both isomers, $[Mn(CO)_4(CNBu^t)]_2$ and $(CO)_5Mn\text{-}Mn(CO)_3(CNBu^t)_2$ (see section 11.4.2.), and of (II) single crystals of one isomer, $(CO)_5Mn\text{-}Mn(CO)_3(CNBu^t)_2$, used in the X-ray diffraction study (Ch.XIV). The mass spectral data for (I) and (II) are given in Table 11.8.

The possible fragmentation paths for $Mn_2(CO)_8(CNBu^t)_2$ are shown in Fig. 11.8(a) (dimeric fragmentation path, ie. Mn_2 unit remains intact), and Fig. 11.8(b) (monomeric fragmentation path, ie. Mn fragment), together with the metastable peaks. The possible cross-overs between the dimeric and monomeric fragmentation paths (eg. $Mn_2(CNBu^t)$ (193) $\xrightarrow{m^* = 99}$ $Mn(CNBu^t)$ (138)) have not been shown. In the case of (II), the monomeric path commencing with the half-dimer fragment $Mn(CO)_4(CNBu^t)^+$ ($^m/_z$ = 250) would be expected to be absent.

Examination of Table 11.8 reveals that the most dramatic relative intensity changes in going from spectrum (I) to spectrum (II) occur for $^m/_z$ = 250 ((I): 76%, cf. (II): 3%) and $^m/_z$ = 305 ((I): 25%, cf. (II): 100%). The diminution of the $^m/_z$ = 250 peak for (II) is as expected, indicating the absence of the $Mn(CO)_4(CNBu^t)^+$ fragment. This peak still occurs due to the $Mn_2(CO)_5^+$ fragment. The effect is less pronounced for peaks lower down in the direct fragmentation path (e.g. $^m/_z$ = 194), because these fragments may be reached by cross-over from other monomeric and dimeric paths, and peak overlap of monomeric and dimeric fragments frequently occurs for this system. The enhancement of the $^m/_z$ = 305 peak for (II) is also expected, since this peak represents the $Mn(CO)_3(CNBu^t)_2$ fragment, the precursor in the only monomeric fragmentation route now available.

The mass spectra data further bear out the conclusion from the IR and ^1H NMR spectra (vide supra), in conjunction with the X-ray diffraction study (ch. XIV) on the nature of the isonitrile substitution in the two isomers of

TABLE 11.8: Mass spectral data for $Mn_2(CO)_8(CNBu^t)_2$

m/z [a]	Relative intensity(%) (I) $Mn_2(CO)_8(CNBu^t)_2$ [b]	(II) $(CO)_5Mn\text{-}Mn(CO)_3(CNBu^t)_2$ [c]	Fragment(s)
55	100	25	Mn^+
57	31	54	Bu^{t+}
81	10	43	$Mn(CN)^+$
82	95	42	$Mn(CNH)^+$
83	10	22	$M(CO)^+$; $CNBu^{t+}$
110	37	6	Mn_2^+
111	8	6	$Mn(CO)_2^+$
136	33	32	$Mn_2(CN)^+$
137	20	9	$Mn_2(CNH)^+$
138	100	67	$Mn_2(CO)^+$; $Mn(CNBu^t)^+$
139	6	6	$Mn(CO)_3^+$
166	36	32	$Mn_2(CO)_2^+$; $Mn(CO)(CNBu^t)_4$
167	3	7	$Mn(CO)_4^+$
193	54	3	$Mn_2(CNBu^t)^+$
194	49	13	$Mn_2(CO)_3^+$; $Mn(CO)_2(CNBu^t)^+$
195	4	1	$Mn(CO)_5^+$
221	34	96	$Mn_2(CO)(CNBu^t)$; $Mn(CNBu^t)_2^+$
222	10	13	$Mn_2(CO)_4^+$; $Mn(CO)_3(CNBu^t)^+$
249	55	20	$Mn_2(CO)_2(CNBu^t)^+$; $Mn(CO)_2(CNBu^t)_2^+$
250	76	3	$Mn_2(CO)_5^+$; $Mn(CO)_4(CNBu^t)^+$ [d]

TABLE 11.8: Mass spectral data for $Mn_2(CO)_8(CNBu^t)_2$ (Contd.)

m/z [a]	Relative intensity(%) (I) $Mn_2(CO)_8(CNBu^t)_2$ [b]	(II) $(CO)_5Mn\text{-}Mn(CO)_3(CNBu^t)_2$ [c]	Fragments
276	1	7	$Mn_2(CNBu^t)_2^+$
277	76	16	$Mn_2(CO)_3(CNBu^t)^+$; $Mn(CO)_2(CNBu^t)_2^+$
278	1	1	$Mn_2(CO)_6^+$
304	1	12	$Mn_2(CO)(CNBu^t)_2^+$
305	25	100	$Mn_2(CO)_4(CNBu^t)^+$; $Mn(CO)_3(CNBu^t)_2^+$
306	6	13	$Mn_2(CO)_7^+$
332	<1	35	$Mn_2(CO)_2(CNBu^t)_2^+$
333	4	24	$Mn_2(CO)_5(CNBu^t)^+$
334	<1	2	$Mn_2(CO)_8^+$
360	<1	13	$Mn_2(CO)_3(CNBu^t)_2^+$
361	<1	3	$Mn_2(CO)_6(CNBu^t)^+$
388	<1	7	$Mn_2(CO)_4(CNBu^t)_2^+$
389	<1	6	$Mn_2(CO)_7(CNBu^t)^+$
416	<2	<1	$Mn_2(CO)_5(CNBu^t)_2^+$
417	<1	<1	$Mn_2(CO)_8(CNBu^t)^+$
444	18	<1	$Mn_2(CO)_6(CNBu^t)_2^+$
472	<1	<1	$Mn_2(CO)_7(CNBu^t)_2^+$
500	<1	6	$Mn_2(CO)_8(CNBu^t)_2^+$

[a] Fragments with m/z <55 are not reported. [b] (I) Polycrystalline sample of $Mn_2(CO)_8(CNBu^t)_2$ containing a mixture of isomers ($[Mn(CO)_4(CNBu^t)]_2$ and $[(CO)_5Mn\text{-}Mn(CO)_3(CNBu^t)_2]$) [c] (II) Single crystals of isomer $[(CO)_5Mn\text{-}Mn(CO)_3(CNBu^t)_2]$ [d] Not applicable for $(CO)_5Mn\text{-}Mn(CO)_3(CNBu^t)_2$(II) (see text)

Figure 11.8(a): Dimeric fragmentation pattern for $Mn_2(CO)_8(CNBu^t)_2$

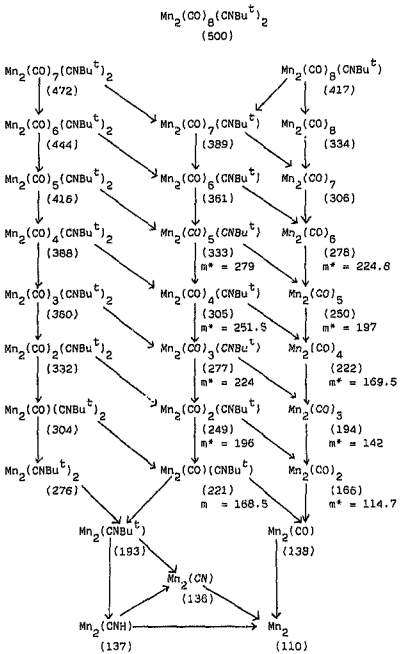
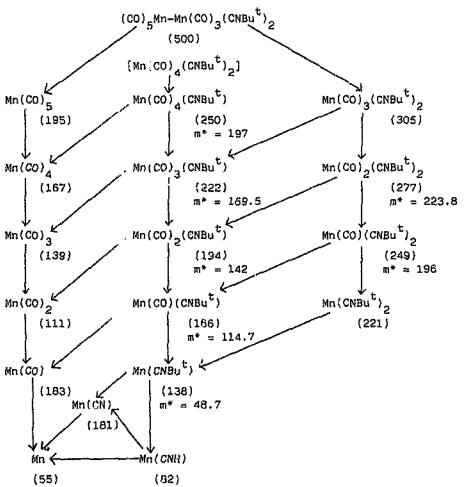


Figure 11.8(b): Monomeric fragmentation pattern for $Mn_2(CO)_8(CNBu^t)_2$



$Mn_2(CO)_8(CNBu^t)_2$ and suggest a method for detecting isomers and of assigning the substitution geometry of $M_2(CO)_8(CNR)_2$ complexes.

(c) Mass spectrum of $Re_2(CO)_8(CNC_6H_3Me_2\text{-}2,6)_2$

The mass spectral data for $Re_2(CO)_8(CNC_6H_3Me_2\text{-}2,6)_2$ is given in Table 11.9. The isotopes $^{185}_{75}Re$ and $^{187}_{75}Re$ give rise to two peaks for monomeric fragments, and three peaks for dimeric fragments (see section 11.4.4(a))

A single crystal sample of $[Re(CO)_4(CNC_6H_3Me\text{-}2,6)]_2$ (used in the X-ray diffraction study (ch.XIV)) was used. Figs. 11.9(a) and (b) show the dimeric (Re_2 unit remains intact) and monomeric (Re fragment) fragmentation paths respectively. Cross-over from dimeric to monomeric paths is of course possible.

As expected, the peaks corresponding to the monomeric fragments $Re(CO)_{3-n}(CNC_6H_3Me_2\text{-}2,6)_2$ (n = 0-3) with two isonitrile ligands on one Re-atom, are not present in the spectrum. (The peak corresponding to the fragment $Re(CO)_5^+$ ($^m/_z$: 325, 327) is likewise absent).

At low temperatures (135°C), the fragmentation pattern of $[Re(CO)_4(CNC_6H_3Me_2\text{-}2,6)]_2$ is dominated by the monomeric fragmentation path(s). However, as the temperature is increased, (probe heated to 175°C), the intensity of the peaks of the monomeric precursor fragment, $[Re(CO)_4(CNC_6H_3Me_2\text{-}2,6)]^+$ ($^m/_z$: 428, 430) and of $[Re(CO)_3(CNC_6H_3Me_2\text{-}2,6)]^+$ ($^m/_z$: 400, 402), decrease drastically, while peaks corresponding to Re_2-fragments previously absent appear, or increase in intensity if previously weakly present. Hence it would appear that for $[Re(CO)_4(CNC_6H_3Me_2\text{-}2,6)]_2$ the monomeric fragmentation path predominates at low temperatures, and the dimeric fragmentation path (ie. ligand loss before metal-metal bond cleavage) is favoured at elevated temperatures.

It is interesting to note that the peaks corresponding to the dirhenium carbonyl fragments, $Re_2(CO)_{8-n}$ (n = 0-4) are entirely absent from the spectrum of $[Re(CO)_4(CNC_6H_3Me_2\text{-}2,6)]_2$. This indicates that for this complex, dimeric

TABLE 11.9: Mass spectral data for the complex $[Re(CO)_4(CNC_6H_3Me_2\text{-}2,6)]_2$

m/z[a]	Relative Intensity(%)[b]	Fragment
185,187	<1	Re^+
211,213	3, 5	$Re(CN)^+$
213,215	5, 5	$Re(CO)^+$
241,243	11,24	$Re(CO)_2^+$
269,271	19,24	$Re(CO)_3^+$
297,299	15,27	$Re(CO)_4^+$
316,318	<1	$Re(CNC_6H_3Me_2\text{-}2,6)^+$
344,346	7,13	$Re(CO)(CNC_6H_3Me_2\text{-}2,6)^+$
372,374	14,11	$Re(CO)_2(CNC_6H_3Me_2\text{-}2,6)^+$
370,372,374	10,14,11	Re_2^+
396,398,400	6, 9,53	$Re_2(CN)^+$
398,400,402	9,53,82	$Re_2(CO)^+$
400,402	53,82 [c]	$Re(CO)_3(CNC_6H_3Me_2\text{-}2,6)^+$
428,430	60,100[c]	$Re(CO)_4(CNC_6H_3Me_2\text{-}2,6)^+$
426,428,430	6,80,100	$Re_2(CO)_2^+$
454,456,458	<1	$Re_2(CO)_3^+$
482,484,486	- [d]	$Re_2(CO)_4^+$
501,503,505	15,17,16	$Re_2(CNC_6H_3Me_2\text{-}2,6)^+$
510,512,514	- [d]	$Re(CO)_5^+$
529,531,533	22,32,28	$Re_2(CO)(CNC_6H_3Me_2\text{-}2,6)^+$
538,540,542	- [d]	$Re_2(CO)_6^+$
557,559,561	11,18,14	$Re_2(CO)_2(CNC_6H_3Me_2\text{-}2,6)^+$
566,568,670	- [d]	$Re_2(CO)_7^+$
585,587,589	5,10, 8	$Re_2(CO)_3(CNC_6H_3Me_2\text{-}2,6)^+$
594,596,598	- [d]	$Re_2(CO)_8^+$
613,615,617	11,33,27	$Re_2(CO)_4(CNC_6H_3Me_2\text{-}2,6)^+$
632,634,636	- [d,e]	$Re_2(CNC_6H_3Me_2\text{-}2,6)_2^+$
641,643,645	<1 [f]	$Re_2(CO)_5(CNC_6H_3Me_2\text{-}2,6)^+$
660,662,664	- [d,e]	$Re_2(CO)(CNC_6H_3Me_2\text{-}2,6)_2^+$
669,671,673	- [d,e]	$Re_2(CO)_6(CNC_6H_3Me_2\text{-}2,6)^+$
688,690,692	<1 [f]	$Re_2(CO)_2(CNC_6H_3Me_2\text{-}2,6)_2^+$
697,699.701	2, 6, 5	$Re_2(CO)_7(CNC_6H_3Me_2\text{-}2,6)^+$

TABLE 11.9: Mass spectral data for the complex $[Re(CO)_4(CNC_5H_3Me_2\text{-}2,6)]_2$ (Contd)

m/z[a]	Relative intensity(%)[b]	Fragment
716,718,720	-[d,e]	$Re_2(CO)_3(CNC_6H_3Me_2\text{-}2,6)_2^+$
725,727,729	-[d,e]	$Re_2(CO)_8(CNC_6H_3Me_2\text{-}2,6)^+$
744,746,748	-[d,e]	$Re_2(CO)_4(CNC_6H_3Me_2\text{-}2,6)_2^+$
772,774,776	-[d,e]	$Re_2(CO)_5(CNC_6H_3Me_2\text{-}2,6)_2^+$
800,802,804	-[d,e]	$Re_2(CO)_6(CNC_6H_3Me_2\text{-}2,6)_2^+$
828,830,832	-[d,e]	$Re_2(CO)_7(CNC_6H_3Me_2\text{-}2,6)_2^+$
856,858,860	-[d,e]	$Re_2(CO)_8(CNC_6H_3Me_2\text{-}2,6)_2^+$

[a] Fragments of m/z <180 are not reported

[b] At an ion chamber temperature of 135°C; probe then heated to 175°C (see c,e,f)

[c] Intensity decreases as temperature is increased

[d] Peak absent

[e] Peak appears as temperature is increased

[f] Intensity increases as temperature is increased

Figure 11.9(a): Dimeric fragmentation pattern for $[Re(CO)_4(CNC_8H_3Me_2\text{-}2,6)]_2$

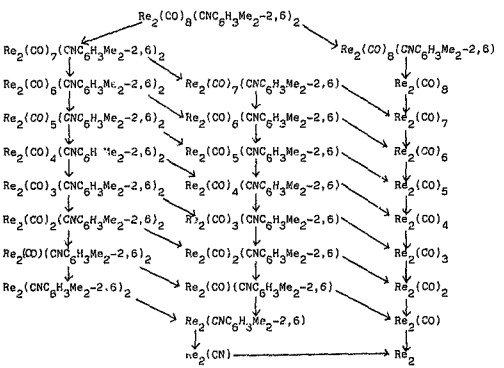
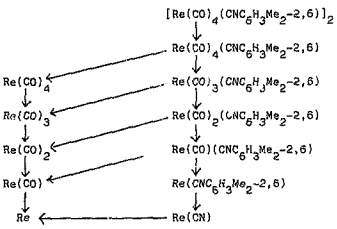


Figure 11.9(b): *Monomeric fragmentation path for* $[Re(CO)_4(CNC_6H_3Me_2\text{-}2,6)]_2$



fragmentation routes involving *loss of* both isonitrile ligands before the loss of at least *five carbonyls* is strongly disfavoured.

11.5 *Mechanism of the reaction of* $M_2(CO)_{10}$ (M = Re, Mn) *with isonitriles*

11.5.1 *Mechanism of the PdO-catalysed reaction between* $Re_2(CO)_{10}$ *and* Bu^tNC *to give* $Re_2(CO)_9(CNBu^t)$ *-* ^{13}CO *labelling study*

The reaction of $Mn_2(CO)_{10}$ and Bu^tNC (thermal, at 80°C, or in the presence of Pd/C (5% Pd) catalyst, at 25°C) to give the monosubstituted $Mn_2(CO)_9(CNBu^t)$, has been demonstrated to proceed without *Mn-Mn* bond scission.[227] In the experiment, $Mn_2(CO)_{10}$ and isotopically labelled $Mn_2(^{13}CO)_{10}$ (1:1 ratio) was used, and the product analysed by mass spectroscopy. The product consisted of $Mn_2(CO)_9(CNBu^t)$ and $Mn_2(^{13}CO)_9(CNBu^t)$ (1:1 ratio), with less than 1% mixed-isotope (ie. *Mn-Mn bond cleavage*) product.

To investigate the *mechanism of the PdO-catalysed* reaction between $Re_2(CO)_{10}$ and RNC, the *PdO- catalysed* reaction of $Re_2(CO)_{10}$ and $Re_2(^{13}CO)_{10}$ with Bu^tNC (1:1:2 *ratio*) at 50°C was performed. The reaction to $Re_2(CO)_9(CNBu^t)$ *was* complete *in less than* 1 min. This product was analysed by mass spectroscopy, *in order to* determine whether any mixing of the labelled carbonyls, indicative *of Re-Re* bond cleavage, had occured. The results clearly indicated that *Re-Re bond* cleavage had not occured. For instance, parent ion peaks (equal intensities) appeared at $^m/_e$ values of 707 and 716, corresponding to $^{187}Re\,^{185}Re(CO)_9(CNBu^t)^+$ and $^{187}Re\,^{185}Re(^{13}CO)_9(CNBu^t)^+$ *respectively*, but there were no peaks at 711 or 712 for $^{187}Re\,^{185}Re(CO)_5(^{13}CO)_4(CNBu^t)^+$ or $^{187}Re\,^{185}Re(CO)_4(^{13}CO)_5(CNBu^t)^+$, the expected bond-*cleavage* products. Hence the PdO- catalysed reaction of $Re_2(CO)_{10}$ with ^tBuNC, like that of $Mn_2(CO)_{10}$, proceeds without metal-metal bond *cleavage*.

11.5.2 *Kinetic studies of the reaction of* $M_2(CO)_{10}$ (M = Mn, Re) with Bu^tNC[225]

The reaction of $Mn_2(CO)_{10}$ with Bu^tNC has been studied kinetically. The PdO-catalysed reaction of $Mn_2(CO)_{10}$ with 2-*equivalents of* Bu^tNC in benzene at 50°C (2 h) yields crude

$Mn_2(CO)_8(CNBu^t)_2$. Recrystallization from hexane (-5°C) yielded a first crop of material which consisted only of 1,1-dieq-$Mn_2(CO)_8(CNBu^t)_2$, isomer A (Fig. 11.6). Repeated recrystallization (-5°C, hexane) yielded 1,2-dieq-$Mn_2(CO)_8(CNBu^t)_2$, isomer B (Fig. 11.6) (fifth crop).

Kinetic studies have shown that isomer B is initially formed, and is converted to isomer A on heating. Kinetic investigation of the isomerization reaction B⇌A have shown that at 50°C, equilibrium is established with the ratio of A:B either 1:3 (benzene) or 1:1 (hexane).

However, with $Re_2(CO)_8(CNBu^t)_2$, only isomer B is formed at 25°C, and the attempted thermal interconversion of B⇌A was unsuccessful even at 125°C. For the $Re_2(CO)_8(CNR)_2$ complexes prepared (see section 11.[illegible]. since isomer A was only observed (in the ^1H NMR spect[illegible] for $Re_2(CO)_8(CNMe)_2$ (see section 11.4.2.), the small size of the MeNC ligand ("fan-shaped" angle[illegible] : 52° (wideness) and 52° (thickness)) and its electronic similarity to CO[1926] may facilitate the interconversion of isomer B to isomer A. The results suggest that for $Re_2(CO)_8(CNR)_2$, isomer A is separated from isomer B by a high energy barrier. This is supported by the inability to convert isomer A, $(CO)_5Re\text{-}Re(CO)_3(CNBu^t)_2$ (prepared indirectly from the reaction of $NaRe(CO)_5$ with $Re(CO)_3(CNBu^t)_2I$[123]), to isomer B, $[Re(CO)_4(CNBu^t)]_2$.[123]

11.6 Experimental

11.6.1 Catalyst testing

To screen potential catalysts, use was made of reaction (11.2)

$$Re_2(CO)_{10} + Bu^tNC \rightarrow Re_2(CO)_9(CNBu^t) + CO \qquad (11.2)$$

$Re_2(CO)_{10}$ (0.20 mmol) and potential catalyst (4 mg; see Table 11.1) were stirred in benzene (4 ml) at 55°C. Bu^tNC (0.22 mmol) was then added to the solution, and the progress of the reaction was monitored by TLC (Silica; eluent: hexane: benzene (20%)). Reaction times for the substitution reaction (11.2) corresponded to the complete conversion of $Re_2(CO)_{10}$ to $Re_2(CO)_9(CNBu^t)$, as detected by TLC.

11.6.2 PdO- catalysed synthesis of $Re_2(CO)_{10-n}(CNR)_n$ (n = 1-3, R = Bu^t, $C_6H_5CH_2$, C_6H_{11}; n = 1-4, R = 2,6-$Me_2C_6H_3$, Me)

$Re_2(CO)_{10}$ (1.0 mmol) and the catalyst, PdO (20 mg) were stirred in toluene (10 mℓ). RNC (n mmol) was then added to the solution and the reaction was monitored by TLC (Silica; eluent: hexane: benzene (20% or 30%)). The reaction was terminated when complete conversion of $Re_2(CO)_{10}$ to $Re_2(CO)_{10-n}(CNR)_n$ had occured, or when no further reaction could be detected (by TLC). Column chromatography (Silica; 20cm x 1cm column; eluent: hexane: benzene (20%)) gave the required products in the indicated yields (Table 11.2). Recrystallization under nitrogen from solutions of dichloromethane-hexane, or benzene-hexane, gave the products as white or yellow crystalline solids. In the case of the $C_6H_{11}NC$ derivatives (n = 1-3), yellow oils were obtained, which on standing solidified over a period of several months.

11.6.3. PdO-catalysed synthesis of $Re_2(CO)_8(CNBu^t)(CNC_6H_3Me_2\text{-}2,6)$

$Re_2(CO)_{10}$ (1.0 mmol) and PdO (20 mg) were stirred in benzene (10 mℓ) at 55°C. RNC (1 mmol, R = Bu^t or 2,6-Me_2-C_6H_3) was then added to the solution, and the reaction monitored by TLC (Silica; eluent: hexane: benzene (30%)). After conversion of the $Re_2(CO)_{10}$ to $Re_2(CO)_9(CNR)$ was judged (by TLC) to be complete, R'NC (1 mmol, R' = 2,6-Me_2-C_6H_3 or Bu^t) was added. The reaction was terminated once all the $Re_2(CO)_9(CNR)$ had been converted to $Re_2(CO)_8(CNR)$-(CNR'). The product, $Re_2(CO)_8(CNBu^t)(CNC_6H_3Me_2\text{-}2,6)$, was isolated using the same procedure as that for the $Re_2(CO)_{10-n}$-$(CNR)_n$ derivates (*vide supra*), and recrystallized from dichloromethane-hexane solution to give a yellow crystalline solid. (70% isolated yield).

11.6.4. PdO-catalysed reaction of $Re_2(CO)_{10}$ and $Re_2(^{13}CO)_{10}$ with Bu^tNC (1:1:2 ratio)

$Re_2(CO)_{10}$ (0.015 mmol) and $Re_2(^{13}CO)_{10}$[117] (0.015 mmol), with catalyst PdO (10 mg), were stirred in benzene at 50°C.

(The reaction vessel was foil-wrapped to exclude all light). Bu^tNC (0.031 mmol) was then added to the solution and the reaction monitored by TLC (Silica; eluent: hexane:benzene (10%)). The reaction to $Re_2(CO)_9(CNBu^t)$ was complete in less than 1 min, and the heating was stopped after 5 min. The product was isolated by plate thin layer chromatography [Silica gel TLC plate (Whatman Chemical Separation Inc., K6F silica gel, 20 x 20 cm, layer thickness 250μ); eluent: hexane: benzene (10%)], extracted with dichloromethane, and recrystallized from dichloromethane-pentane solution, to give a white material, $Re_2(CO)_9(CNBu^t)$ (90% isolated yield].

XII. THE MODIFICATION OF $Re_2(CO)_{10}$ BY LIGANDS L

12.1 Introduction

Dirhenium decacarbonyl, $Re_2(CO)_{10}$, together with its analogue, *dimanganese* decacarbonyl, $Mn_2(CO)_{10}$, is an example of a simple *metal carbonyl* dimer, with a single metal-metal bond, and no bridging *ligands*. Owing to their relative chemical simplicity, these complexes *have been* used as model compounds in theoretical calculations,[95] and *extensively* studied by spectroscopic and diffraction methods.[105-139]

Substituted *derivatives* of the type $Re_2(CO)_{10-n}(L)_n$ (n = 1-4), have been less *extensively investigated*, possibly due to synthetic difficulties encountered *in such* carbonyl substitution reactions (ch. X). Substitution of *one or more* carbonyls for ligand(s) L can result in extensive *structural changes*, relative to the parent carbonyl, $Re_2(CO)_{10}$. *In the extreme* case, under suitable chemical conditions, the reaction *between* $Re_2(CO)_{10}$ and ligand L may result in the cleavage of the Re-Re *bond, and the* formation of mononuclear products of the type $Re(CO)_{5-n}(L)_n$.[140] *Reaction* between $Re_2(CO)_{10}$ and L may also yield dinuclear products *in which* the Re-Re bond has been cleaved,[133-8] the two halves *of the dimer* being held together by bridging ligand(s) L. *In cases where* the Re-Re bond remains intact (or acquires some multiple bond *character*) in the $Re_2(CO)_{10-n}(L)_n$ dimer, the structural changes *in the product* can be rationalized in terms of the steric and electronic *properties* of the ligand L. An understanding of the structural *features* of $Re_2(CO)_{10}$ is fundamental to an analysis of the structural *modifications* of the molecule by ligands L.

12.2 The Structure of $Re_2(CO)_{10}$

The (partial) X-ray crystal structures *of the isomorphous* $Re_2(CO)_{10}$ and $Mn_2(CO)_{10}$ were first determined by Dahl, *Ishishi* and Rundle in 1957,[137a] and a refined structure of $Mn_2(CO)_{10}$ was published by Dahl and Rundle in 1963.[137b]

Both structures were redetermined by Churchill, Amoh and Wasserman in 1981,[158] the main changes being in the M-M bond length distances. An X-ray crystal structure study at 74K of $Mn_2(CO)_{10}$ has also been published by Martin, Rees and Mitschler in 1982.[159] Prior to the full X-ray crystal structure of $Re_2(CO)_{10}$ by Churchill et al in 1981, the only full structural determination of this molecule was an electron diffraction study in the gas phase by Gapotchenko et al in 1972.[156] Similar studies have been reported for $Mn_2(CO)_{10}$, by Gapotchenko et al (1968)[155b] and Almenningen et al (1969).[155a]

$Re_2(CO)_{10}$ crystallizes in the monoclinic space group, I2/a, with 4 molecules in the unit cell, the two halves of the dimer being related by a crystllographic 2-fold axis. The molecular symmetry is D4d, each Re-atom being octahedrally coordinated to 5 CO groups and the other Re atom, with the equatorial carbonyls on the two halves of the dimer in a staggered configuration. The main structural features of the molecule are discussed below, in terms of the underlying electronic and/or steric factors determining the observed geometry.

12.2.1 The Re-Re bond length

The $Re_2(CO)_{10}$ molecule is diamagnetic, and obeys the 18-Electron Rule.[228] The rhenium atoms are connected by a single bond, the Re-Re bond length[158] in the crystal being 3.0413(11)Å. In $Mn_2(CO)_{10}$, the Mn-Mn bond length[159] is 2.9038(6)Å.

Bond length is generally taken as a reflection of bond strength. Measurements of bond strengthe (where reported) are often subject to large experimental uncertainties. The earliest thermochemical measurement of the Mn-Mn bond enthalpy for $Mn_2(CO)_{10}$ gave a ΔH value of 142kJ mol^{-1}.[229] Subsequent calorimetric measurements[163] for $Mn_2(CO)_{10}$ and $Re_2(CO)_{10}$ have given values for D(Mn-Mn) and D(Re-Re) of 67 and 128 kJ mol^{-1} respectively.

Estimates of metal-metal bond energies of $M_2(CO)_{10}$ (M = Re, Mn), have been made using indirect methods.

Several groups have carried out mass spectral studies[154] of $Mn_2(CO)_{10}$ and $Re_2(CO)_{10}$. From appearance and ionization potentials, the average metal-metal bond dissociation energy may be calculated for the process $M_2(CO)_{10} \longrightarrow 2{\cdot}M(CO)_5$ (M = Mn, Re). A range of D(M-M) values have been reported. (D(Mn-Mn): 79.0,[154a] 87.9,[154b] 92.5,[154c] 104.1[154d] kJ mol^{-1}; D(Re-Re): 213.9,[154c] 186.9[154d] kJ mol^{-1}).

A correlation between metal-metal stretching force constants and metal-metal dissociation energies (derived from electron impact measurements), has been found for $M_2(CO)_{10}$ (M = Mn, Re).[147b] From Raman spectra, metal-metal bond stretching force constants have been calculated using the method of normal co-ordinate analysis.[147] (f(Mn-Mn): 0.59 mdyn/Å,[147b] f(Re-Re): 0.82 mdyn/Å;[147a-b] another study[147c] gave values of 1.4 and 1.6 mdyn/Å respectively).

From kinetic studies of the decomposition of $M_2(CO)_{10}$ (M = Mn, Re), the energy of activation $\Delta H^{\ddagger}$ for M-M bond homolysis has been calculated. (For $M_2(CO)_{10}$,[230-2,161a] $\Delta H^{\ddagger}$ = 151 kJ mol^{-1}, and for $Re_2(CO)_{10}$,[231] $\Delta H^{\ddagger}$ = 162 kJ mol^{-1}). However, the estimates of the Mn-Mn bond strength have subsequently been felt[224] to be too low, in the light of the recent result[127] that the thermal reaction between $Mn_2(CO)_{10}$ and PR_3 to give $Mn_2(CO)_9(PR_3)$ proceeds without Mn-Mn bond scission (see Section 15C).

Metal-metal bond energies have been calculated from bond length (d) - enthalpy (E) relationship of the form $E = Ad^{-6.6}$ (A a constant).[172] Using bond lengths of 3.04Å and 2.92Å for Re-Re and Mn-Mn respectively, E(M-M) was calculated as 80 and 35 kJ mol^{-1} respectively for $Re_2(CO)_{10}$ and $Mn_2(CO)_{10}$. However, it should be noted that the M-M bond lengths used are those from the electron diffraction gas phase study of $Re_2(CO)_{10}$,[156] and from the early X-ray crystal study of $Mn_2(CO)_{10}$.[157] These values, especially for $Mn_2(CO)_{10}$, differ significantly from the refined values of the redetermined structures,[158] and, as acknowledged by

the authors, the use of incorrect bond length data could affect the accuracy of the results. Using ΔH (disrupt) values of 2029 and 1068 kJ mol^{-1} for $Re_2(CO)_{10}$ and $Mn_2(CO)_{10}$ respectively, where ΔH (disrupt) represents the enthalpy change for the process $M_2(CO)_{10} \longrightarrow 2M + 10\ CO$, the average enthalpy contribution assignable to the bonding of each carbonyl ligand to the metal (D(M-CO)) was calculated from the relationship

$$\Delta H(\text{disrupt}) = E(M\text{-}M) + 10\ D(M\text{-}CO),$$

and found to be 195 and 103 kJ mol^{-1} for $Re_2(CO)_{10}$ and $Mn_2(CO)_{10}$ respectively. Hence the percentage ΔH (disrupt) due to M-M bonding (ie. 100 (E(M-M))/ΔH (disrupt)) was calculated as 4% and 3% respectively for $Re_2(CO)_{10}$ and $Mn_2(CO)_{10}$, ie. less than 5% of the total disruption enthalpy is due to metal-metal bond cleavage.

As is apparent from the foregoing analysis, controversy surrounds the exact values of D(Re-Re) and D(Mn-Mn) in $Re_2(CO)_{10}$ and $Mn_2(CO)_{10}$. However, there is no doubt as to the relative order of the M-M bond strengths, viz. *D(Re-Re)> D(Mn-Mn)*.

On the basis of their MO calculations, Brown et al[235] have suggested that the term "unsupported" metal-metal bond applied to dirhenium decacarbonyl and dimanganes decacarbonyl requires modification, since an important contribution to the metal-metal bond energy in these dimers arises by interaction of metal orbitals with ligand orbitals on the opposite metal. However, this conclusion has been questioned[155] as other theoreticians[236] find no evidence of this cross-interaction from the results of their MO calculations. This effect is nevertheless evoked by some authors in explaining certain structural effects (vide infra).

12.2.2 The Re-CO bond lengths

From the X-ray crystal structure of $Re_2(CO)_{10}$,[188] the Re-COax bond length is 1.929(7)Å, compared to an average value for Re-COeq of 1.987(15)Å. The shorter M-COax than M-COeq bond length, also observed in the X-ray crystal

structure of $Mn_2(CO)_{10}$,[150-9] is ascribed to competition for dπ -electron density between mutually trans pairs of equatorial CO ligands. Low temperature electron density studies of $Mn_2(CO)_{10}$[159] have shown a greater electron deficiency in the axial than the equatorial carbonyls, again indicative of a stronger bonding to the metal of the axial than the equatorial carbonyl ligands.

As a result of the above electronic effect, CO has a larger trans influence that $M(CO)_5$.[159] Consequently, in reactions of $M_2(CO)_{10}$ with ligand L, equatorial substitution is expected, unless steric factors dominate with bulky ligands, eg. phosphines, to give products of the type ax-$M_2(CO)_9L$ eg. ax-$Mn_2(CO)_9(PMe_2Ph)$.[224]

12.2.3 Molecular Conformation

In the crystal, the $Re_2(CO)_{10}$ molecule adopts a staggered configuration, of molecular symmetry D4d, with OC-Re-Re-CO torsional angles close to the ideal 45°.[158] Repulsive interactions between equatorial CO groups might be expected to be less in the staggered than in the eclipsed conformation.[159]

The results of an electron diffraction study of $Re_2(CO)_{10}$ in the gas phase[156] were interpreted in terms of an eclipsed configuration, of molecular symmetry D4h. However, the validity of this anomalous result has been questioned,[144b] and force field calculations have shown that the difference in values of the eq-eq' interaction constants influenced by the change in molecular geometry from the staggered D4d, to the eclipsed D4h conformation, is small.[144b] Further, electron diffraction studies of $Mn_2(CO)_{10}$ in the gas phase[155] have indicated a staggered conformation, of molecular symmetry D4d, with the barrier to internal rotation estimated at ca. 8.4 KJ mol^{-1} or more.[155a] The agreement between experimental and theoretical curves for $Mn_2(CO)_{10}$ does not differ substantially for models with D4h and D4d symmetry, suggestive of an error of interpretation in the case of the $Re_2(CO)_{10}$ study.[144b]

In high pressure solid state Raman spectroscopic studies,[149] at ca. 8 Kbar for $Re_2(CO)_{10}$, and ca. 5 Kbar for $Mn_2(CO)_{10}$, changes were observed in the spectra indicative of a phase change and a repacking of the molecules, consistent with a transition from the staggered D4d conformation to the eclipsed D4h form. For $Re_2(CO)_{10}$, observation of spectral shifts at the phase transition provides evidence that in becoming eclipsed, the back-bonding from Re to axial-CO is sharply increased.

12.2.4 OC-Re-CO bond angles

A feature of the structure of $Re_2(CO)_{10}$ (and $Mn_2(CO)_{10}$) is the obtuse axOC-M-COeq, and the acute eqOC-M-COeq bond angles. This is also reflected in M-M-COeq angles of less than 90°, and is apparent in both the gas phase ($Mn_2(CO)_{10}$)[155a] and the crystalline state.[156-9]

This bending in of the M-COeq bonds towards the M-M bond has been variously ascribed to electronic and/or steric factors:-

(a) Steric

(i) C...C repulsions between equatorial carbonyls of the two halves of the dimer.[157b]

(ii) Repulsive interactions between axial and equatorial carbonyls in one half of the molecule.[157b,159] (In terms of non-bonding interactions, C...C repulsions of type (ii) are stronger than those of type (i).)[157b]

(iii) Influence of neighbouring molecules which increases O...O distances.[157b] (ie., crystal packing effects). However, this could not account for the gas phase observations (for $Mn_2(CO)_{10}$).[155a]

(b) Electronic

(i) Bonding interactions between a metal atom and the equatorial carbonyls on the opposite metal atom, ie., a back-bonding interaction of the type M (filled d orbital) ⟶ CO(π* orbital), where M, CO are not bonded directly.[215,217]

(ii) Rehybridization which decreases repulsions between the non-bonding d-electrons on the two metals, by mixing of p-character into the non-bonding orbitals dxz and dyz.[129-32]

(iii) An increase in the angle between the multiple-bonded M-CO bonds and a decrease in the angle between the single M-M bond and the equatorial bonds would decrease repulsions between the bonding electrons.[129]

(iv) Molecular orbital energy level diagrams (Elian and Hoffmann, 1975[38]) have shown that for 5-co-ordinate metal carbonyl fragments, the energetically most favoured geometry corresponds to an eqC-M-Cax angle of slightly greater than 90°, at which point π-interaction is maximized and anti-bonding interaction minimized.

This latter explanation receives further experimental support from the X-ray crystal structure of $HMn(CO)_5$,[229] which also showed a bending of the equatorial carbonyls towards the axial H-atom. Here the acute axOC-Mn-COeq angles cannot be ascribed to metal-carbonyl cross interaction (i). Further, it has been shown by a combination of ^{13}CO enrichment and IR spectroscopy,[119] that axOC-Mn-COeq bond angle in $Mn(CO)_5$ (molecular symmetry C4v) is 96(3)°. Explanations such as (i), (ii) would also not be applicable here. Clearly, if this effect were (partly) steric in origin, repulsive interactions of the type (i) would also be eliminated.

12.2.5 Re-C-O bond angles

In $Re_2(CO)_{10}$, (and $Mn_2(CO)_{10}$) the carbonyl ligands are close to linear, with M-C-O bond angles in the range 176 - 180°.[158]

Non-linearity of M-C-O fragments in $M(CO)_n$ (n = 2-4) groups has been examined,[19] and is a consequence of bonding and not solely a result of crystal packing forces. The M-C-O fragments are bent (ca. 5° deviation from linearity) due to different occupation of the two antibonding π* orbitals on a carbonyl ligand. (Hence linearity is expected for M(CO) only).

The reason for the different M-C-O angles within one $M(CO)_n$ group (often equal within experimental error) must lie in crystal packing forces[19] (eg. for $Re_2(CO)_{10}$, repulsive non-bonded O...O interactions between neighbouring

molecules which increases O...O distances [157b], or in the influence of other groups within the molecule which may lower the symmetry of the ML_n group. [39]

12.2.6 Packing

$Re_2(CO)_{10}$ crystallizes in the monoclinic space group I2/a. The Re-Re distances in the dimeric molecules are required by crystallographic symmetry to be parallel to one another. [157b] Hence repulsive non-bonding interactions between O-atoms of carbonyls on neighbouring molecules could be in part responsible for small deviations observed from the molecular D4d symmetry. [154]

Johnson [240] has proposed a model for the rationalization of the structures of simple binary carbonyls by considering the M_n unit as surrounded by a close-packed array of CO groups, with the M-atoms occupying the interstices. Thus anomalous bond lengths and distortions could be due to packing forces.

12.3 Ringing the changes: the effect of ligand substitution on molecular geometry

In derivatives of the type $Re_2(CO)_{10-n}(L)_n$ (n = 1-10), where a metal-metal bond is retained in the dimer, the substitution of carbonyl group(s) for ligand(s) L may nevertheless drastically affect the structure of the molecule relative to the parent carbonyl, $Re_2(CO)_{10}$. Such changes can be rationalized in terms of the steric and electronic properties of the ligand L relative to CO.

12.3.1 The Re-Re bond length

The Re-Re bond length is sensitive to changes in the metal co-ordination sphere. However, such variations should be interpreted with caution, as the metal-metal bond length is governed by an often complex set of factors, which may give rise to opposing trends.

Factors affecting the Re-Re bond length

(a) Bond Order

Problems arise as it is by no means always apparent whether a metal-metal bond exists, or what the bond order

is. In general, the possibility of a metal-metal bond is considered when the metal-metal distance is of the same order as in the bulk metal,[2a] but variability of metal-metal distances due to other factors (vide infra) precludes a conclusion based solely on bond length. The metal-metal bond defines a relatively flat energy minimum as a function of interatomic distance.[2a] Experimental data, such as metal-metal distances and magnetic properties, provide information, but not an unequivocal delineation.

Spiro[2c] has proposed that quantitative Raman intensity data for metal-metal stretching modes be used to establish a scale of metal-metal force constants, reflecting relative metal-metal bond strengths, with the view to the eventual establishment of a quantitative scale of metal-metal bond orders. The relation between force constants and bond strengths is a general, though not necessary one.[2c] For $M_2(CO)_{10}$ (M = Re, Mn), a correlation between M-M stretching force constants derived from Raman spectra, and metal-metal dissociation energies obtained from mass-spectral studies, is found[17b] (see section 12.2.1).

Recently Boeyens[2d] has proposed a general relationship between bonds that differ in order only. This method assumes that bond order derives essentially from changes in the repulsive part of covalent interactions, specifically from a modification of the internuclear repulsion due to electronic screening. Since the electron density in the region between atomic cores is sensitive to the nature of the ligands attached to the bonded atoms, in a series of compounds, metal-metal bond orders are expected over the whole range from 1 to 4, including non-integral bond orders, which in practice are often obtained.

In Organometallic chemistry, the metal-metal bond order has been based largely on Tolman's "18-Electron" or "Effective Atomic Number" (EAN) Rule.[22] In metal complexes, there is a tendency to achieve an 18-electron configuration, often by metal-metal bonding. Metal-metal bonding may be a compromise in the absence of other bonding partners.[2a]

However, this is not always unambiguous, as the number of electrons donated by a ligand can vary according to the mode of bonding of the ligand. Ambiguity arises as to the presence of a metal-metal bond where the compound can be formulated on electronic structure according to the 18-electron rule without a metal-metal bond, especially where the metal-metal distance is shorter than that in related compounds containing a metal-metal bond. However, structural constraints such as crystal lattice effects or bridging ligands, may force the metal atoms closer together. Often in the literature a shorter than "normal" Re-Re single bond is taken as indicative of some degree of multiple bonding.[212,244]

Although it is true in general that when two atoms are directly bonded to each other, the shorter the internuclear distance, the stronger the bond and the lower the bond order,[172] metal-metal bond distances do not provide reliable estimates of the metal-metal bond order, especially when bridging ligands are present,[245] as metal-metal bond order is dependent on other geometric, steric and/or electronic factors (vide infra). Cotton[245] has pointed out that with multiple metal-metal bonds, bond length is no indication of bond order, especially in the cases of triple and quadruple bonds.

At best, in a series of closely related complexes, a higher metal-metal bond order, or a stronger metal-metal bond, might be reflected in a shorter metal-metal bond length, where other structural differences are not significant. Hence X-ray analysis data alone cannot provide unequivocal information on the nature of the metal-metal bond, but electron density studies could prove useful in this regard.

(b) Electronic nature of ligands

The σ- or π- donor/acceptor properties of the ligand L in $Re_2(CO)_{10-n}L_n$, relative to CO, affect the bonding of the ligand L to the Re-atoms, and hence the Re-Re bond length. With ligands such as isonitriles, phosphines, hydrides, which are weaker π-acceptors than CO, [43,202] an increase in the Re-Re bond length can be expected,[192b,202] since more

However, this is not always unambiguous, as the number of electrons donated by a ligand can vary according to the mode of bonding of the ligand. Ambiguity arises as to the presence of a metal-metal bond where the compound can be formulated on electronic structure according to the 18-electron rule without a metal-metal bond, esp cially where the metal-metal di ance is shorter than that in related compounds containi a metal-metal bond. However, structural constraints such as crystal lattice effects or bridging ligands, may force the metal atoms closer together. Often in the literature a shorter than "normal" Re-Re single bond is taken as indicative of some degree of multiple bonding.[212,244]

Although it is true in general that when two atoms are directly bonded to each other, the shorter the internuclear distance, the stronger the bond and the lower the bond order,[172] metal-metal bond distances do not provide reliable estimates of the metal-metal bond order, especially when bridging ligands are present,[243] as metal-metal bond order is dependent on other geometric, steric and/or electronic factors (vide infra). Cotton[246] has pointed out that with multiple metal-metal bonds, bond length is no indication of bond order, especially in the cases of triple and quadruple bonds.

At best, in a series of closely related complexes, a higher metal-metal bond order, or a stronger metal-metal bond, might be reflected in a shorter metal-metal bond length, where other structural differences are not significant. Hence X-ray analysis data alone cannot provide unequivocal information on the nature of the metal-metal bond, but electron density studies could prove useful in this regard.

(b) Electronic nature of ligands

The σ- or π- donor/acceptor properties of the ligand L in $Re_2(CO)_{10-n}L_n$, relative to CO, affect the bonding of the ligand L to the Re-atoms, and hence the Re-Re bond length. With ligands such as isonitriles, phosphines, hydrides, which are weaker π-acceptors than CO,[47,267] an increase in the Re-Re bond length can be expected,[192b,228] since more

negative π-electron charge becomes localized on the metal, increasing the π-electron repulsions which weaken the metal-metal bond.

(c) Steric factors

Steric strain with bulky ligands may result in a lengthening of the Re-Re bond, to relieve interatomic non-bonded repulsions.

Where the molecule is forced into an eclipsed conformation by bridging ligands, repulsive interactions between eclipsed equatorial carbonyls might give rise to a longer Re-Re bond length.[202b,202]

(d) Bridging ligands

In ligand-bridged $Re_2(CO)_{10-n}(L)_n$ complexes, the metal-metal bond length is dependent on the particular ligand-bridged geometry, viz. the metal-to-bridging atom distance, and the M-B-M angle size[243,247] (B = bridging ligand). In general, in bridged dimeric systems, the M-B-M angle is sharply acute (ca. 70-75°) where a M-M bond exists, and obtuse (ca. 90-100°) where no direct M-M bond exists.[246] An acute M-B-M angle with no metal-metal bond, however, could be due to repulsions between large bridging atoms, eg. halogens.[201] Stability of an M_2B_2 bridged system is governed not only by the minimization of all non-bonded repulsions between atoms, but also by interorbital electron-pair interactions, which for a more electronegative bridging atom favours a wider bridging angle.[248]

With bridging ligands, two opposing factors may operate in determining the Re-Re bond length observed, viz. the "bite" of the bridging ligand, a ligand with a small bite size forcing the metal atoms closer together, and O...O repulsions between eclipsed carbonyl groups, which favour a longer Re-Re bond distance.[202b,202] The number of bridging ligands also plays a role in determining the Re-Re bond length. In similar complexes, the one with more bridging groups usually has a shorter metal-metal bond.[202] However, this could in part be due to the reduced number of eclipsed CO groups in the more highly bridged species.[202]

12.3.2 *The Re-CO bond lengths*

The stronger bonding of *Re-COax than Re-COeq* observed in $Re_2(CO)_{10}$ (section 12.2.2), *might* be expected also in $Re_2(CO)_{10-n}(L)_n$ derivatives. *However, in* substituted derivatives, bonding effects *due to the* electronic nature of the ligand L must also *be considered*, and these may alter or obscure the above *effect*.

Since π-acceptor ligands must compete *for the two* metal dπ orbitals,[102] the π-bonding between *the metal atom* and a CO trans to a ligand L, which is a weaker π-*acceptor* than CO, is greater than that to a CO cis to L.[102] *Hence a* shortening of the Re-CO (trans to L) relative to the (cis to L) bond length is expected with poor π-acceptor ligands L.[102] This is also the origin of the cis-labilization effects observed with poor π-acceptors L, resulting in initial cis-eq substitution for $Re_2(CO)_8(L)_2$ complexes.[102] Final substitution geometry is thus expected to cis-dieq-$Re_2(CO)_8(L)_2$, unless steric factors predominate, as in the case of bulky phosphine ligands, to give diax-$Re_2(CO)_8(L)_2$ complexes (*vide infra*).

Isonitrile (RNC) ligands are better σ-donors, but weaker π-acceptors than CO,[43] but stronger π-acceptors than phosphines (PR_3).[43a] With isonitrile ligands, one would expect to observe the above effects. Phosphines however, have a larger cone angle[85] than isonitriles,[44] and steric effects may dominate. In the reaction of $Mn_2(CO)_{10}$ with PR_3, to give diax-$Mn_2(CO)_8(PR_3)_2$, the cis-labilization *effect* accounts for the observation that the rate constant *for the second substitution* is larger than that for the *first*.[102] According to the proposed mechanism, the first *step is mono*-substitution to give ax-$Mn_2(CO)_9L$ (steric *factors governing* axial substitution), then loss of a CO cis *to the* PR_3 group on the same Mn-atom, followed by *exchange of* CO via a bridging mechanism, and PR_3 substitution on *the other* Mn-atom, steric consideration necessitating diaxial *substitution*.

12.3.3 Molecular Conformation

On steric ground, staggered molecular conformation is favoured, as this minimizes repulsive interactions.[131] However, bridging ligands necessitate an eclipsed configuration, where O...O repulsions between eclipsed equatorial carbonyls may result in distortions from the ideal molecular geometry.[21a,b]

12.3.4 OC-Re-CO bond angles

As discussed above (section 12.2.4.) the bending in towards the Re-Re bond of the equatorial carbonyls in Re[illegible] could be due to steric and/or electronic factors. [illegible]steric in origin (due to attempts to minimize re[illegible] interactions), a more pronounced effect might be expected with bulky ligands more sterically demanding than relatively small CO ligand (Tolman cone angle estimated at ca. 95°).[45a] If the origin of this effect is predominately electronic in nature, however, for ligands electronically similar to CO, eg. the isoelectronic RNC,[41] similar trends might be expected to be observed as with $Re_2(CO)_{10}$, especially if the ligand itself, although bulkier than CO, is not very sterically demanding, a situation which might impose severe steric constraints on the structure of the $Re_2(CO)_{10-n}(L)_n$ derivative.

12.3.5 Re-C-O bond angles

The analysis of non-linearity of M-C-O fragments in $M(CO)_n$ ($n = 2$-4) groups[35] applies to other MR_n groups also, eg. R = CN, NO. Hence near-linear co-ordination of those ligands (M-C-N ca. 175°) is predicted.

12.3.6 Packing

The packing of the molecules in the crystal is determined by the molecular geometry, crystallographic symmetry demands, and the principle of dense packing.[32] The molecules pack in such a way as to make the most efficient use of space ie. maximum closeness, without causing repulsive intermolecular interactions. Hence structural changes in the molecule may result in differences in

crystallographic space group and packing order. Further, interactions between groups on neighbouring molecules may cause anomalous structural features. Deviations from ideal geometry could reflect packing requirements in the crystal lattice.[285]

XIII X-RAY CRYSTALLOGRAPHIC STUDIES OF DIRHENIUM CARBONYL DERIVATIVES - A SURVEY OF THE LITERATURE

13.1 Introduction

As discussed in the previous chapter, the basic structure of the dirhenium decacarbonyl dimer may be changed (to a lesser or greater extent) by the substitution of one or more carbonyl groups for ligand(s) L. These structural effects can be rationalized in terms of the steric and/or electronic properties of ligand L relative to CO.

Despite the tremendous growth in recent years of the use of single crystal X-ray diffraction methods in product characterization, relatively few X-ray structures have been reported of dirhenium decacarbonyl derivatives. This could be due in part to synthetic difficulties often encountered in the preparation of such substituted derivatives of $Re_2(CO)_{10}$ (ch. X).

This review briefly describes the derivatives of dirhenium decacarbonyl for which an X-ray crystal and molecular structure has been reported in the Literature. Only those complexes with a direct Re-Re bond will be considered. The majority of these complexes were synthesized from the direct reaction of $Re_2(CO)_{10}$ with ligand L (ch. X), but some were prepared from the reaction of higher rheni clusters, eg. $[Re_3(H)_3(CO)_{12}]$.[165] The purpose of this review is to assess the effect of ligand substitution on molecular conformation and bond parameters, for a wide variety of ligands L.

Dirhenium carbonyl complexes which contain bridging bidentate ligands and/or bridging halogen atoms, but no direct Re-Re bond, will not be included in this review. For example, dirhenium complexes of the type $(\mu\text{-X})_2Re_2(CO)_6(L)_2$ (eg. X = Br, L = THF[249a]; X = Br, $(L)_2$ = μ-S_2Ph_2,[249b] μ-S_2Me_2,[249c] μ-Se_2Ph_2,[249d] μ-P_2Ph_4,[249c] X = Cℓ, $(L)_2$ = μ-$Ph_2AsCH_2AsPh_2$[250b]), prepared indirectly from monomeric rhenium halocarbonyl compounds,[249a,250a] (Re...Re distances range from 3.81 to 3.97Å).[249-250] Further, dirhenium complexes formed from reactions of

$Re_2(CO)_{10}$ (or derivatives thereof) with ligand L, but which lack a direct Re-Re bond, will also not be included in this review (eg. $(CO)_4Re\text{-}\mu\text{-}(\eta^3{:}\eta^1C_8H_5)\text{-}Re(CO)_5$,[193] formed from the photolysis of $Re_2(CO)_{10}$ with cyclooctatetraene; $(\mu\text{-Br})\text{-}Re_2(CO)_8[\mu\text{-CPh}]$,[251] formed from the reaction of $Re_2(CO)_9\text{-}[C(OMe)Ph]$ with $AlBr_3$). The so-called "metal-ring" compounds, eg. $[Re_2(CO)_8(Sn(I)Re(CO)_4(PPh_3))]$[252] (formed from reaction of $Re_2(CO)_8(PPh_3)_2$ with SnI_2), with a non-bonded Re-Re distance of 3.176(1)Å across the metal ring, are likewise excluded.

Those derivatives of $Re_2(CO)_{10}$, in which the direct Re-Re bond has been retained, for which X-ray crystal and molecular structures have been reported in the Literature, are listed in Table 13.1. In all the rhenium-rhenium bonded structures listed in Table 13.1, the basic dimeric unit has been retained, although a change in the metal-metal bond order may have resulted. The Re-Re bond length distances for each structure are also given in Table 13.1. A brief description of the salient features of these complexes, in terms of the electronic and steric effects of the ligand(s) L, will be given.

13.2 Literature Structures

13.2.1 Structures without bridging ligands

(a) Mono-substitution: eq-$Re_2(CO)_9(L)$, (L = CH(OMe); C(OR)($SiPh_3$), R = Me, Et

To date, the only mono-substituted derivatives of $Re_2(CO)_{10}$ reported are eq-$Re_2(CO)_9[CH(OMe)]$[211] (i), eq-$Re_2(CO)_8[C(OMe)(SiPh_3)]$[253] (ii) and eq-$Re_2(CO)_9\text{-}[Re_2(CO)_4(CNBut)(SiPh_3)]$[174a,251] (iii). All three molecules are equatorially substituted, as expected,[159,253] and adopt a staggered conformation, like the parent carbonyl, $Re_2(CO)_{10}$[85b] to minimize repulsive interactions between equatorial CO groups.[120]

The Re-Re bond lengths for compounds (i), (ii) and (iii), (see Table 13.1) are the same within error limits (ca. 3.05Å) and slightly longer (ca. 0.009Å) than that for $Re_2(CO)_{10}$ (3.0413(11)Å). Although significance cannot be

TABLE 13.1: *X-ray crystal structures of dirhenium carbonyl derivatives, with a direct Re-Re bond*

Complex	Space group, Z	Re-Re bond length(Å)	Reference
$Re_2(CO)_{10}$	I2/a,4 [a]	3.0413(11)	158
eq-$Re_2(CO)_9$[CH(OMe)]	Cc,8 [b]	3.047, 3.051	211 [c]
eq-$Re_2(CO)_9$[C(OMe)($SiPh_3$)]	$P2_1/c$,4	3.052(1)	253
eq-$Re_2(CO)_9$[C(OEt)($SiPh_3$)]	Cc,8 [b]	3.050(3), 3.052(4)	1?3a,253
1,2-ax,eq-$Re_2(CO)_8$[C(OEt)$SiPh_3$)]$_2$	Pc,2	3.091(2)	253
$Re_2(CO)_8$[μ-(η^2,η^2-C_6H_6)]	$P2_1/n$,4	3.114(1)	195
$Re_2(CO)_8$[μ-(η^1,η^3-CH·CH·CMe_2)]	$P2_1/c$,4	3.058(1)	199
$Re_2(CO)_8$[μ-NC_5H_4)(μ-H)	$P\bar{1}$,4 [b]	3.2088(4), 3.1956(5)	168
$Re_2(CO)_7$(ONMe$_3$)(μ-NC_5H_4)(μ-H)	Pbca,8	3.2324(5)	168
$Re_2(CO)_8$[μ-$SiPh_2$]$_2$	[d]	3.001(1)	202-3
$Re_2(CO)_8(H)_2$[μ-$SiPh_2$]	Pnn,8	3.121(2)	200
$Re_2(CO)_7(H)_2$[μ-$SiEt_2$]$_2$	$P\bar{1}$,2	3.052(1)	202
$Re_2(CO)_6(H)_4$[μ-$SiEt_2$]$_2$	$P\bar{1}$,1 [e]	3.084(1)	201
$Re_2(CO)_8$[μ-C(OMe)(C_6H_4Me-p)]$_2$	C2/c,4 [a]	2.81(3)	177b
(CO)$_4$Re[μ-C($SiPh_3$)CO(OEt)]Re(CO)$_3$-[C(OEt)($SiPh_3$)]	$P2_1/c$,4	2.937(1)	178c
$Re_2(CO)_8$[μ-(C($SiPh_3$)(CO))](μ-H)	$P2_1/c$,4	3.036(2)	178c
$Re_2(CO)_8(\mu\text{-H})_2$	$P2_1/c$,4	2.90 [f]	204
$Re_2(CO)_6(\mu\text{-H})_2$[$\mu$-$Ph_2PCH_2PPh_2$]	Pbca,8	2.893(2)	244a,b
$Re_2(CO)_6$(μ-H)(μ-NCHMe)[μ-$Ph_2PCH_2PPh_2$]	$P2_1/n$,4	3.035(3)	244a,c

TABLE 13.1: X-ray crystal structures of dirhenium carbonyl derivatives, wtih a direct Re-Re bond (Contd)

Complex	Space group, Z	Re-Re bond length(A)	Reference
$Re_2(CO)_6(\mu\text{-}H)(\mu\text{-}OH)[\mu\text{-}Ph_2PCH_2PPh_2]$	$P\bar{1}$,2	3.030(1)	198
$Re_2(CO)_4(PhCCPh)_3(CNCH_2SO_2C_6H_4Me\text{-}p)_2$	$P\bar{1}$,2	2.786(1)	212
$Re_2(CO)_4(PhCCPh)_4$	[d]	2.78 [f]	212

[a] Molecule possesses crystallographic C_2 symmetry

[b] Two crystallographically independent molecules in the asymmetric unit

[c] Data obtained from the Cambridge Crystallographic Data Base

[d] Unpublished structure; data not quoted in reference

[e] Molecule possesses crystallographic $\bar{1}$ symmetry

[f] Unrefined bond length value

attached to such a small difference, the slight increase could reflect the weaker π-acceptor ability of the carbene ligands relative to CO.[233]

Of note are the acute *Re-Re-CO angles*, and the obtuse Re-Re-C (carbene) angles observed for all three complexes (see Table 13.2). The bending in of the carbonyl ligands, reflected by the acute *Re-Re-CO angles*, *is in accord* with electronic predictions[88] (see section 12.2.4). The reversal of this trend for the carbene ligands could be due to steric interaction between the phenyl rings and eq-carbonyls for (i) and (ii), or, since steric crowding would not be expected to be severe with the [C(OMe)H] ligand in (i), a result of the electronic nature of the carbene ligand and its bonding to the Re-centre.

(b) Di-substitution: 1,2-ax,eq-$Re_2(CO)_8[C(OEt)(SiPh_3)]_2$

The only di-substituted derivative of $Re_2(CO)_{10}$ without a bridging ligand reported to date is 1,2-ax,eq-$Re_2(CO)_8[C(OEt)(SiPh_3)]_2$.[233] This complex, like that of the eq-$Re_2(CO)_9$ (carbene) complexes (i), (ii) and (iii) (vide supra) is staggered. One $[C(OEt)(SiPh_3)]$ ligand occupies an equatorial position of Re(1), while the second carbene occupies the axial site on Re(2). The overall electronic stabilization of the complex governs this 1,2-ax,eq-substitution geometry.[233] In an axial position, the carbene ligand is a stronger π-donor than in an equatorial position. The resultant increased electron density on the Re-atom is reflected in the lengthening of the Re-Re bond length in 1,2-ax,eq-$Re_2(CO)_8[C(OEt)(SiPh_3)]_2$ (3.091(2)Å) relative to that in eq-$Re_2(CO)_9$ (carbene) (see Table 13.1), eg. av. 3.051(3)Å for eq-$Re_2(CO)_9[C(OEt)(SiPh_3)]$.

The effect of acute *Re-Re-CO* and obtuse *Re-Re-CO*-(carbene) angles observed for eq-$Re_2(CO)_9$ (carbene) complexes (i)-(ii), (Table 13.2), is also found for 1,2-ax,eq-$Re_2(CO)_8[C(OEt)(SiPh_3)]_2$,[233] viz. av. *Re(1)-Re(2)-CO*: 83°; av. Re(2)-Re(1)-CO: 86° and Re(2)-Re(1)-C(eq carbene):96.9(8)° (Re(1)-Re(2)-C(ax carbene): 178.7(9)°).

TABLE 13.2: Average values of the Re-Re-C bond angles(°) for the eq-$Re_2(CO)_9$(carbene) structures (i)-(iii)

Complex	(i) eq-$Re_2(CO)_9[CH(OMe)]$ [a]	(ii) eq-$Re_2(CO)_9[C(OMe)(SiPh_3)]$ [b]	(iii) eq-$Re_2(CO)_9[C(OEt)(SiPh_3)]$ [b]
av. Re(2)-Re(1)-CO	82.8, 83.9 [c]	84	83, 84 [c]
av. Re(1)-Re(2)-CO	86.5, 84.2 [c]	87	85, 85 [c]
Re(2)-Re(1)-C(carbene)	94.5, 97.9 [c]	98.1(8)	94(1), 98(1) [c]

[a] *Data obtained from the* Cambridge Crystallographic Data Base

[b] Ref. 253

[c] Two crystallographically *independent molecules in the* asymmetric unit

13.2.2 Structures with bridging ligands

(a) A bridging olefin - $Re_2(CO)_8[\mu\text{-}(\eta^2,\eta^2\text{-}C_4H_6)]$

In $Re_2(CO)_8[\mu\text{-}(\eta^2,\eta^2\text{-}C_4H_6)]$,[193] the $Re_2(CO)_8$ fragment, in which the carbonyl groups are eclipsed (as necessitated by the bridging olefin), is co-ordinated to the bridging 1,3-butadiene ligand in the trans-configuration. With the alkyl ligand acting as a 2-electron donor to each Re-atom, the compound obeys the 18-Electron Rule,[228] the Re-Re single bond being 3.114(1)Å.[193] Re-COax and Re-CO(trans to alkyl ligand) bond lengths are approximately the same, and ca. 0.1Å shorter than the Re-CO(trans to CO) bonds, in accordance with electronic expectations.[150-6,162] Further, Re-Re-COeq bond angles are less than or equal to 90°, ie. the carbonyl ligands bend in towards the Re-Re bond, as noted for $Re_2(CO)_{10}$.[98,158] As expected,[19] the carbonyl ligands are slightly bent, with Re-C-O bond angles in the range 173 - 179°, averaging 177°.

(b) A bridging carbene - $Re_2(CO)_8(\mu\text{-}\eta^1,\eta^3\text{-}CH\cdot CH\cdot CMe_2)$

In $Re_2(CO)_8[\mu\text{-}\eta^1,\eta^3\text{-}CH\cdot CH\cdot CMe_2]$,[172] the two $Re(CO)_4$ fragments, which are eclipsed with respect to each other, are bridged by a μ-allylidine ligand formed by ring opening of the cyclopropene. The $\mu\text{-}(CH\cdot CH\cdot CMe_2)$ moiety is η^1-bonded to Re(1) and η^3-bonded to Re(2), resulting in the carbene ligand bridging the dirhenium unit in a highly asymmetric fashion. In accordance with the 18-Electron Rule,[228] a formal Re-Re single bond is required by the total of 34 valence electrons around the dirhenium unit. The Re-Re bond length of 3.056(1)Å is comparable to that of other Re-Re single bonded complexes (Table 13.1).

(c) $Re_2(CO)_8(\mu\text{-}NC_5H_4)(\mu\text{-}H)$ and $Re_2(CO)_7(ONMe_3)\text{-}(\mu\text{-}NC_5H_4)(\mu\text{-}H)$

The complex $Re_2(CO)_8(\mu\text{-}NC_5H_4)(\mu\text{-}H)$, and its derivative, $Re_2(CO)_7(ONMe_3)(\mu\text{-}NC_5H_4)(\mu\text{-}H)$, are closely related structurally. In the case of $Re_2(CO)_8(\mu\text{-}NC_5H_4)(\mu\text{-}H)$,[168] the two crystallographically independent molecules ($P\bar{1}$, Z = 4) are structurally very similar, with small differences attributable to crystal packing forces. An eclipsed conformation is

necessitated by the bridging pyridyl ligand, which is opposite to a symmetrical hydride bridge. (Re-H-Re bond angles of 120(6) and 116(5)°). Each Re-atom has a distorted octahedral co-ordination geometry, with C-Re-Re-C torsion angles of less than 6°. The Re-Re-COeq bond angles are less than or equal to 90°, ie. the carbonyls bend in towards the Re-Re bond. The av. Re-CO (trans to CO) (1.99(1) and 2.00(2)Å) are greater than the av. Re-CO (not trans to CO) (1.94(3) and 1.95(2)Å) bond lengths, as predicted on electronic grounds.[102] Of the latter Re-CO bonds, the longest is that trans to C(pyridyl). Re-C-O bond angles are in the 175 - 179° range.

Closely related to the structure of $Re_2(CO)_8(\mu\text{-}NC_5H_4)(\mu\text{-}H)$, is that of the $Re_2(CO)_7(ONMe_3)(\mu\text{-}NC_5H_4)(\mu\text{-}H)$ molecule,[155] in which one of the equatorial carbonyl ligands trans to another CO-group, has been substituted with the $-ONMe_3$ group. The eclipsed structure is maintained, but there are larger distortions from octahedral symmetry, with C-Re-Re-C torsion angles of ca. 10°, due to the bulkier (relative to CO) Me_3NO-group. The Re-H-Re angle is slightly larger at 131(17)°. Re-Re-C angles range from 83-110°. It is noteworthy that the Re-Re-O bond angle is acute (83.7(2)°). The remaining pair of trans carbonyls have the longest Re-CO bonds, with the shorter Re-CO bond being than trans to the $ONMe_3$ ligand. Again the Re-C-O bond angles range from 175 - 179°.

The Re-Re bond length of 3.2324(5)Å in $Re_2(CO)_7(ONMe_3)(\mu\text{-}NC_5H_4)(\mu\text{-}H)$ is longer than that for $Re_2(CO)_8(\mu\text{-}NC_5H_4)(\mu\text{-}H)$ (3.2088(4) and 3.1954(5)Å). This is ascribed to the larger steric requirements of the Me_3NO ligand.[68] Both the Re-Re bonds are single (in accordance with the 18-Electron Rule).

(d) $Re_2(CO)_8[\mu\text{-}SiPh_2]_2$, $Re_2(CO)_8(H)_2[\mu\text{-}SiPh_2]$, $Re_2(CO)_7(H)_2[\mu\text{-}SiEt_2]_2$ and $Re_2(CO)_6(H)_4[\mu\text{-}SiEt_2]_2$

The above four complexes form a series of chemically and structurally related compounds. In all four molecules, an eclipsed conformation is necessitated by the bridging silane ligand(s), although molecular symmetry differs $(Re_2(CO)_8[\mu\text{-}SiPh_2]_2$,[164] D_{2h}; $Re_2(CO)_8(H)_2[\mu\text{-}SiPh_2]$,[165] C_{2v}

$Re_2(CO)_7(H)_2[\mu\text{-}SiEt_2]_2$,[202] Cs; $Re_2(CO)_6(H)_4[\mu\text{-}SiEt_2]_2$,[201] C_2h (molecule possesses crystallographic $\bar{1}$ symmetry). The non-bridging hydrogen atoms were *not located* directly, their positions being inferred from vacancies in the (distorted) octahedral metal co-ordination sphere; spectroscopic evidence indicated that the hydride ligands are *terminally bonded to the rhenium atoms* with no attractive interactions with the silicon atoms.[202]

In all four structures,[200-3] the Re-Si bond length is approximately constant, with acute Re-Si-Re bond angles in the range 74 - 76°. There are, however, significant variations in the Re-Re single bond length, which has values of 3.001(1), 3.052(1), 3.084(1) and 3.121(2)Å for the complexes $Re_2(CO)_8[\mu\text{-}SiPh_2]_2$,[202] $Re_2(CO)_7(H)_2[\mu\text{-}SiEt_2]_2$,[202] $Re_2(CO)_6(H)_4[\mu\text{-}SiEt_2]_2$[201] and $Re_2(CO)_8(H)_2[\mu\text{-}SiPh_2]$,[203] respectively. Considering the first three cases, this *increase* in Re-Re bond length is due to the progressive replacement of a carbonyl by hydride ligands, which are weaker π-acceptors than CO.[202] This electronic effect is strong enough to counteract any possible Re-Re bond shortening due to reduced non-bonded repulsions with fewer eclipsed carbonyl groups (the above four complexes have 4, 2, 3 and 4 eclipsed CO pairs respectively). In the case of $Re_2(CO)_8(H)_2[\mu\text{-}SiPh_2]$, with only one silane bridge, the longer bond is ascribed to O...O repulsions between the two extra pairs of eclipsed carbonyls,[202] compared to $Re_2(CO)_7(H)_2[\mu\text{-}SiEt_2]_2$, which also has two hydride ligands.

Full details of the structure of $Re_2(CO)_8[\mu\text{-}SiPh_2]_2$[202-3] have not been reported. For the other three structures, the av. Re-Re-CO bond angle is ca. 90° ($Re_2(CO)_8(H)_2[\mu\text{-}SiPh_2]$, 89.6(9)°; $Re_2(CO)_7(H)_2[\mu\text{-}SiEt_2]_2$, 90.4(5)°, and $Re_2(CO)_6(H)_4[\mu\text{-}SiEt_2]_2$, 90.2(3)°). In the case of $Re_2(CO)_8(H)_2[\mu\text{-}SiPh_2]$,[200] the Re-COax bond lengths are shorter than the Re-COeq bond lengths. This is also true for $Re_2(CO)_6(H)_4[\mu\text{-}SiEt_2]_2$,[201] but the differences are too slight to be significant. Further, for $Re_2(CO)_8(H)_2[\mu\text{-}SiPh_2]$, the bond Re-CO (trans to H) is longer than that trans to another CO. There are no significant

differences between the Re-CO bond lengths in $Re_2(CO)_7(H)_2[\mu\text{-}SiEt_2]_2$.[212] In all these three structures, the Re-C-O bond angles are in the range 170 - 179°, as expected.[39]

(e) $\underline{Re_2(CO)_8[\mu\text{-}C(OMe)(C_6H_4Me\text{-}p)]_2}$

The structure of $Re_2(CO)_8[\mu\text{-}C(OMe)(C_6H_4Me\text{-}p)]_2$ resembles that of $Re_2(CO)_8[\mu\text{-}SiPh_2]_2$ (vide supra). The $Re_2(CO)_8[\mu\text{-}C(OMe)(C_6H_4Me\text{-}p)]_2$[177b] molecule adopts an eclipsed structure, necessitated by the bridging ligands, and has crystallographic C_2 symmetry. The Re-C-Re bridging angle is an acute 77(1)°, and the Re-Re bond short at 2.81(3)Å. The shortness of the Re-Re bond (Table 13.1) would seem to indicate some degree of multiple bonding, but more than a single Re-Re bond is not required by the 18-Electron Rule.

(f) $\underline{(CO)_4Re[\mu\text{-}C(SiPh_3)CO(OEt)]Re(CO)_3[C(OEt)(SiPh_3)]}$ - a carbonyl-ligand bonded derivative of 1,2-ax,eq-$\underline{Re_2(CO)_8[C(OEt)(SiPh_3)]_2}$

The molecule $(CO)_4(Re[\mu\text{-}C(SiPh_3)CO(OEt)]Re(CO)_3(C(OEt)\text{-}(SiPh_3))$[178c] can be viewed as a derivative of 1,2-ax,eq-$Re_2(CO)_8[C(OEt)(SiPh_3)]_2$ (see section 13.2.1(b), in which the equatorially co-ordinated $[C(OEt)SiPh_3]$ ligand on Re(2) has become bridging, and a CO-group has formally inserted into the C-OEt bond, with the oxygen of the CO being bonded to Re(1) (Re(1)-O: 2.217(13)Å), Re(1) bearing the second axially substituted $[C(OEt)(SiPh_3)]$ ligand. (See Fig. 13.1).

The Re-Re bond is short at 2.937(1)Å. In terms of the 18-Electron Rule, a non-integral Re-Re bond order of 1½ is found. The bridging Re-C-Re angle is an acute 81.7(6)°. The C-C-(OEt)-O is essentially planar. The geometry of this complex is determined by the unusual double-bridging ligand.

(g) $\underline{Re_2(CO)_8[\mu\text{-}(C(SiPh_3)(CO))](\mu\text{-}H)}$, and $\underline{Re_2(CO)_8\text{-}[\mu\text{-}(CPh)](\mu\text{-}Br)}$

The geometry of the $Re_2(CO)_8[\mu\text{-}(C(SiPh_3)(CO))](\mu\text{-}H)$[178c] molecule resembles that of $Re_2(CO)_8[\mu\text{-}(CPh)][\mu\text{-}Br)$.[251] For both molecules, the four carbonyls of the $Re_2(CO)_8$-unit are eclipsed, as necessitated by the bridging carbene ligand, which is opposite to a bridging hydride (located indirectly) or bromide atom respectively. However, in the case of

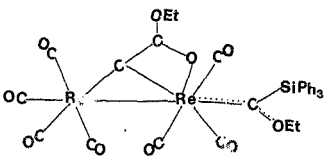


Figure 13.1: Schematic representation of the structure of $(CO)_4Re[\mu\text{-}C(SiPh_3)C\overline{O(OEt)}]\overline{Re}[C(OEt)(SiPh_3)]$

$Re_2(CO)_8[\mu\text{-}(CPh)](\mu\text{-}Br)$, the 18-Electron count can be satisfied without a rhenium-rhenium bond. (The rhenium-*rhenium distance* is not quoted for this complex[231]). For the related $Re_2(CO)_8[\mu\text{-}(C(SiPh_3)(CO)](\mu\text{-}H)$, application of the 18-Electron Rule gives a non-integral Re-Re bond order of 1½. *Some degree* of multiple bonding is supported by the relatively short Re-Re bond length of 3.036(2)Å. (Table 13.1). A Re-Re bond order of 1½ is also found for the complex $(CO)_4Re[\mu\text{-}C(SiPh_3)C\overline{O(OEt)}]\overline{Re}(CO)_3[C(OEt)(SiPh_3)]$ with a Re-Re bond length of 2.937(1)Å (vide supra).

(h) $Re_2(CO)_8(\mu\text{-}H)_2$ - an Re-Re double bond?

The $Re_2(CO)_8(\mu\text{-}H)_2$ *molecule*,[233] with two hydride bridges (not located directly), adopts an eclipsed configuration, of molecular symmetry D2h, and no significant differences *from idealized octahedral* metal co-ordination geometry.

The Re-Re bond length is short at 2.90Å. In accordance with the *formal application* of the 18-Electron Rule,[228] each

hydrogen donates *half* an electron to each Re-atom, requiring a double Re-Re bond. However, it has been suggested that the bonding in this complex can be described in alternate manners in terms of which a double Re-Re bond is not needed to balance the electron-*counting*.[89]

In such *cases*, *molecular* orbital calculations may be *needed* to evaluate the possible bonding modes, and electron density studies might provide useful information. However, owing to the relatively short Re-Re bond length, some degree of multiple bonding is usually ascribed to $Re_2(CO)_8(\mu\text{-}H)_2$. This is probably backed up by the formal application of the 18-Electron Rule, giving an Re-Re bond order of 2.

(i) An $Re_2(CO)_8(\mu\text{-}H)_2$ derivative - $Re_2(CO)_6(\mu\text{-}H)_2[Ph_2PCH_2PPh_2]$

$Re_2(CO)_6(\mu\text{-}H)_2[Ph_2PCH_2PPh_2]$[244a,b] can be regarded as a derivative of $Re_2(CO)_8(\mu\text{-}H)_2$, with two of the CO ligands trans to CO replaced by the bis-phosphine ligand. The two hydrides (located *indirectly* from the distribution of carbonyls) bridge the Re-Re bond, and lie on either side of the Re_2P_2-plane.

For the 18-Electron Rule to hold, a double Re-Re bond is required. This supports the formal application of the 18-Electron Rule to $Re_2(CO)_8(\mu\text{-}H)_2$, to give a double Re-Re bond also. The bond length for $Re_2(CO)_6(\mu\text{-}H)_2[Ph_2PCH_2PPh_2]$ and $Re_2(CO)_8(\mu\text{-}H)_2$ are similar, and relatively short (2.893(2)[244a,b] and 2.90Å[245]) respectively.)

The structure of $Re_2(CO)_6(\mu\text{-}H)_2(Ph_2PCH_2PPh_2]$ is eclipsed. Four of the carbonyls bend away from the Re-Re bond, with the av. Re-Re-CO angle of 134.6(10)°, cf ca. 90° for octahedral co-ordination of Re without bridging hydrides; this observed configuration has b[illegible]firmed by potential energy calculations. The dev[illegible] octahedral co-ordination are probably due to [illegible]strictions imposed by the bulky bis-phosphine ligand [illegible]man cone angle [83a] for half $Ph_2PCH_2PPh_2$ chelate: 121°).

The two phosphine atoms exhibit distorted tetrahedral co-ordination geometry. The two phenyl rings are

approximately parallel, with interplanar distances of 3.4Å, indicative of graphite packing. Hence packing forces could be responsible for distortions from idealized geometry. The carbonyl ligands are near-linear, with Re-C-O angles ranging from 175 - 180°.

(j) Re$_2$(CO)$_6$(μ-H)(μ-NCHMe)(Ph$_2$PCH$_2$PPh$_2$) - derivative of Re$_2$(CO)$_6$(μ-H)$_2$(Ph$_2$PCH$_2$PPh$_2$)

Re$_2$(CO)$_6$(μ-H)(μ-NCHMe)(Ph$_2$PCH$_2$PPh$_2$) is derived from Re$_2$(CO)(μ-H)$_2$(Ph$_2$PCH$_2$PPh$_2$) by insertion of MeCN into an Re-H bond.[244a,c] The NCHMe ligand symmetrically bridges the metal-metal bond, as does the hydride (from analysis of the carbonyl distribution) with the carbonyl groups eclipsed, as in Re$_2$(CO)$_6$(μ-H)(Ph$_2$PCH$_2$PPh$_2$).

The complex Re$_2$(CO)$_6$(μ-H){μ-NCHMe)(Ph$_2$PCH$_2$PPh$_2$) is electron precise, and in accordance with the 18-Electron Rule, the Re-Re bond is single. This is reflected in the Re-Re bond length of 3.035(3)Å, compared to that of 2.893(2)Å for Re$_2$(CO)$_6$(μ-H)(Ph$_2$PCH$_2$PPh$_2$), for which a double Re-Re bond is required in terms of the 18-Electron Rule.

(k) Re$_2$(CO)$_6$(μ-H)(μ-OH)[μ-Ph$_2$PCH$_2$PPh$_2$] - a formal derivative of Re$_2$(CO)$_6$(μ-H)$_2$[μ-Ph$_2$PCH$_2$PPh$_2$]

Re$_2$(CO)$_6$(μ-H)(μ-OH)[μ-Ph$_2$PCH$_2$PPh$_2$][199] may be regarded as a formal derivative of Re$_2$(CO)$_6$(μ-H)$_2$[μ-Ph$_2$PCH$_2$-PPh$_2$],[244a,b] with one bridging hydride replaced by a bridging hydroxide ligand. For both complexes, an Re-Re double bond is required in terms of the 18-Electron Rule. In the case of Re$_2$(CO)$_6$(μ-H)$_2$[μ-Ph$_2$PCH$_2$PPh$_2$], the Re-Re bond is short at 2.893(2)Å, but for Re$_2$(CO)$_6$(μ-H)(μ-OH)-[μ-Ph$_2$PCH$_2$PPh$_2$], the Re-Re bond is surprisingly long at 3.030(1)Å (cf. Re-Re single bond value of 3.035(3)Å for the related Re$_2$(CO)$_6$(μ-H)(μ-NCHMe)[Ph$_2$PCH$_2$PPh$_2$] (vide supra)).

Like Re$_2$(CO)$_6$(μ-H)$_2$[μ-Ph$_2$PCH$_2$PPh$_2$], Re$_2$(CO)$_6$(μ-H)-(μ-OH)[μ-Ph$_2$PCH$_2$PPh$_2$][199] has a distorted octahedral co-ordination geometry about each rhenium atom. The hydrido and hydroxo bridges are both slightly asymmetric, and lie opposite each other on either side of the Re$_2$P$_2$-plane.

The Re-O-Re angle is 88.6(2)°. The structure is eclipsed. The Re-Re-P and Re-Re-CO(trans to P) angles are ca. 90°, but the remaining four carbonyls bend away from the Re-Re bond, with the av. Re-Re-CO angle of 135.3(2)°. Similar deviations are observed for the related $Re_2(CO)_6(\mu\text{-H})_2[\mu\text{-}Ph_2PCH_2PPh_2]$ (section 13.2.2(i)), and probably reflect steric repulsions between the carbonyls and the bulky phosphine ligand (Tolman cone angle[85a] for half of $Ph_2PCH_2PPh_2$: 121°). The phenyl rings are approximately parallel, as for $Re_2(CO)_6(\mu\text{-H})_2$-$[\mu\text{-}Ph_2PCH_2PPh_2]$.

In $Re_2(CO)_6(\mu\text{-H})(\mu\text{-OH})[\mu\text{-}Ph_2PCH_2PPh_2]$,[198] the av. Re-CO bond length (1.921Å) is significantly shorter than in $Re_2(CO)_{10}$ (1.975Å).[15e] This may reflect stronger Re-CO bonding due to increased electron d[illegible] on the metal atoms, since phosphine is a poor π-ac[illegible]an CO.[92a] Further, the Re-CO(trans to P) bond lengths are longer than those trans to H or OH ligands, which do not have π-acceptor character[198] (av. 1.950Å and 1.907Å respectively). This difference is due to competition for π-electron density[112] between the carbonyl and trans-phosphine ligand. The carbonyl ligands are near-[illegible]ar, with Re-C-O angles ranging from 175 - 180°.

(ii) $[Re_2(CO)_4(PhCCPh)_3(CNCH_2SO_2C_6H_4Me\text{-}p)_2]$, and $[Re_2(CO)_4(PhCCPh)_4]$

The mixed acetylene-isonitrile derivative, $[Re(CO)_4(PhCCPh)_3(CNCH_2SO_2C_6H_4Me\text{-}p)]$,[112] has an interesting structure. The three acetylene molecules are linked in a chain, with the end carbon atoms of the chain each σ-bonded to one rhenium atom, and, with the two neighbouring carbon atoms, forming an η^3-allyl link to the other rhenium atom. The two isonitrile ligands are terminally bonded to one Re-atom only, occupying positions cis to each other. The RNC ligands are slightly bent with av. C-N-C angle of 167.6(7)°, a C-N-R angle greater than 170° being considered linear for terminal RNC ligands.[91b] Slight deviations from linearity could be due to steric crowding. Both the isonitrile and carbonyl ligands co-ordinate in a near-linear fashion, with av. values of 174.6(7) and 176.5(9)° for Re-C-N and Re-C-O angles respectively.

Although the Re-Re bond length of 2.786(1)Å is relatively short, the Re-Re bond is only a single bond if the 18-Electron Rule is applied, with $(PhCCPh)_3$ acting as an 8-electron donor. The relatively short Re-Re bond length could be largely due to the steric restrictions imposed by the 6-atom carbon chain linked to the two metal atoms.

A partial crystal structure of the related complex, $[Re_2(CO)_4(PhCCPh)_4]$,[212] has been determined, but disorder problems prevented refinement. The chain of three acetylene molecules is bonded as in $[Re_2(CO)_4(PhCCPh)_3(CNCH_2SO_2C_6H_4Me\text{-}p)_2]$, with the fourth acetylene molecule separately bonded to one Re-atom only, taking the place of the two RNC ligands.

The Re-Re bond length is ca. 2.78Å, once again relatively short, but similar to the above single Re-Re bond length of 2.786(1)Å. However, in the case of $[Re_2(CO)_4(PhCCPh)_4]$, the Re-Re bond is probably a double bond, since with the fourth PhCCPh ligand (replacing the two RNC ligands) co-ordinated to only one Re-atom acting as a 2-electron donor, the 18-Electron Rule requires a double Re-Re bond, and it is difficult to envisage how the lone PhCCPh ligand can act as more than a two-electron donor when co-ordinated to only one metal atom. This example demonstrates that metal-metal bond length is not a reliable indication of metal-metal bond order, especially where geometric constraints may be important.

13.3 Assessment

From the foregoing structural study of dirhenium decacarbonyl derivatives, it is possible to draw some general conclusions regarding the modification of $Re_2(CO)_{10}$ by ligands L. These are outlined below.

13.3.1 The Re-Re bond length

The Re-Re bond length alone provides little information on the nature of the metal-metal bonding. All factors must be considered.

(a) Bond Order: Bond order is usually assigned on the basis of the 18-Electron Rule. Where ambiguities arise, the answer is uncertain. A more reliable method is needed for such cases.

(b) Electronic nature of ligands: In a closely related series, a ligand L which is a weaker π-acceptor than CO, may significantly increase the Re-Re bond length.

(c) Steric factors: Repulsive interactions between eclipsed carbonyl groups may increase the Re-Re bond length.

(d) Bridging ligands: A bridging ligand with a small bite may result in a seemingly anomalous short Re-Re bond length.

13.3.2 The Re-CO bond lengths

The Re-COax bonds are shorter than Re-COeq bonds; eq-$Re_2(CO)_9L$ substitution results, unless steric factors dominate. The Re-CO bond trans to L, a poorer π-acceptor than CO, is shorter than that trans to another CO; cis-dieq-$Re_2(CO)_8(L)_2$ substitution results, in the absence of steric constraints.

13.3.3 Molecular conformation

Molecules without bridging ligands adopt a staggered conformation. Bridging ligands necessitate an eclipsed conformation.

13.3.4 OC-Re-CO bond angles

Generally, Re-Re-CO bond angles are less than or equal to 90° ie. the carbonyls bend in towards the Re-Re bond. Where this is not the case, severe steric restraints are imposed on the structure by bulky ligands, resulting in pronounced distortions from the ideal geometry.

13.3.5 Re-C-O bond angles

The Re-C-O bond angles are always in the range 170 - 179°. The same is true for Re-C-N bond angles of isonitrile ligands.

13.3.6 Packing

Small deviations in structure (from ideal geometry) probably stem from interaction with neighbouring molecules ie. crystal packing.

XIV. X-RAY CRYSTALLOGRAPHIC STUDIES OF ISONITRILE DERIVATES OF $M_2(CO)_{10}$ (M = Re,Mn)

14.1 Introduction

Although the structures of the parent carbonyls, $Re_2(CO)_{10}$ and $Mn_2(CO)_{10}$, have been determined,[156] and studies made of the bonding in these complexes,[159] no X-ray crystal structures have been reported of isonitrile substituted derivatives, $Mn_2(CO)_{10-n}(CNR)_n$ (M = Re,Mn). As part of a systematic study of the structural and chemical properties of isonitrile derivatives of dirhenium carbonyl, $Re_2(CO)_{10-n}(CNR)_n$ (n = 1-4), an X-ray crystallographic study of a series of representative complexes was undertaken.

Specifically, this X-ray Crystallographic study was undertaken with the aim, firstly, of establishing the stereochemistry of the mono-to tetra-isonitrile-substituted dirhenium carbonyl derivatives, and secondly, of obtaining bond length and bond angle data relating to the structural effect (if any) of increasing degree of isonitrile substitution. In particular, any weakening of the metal-metal bond would be expected to be reflected in an increase in the M-M bond length. Since isonitriles are weaker π-acceptors than carbonyls,[43] substitution of isonitriles for carbonyls in $M_2(CO)_{10}$ would result in increased localization of π-electron charge on the metal, increasing π-electron repulsions and thereby weakening the M-M bond.[192b]

Obviously, the structure of the parent carbonyl, $Re_2(CO)_{10}$, is of interest in the context of this study, and this structure has been reported in the literature,[159] together with the structure of the isomorphous $Mn_2(CO)_{10}$. (Monoclinic space group I2/a, Z = 4). The molecules adopt a staggered conformation, with point group symmetry D4d. A feature of both structures is the shorter M-COax bond length, compared to the M-COeq bond lengths. This is ascribed to the competition for $d\pi$ -electrons between pairs of mutually trans CO ligands.[156]

Consequently, on electronic grounds, substitution would be predicted to be equatorial rather than axial. However,

with bulky ligands such as phosphines, *steric factors may* dominate, resulting in axial substitution, *as has been* shown by the X-ray crystal structure of *ax*-$[Mn_2(CO)_9(PMe_2Ph)]$[224] (Tolman cone angle for PMe_2Ph: 122°[23] 141.7°[224]). *Hence,* for monosubstituted derivatives of $M_2(CO)_{10}$ (M = Re, Mn), there are two possibilities (Fig. 14.1), viz. (IA) equatorial, or (IB) axial substitution.

With disubstituted complexes, *there are more* possibilities. With bulky phosphine ligands, *diaxial* substitution may be found, as has been shown by *X-ray crystal* structures of *diax*-$[Mn_2(CO)_8(PMePh_2)_2]$[23] (*Tolman cone* angle for $PMePh_2$: 136°[85]), *diax*-$[Mn_2(CO)_8(PEt_3)_2]$ (*Tolman* cone angle for PEt_3: 132°[85]; 166.4°[224]) and *diax*-$[Re_2(CO)_8(PMe_2Ph)_2]$ (see ch 15E) (Tolman cone angle for PMe_2Ph: 122°[85]; 141.7°[224]). However, for di-isonitrile derivatives, diaxial substitution is not expected, because for this geometry of point group D4d, only two ν(CO) bands are predicted *in the IR spectrum* (as is indeed observed *for the above* biphosphine derivatives, see ch XV), but *the IR spectra* of the di-isonitrile derivatives are much more *complex* (see ch XI). Axial-equatorial substitution *is also* a possibility, and has been observed for some $Re_2(CO)_8(PR_3)_2$ complexes (see ch XV), but is *considered unlikely* for the smaller isonitrile ligands, in *view of the electronic* factors favouring equatorial *substitution* (*vide supra*). Further, *trans*-substitution is *electronically* disfavoured.[102] Even considering only *cis*-*diequatorial* substitution, there are still two possibilities (*Fig 14.2*), viz. (IIa) with the two RNC ligands on the *same* metal atom, or on different metal atoms (conformers (IIb) and (IIc)).

Several structures are also possible for the trisubstituted case, considering only cis-equatorial substitution (*vide supra*). (Fig. 14.3, IIIa-c). Considering the case of tetrasubstitution, there are again several cis-equatorially substituted possibilities, assuming two RNC ligands on each metal atom (Fig 14.4, IVa-c). Although repulsive interactions between equatorial CO groups are expected to be less in the staggered than eclipsed conformation,[130]

here the eclipsed conformation (IVc) is considered as well, since from steric considerations of the RNC ligands, this might be expected to be the most favourable structure.

The crystal and molecular structures were determined of the complexes $Re_2(CO)_9(CNBu^t)$(I), $Re_2(CO)_8(CNC_6H_3Me_2\text{-}2,6)_2$ (II), $Re_2(CO)_7(CNMe)_3$(III) and $Re_2(CO)_6(CNC_6H_3Me_2\text{-}2,6)_4$(IV). The X-ray structure of the di-isonitrile dimanganese carbonyl derivative, $Mn_2(CO)_8(CNBu^t)_2$(V), was also determined, in order to establish whether certain differences observed in the IR and ^1H NMR spectra of $Re_2(CO)_8(CNR)_2$ and of $Mn_2(CO)_8(CNR)_2$ complexes (see sections 11.4.1 and 11.4.2) could be correlated with structural differences on the molecular level. The structure of $Mn_2(CO)_6(CNC_6H_3Me_2\text{-}2,6)_4$ (VI) was also investigated by X-ray Crystallography, with the aims of obtaining bond parameter data for a tetra-isonitrile dimanganese derivative, and establishing whether differences observed in the IR and ^1H NMR spectra of $Re_2(CO)_6(CNC_6H_3Me_2\text{-}2,6)_4$ and $Mn_2(CO)_6(CNC_6H_3Me_2\text{-}2,6)_4$ (see sections 11.4.1 and 11.4.2) could have a structural basis.

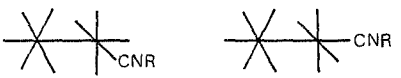
14.2 X-ray Crystallographic Studies

14.2.1 Structure of $Re_2(CO)_9(CNBu^t)$(I)

The molecular structure of $Re_2(CO)_9(CNBu^t)$ and the numbering system used in the crystal structure determination is shown in Fig. 14.5. Bond lengths and bond angles are given in Tables 14.1 and 14.2 respectively. The compound crystallizes in the orthorhombic space group Pbca, with $Z = 8$. A view of the unit cell, looking down the b-axis is shown in Fig. 14.6.

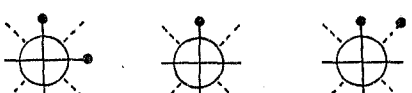
Substitution was found to be equatorial (Fig. 14.1(Ia)), as predicted (*vide supra*). This equatorial substitution of CO by $CNBu^t$ is in keeping with previous arguments on the *final* position of the incoming ligand in an octahedral environment.[102]

The two halves of the molecule are staggered with respect to each other, as in the parent carbonyl, $Re_2(CO)_{10}$.[138] This staggered geometry presumably arises from steric considerations (ie. reduced interaction of equatorial CO



Ia

Figure 14.1: The two possible structures of $Re_2(CO)_9(CNR)$: (Ia) equatorial substitution, (Ib) axial substitution



IIa IIb IIc

Figure 14.2: Newman projections of possible structures of $M_2(CO)_8(CNR)_2$ (M = Re, Mn), as viewed down the M-M axis (● = RNC)

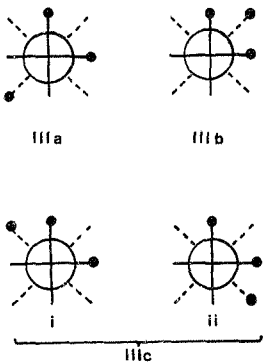


Figure 14.3: *Newman* projections of possible conformations of $Re_2(CO)_7(CNR)_3$, as viewed down the Re-Re axis (● = RNC)

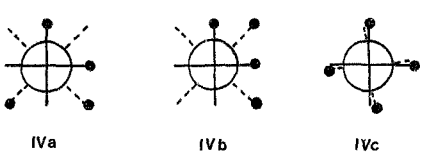


Figure 14.4: Newman projections of possible conformations of $M_2(CO)_6(CNR)_4$ (M = Re,Mn), as viewed down the M-M axis (● = RNC)

groups on the two Re atoms),[131] and has been observed in all previously reported structures of $Re_2(CO)_{10-n}(L)_n$ (n = 1,2) derivatives not containing bridging ligands (*see* ch. XIII).

The axial Re-CO bond distance (av. 1.902(19)Å) is shorter than the average equatorial Re-CO bond distance (av. 1.983(20)Å), *excluding* Re-C(1) in which the CO group is trans to the Bu^tNC group (1.916(18)Å). This effect of a shorter Re-COax bond length relative to the Re-COeq bond length has been observed in the *structure* of $Re_2(CO)_{10}$,[158] and is ascribed to competition for $d\pi$-electron density between mutally trans pairs of equatorial carbonyls. The shorter Re-C(1) bond length (cf. av. Re-COeq) *could also reflect* the greater π-acceptor ability of the CO group relative to the Bu^tNC group.[43]

14.2.2. Structure of $Re_2(CO)_8(CNC_6H_3Me_2\text{-}2,6)_2$(II)

The compound (II) was found to crystallize in the *centrosymmetric* triclinic space group $P\bar{1}$, with Z = 2. The molecular structure of $Re_2(CO)_8(CNC_6H_3Me_2\text{-}2,6)_2$, and the numbering system used in the crystal structure determination is shown in Fig. 14.7. *Bond lengths* and bond angles are given in Tables 14.3 and 14.4 respectively.

Viewed down the Re-Re bond, the conformation is staggered, as expected.[132] *In the crystal, the molecule* adopts conformation (IIb)(Fig. 14.2), with the two isonitrile ligands on different Re-atoms. This conformation might be expected to be sterically most favourable, since the *bulky* 2,6-$Me_2C_6H_3NC$ ligands ("fan-shaped" angles[44]: 106° (wideness) and 53° (thickness)) are as far away from each other as possible, but in the crystal the conformation adopted is probably *also determined* by crystal packing considerations (vide infra).

The phenyl rings are essentially planar. The mean planes of the C6-rings *are 73.1° to each other*. This is probably determined mainly by crystal packing forces. As can be seen from the packing diagram (Fig. 14.8), viewed down the b-axis, the molecules pack in rows, *with the*

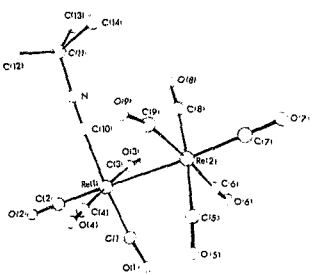


Figure 14.5: ORTEP[45] view of the $Re_2(CO)_9(CNBu^t)$ molecule(I), showing the numbering system used

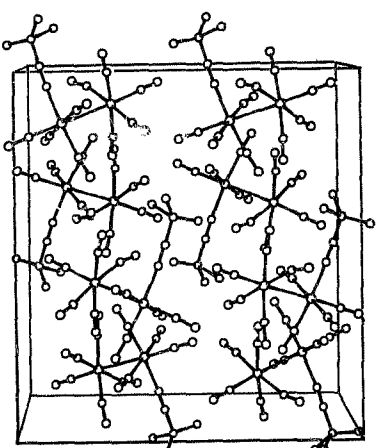


Figure 14.6: ORTEP[*5] view of the unit cell of $Re_2(CO)_9(CNBu^t)$(I), looking down the b-axis

TABLE 14.1: Bond lengths (Å) for $Re_2(CO)_9(CNBu^t)(I)$

Re(1)-Re(2)	3.048(1)		
Re(1)-C(1)	1.916(18)	C(1)-O(1)	1.149(18)
Re(1)-C(2)	1.916(18)	C(2)-O(2)	1.142(17)
Re(1)-C(3)	2.089(20)	C(3)-O(3)	1.077(18)
Re(1)-C(4)	1.974(21)	C(4)-O(4)	1.144(19)
Re(1)-C(10)	2.068(15)	C(10)-N	1.130(16)
Re(2)-C(5)	1.943(20)	C(5)-O(5)	1.139(20)
Re(2)-C(6)	1.999(22)	C(6)-O(6)	1.151(20)
Re(2)-C(7)	1.887(21)	C(7)-O(7)	1.158(20)
Re(2)-C(8)	1.928(18)	C(8)-O(8)	1.169(18)
Re(2)-C(9)	1.965(20)	C(9)-O(9)	1.133(18)
N-C(11)	1.481(20)	C(11)-C(12)	1.503(39)
C(11)-C(14)	1.667(48)	C(11)-C(13)	1.486(33)

TABLE 14.2: Bond angles (°) for $Re_2(CO)_9(CNBu^t)$(I)

C(10)-N-C(11)	175.7(18)		
Re(1)-C(1)-O(1)	176.1(15)	Re(2)-C(5)-O(5)	176.5(18)
Re(1)-C(2)-O(2)	178.8(15)	Re(2)-C(6)-O(6)	174.6(18)
Re(1)-C(3)-O(3)	175.3(16)	Re(2)-C(7)-O(7)	178.2(18)
Re(1)-C(4)-O(4)	177.1(16)	Re(2)-C(8)-O(8)	175.8(16)
Re(1)-C(10)-N	175.5(13)	Re(2)-C(9)-O(9)	175.7(17)
C(1)-Re(1)-Re(2)	87.4(5)	C(5)-Re(2)-Re(1)	88.2(5)
C(1)-Re(1)-C(2)	93.1(7)	C(5)-Re(2)-C(6)	87.8(8)
C(1)-Re(1)-C(3)	90.1(7)	C(5)-Re(2)-C(7)	93.2(8)
C(1)-Re(1)-C(4)	89.7(7)	C(5)-Re(2)-C(8)	172.6(7)
C(1)-Re(1)-C(10)	174.9(6)	C(5)-Re(2)-C(9)	92.8(8)
C(2)-Re(1)-Re(2)	177.4(5)	C(6)-Re(2)-Re(1)	88.8(6)
C(2)-Re(1)-C(3)	93.5(7)	C(6)-Re(2)-C(7)	94.4(8)
C(2)-Re(1)-C(4)	91.3(7)	C(6)-Re(2)-C(8)	93.1(8)
C(2)-Re(1)-C(10)	92.1(6)	C(6)-Re(2)-C(9)	172.2(8)
C(3)-Re(1)-Re(2)	89.0(5)	C(7)-Re(2)-Re(1)	176.5(6)
C(3)-Re(1)-C(4)	175.2(7)	C(7)-Re(2)-C(8)	94.1(8)
C(3)-Re(1)-C(10)	89.7(6)	C(7)-Re(2)-C(9)	93.4(8)
C(4)-Re(1)-Re(2)	86.2(5)	C(8)-Re(2)-Re(1)	84.4(5)
C(4)-Re(1)-C(10)	90.1(7)	C(8)-Re(2)-C(9)	85.4(7)
C(10)-Re(1)-Re(2)	87.5(4)	C(9)-Re(2)-Re(1)	83.4(5)
N-C(11)-C(12)	111.2(22)	C(12)-C(11)-C(13)	126.6(26)
N-C(11)-C(13)	110.1(19)	C(12)-C(11)-C(14)	96.1(23)
N-C(11)-C(14)	104.9(21)	C(13)-C(11)-C(14)	104.6(23)

orientation of the rings alternating along a row, and with the rings lining up in a coplanar manner (less than 2° deviation) with those of the row above.

14.2.3. Structure of $Mn_2(CO)_8(CNBu^t)_2$ (V)

The molecular structure of $Mn_2(CO)_8(CNBu^t)_2$ and the numbering system used in the crystal structure determination is shown in Fig. 14.9. Bond lengths and bond angles are given in Tables 14.5 and 14.6 respectively. The compound crystallizes in the monoclinic space group $P2_1/n$, with $Z = 4$. Fig. 14.10 shows the unit cell, viewed down the b-axis.

In contrast to $Re_2(CO)_8(CNC_6H_3Me_2\text{-}2,6)_2$ (vide supra), the conformation of the $Mn_2(CO)_8(CNBu^t)_2$ molecule is (IIa) (Fig. 14.2), with both isonitrile ligands in cis-equatorial positions on the same Mn-atom. Electronically, this might be expected to be the most favourable geometry, since the isonitrile ligand is a stronger σ-donor, but weaker π-acceptor than carbonyl,[87] resulting in a cis-labilization effect[102] (but see section 14.4).

From ^1H NMR data (section 11.4.2.), in the case of the di-isonitrile derivatives of dimanganese carbonyl, two isomers, (IIa) and (IIb) (or (IIc)) (Fig. 14.2) appear to exist in solution, the isomer (IIa) (which is the minor component-ratio of (IIa):(IIb) is 1:5) having been preferentially crystallized out of solution (pentane, ~5°C) in the case of $Mn_2(CO)_8(CNBu^t)_2$. However, with the di-isonitrile derivatives of dirhenium carbonyl, (with the exception of MeNC) the ^1H NMR spectra give no evidence of another isomer in addition to (IIb). The formation of isomers for $Mn_2(CO)_8(CNBu^t)_2$ will be further discussed in section 14.4.

14.2.4 Structure of $Re_2(CO)_7(CNMe)_3$ (III)

Complex (III) crystallizes in the monoclinic space group $P2_1/n$, with $Z = 4$. Unfortunately the structure displayed disorder (vide infra). Fig. 14.11 shows the molecular structure, and the numbering system used in the crystal structure analysis. Bond lengths and bond angles

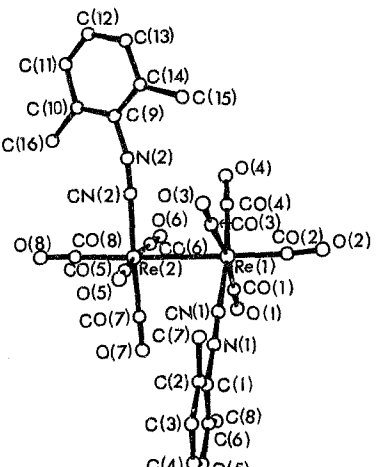


Figure 14.7. ORTEP[14] view of the $Re_2(CO)_8(CNC_6H_3Me_2\text{-}2,6)_2$ molecule (II), showing the numbering system used.

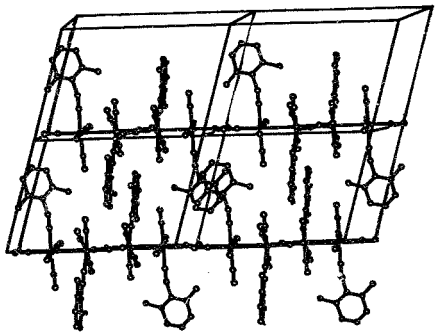


Figure 14.8: ORTEP[21] view of the unit cell of $Re_2(CO)_8(CNC_6H_3Me_2\text{-}2,6)_2$(II), looking down the b-axis

TABLE 14.3: Bond lengths (Å) for $Re_2(CO)_8(CNC_6H_3Me_2\text{-}2,6)_2$(II)

Re(1)-Re(2)	3.047(0)		
Re(1)-C0(1)	1.982(6)	C0(1)-O(1)	1.131(6)
Re(1)-C0(2)	1.916(6)	C0(2)-O(2)	1.151(6)
Re(1)-C0(3)	1.976(6)	C0(3)-O(3)	1.138(6)
Re(1)-C0(4)	1.980(7)	C0(4)-O(4)	1.125(7)
Re(2)-C0(5)	1.951(6)	C0(5)-O(5)	1.141(6)
Re(2)-C0(6)	1.995(7)	C0(6)-O(6)	1.117(6)
Re(2)-C0(7)	1.969(6)	C0(7)-O(7)	1.126(6)
Re(2)-C0(8)	1.931(6)	C0(8)-O(8)	1.143(6)
Re(1)-CN(1)	2.041(6)	CN(1)-N(1)	1.157(6)
Re(2)-CN(2)	2.059(6)	CN(2)-N(2)	1.138(6)
N(1)-C(1)	1.444(7)	N(2)-C(9)	1.413(7)
C(1)-C(2)	1.373(8)	C(9)-C(10)	1.407(7)
C(2)-C(3)	1.465(9)	C(10)-C(11)	1.427(8)
C(3)-C(4)	1.418(9)	C(11)-C(12)	1.340(9)
C(4)-C(5)	1.318(9)	C(12)-C(13)	1.403(8)
C(5)-C(6)	1.441(8)	C(13)-C(14)	1.467(8)
C(6)-C(1)	1.417(8)	C(14)-C(9)	1.406(7)
C(2)-C(7)	1.526(8)	C(10)-C(16)	1.487(9)
C(6)-C(8)	1.495(9)	C(14)-C(15)	1.533(8)

TABLE 14.4: Bond angles(°) for $Re_2(CO)_8(CNC_6H_3Me_2\text{-}2,6)_2$(II)

Re(1)-CO(1)-O(1)	177.8(6)	Re(2)-CO(5)-O(5)	178.8(5)
Re(1)-CO(2)-O(2)	175.7(5)	Re(2)-CO(5)-O(6)	177.6(5)
Re(1)-CO(3)-O(3)	177.8(5)	Re(2)-CO(7)-O(7)	179.8(2)
Re(1)-CO(4)-O(4)	177.8(5)	Re(2)-CO(8)-O(8)	178.2(5)
Re(1)-CN(1)-N(1)	178.0(5)	Re(2)-CN(2)-N(2)	176.8(5)
CN(1)-N(1)-C(1)	175.9(5)	CN(2)-N(2)-C(9)	166.1(5)
CO(1)-Re(1)-Re(2)	88.0(2)	CO(5)-Re(2)-Re(1)	86.4(1)
CO(1)-Re(1)-CO(2)	94.0(2)	CO(5)-Re(2)-CO(6)	172.0(2)
CO(1)-Re(1)-CO(3)	171.1(2)	CO(5)-Re(2)-CO(7)	91.3(2)
CO(1)-Re(1)-CO(4)	91.0(2)	CO(5)-Re(2)-CO(8)	92.3(2)
CO(1)-Re(1)-CN(1)	88.1(2)	CO(5)-Re(2)-CN(2)	91.0(2)
CO(2)-Re(1)-Re(2)	178.0(2)	CO(6)-Re(2)-Re(1)	85.7(1)
CO(2)-Re(1)-CO(3)	94.2(2)	CO(6)-Re(2)-CO(7)	89.4(2)
CO(2)-Re(1)-CO(4)	94.4(2)	CO(6)-Re(2)-CO(8)	95.6(2)
CO(2)-Re(1)-CN(1)	93.8(2)	CO(6)-Re(2)-CN(2)	88.0(2)
CO(3)-Re(1)-Re(2)	83.8(1)	CO(7)-Re(2)-Re(1)	87.9(1)
CO(3)-Re(1)-CO(4)	91.8(2)	CO(7)-Re(2)-CO(8)	94.0(2)
CO(3)-Re(1)-CN(1)	87.9(2)	CO(7)-Re(2)-CN(2)	176.7(2)
CO(4)-Re(1)-Re(2)	85.3(2)	CO(8)-Re(2)-Re(1)	177.8(2)
CO(4)-Re(1)-CN(1)	171.8(2)	CO(8)-Re(1)-CN(2)	88.3(2)
CN(1)-Re(1)-Re(2)	86.5(1)	CN(2)-Re(2)-Re(1)	89.9(1)
C(6)-C(1)-C(2)	125.7(6)	C(14)-C(9)-C(10)	124.9(6)
C(1)-C(2)-C(3)	117.1(6)	C(9)-C(10)-C(11)	115.3(6)
C(2)-C(3)-C(4)	115.5(7)	C(10)-C(11)-C(12)	121.7(6)
C(3)-C(4)-C(5)	126.7(8)	C(11)-C(12)-C(13)	124.4(7)
C(4)-C(5)-C(6)	119.3(7)	C(12)-C(13)-C(14)	116.5(6)
C(5)-C(6)-C(1)	115.6(6)	C(13)-C(14)-C(9)	117.1(8)
N(1)-C(1)-C(2)	115.7(5)	N(2)-C(9)-C(10)	117.3(5)
N(1)-C(1)-C(6)	118.6(5)	N(2)-C(9)-C(14)	117.8(5)
C(1)-C(2)-C(7)	124.5(6)	C(9)-C(10)-C(16)	122.2(6)
C(3)-C(2)-C(7)	118.4(6)	C(11)-C(10)-C(16)	122.5(6)
C(1)-C(6)-C(8)	119.5(6)	C(9)-C(14)-C(15)	121.7(5)
C(5)-C(6)-C(8)	124.8(6)	C(13)-C(14)-C(15)	121.2(5)

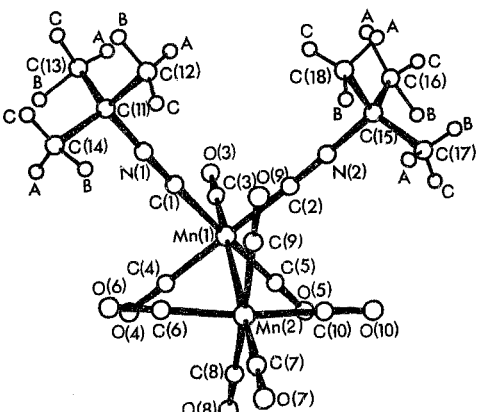


Figure 14.9: ORTEP[13] view of the $Mn_2(CO)_8(CNBu^t)_2$ molecule (V), showing the numbering system used.

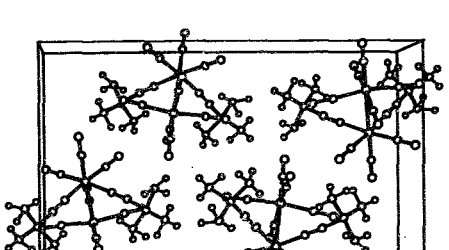


Figure 14.10: ORTEP[45] view of the unit cell of $Mn_2(CO)_8(CNBu^t)_2$(V), looking down the b-axis

TABLE 14.5: Bond lengths (Å) for $Mn_2(CO)_8(CNBu^t)_2$[VI]

Mn(1)-Mn(2)	2.924(1)		
Mn(1)-C(1)	1.947(4)	C(1)-N(1)	1.150(5)
Mn(1)-C(2)	1.941(4)	C(2)-N(2)	1.158(5)
Mn(1)-C(3)	1.779(5)	C(3)-O(3)	1.149(6)
Mn(1)-C(4)	1.833(5)	C(4)-O(4)	1.143(6)
Mn(1)-C(5)	1.814(4)	C(5)-O(5)	1.152(6)
Mn(2)-C(6)	1.837(5)	C(6)-O(6)	1.140(6)
Mn(2)-C(7)	1.788(5)	C(7)-O(7)	1.144(7)
Mn(2)-C(8)	1.837(5)	C(8)-O(8)	1.150(7)
Mn(2)-C(9)	1.845(5)	C(9)-O(9)	1.132(6)
Mn(2)-C(10)	1.843(5)	C(10)-C(10)	1.138(6)
N(1)-C(11)	1.448(6)	N(2)-C(15)	1.464(6)
C(11)-C(12)	1.529(10)	C(15)-C(16)	1.547(11)
C(11)-C(13)	1.529(11)	C(15)-C(17)	1.479(11)
C(11)-C(14)	1.534(10)	C(15)-C(18)	1.513(10)
C(12)-H(12A)	0.90(10)	C(16)-H(16A)	1.22(14)
C(12)-H(12B)	1.02(6)	C(16)-H(16B)	1.17(9)
C(12)-H(12C)	0.98(9)	C(16)-H(16C)	0.75(6)
C(13)-H(13A)	0.84(7)	C(17)-H(17A)	0.97(7)
C(13)-H(13B)	1.13(10)	C(17)-H(17B)	0.85(7)
C(13)-H(13C)	1.04(8)	C(17)-H(17C)	0.98(8)
C(14)-H(14A)	0.92(8)	C(18)-H(18A)	1.03(8)
C(14)-H(14B)	1.05(6)	C(18)-H(18B)	0.91(8)
C(14)-H(14C)	0.96(6)	C(18)-H(18C)	1.01(8)

TABLE 14.6: Bond angles (°) for $Mn_2(CO)_8(CNBu^t)_2$ (V)

Mn(1)-C(1)-N(1)	177.7(4)	Mn(2)-C(6)-O(6)	177.6(4)
Mn(1)-C(2)-N(2)	177.5(4)	Mn(2)-C(7)-O(7)	178.6(5)
Mn(1)-C(3)-O(3)	177.6(4)	Mn(2)-C(8)-O(8)	178.9(5)
Mn(1)-C(4)-O(4)	178.0(4)	Mn(2)-C(9)-O(9)	176.9(4)
Mn(1)-C(5)-O(5)	177.6(4)	Mn(2)-C(10)-(10)	178.1(4)
C(1)-N(1)-C(11)	178.1(4)	C(2)-N(2)-C(15)	175.3(4)
C(12)-C(11)-C(13)	112.2(6)	C(16)-C(15)-C(17)	112.9(7)
C(12)-C(11)-C(14)	111.5(6)	C(16)-C(15)-C(18)	110.0(6)
C(13)-C(11)-C(14)	110.2(6)	C(17)-C(15)-C(18)	114.6(7)
C(12)-C(11)-N(1)	107.6(4)	C(16)-C(15)-N(2)	104.7(5)
C(13)-C(11)-N(1)	107.7(5)	C(17)-C(15)-N(2)	106.7(5)
C(14)-C(11)-N(1)	107.4(5)	C(18)-C(15)-N(2)	107.2(4)
C(1)-Mn(1)-Mn(2)	90.7(1)	C(6)-Mn(2)-Mn(1)	84.0(2)
C(1)-Mn(1)-C(2)	86.1(2)	C(6)-Mn(2)-C(7)	95.6(2)
C(1)-Mn(1)-C(3)	93.0(2)	C(6)-Mn(2)-C(8)	90.3(3)
C(1)-Mn(1)-C(4)	91.0(2)	C(6)-Mn(2)-C(9)	89.0(2)
C(1)-Mn(1)-C(5)	175.3(2)	C(6)-Mn(2)-C(10)	168.8(2)
C(2)-Mn(1)-Mn(2)	89.2(1)	C(7)-Mn(2)-Mn(1)	177.1(2)
C(2)-Mn(1)-C(3)	93.3(2)	C(7)-Mn(2)-C(8)	98.1(2)
C(2)-Mn(1)-C(4)	174.1(2)	C(7)-Mn(2)-C(9)	94.9(2)
C(2)-Mn(1)-C(5)	91.4(2)	C(7)-Mn(2)-C(10)	95.6(2)
C(3)-Mn(1)-Mn(2)	175.6(2)	C(8)-Mn(2)-Mn(1)	84.8(2)
C(3)-Mn(1)-C(4)	91.9(2)	C(8)-Mn(2)-C(9)	167.0(2)
C(3)-Mn(1)-C(5)	91.0(2)	C(8)-Mn(2)-C(10)	88.4(2)
C(4)-Mn(1)-Mn(2)	85.7(1)	C(9)-Mn(2)-Mn(1)	82.2(1)
C(4)-Mn(1)-C(5)	91.1(2)	C(9)-Mn(2)-C(10)	89.8(2)
C(5)-Mn(1)-Mn(2)	85.4(1)	C(10)-Mn(2)-Mn(1)	84.8(1)
H(12A)-C(12)-H(12B)	103(7)	H(16A)-C(16)-H(16B)	163(8)
H(12A)-C(12)-H(12C)	133(8)	H(16A)-C(16)-H(16C)	83(8)
H(12B)-C(12)-H(12C)	110(6)	H(16B)-C(16)-H(16C)	93(7)
H(13A)-C(13)-H(13B)	146(7)	H(17A)-C(17)-H(17B)	96(6)
H(13A)-C(13)-H(13C)	106(6)	H(17A)-C(17)-H(17C)	123(6)
H(13B)-C(13)-H(13C)	100(7)	H(17B)-C(17)-H(17C)	111(6)
H(14A)-C(14)-H(14B)	110(6)	H(18A)-C(18)-H(18B)	104(7)
H(14A)-C(14)-H(14C)	115(6)	H(18A)-C(18)-H(18C)	109(6)

TABLE 14.6: Bond angles (°) for $Mn_2(CO)_8(CNBu^t)_2$(V) (Contd)

H(14B)-C(14)-H(14C)	116(5)	H(18B)-C(18)-H(18C)	134(7)
H(12A)-C(12)-C(11)	101(6)	H(16A)-C(16)-C(15)	98(7)
H(12B)-C(12)-C(11)	105(3)	H(16B)-C(16)-C(15)	99(5)
H(12C)-C(12)-C(11)	102(5)	H(16C)-C(16)-C(15)	105(5)
H(13A)-C(13)-C(11)	105(5)	H(17A)-C(17)-C(15)	100(4)
H(13B)-C(13)-C(11)	97(5)	H(17B)-C(17)-C(15)	113(4)
H(13C)-C(13)-C(11)	99(4)	H(17C)-C(17)-C(15)	112(5)
H(14A)-C(14)-C(11)	112(5)	H(18A)-C(18)-C(15)	108(4)
H(14B)-C(14)-C(11)	95(4)	H(18B)-C(18)-C(15)	91(5)
H(14C)-C(14)-C(11)	107(4)	H(18C)-C(18)-C(15)	109(5)

are given in Tables 14.7 and 14.8 respectively. The unit cell, viewed down the b-axis, is shown in Fig. 14.12.

The complex $Re_2(CO)_7(CNMe)_3$ might be expected on steric grounds to adopt conformation (IIIa) (Fig. 14.3), but the structure found in the crystal is (IIIc) (Fig. 14.3). Again the structure is staggered, with two methyl isonitrile ligands occupying cis-equatorial positions on Re(2), but the third MeNC ligand on Re(1) is disordered with respect to the carbonyl trans to it, with 50% occupancy of both sites, which are equivalent with respect to the two isonitrile ligands on Re(2) (Fig. 14.3 ((c) (i) and (ii)). Disorder of this type has been observed previously with MeNC ligands,[192b] and is thought to be due to the relatively small size of the MeNC ligand ("fan-shaped" angle[44] for MeNC: 52° (wideness) and 52° (thickness), cf. cone-angle[42a] for CO ca 95°, an estimate which may be too large), and its electronic similarity to CO.[192b] The distance C(11A)...C(11B) between the methyl atom C(11A) and the methyl atom C(12B) of a neighbouring molecule (translated by (0 0 1)) is within bonding distance (1.57(4)Å). However, the atoms C(11A) and C(11B) consitute the disordered methyl isonitrile group, with site occupancy factors of 0.5.

14.2.5 Structure of $Re_2(CO)_6(CNC_6H_3Me_2\text{-}2,6)_4$(IV)

Compound (IV) crystallizes in the orthorhombic space group Pccn with Z = 4, an asymmetric unit being an $Re(CO)_3(CNC_6H_3Me_2\text{-}2,6)_2$-fragment, the two halves of the molecule being related by a crystallographic 2-fold axis, generating the equivalent position (x-½,y-½, z). The molecular structure and the numbering system used in the crystal structure analysis, is shown in Fig. 14.13. Bond lengths and bond angles are given in Tables 14.9 and 14.10 respectively.

From steric considerations of the RCN ligand, the $Re_2(CO)_8(CNC_6H_3Me_2\text{-}2,6)_4$ molecule might have been expected to adopt the eclipsed conformation (IVc) (Fig. 14.4). Of the possible staggered conformations, (IVa) and (IVb) (Fig. 14.4), (IVb) would be less favourable on steric grounds. The molecular geometry found in the crystal is that of (IVa), with cis-equatorial substitution of a pair

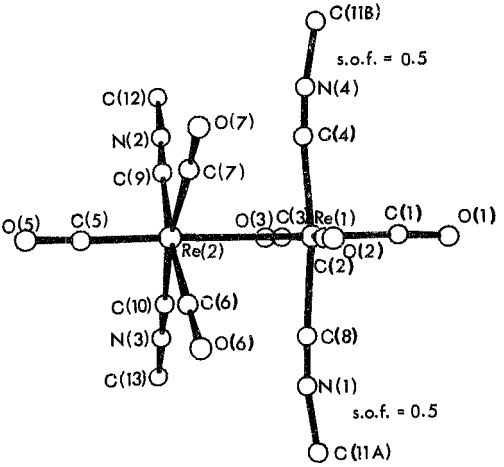


Figure 14.11: ORTEP[43] view of the $Re_2(CO)_7(CNMe)_3$ molecule (III), showing the numbering system used. (Site occupancy factor (s.o.f.) of 0.5 for N(1), N(4), and C(11A), C(11B))

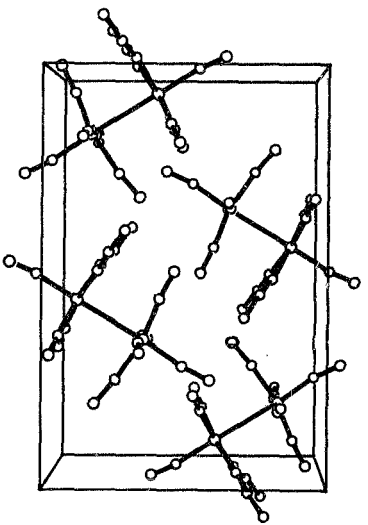


Figure 14.12: ORTEP[15] view of the unit cell of $Re_2(CO)_7(CNMe)_3$(III), looking down the b-axis

TABLE 14.7: Bond lengths (Å) for $Re_2(CO)_7(CNMe)_3$ (III)

Re(1)-Re(2)	3.049(1)		
Re(1)-C(1)	1.908(16)	C(1)-O(1)	1.160(17)
Re(1)-C(2)	1.916(16)	C(2)-O(2)	1.174(17)
Re(1)-C(3)	1.937(18)	C(3)-O(3)	1.126(19)
Re(2)-C(5)	1.870(16)	C(5)-O(5)	1.156(17)
Re(2)-C(6)	1.921(16)	C(6)-O(6)	1.175(17)
Re(2)-C(7)	1.936(17)	C(7)-O(7)	1.139(18)
Re(2)-C(9)	2.044(13)	C(9)-N(2)	1.140(15)
Re(2)-C(10)	2.095(15)	C(10)-N(3)	1.137(16)
Re(1)-C(8)	2.121(17)	C(8)-N(1)	1.066(19)
Re(1)-C(4)	2.127(17)	C(4)-N(4)	1.045(19)
N(1)-C(21A)	1.420(30)	N(2)-C(12)	1.455(20)
N(4)-C(11B)	1.414(29)	N(3)-C(13)	1.431(20)

TABLE 14.8: Bond angles (°) for $Re_2(CO)_7(CNMe)_3$ (III)

Re(1)-C(1)-O(1)	175.4(15)	Re(2)-C(5)-O(5)	172.0(16)
Re(1)-C(2)-O(2)	179.4(13)	Re(2)-C(6)-O(6)	178.1(14)
Re(1)-C(3)-O(3)	179.7(10)	Re(2)-C(7)-O(7)	178.0(15)
Re(1)-C(4)-N(4)	173.0(16)	Re(2)-C(9)-N(2)	176.7(12)
Re(1)-C(8)-N(1)	175.1(15)	Re(2)-C(10)-N(3)	179.0(14)
C(4)-N(4)-C(11B)	172.2(22)	C(9)-N(2)-C(12)	175.9(15)
C(8)-N(1)-C(11A)	170.4(22)	C(10)-N(3)-C(13)	177.1(14)
C(1)-Re(1)-Re(2)	179.2(5)	C(5)-Re(2)-Re(1)	178.4(5)
C(1)-Re(1)-C(2)	96.2(6)	C(5)-Re(2)-C(6)	93.6(7)
C(1)-Re(1)-C(3)	96.5(6)	C(5)-Re(2)-C(7)	96.3(7)
C(1)-Re(1)-C(4)	93.9(6)	C(5)-Re(2)-C(9)	92.8(6)
C(1)-Re(1)-C(8)	94.2(6)	C(5)-Re(2)-C(10)	92.2(6)
C(2)-Re(1)-Re(2)	83.7(4)	C(6)-Re(2)-Re(1)	86.4(4)
C(2)-Re(1)-C(3)	167.2(6)	C(6)-Re(2)-C(7)	89.8(7)
C(2)-Re(1)-C(4)	89.6(6)	C(6)-Re(2)-C(9)	173.4(5)
C(2)-Re(1)-C(8)	88.2(6)	C(6)-Re(2)-C(10)	91.2(6)
C(3)-Re(1)-Re(2)	83.6(4)	C(7)-Re(2)-Re(1)	85.3(4)
C(3)-Re(1)-C(4)	90.5(7)	C(7)-Re(2)-C(9)	91.2(6)
C(3)-Re(1)-C(8)	89.9(7)	C(7)-Re(2)-C(10)	171.4(6)
C(4)-Re(1)-Re(2)	85.2(4)	C(9)-Re(2)-Re(1)	87.2(3)
C(4)-Re(1)-C(8)	171.7(6)	C(9)-Re(2)-C(10)	86.7(5)
C(8)-Re(1)-Re(2)	86.6(4)	C(10)-Re(2)-Re(1)	86.3(4)

of isonitrile ligands on each Re-atom.

The relative arrangements of the xylyl (xylyl = 2,6-$Me_2C_6H_3$) isonitrile ligands, adopted (vide supra), as well as the relative orientation of the xylyl rings, probably reflects both steric requirements and crystal packing forces. The C6 rings are essentially planar. The xylyl rings are all close to being coplanar, the angles between the mean planes through rings A and B (A' and B'), A and B' (A' and B), A and A', and B and B' being 6.6, 5.7, 4.8, and 2.4° respectively. Fig. 14.14 shows the packing of the molecules in the unit cell, viewed down the b-axis. The xylyl rings of one molecule fit neatly into the gaps between the xylyl rings of adjacent molecules.

14.2.6 Structure of $Mn_2(CO)_6(CNC_6H_3Me_2\text{-}2,6)_4$(VI)

The complex $Mn_2(CO)_8(CNC_6H_3Me_2\text{-}2,6)_4$(VI) is isomorphous with the rhenium analogue, $Re_2(CO)_6(CNC_6H_3Me_2\text{-}2,6)_4$ (IV) (Space group Pccn, Z = 4), which is not surprising in view of the similarity of the two complexes.

The molecular structure and the numbering system used in the crystal structure analysis is shown in Fig. 14.15. Bond lengths and bond angles are given in Tables 14.11 and 14.12 respectively.

Fig. 14.16 shows the packing of the molecules in the unit cell, viewed down the b-axis. The xylyl rings are are close to being coplanar, with angles between the mean planes through rings A and B (A' and B'), A and B' (A' and B), A and A', and B and B', of 7.9, 7.4, 3.0 and 2.6° respectively. Slight structural differences between (VI) and (IV) are due to the shorter Mn-Mn and Mn-C bond distances relative to the Re-Re and Re-C bond lengths.

Since the structure of (VI) is the same as that of (IV) in the crystal, this cannot provide an explanation of the spectral (IR, ^{1}H NMR) differences between the two compounds in solution.

...3 Structural Trends

One of the main aims in undertaking the crystal structure determinations was to obtain bond parameter data and to

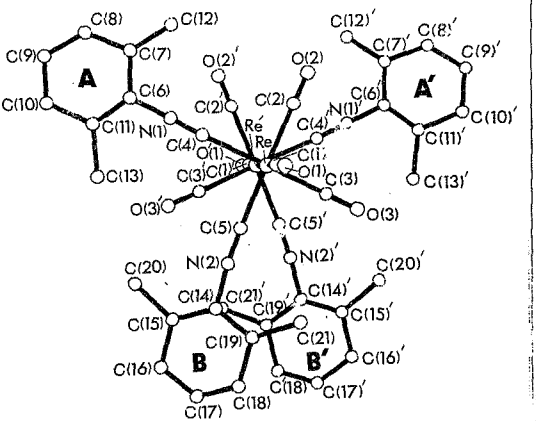


Figure 14.13: ORTEP*[8] view of the $Re_2(CO)_6(CNC_6H_3Me_2\text{-}2,6)_4$ molecule (IV), showing the numbering system used (Re related to Re' by a 2-fold axis, generating the equivalent position ($x-\frac{1}{2}$, $y-\frac{1}{2}$, z), and similarly for the other atoms).

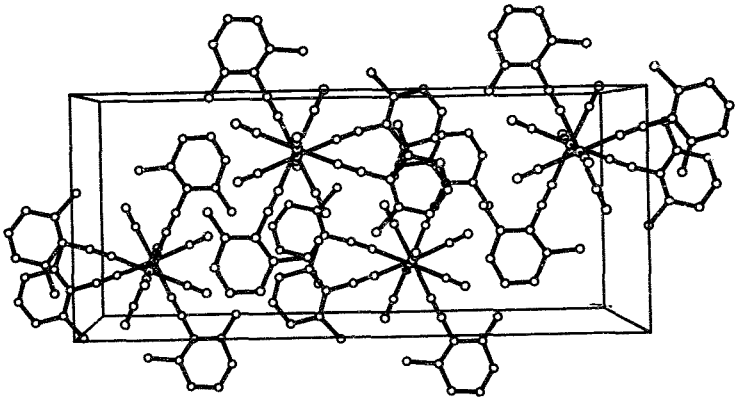


Figure 14.4: ORTEP[45] view of the unit cell of $Re_2(CO)_6(CNC_6H_3Me_2\text{-}2,6)_4$, looking down the b-axis

TABLE 14.9: Bond lengths (Å) for $Re_2(CO)_6(CNC_6H_3Me_2\text{-}2,6)_4$ (IV)

Re(x,y,z)-Re(½-x,½-y,z): 3.081(2)

Re-C(1)	1.968(20)	C(1)-O(1)	1.088(21)
Re-C(2)	1.980(20)	C(2)-O(2)	1.093(21)
Re-C(3)	1.924(21)	C(3)-O(3)	1.174(23)
Re-C(4)	2.031(22)	C(4)-N(1)	1.171(25)
Re-C(5)	2.027(18)	C(5)-N(2)	1.161(22)
N(1)-C(6)	1.407(24)	N(2)-C(14)	1.413(22)
C(6)-C(7)	1.391(26)	C(14)-C(15)	1.438(29)
C(7)-C(8)	1.448(32)	C(15)-C(16)	1.472(30)
C(8)-C(9)	1.413(35)	C(16)-C(17)	1.395(34)
C(9)-C(10)	1.396(31)	C(17)-C(18)	1.263(37)
C(10)-C(11)	1.428(32)	C(18)-C(19)	1.1472(35)
C(11)-C(6)	1.381(27)	C(19)-C(14)	1.396(19)
C(7)-C(12)	1.524(33)	C(15)-C(20)	1.573(32)
C(11)-C(13)	1.545(28)	C(19)-C(21)	1.485(34)

TABLE 14.10: Bond angles (°) for $Re_2(CO)_6\{CNC_6H_3Me_2\text{-}2,6\}_4$(IV)

Re-C(1)-O(1)	172.8(19)	C(1)-Re-C(2)	92.5(7)
Re-C(2)-O(2)	174.0(19)	C(1)-Re-C(3)	95.5(8)
Re-C(3)-O(3)	175.7(20)	C(1)-Re-C(4)	93.8(8)
Re-C(4)-N(1)	178.1(18)	C(1)-Re-C(5)	92.6(7)
Re-C(5)-N(2)	174.2(18)	C(2)-Re-C(3)	90.2(8)
C(4)-N(1)-C(6)	177.0(20)	C(2)-Re-C(4)	89.3(8)
C(5)-N(2)-C(14)	176.6(22)	C(3)-Re-C(5)	87.2(8)
C(2)-Re-Re´[a]	86.6(8)	C(4)-Re-C(5)	92.6(7)
C(3)-Re-Re´[a]	83.5(8)	C(2)-Re-C(5)	174.5(7)
C(4)-Re-Re´[a]	87.3(8)	C(3)-Re-C(4)	170.7(8)
C(5)-Re-Re´[a]	88.4(8)	C(1)-Re-Re´[a]	178.5(8)
C(11)-C(6)-C(7)	124.8(18)	C(19)-C(14)-C(15)	126.3(19)
C(6)-C(7)-C(8)	115.1(20)	C(14)-C(15)-C(16)	114.6(19)
C(7)-C(8)-C(9)	120.7(23)	C(15)-C(16)-C(17)	116.3(23)
C(8)-C(9)-C(10)	121.5(25)	C(16)-C(17)-C(18)	127.6(28)
C(9)-C(10)-C(11)	117.6(23)	C(17)-C(18)-C(19)	121.5(27)
C(10)-C(11)-C(6)	119.9(18)	C(18)-C(19)-C(14)	113.4(21)
C(12)-C(7)-C(6)	120.9(20)	C(20)-C(15)-C(14)	124.4(19)
C(12)-C(7)-C(8)	123.9(20)	C(20)-C(15)-C(16)	120.8(20)
C(13)-C(11)-C(6)	120.6(19)	C(21)-C(19)-C(14)	121.8(21)
C(13)-C(11)-C(10)	119.5(19)	C(21)-C(19)-C(18)	124.5(23)
N(1)-C(6)-C(7)	117.7(18)	N(2)-C(14)-C(15)	118.5(19)
N(1)-C(6)-C(11)	117.5(17)	N(2)-C(14)-C(19)	115.1(19)

[a] Re´ is related to Re by a 2-fold axis, generating the equivalent position ($\frac{1}{2}$-x, $\frac{1}{2}$-y, z).

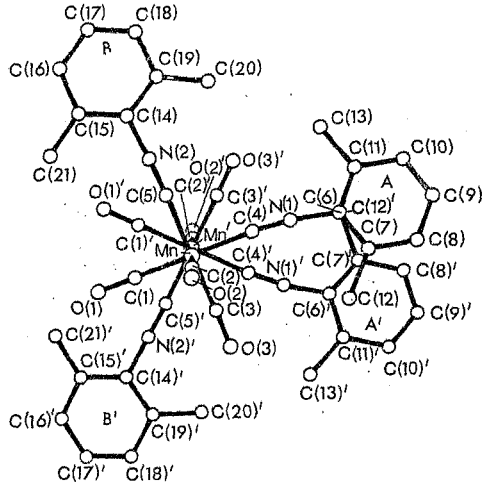


Figure 14.15: ORTEP[13] view of the $Mn_2(CO)_6(CNC_6H_3Me_2\text{-}2,6)_4$ molecule (VI), showing the numbering system used (Mn' related to Mn by a 2-fold axis generating the equivalent position (x-½, y-½, z), and similarly for other atoms).

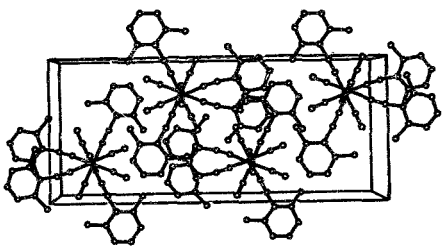


Figure 14.16: ORTEP view of the unit cell of $Mn_2(CO)_6(CNC_6H_3Me_2\text{-}2,6)_4$(VI), looking down the b-axis

TABLE 14.11: Bond lengths (Å) for $Mn_2(CO)_8(CNC_6H_3Me_2\text{-}2,6)_4$(VI)

Mn(x,y,z)-Mn(½-x, ½-y, z) :		2.946(6)	
Mn-C(1)	1.80(2)	C(1)-O(1)	1.15(2)
Mn-C(2)	1.72(2)	C(2)-O(2)	1.20(2)
Mn-C(3)	1.81(2)	C(3)-O(3)	1.16(2)
Mn-C(4)	1.90(2)	C(4)-N(1)	1.15(2)
Mn-C(5)	1.90(2)	C(5)-N(2)	1.17(2)
N(1)-C(6)	1.42(2)	N(2)-C(14)	1.41(2)
C(6)-C(7)	1.35(2)	C(14)-C(15)	1.41(2)
C(7)-C(8)	1.43(3)	C(15)-C(16)	1.40(3)
C(8)-C(9)	1.38(3)	C(16)-C(17)	1.40(3)
C(9)-C(10)	1.37(3)	C(17)-C(18)	1.38(3)
C(10)-C(11)	1.43(3)	C(18)-C(19)	1.44(2)
C(11)-C(6)	1.39(3)	C(19)-C(14)	1.42(2)
C(7)-C(12)	1.54(3)	C(15)-C(21)	1.48(3)
C(11)-C(13)	1.53(3)	C(19)-C(20)	1.51(3)

TABLE 14.12: Bond angles (°) for $Mn_2(CO)_6(ONC_6H_3Me_2\text{-}2,6)_4$ (VI)

Mn-C(1)-O(1)	177(2)	C(1)-Mn-C(2)	92.4(10)
Mn-C(2)-O(2)	179(2)	C(1)-Mn-C(3)	91.2(8)
Mn-C(3)-O(3)	173(2)	C(1)-Mn-C(5)	88.6(8)
Mn-C(4)-N(1)	175(2)	C(2)-Mn-C(3)	92.7(8)
Mn-C(5)-N(2)	177(2)	C(2)-Mn-C(4)	92.5(9)
C(4)-N(1)-C(6)	172(2)	C(2)-Mn-C(5)	96.0(8)
C(5)-N(2)-C(14)	179(2)	C(3)-Mn-C(4)	88.3(8)
C(1)-Mn-Mn'[a]	85(1)	C(4)-Mn-C(5)	91.2(7)
C(3)-Mn-Mn'[a]	81(1)	C(1)-Mn-C(4)	178.1(9)
C(4)-Mn-Mn'[a]	90(1)	C(3)-Mn-C(5)	171.4(8)
C(5)-Mn-Mn'[a]	90(1)	C(2)-Mn-Mn'[a]	173(1)
C(11)-C(6)-C(7)	123(2)	C(19)-C(14)-C(15)	125(2)
C(6)-C(7)-C(8)	118(2)	C(14)-C(15)-C(16)	115(2)
C(7)-C(8)-C(9)	119(2)	C(15)-C(16)-C(17)	122(2)
C(8)-C(9)-C(10)	123(2)	C(16)-C(17)-C(18)	123(2)
C(9)-C(10)-C(11)	118(2)	C(17)-C(18)-C(19)	118(2)
C(10)-C(11)-C(6)	119(2)	C(18)-C(19)-C(14)	118(2)
C(12)-C(7)-C(6)	121(2)	C(21)-C(15)-C(14)	121(2)
C(12)-C(7)-C(8)	121(2)	C(21)-C(15)-C(16)	124(2)
C(13)-C(11)-C(6)	122(2)	C(20)-C(19)-C(14)	122(2)
C(13)-C(11)-C(10)	119(2)	C(20)-C(19)-C(18)	120(2)
N(1)-C(6)-C(7)	119(2)	N(2)-C(14)-C(15)	120(2)
N(1)-C(6)-C(11)	118(2)	N(2)-C(14)-C(19)	118(2)

[a] Mn' is related to Mn by a 2-fold axis, generating the equivalent position ($\frac{1}{2}$-x, $\frac{1}{2}$-y, z).

see if any trends could be observed, relating to the structural effect (if any) of increasing isonitrile substitution.

14.3.1 The M-M bond length

Specifically, the effect of increasing isonitrile substitution on the metal-metal bond was of interest. Since isonitriles are weaker π-acceptors than carbonyls,[41] increasing isonitrile substitution would be expected to result in a weakening and hence a lengthening of the metal-metal bond.[192b] As can be seen from the Re-Re bond length data given for a series of $Re_2(CO)_{10-n}(CNR)_n$ (n = 0-4) complexes (Table 14.13a), there is a slight lengthening of the Re-Re bond with increasing n, but this only becomes significant at the n = 4 level. This effect is more apparent for the $Mn_2(CO)_{10-n}(CNR)_n$ (n = 0,2,4) series (Table 14.13b), possibly due to the weaker Mn-Mn bond relative to the Re-Re bond (see section 12.2.1), or to steric effects (greater steric crowding with Mn). The inference is that the isonitrile ligands are not having as great an effect (in the ground state) of weakening the metal-metal bond as might have been anticipated.[192b]

A lengthening of the metal-metal bond on increasing isonitrile substitution could also be expected on purely steric grounds in order to reduce repulsions between bulky isonitrile groups. For instance, as no significant bond lengthening is observed for the series $Re_2(CO)_{10-n}(CNR)_n$ (n = 0-3), and the Re-Re-Ceq angles are acute i.e. no bending out of CNR (or CO) ligands (see section 14.3.4), there seems to be little steric effect observed, except possibly for $Re_2(CO)_6(CNC_6H_3Me_2\text{-}2,6)_4$ ("fan-shaped" angle[44] for $CNC_6H_3Me_2$-2,6: 106° (wideness) and 53° (thickness)), where a lengthening of the Re-Re bond is observed.

14.3.2 The M-CO bond lengths

Studies of $M_2(CO)_{10}$ (M = Re,Mn)[138-9] have shown that the M-COax bonds are shorter than the M-COeq bonds (see Table 14.14), implying stronger bonding of axial carbonyls. However, when considering the substituted isonitrile

TABLE 14.13: Metal-metal bond length data for the complexes $M_2(CO)_{10-n}(CNR)_n$ (M = Re,Mn; n = 0-4)

(a) $Re_2(CO)_{10-n}(CNR)_n$ (n = 0-4)

Complex	Re-Re Bond length(Å)
$Re_2(CO)_{10}$	3.041(1)[a]
$Re_2(CO)_9(CNBu^t)$	3.048(1)
$Re_2(CO)_8(CNC_6H_3Me_2\text{-}2,6)_2$	3.047(1)
$Re_2(CO)_7(CNMe)_3$	3.049(1)
$Re_2(CO)_6(CNC_6H_3Me_2\text{-}2,6)_4$	3.081(2)

(b) $Mn_2(CO)_{10-n}(CNR)_n$ (n = 0,2,4)

Complex	Mn-Mn bond length(Å)
$Mn_2(CO)_{10}$	2.904(1)[a]
$Mn_2(CO)_8(CNBu^t)_2$	2.924(1)
$Mn_2(CO)_6(CNC_6H_3Me_2\text{-}2,6)_4$	2.946(6)

[a] Ref. 158

derivatives, the possible effect of the isonitrile ligand on the trans carbonyl could also be important.[132] Since the isonitrile ligand is a poorer π-acceptor than carbonyl,[43] it would be expected that the M-CO bond trans to an RNC ligand would be shorter than that trans to another CO.[102]

Although this effect is indeed observed for $Re_2(CO)_9(CNBu^t)$, with *Re-C(1) trans to CNBu^t* (1.916(18)Å) *significantly shorter* than the av. value of the other *Re-COeq* bonds (av. 1.983(20)Å), this trend does not continue for the $Re_2(CO)_{10-n}(CNR)_n$ (n = 2-4) derivatives (see Table 14.14(a)). However, for the $Re_2(CO)_{10-n}(CNR)_n$ (n = 1-3) complexes, the av. Re-COax bond is significantly shorter than the av. Re-COeq (trans to CO or CN) bonds, *as expected* (vide supra). However, for $Re_2(CO)_8(CNC_6H_3Me_2\text{-}2,6)_4$, the Re-COax bond (1.968(20)Å) is longer than the av. Re-COeq (*all trans to CN*) bonds (av. 1.952(20)Å), indicative of a strong trans effect of the isonitrile ligands.[102] The Re-CN bond lengths are relatively constant for the series $Re_2(CO)_{10-n}(CNR)_n$ (n = 1-4) (see Table 14.14(a)).

For the $Mn_2(CO)_{10-n}(CNR)_n$ (n = 2,4) complexes, the Mn-COax bond lengths are significantly shorter than the Mn-COeq (trans to CO or CN) bonds (Table 14.14(b)). This effect is more pronounced than in the parent $Mn_2(CO)_{10}$.[133] In the case of $Mn_2(CO)_8(CNBu^t)_2$, the Mn-CO (trans to CN) bonds (av. 1.814(5)Å) are shorter than the Mn-CO (trans to CO) bonds (av. 1.841(5)Å), as expected (vide supra).

14.3.3 Molecular conformation

In all the structures discussed (I-VI), the molecule adopts a staggered conformation, like the parent carbonyls, $M_2(CO)_{10}$ (M = Re, Mn),[134] with C-M-M-C torsional angles close to the ideal 45°. (Torsional angles of structures (I)-(VI) are listed in Appendix C). A staggered conformation is expected to minimize repulsions between equatorial ligands.[135]

The axC-M-M-Cax fragement is essentially linear, as evidenced by M-M-COax bond angles of ca. 177° (see Table 14.15).

TABLE 14.14: Average M-C bond length data for the complexes $M_2(CO)_{10-n}(CNR)_n$ (M = Re,Mn; n = 0-4)

(a) $Re_2(CO)_{10-n}(CNR)_n$ (n = 0-4)

Complex	av. Re-C bond length(Å)			
	Re-COax	Re-COeq		Re-CN
		trans to CO	trans to CN	
$Re_2(CO)_{10}$ [a]	1.929(7)	1.987(6)	-	-
$Re_2(CO)_9(CNBu^t)$	1.902(19)	1.983(20)	1.916(18)	2.068(15)
$Re_2(CO)_8(CNC_6H_3Me_2\text{-}2,6)_2$	1.924(6)	1.976(6)	1.975(7)	2.050(6)
$Re_2(CO)_7(CNMe)_3$ [b]	1.889(16)	1.927(16)	1.929(17)	2.070(14)
				2.124(17) [c]
$Re_2(CO)_6(CNC_6H_3Me_2\text{-}2,6)_4$	1.968(20)	-	1.952(20)	2.029(20)

(b) $Mn_2(CO)_{10-n}(CNR)_n$ (n = 0,2,4)

Complex	av. Mn-C bond length(Å)			
	Mn-COax	Mn-COeq		Mn-CN
		trans to CO	trans to CN	
$Mn_2(CO)_{10}$ [a]	1.811(3)	1.856(2)	-	-
$Mn_2(CO)_8(CNBu^t)_2$	1.784(5)	1.841(5)	1.814(5)	1.944(4)
$Mn_2(CO)_6(CNC_6H_3Me_2\text{-}2,6)_4$	1.72(2)	-	1.81(2)	1.90(2)

[a] Ref. 158

[b] Disordered structure

[c] av. for disordered MeNC ligand

14.3.4 C-M-C and M-M-Ceq bond angles

In structures (I)-(VI), all the C-M-C angles are close to 90°, but significantly, the axC-M-Ceq angles are all greater than 90°, while the eqC-M-Ceq angles are ca. 90°. (See Table 14.16). This is true whether the equatorial ligand is a carbonyl or isonitrile ligand. Hence the ligands are all bending slightly inwards towards the M-M bond. This is also reflected in the acute M-M-Ceq angles (ca. 86°) (see Table 14.15). Similar trends were observed for $M_n(CO)_{10}$ (M = Re,Mn).[158-9]

This is thought to be a genuine electronic effect, and has been rationalized by Elian and Hoffmann[93] on the basis of MO Theory. From a consideration of energy level diagrams, theoretical predictions indicate that the energetically most favourable geometry corresponds to an eqC-M-Cax angle of slightly greater than 90°, at which point π-interaction is maximized, and anti-bonding interaction minimized.

The consistency of the axC-M-Ceq (93-96°), eqC-M-eq (ca. 90°) and M-M-Ceq (85-88°) bond angles for the series $M_2(CO)_{10-n}(CNR)_n$ (M = Re, n = 0-4; M = Mn, n = 0,2,4) (see Tables 14.15-16), indicate that this effect is genuine. Also significant is the observation that the M-M-CN angles are less than 90° for these structures (Table 14.15). Since isonitriles such as $CNC_6H_3Me_2$-2,6 ("fan-shaped" angles,[94] 105° (wideness) and 53° (thickness)) have greater steric bulk than CO (cone angle ca. 95°;[94a] this estimate, however, seems too large) this would indicate that any steric factors are less important than electronic factors in determining the direction of the bending of the equatorial ligands. Again no structural effect of increasing isonitrile substitution is apparent.

14.3.5 M-C-O, M-C-N and C-N-C bond angles

In all the structures (I-VI), both the carbonyl and the isonitrile ligands co-ordinate in an essentially linear fashion, with M-C-O and M-C-N bond angles all in the range 170 - 179° (see Table 14.17). Near-linearity of

TABLE 14.15: Average M-M-C bond angle data (°) for the complexes $M_2(CO)_{10-n}(CNR)_n$ ((a) M = Re, n = 0-4; (b) M = Mn, n = 0,2,4)

Complex	M-M-COax	M-M-COeq	M-M-CN
(a)			
$Re_2(CO)_{10}$ [a]	176.3(2)	86.4(2)	-
$Re_2(CO)_9(CNBu^t)$	177.0(6)	86.8(5)	87.5(4)
$Re_2(CO)_8(CNC_6H_3Me_2\text{-}2,6)_2$	177.9(2)	86.2(1)	88.2(1)
$Re_2(CO)_7(CNMe)_3$ [b]	178.8(5)	84.8(4)	86.3(4)
$Re_2(CO)_6(CNC_6H_3Me_2\text{-}2,6)_4$	178.5(8)	85.1(8)	87.9(8)
(b)			
$Mn_2(CO)_{10}$ [a]	177.03(9)	86.38(7)	-
$Mn_2(CO)_8(CNBu^t)_2$	176.4(2)	84.5(1)	90.0(1)
$Mn_2(CO)_6(CNC_6H_3Me_2\text{-}2,6)_4$	173(1)	83(1)	90(1)

[a] Ref. 158

[b] Disordered structure

TABLE 14.16: Average cis C-M-C bond angle data (°) for the complexes $M_2(CO)_{10-n}(CNR)_n$ ((a) M = Re, n = 0-4; (b) M = Mn , n = 0,2,4)

Complex	axCO-M-COeq	axCO-M-CN	eqCO-M-COeq	eqCO-M-CN	CN-M-CN
(a)					
$Re_2(CO)_{10}$ [a]	93.7(3)	-	89.8(2)	-	-
$Re_2(CO)_9(CNBu^t)$	93.3(8)	92.1(6)	89.8(8)	89.9(7)	-
$Re_2(CO)_8(CNC_6H_3Me_2\text{-}2,6)_2$	94.1(2)	91.1(2)	90.9(2)	88.8(2)	-
$Re_2(CO)_7(CNMe)_3$ [b]	95.7(7)	93.3(6)	89.8(6)	90.1(6)	86.7(5)
$Re_2(CO)_6(CNC_6H_3Me_2\text{-}2,6)_4$	94.0(8)	93.2(8)	90.2(8)	88.3(8)	92.6(7)
(b)					
$Mn_2(CO)_{10}$ [a]	93.65(11)	-	89.79(10)	-	-
$Mn_2(CO)_8(CNBu^t)_2$	94.5(2)	93.2(2)	89.7(2)	91.2(2)	86.1(2)
$Mn_2(CO)_6(CNC_6H_3Me_2\text{-}2,6)_4$	92.6(9)	94.3(9)	91.2(8)	88.5(8)	91.2(7)

[a] Ref. 158

[b] Disordered structure

M-C-R bonds for $M(CR)_n$ (R = O,N, n>1) groups has been predicted on electronic grounds. [39]

The observation that deviations from linearity are not greater for the M-C-N bonds than for the M-C-O bonds (see Table 14.17), nor indeed do more highly substituted complexes show any greater distortions, is indicative of the apparent lack of any noticeable effect of the steric bulk[41] of the isonitrile ligands on the molecular geometry.

Further, the isonitrile ligands themselves show only small deviations from linearity, the C-N-C angles being generally in the range 170-180° (see Table 14.17). This slight deviation from linearity is normal for terminal isonitrile ligands (isonitriles with C-N-C angles > . are considered to be essentially linear[41b]). Individual isontrile ligands which show slight deviations from linearity (eg. (II): CN(2)-N(2)-C(9): 166.1(5)°; (III): C(8)-N(1)-C(11A): 170.4(22)°) probably reflect the influence of crystal packing forces. A greater bending of the isonitrile ligands in the more highly substituted complexes is not observed.

14.3.6 Packing

The role of crystal packing forces in determining structure should not be neglected. In the case of $Re_2(CO)_8(CNC_6H_3Me_2\text{-}2,6)_2$(II) (see section 14.2.2) and $Re_2(CO)_6(CNC_6H_3Me_2\text{-}2,6)_4$(IV) (see section 14.2.5) (and the isomorphous $Mn_2(CO)_6(CNC_6H_3Me_2\text{-}2,6)_4$(VI), section 14.2.6), the conformation adopted in the crystal, as well as the relative orientation of the xylyl rings, is probably determined largely by the influence of packing forces. (See packing diagram of (II), (IV) and (VI), Figs. 14.8, 14.14 and 14.16 respectively.) For the tri-substituted $Re_2(CO)_7(CNMe)_3$, the conformation adopted in the crystal, (IIIc) (Fig. 14.3), is probably favoured over the other possible conformations (IIIa) and (IIIb) (Fig. 14.3) due to packing considerations. In solution all isomers probably co-exist.

Packing forces could also be responsible for small

TABLE 14.17 Average bond data (°) for the M-C-O, M-C-N and C-N-C bond angles of the complexes $M_2(CO)_{10-n}(CNR)_n$ ((a) M = Re, n = 0-4; (b) M = Mn, n = 0,2,4)

Complex	M-C-Oax	M-C-Oeq	M-C-N	C-N-C
(a)				
$Re_2(CO)_{10}$ [a]	177.5(7)	178.0(5)	-	-
$Re_2(CO)_9(CNBu^t)$	177.0(17)	175.9(17)	175.5(13)	175.7(18)
$Re_2(CO)_8(CNC_6H_3Me_2\text{-}2,6)_2$	177.0(5)	178.3(5)	177.4(5)	171.0(5)
$Re_2(CO)_7(CNMe)_3$ [b]	173.7(16)	178.8(13)	177.9(13)	176.5(15)
			174.1(14) [c]	171.3(22) [c]
$Re_2(CO)_6(CNC_6H_3Me_2\text{-}2,6)_4$	172.8(19,	174.9(20)	176.3(18)	176.8(21)
(b)				
$Mn_2(CO)_{10}$ [a]	179.21(27)	177.89(23)	-	-
$Mn_2(CO)_8(CNBu^t)_2$	178.1(5)	177.9(4)	177.6(4)	176.7(4)
$Mn_2(CO)_6(CNC_6H_3Me_2\text{-}2,6)_4$	179(2)	175(2)	176(2)	176(2)

[a] Ref. 158

[b] Disordered structure

[c] av. for disordered MeNC ligand

deviations in geometry. For example, non-bonded O...O interactions could result in M-C-O bonds deviating from linearity by 5-10°. Hence deviations from ideal geometry might occur in order to achieve close-packing.[243]

14.4 Relating structure to chemical reactivity

Investigations of the reaction (14.1) of $Re_2(CO)_{10}$ with RNC to give products $Re_2(CO)_{10-n}(CNR)_n$ (n = 1-4) (see ch. XI).

$$Re_2(CO)_{10} + nRNC \longrightarrow Re_2(CO)_{10-n}(CNR)_n + nCO \qquad (14.1)$$

showed that

(i) reaction proceeds more slowly as n increases, and

(ii) direct substitution with n>4 could not be achieved (except perhaps for R = 2,6-$Me_2C_6H_3$).

This can be explained in terms of

(i) increasing electron density on the metal atom, and

(ii) a fifth RNC ligand would have to occupy an electronically less favourable equatorial trans to RNC,[162] or axial[159] site.

^{13}CO labelling studies have shown that for the thermal (80°, 4h) and Pd/C (10%) catalysed (25°C, 10 min) reaction (14.2),[277] and the PdO-catalysed (55°C, 5 min) reaction (14.3) (see ch. XI),

$$Mn_2(CO)_{10} + {}^tBuNC \longrightarrow Mn_2(CO)_9(CNBu^t) + CO \qquad (14.2)$$

$$Re_2(CO)_{10} + {}^tBuNC \longrightarrow Re_2(CO)_9(CNBu^t) + CO \qquad (14.3)$$

no metal-metal bond cleavage occurs. However total scrambling was observed for the $Mn_2(CO)_{10-n}(CNBu^t)_n$ (n = 2,3) products also formed in the thermal reaction (14.2).[277] Hence an alternate mechanism for the synthesis of the higher derivatives, $M_2(CO)_{10-n}(CNR)_n$ (n>1), involving metal-metal bond cleavage cannot be ruled out on the basis of available data.

An interesting result is that of the different substitution geometries observed for the $M_2(CO)_8(CNR)_2$ structures, viz. 1,2-cis-dieq-$Re_2(CO)_8(CNC_6H_3Me_2\text{-}2,6)_2$ and 1,1-cis-dieq-$Mn_2(CO)_8(CNBu^t)_2$. This latter isomer might be expected to be the electronically favoured product in a direct substitution reaction not involving metal-metal bond cleavage, in accordance with the so-called cis-labilization

effect.[182] However, kinetic studies[225] on the PdO-catalysed reaction (14.4) at 25°C in benzene,

$$Mn_2(CO)_{10} + 2Bu^tNC \longrightarrow Mn_2(CO)_8(CNBu^t)_2 + 2CO \quad (14.4)$$

have shown the 1,2-isomer (*Isomer(B)*, *Fig.* 11.5) is formed first. The 1,2-isomer (B) can be isomerized to the 1,1-isomer (A) (Fig. 11.5) on heating. (Ratio of B:A, 3:1 (benzene); 1:1 (hexane)). *These results show* that cis-labilization is not necessarily implicated in the reaction of $Mn_2(CO)_{10}$ with RNC ligands. Further, isomer (A) reacts faster than isomer (B) with RNC to give 1,1-*cis*-*diax*, 2-*eq*-$Mn_2(CO)_7(CNBu^t)_3$, which is the opposite to the expected result in terms of the cis-labilization effect. The reaction of both the isomers (A) and (B) to give the tri-substituted product *is faster than* the isomerization of (B) to (A).

In the case of the analogous reaction (14.5) with $Re_2(CO)_{10}$,[225]

$$Re_2(CO)_{10} + 2Bu^tNC \longrightarrow Re_2(CO)_8(CNBu^t)_2 + 2CO \quad (14.5)$$

only isomer (B) is formed, and isomerization to isomer (A) *cannot be achieved* even on extended heating at 125°C. Hence there would appear to be a substantial barrier to the isomerization reaction (B) to (A) for $Re_2(CO)_8(CNBu^t)_2$. This is supported *by the inability* to convert isomer (A) to (B),[225] isomer (A), $(CO)_5Re\text{-}Re(CO)_3(CNBu^t)_2$, being prep.. indirectly from the reaction of $NaRe(CO)_5$ with $Re(CO)_3(CNBu^t)_2I$.[225]

From the above kinetic results it is apparent that the differences in the $M_2(CO)_8(CNR)_2$ (M = Re, Mn) structures determined reflect the kinetics of the *reaction of* $M_2(CO)_{10}$ with RNC ligands.

14.5 Experimental

14.5.1 Data collection

The synthesis of the complexes $Re_2(CO)_9(CNBu^t)$(I), $Re_2(CO)_8(CNC_6H_3Me_2\text{-}2,6)_2$(*II*), $Re_2(CO)_7(CNMe)_3$(III) and $Re_2(CO)_6(CNC_6H_3Me_2\text{-}2,6)_4$(IV) is described in ch. XI, and of $Mn_2(CO)_8(CNBu^t)_2$(V) and $Mn_2(CO)_6(CNC_6H_3Me_2\text{-}2,6)_4$(VI) in Ref. 220. Crystals of the complexes were grown under

nitrogen at 20°C from solutions of dichloromethane-hexane (I,II,IV) or benzene-hexane (III), or from deoxygenated pentane solutions at -5°C (V,VI).

In each case, preliminary investigation was done using standard Weissenberg and precession photography. Refined cell constants were obtained during data collection on a Philips PW1100 four-circle diffractometer at 20°C, using either MoKα (I,II,III,V and VI) or CuKα (IV) graphite-monochromated radiation (see Appendix 8(d) for details). Lorentz and polarization corrections were applied in all cases. For the rhenium structures (I-IV), the data was corrected for absorption using the computer program DIFABS, an empirical method for correcting diffractometer data for absorption effects, written by N. Walker and D. Stuart,[257a] and adapted by G. Kruger.[257b]

Crystal data and details of the data collections and structural analyses are summarized in Tables 14.18 (I-IV) and 14.19 (V and VI). Definitions of the crystallographic R-indices used are given in Appendix B(f).

14.5.2 Structure solution and refinement

The structures were solved and refined using the program SHELX82.[46a] The metal atom(s) were placed by a Patterson synthesis, and the positions of the other non-hydrogen atoms, and hydrogen atoms, if located (V only), were found by difference Fourier syntheses. Refinement of positional parameters of all atoms, and anisotropic temperature factors for the non-carbon (II-IV,VI) or non-hydrogen (V) atoms, was done by full-matrix least-squares methods, and was considered complete when all parameter shifts were less than 0.5σ. Scattering factors for Re(0) and Mn(0) were taken from "International Tables for X-ray Crystallography",[46b] and anomalous dispersion corrections[46c] were made for the rhenium and manganese atoms. Final fractional atomic co-ordinates, together with isotropic temperature factors for the carbon (I-IV,VI) or hydrogen (V) atoms for structures (I)-(VI) are given in Tables 14.20 to 14.25 respectively, and anisotropic temperature factors for the non-carbon (I-IV,VI) or non-hydrogen (V) atoms in Tables 14.26 to 14.31

TABLE 14.18: Crystal data and details of structure analyses for the $Re_2(CO)_{10-n}(CNR)_n$ (n = 1–4) complexes (I–IV)

	(I)	(II)	(III)	(IV)
Complex	$Re_2(CO)_9(CNBu^t)$	$Re_2(CO)_8(CNC_6H_3Me_2\text{-}2,6)_2$	$Re_2(CO)_7(CNMe)_3$	$Re_2(CO)_6(CNC_6H_3Me_2\text{-}2,6)_4$
Formula	$Re_2C_{14}H_9NO_9$	$Re_2C_{25}H_{10}N_2O_8$	$Re_2C_{13}H_9N_3O_7$	$Re_2C_{42}H_{36}N_4O_6$
Mr	707.62	850.76	691.63	1065.15
Colour, shape	white, needles	cream, needles	yellow, cylindrical	yellow, rectangular
Crystal dimensions (mm)	0.19x0.18x0.13	0.20x0.12x1.10	0.20x0.19x0.14	0.60x0.40x0.40
Space Group	Pbca (No. 61)	$P\bar{1}$ (No. 2)	$P2_1/n$ (No. 14[a])	Pccn (No. 56)
a(Å)	17.160(7)	15.145(7)	10.874(5)	13.832(6)
b(Å)	18.300(7)	9.294(4)	16.175(7)	11.322(5)
c(Å)	12.370(5)	10.328(5)	10.711(5)	26.401(11)
α(°)	90	92.70(3)	90	90
β(°)	90	74.47(2)	90.07(3)	90
γ(°)	90	98.85(3)	90	90
U(Å^3)	3884.53	1383.94	1883.92	4134.55
Z	8	2	4	4
F(000)	2575.22	807.80	1255.61	2055.61
Dc(gcm^{-3})	2.42	2.04	2.44	1.71
μ(cm^{-1})	119.71	84.10	123.37	104.39
λ(Å)	0.7107(MoKα)	0.7107(MoKα)	0.7107(MoKα)	1.5418(CuKα)
Scan Mode	ω/2θ	ω/2θ	ω/2θ	ω/2θ

TABLE 14.18: Crystal data and details of structure analyses for the $Re_2(CO)_{10-n}(CNR)_n$ (n = 1-4) complexes (I-IV)

	(I)	(II)	(III)	(IV)
Range (°)	$3 \leq \theta \leq 26$	$3 \leq \theta \leq 23$	$3 \leq \theta \leq 26$	$3 \leq \theta \leq 68$
Scan width (°)	0.90	1.40	1.30	1.60
Scan speed ($°sec^{-1}$)	0.030	0.047	0.043	0.052
Range of hkℓ	$+h,+k,+\ell$	$\pm h,\pm k,+\ell$	$\pm h,+k,+\ell$	$+h,+k,+\ell$
Measured intensities	2520	3815	3828	3470
Unique reflections	2168	3749	3631	3052
Internal consistency R-index	0.0000	0.0117	0.0000	0.0000
Omitted reflections	272	347	236	160
Cut-off criterion	$F<\sigma F$	$F<\sigma F$	$F<\sigma F$	$F<\sigma F$
R	0.0505	0.0386	0.0596	0.1090
Rw	0.0391	0.0334	0.0467	0.1112
k (weight $w=k/(\sigma^2 F)$)	0.2600	0.3329	0.4835	3.1265

[a] Cell choice 2 ("International Tables for Crystallography Vol. A. Space Group Symmetry", T. Hahn (Ed.), D. Reidel Publishing Co., Dordrecht, Holland (1983), p 177).

TABLE 14.19: Crystal data and details of structure analyses for the $Mn_2(CO)_{10-n}(CNR)_n$ (n = 2,4) complexes (V,VI)

	(V)	(VI)
Complex	$Mn_2(CO)_8(CNBu^t)_2$	$Mn_2(CO)_6(CNC_6H_3Me_2\text{-}2,6)_4$
Formula	$Mn_2C_{18}H_{18}N_2O_8$	$Mn_2C_{42}H_{36}N_4O_6$
Mr	500.21	802.63
Colour, shape	*yellow, rectangular*	*orange, rectangular*
Crystal dimensions (mm)	0.17x0.16x0.13	0.16x0.16x0.14
Space Group	$P2_1/n$ (No. 14[b])	Pccn (No. 56)
a(Å)	20.535(8)	13.895(6)
b(Å)	12.291(5)	11.131(4)
c(Å)	9.289(4)	26.125(10)
α(°)	90	90
β(°)	90.38(3)	90
γ(°)	90	90
U(Å^3)	2344.45	4040.63
Z	4	4
F(000)	1519.94	1555,97
Dc(gcm^{-3})	1.42	1.32
μ(cm^{-1})	10.71	6.25
λ(Å)	0.7107(MoKα)	0.7107(MoKα)
Scan mode	ω/2θ	ω/2θ
Range (°)	3≤θ≤26	3≤θ≤26
Scan width (°)	0.60	0.40
Scan speed (°sec^{-1})	0.020	0.016
Range of h,k,ℓ	±h,+k,+ℓ	+h,+k,+ℓ
Measured intensities	4178	3184
Unique *reflections*	3798	2690
Internal consistency R-index	0.0000	0.0223
Omitted reflections	-	1111
Cut-off criterion	-	F<2σF
R = Rw [a]	0.0563	0.1320

[a] Unit weights used

[b] Cell choice 2 ("International Tables for Crystallography Vol. A. Space Group Symmetry", T. Hahn (Ed.), D. Reidel Publishing Co., Dordrecht, Holland (1983), p 177).

respectively. Appendix D contains a listing of the Structure Factors.

14.5.3 Refinement problems with $Mn_2(CO)_6(CNC_6H_3Me_2\text{-}2,6)_4$ (VI)

Problem was experienced with the refinement of (VI). Initially a data set was collected under CuKα radiation (λ = 1.5418Å). The structure was solved using this data set (2822 unique reflections), but refinement of the structure below an R-value of 0.19 could not be achieved. Data was re-collected, using MoKα radiation (λ = 0.7107Å). With this new data set (2690 unique reflections), refinement of the structure could proceed. However, refinement below an R-value of ca. 0.17 could only be achieved after omitting all reflections (1111) with $F<2\sigma F$. The final R-value of the refined structure was 0.1320. At this stage, all parameter shifts were less than 0.5σ, and there was no residual electron density. Inability to refine the structure further could be due to (i) a too small an effective data set (1579 unique reflections), (ii) a poor data set due to inferior quality crystals, or (iii) compound deterioration before data collection (crystal decomposition during data collection was not, however, observed).

TABLE 14.20: Final atomic co-ordinates, and isotropic temperature factors of the C-atoms, for $Re_2(CO)_9(CNBu^t)$(I)

Atom	x/a	y/b	z/c	U(Å²)
Re(1)	0.3693(0)	-0.1472(0)	-0.2293(1)	
Re(2)	0.2234(0)	-0.0982(0)	-0.1789(1)	
O(1)	0.2849(8)	-0.2931(7)	-0.3315(11)	
O(2)	0.5176(7)	-0.2018(7)	-0.4099(10)	
O(3)	0.2896(8)	-0.0911(7)	-0.5146(10)	
O(4)	0.4277(9)	-0.1994(9)	-0.0736(12)	
O(5)	0.2237(8)	-0.2496(8)	-0.0697(11)	
O(6)	0.1240(7)	-0.1643(8)	-0.3690(11)	
O(7)	0.0842(8)	-0.0405(8)	-0.0524(11)	
O(8)	0.2476(6)	0.0439(7)	-0.3101(11)	
O(9)	0.3443(7)	-0.0385(7)	-0.0154(9)	
N	0.4350(7)	0.0138(7)	-0.2579(11)	
C(1)	0.3191(9)	-0.2397(10)	-0.3195(14)	0.053(5)
C(2)	0.4633(10)	-0.1787(9)	-0.3690(15)	0.052(5)
C(3)	0.3197(10)	-0.1090(10)	-0.4428(17)	0.057(5)
C(4)	0.4082(10)	-0.1806(10)	-0.1575(17)	0.060(5)
C(5)	0.2223(11)	-0.1928(11)	-0.1073(16)	0.067(5)
C(6)	0.1589(12)	-0.1428(11)	-0.2962(17)	0.079(6)
C(7)	0.1368(11)	-0.0636(11)	-0.1000(16)	0.071(6)
C(8)	0.2375(10)	-0.0081(10)	-0.2573(15)	0.051(5)
C(9)	0.2992(11)	-0.0576(10)	-0.0760(16)	0.065(6)
C(10)	0.4146(8)	-0.0443(8)	-0.2706(12)	0.036(4)
C(11)	0.4627(11)	0.0886(10)	-0.2327(16)	0.068(5)
C(12)	0.5457(24)	0.0877(23)	-0.1941(31)	0.250(20)
C(13)	0.4272(21)	0.1419(18)	-0.3087(26)	0.194(14)
C(14)	0.4231(27)	0.1084(26)	-0.1132(39)	0.276(23)

TABLE 14.21: Final atomic co-ordinates, and isotropic temperature factors of the C-atoms, for $Re_2(CO)_8(CNC_6H_3Me_2\text{-}2,6)_2$ (II)

Atom	x/a	y/b	z/c	$U(Å^2)$
Re(1)	0.3591(0)	-0.2532(0)	-0.0150(0)	
Re(2)	0.1661(0)	-0.1993(0)	-0.0172(0)	
N(1)	0.3659(5)	-0.4271(9)	-0.2913(8)	
N(2)	0.0923(5)	-0.2582(9)	0.2985(8)	
O(1)	0.4388(5)	0.0250(9)	-0.1890(9)	
O(2)	0.5479(4)	-0.3179(9)	0.0029(8)	
O(3)	0.2543(5)	-0.5381(8)	0.1347(7)	
O(4)	0.3248(5)	-0.0727(9)	0.2497(8)	
O(5)	0.1273(5)	-0.5267(8)	-0.0846(9)	
O(6)	0.2334(5)	0.1202(8)	0.0551(8)	
O(7)	0.2449(5)	-0.1250(8)	-0.3191(7)	
O(8)	-0.0316(4)	-0.1566(8)	-0.0144(8)	
CN(1)	0.3619(6)	-0.3657(10)	-0.1902(10)	0.048(2)
CN(2)	0.1201(6)	-0.2407(10)	0.1858(10)	0.051(2)
CO(1)	0.4097(7)	-0.0743(12)	-0.1234(10)	0.060(3)
CO(2)	0.4785(7)	-0.2925(11)	-0.0091(10)	0.060(3)
CO(3)	0.2917(6)	-0.4323(12)	0.0820(10)	0.054(3)
CO(4)	0.3391(7)	-0.1372(12)	0.1534(11)	0.064(3)
CO(5)	0.1420(6)	-0.4063(12)	-0.0586(10)	0.054(3)
CO(6)	0.2076(6)	0.0065(12)	0.0296(10)	0.056(3)
CO(7)	0.2163(6)	-0.1522(11)	-0.2092(11)	0.057(3)
CO(8)	0.0418(7)	-0.1711(11)	-0.0135(10)	0.059(3)
C(1)	0.3652(6)	-0.5109(11)	-0.4124(10)	0.051(2)
C(2)	0.3346(7)	-0.6574(12)	-0.3946(11)	0.069(3)
C(3)	0.3335(8)	-0.7459(14)	-0.5155(13)	0.092(4)
C(4)	0.3663(9)	-0.6695(15)	-0.6388(13)	0.097(4)
C(5)	0.3979(7)	-0.5295(13)	-0.6546(11)	0.075(3)
C(6)	0.3984(7)	-0.4386(12)	-0.5377(11)	0.072(3)
C(7)	0.3029(7)	-0.7330(13)	-0.2585(11)	0.076(3)
C(8)	0.4292(8)	-0.2778(14)	-0.5409(12)	0.088(4)
C(9)	0.0401(6)	-0.2632(11)	0.4344(10)	0.060(3)

TABLE 14.21: Final atomic co-ordinates, and isotropic temperature factors of the C-atoms, for $Re_2(CO)_8(CNC_6H_3Me_2\text{-}2,6)_2$(II) (Contd)

Atom	x/a	y/b	z/c	U(Å²)
C(10)	-0.0419(7)	-0.2003(12)	0.4967(11)	0.075(3)
C(11)	-0.0917(8)	-0.2064(14)	0.6053(12)	0.086(4)
C(12)	-0.0836(8)	-0.2734(14)	0.6959(12)	0.088(4)
C(13)	0.0169(8)	-0.3395(14)	0.6665(12)	0.086(4)
C(14)	0.0737(7)	-0.3304(12)	0.5268(11)	0.067(3)
C(15)	0.1829(7)	-0.3993(13)	0.4828(11)	0.079(3)
C(16)	-0.0732(8)	-0.1300(14)	0.3639(13)	0.093(4)

TABLE 14.22: Final atomic co-ordinates, and isotropic temperature factors of the C-atoms, for $Re_2(CO)_7(CNMe)_3$ (III)

Atom	x/a	y/b	z/c	U(Å²)
Re(1)	0.3462(0)	0.3410(0)	0.2501(0)	
Re(2)	0.1060(0)	0.4383(0)	0.2499(1)	
O(1)	0.5907(10)	0.2467(10)	0.2489(13)	
O(2)	0.1745(11)	0.1889(7)	0.2470(13)	
O(3)	0.4638(10)	0.5131(9)	0.2486(16)	
O(5)	-0.1363(10)	0.5293(9)	0.2472(15)	
O(6)	0.0208(13)	0.3164(9)	0.0446(12)	
O(7)	0.0213(12)	0.3175(9)	0.4541(13)	
N(2)	0.2315(10)	0.5527(8)	0.4556(11)	
N(3)	0.2327(10)	0.5564(9)	0.0433(11)	
N(1)[a]	0.3377(12)	0.3453(10)	-0.0470(13)	0.014(2)
N(4)[a]	0.3337(12)	0.3432(10)	0.5454(13)	0.014(2)
C(1)	0.4963(13)	0.2799(10)	0.2527(14)	0.063(4)
C(2)	0.2392(12)	0.2469(10)	0.2478(14)	0.056(4)
C(3)	0.4206(13)	0.4498(11)	0.2488(15)	0.061(4)
C(4)	0.3314(14)	0.3455(11)	0.4479(16)	0.073(5)
C(5)	-0.0395(14)	0.4999(11)	0.2464(15)	0.066(4)
C(6)	0.0511(13)	0.3627(10)	0.1234(14)	0.059(4)
C(7)	0.0541(13)	0.3612(11)	0.3776(15)	0.063(4)
C(8)	0.3349(14)	0.3437(11)	0.0524(16)	0.076(5)
C(9)	0.1844(10)	0.5138(8)	0.3808(11)	0.039(3)
C(10)	0.1886(11)	0.5142(10)	0.1155(13)	0.051(4)
C(11A)[a]	0.3489(23)	0.3337(19)	-0.1779(25)	0.052(5)
C(11B)[a]	0.3455(23)	0.3299(19)	0.8754(25)	0.052(5)
C(12)	0.2914(15)	0.6073(12)	0.5448(16)	0.078(5)
C(13)	0.2931(15)	0.6101(12)	-0.0432(16)	0.079(5)

[a] Disordered isonitrile: Atoms N(1), N(4), C(11A) and C(11B) have s.o.f. of 0.5; Atoms N(1) and N(4), and C(11A) and C(11B), assigned common isotropic temperature factors.

TABLE 14.23: Final atomic co-ordinates, and isotropic temperature factors of the C-atoms, for $Re_2(CO)_6(CNC_6H_3Me_2\text{-}2,6)_4$(IV)

Atom	x/a	y/b	z/c	U(Å^2)
Re	0.1394(1)	0.2342(1)	0.6076(0)	
N(1)	0.1248(11)	0.4887(16)	0.6599(6)	
N(2)	0.1333(11)	0.1320(20)	0.4946(5)	
O(1)	-0.0774(11)	0.1845(17)	0.6081(5)	
O(2)	0.1684(12)	0.1326(19)	0.7143(5)	
O(3)	0.1819(13)	-0.0077(14)	0.5577(5)	
C(1)	-0.0015(14)	0.2098(15)	0.6082(6)	0.049(4)
C(2)	0.1549(13)	0.1637(17)	0.6758(7)	0.059(5)
C(3)	0.1697(15)	0.0845(19)	0.5470(8)	0.064(5)
C(4)	0.1309(15)	0.3905(19)	0.6401.7)	0.063(5)
C(5)	0.1371(13)	0.3024(16)	0.5366(7)	0.052(4)
C(6)	0.1228(13)	0.6001(17)	0.6835(7)	0.056(5)
C(7)	0.1173(15)	0.6030(20)	0.7361(3)	0.067(6)
C(8)	0.1178(18)	0.7201(23)	0.7582(10)	0.089(8)
C(9)	0.1164(18)	0.8218(24)	0.7272(10)	0.089(7)
C(10)	0.1227(16)	0.8138(23)	0.6745(9)	0.080(6)
C(11)	0.1246(14)	0.6984(19)	0.6526(7)	0.058(5)
C(12)	0.1171(18)	0.4894(26)	0.7670(10)	0.099(8)
C(13)	0.1226(16)	0.6851(23)	0.5944(9)	0.077(6)
C(14)	0.1327(14)	0.3823(18)	0.4427(7)	0.060(5)
C(15)	0.1449(15)	0.4847(20)	0.4290(8)	0.070(6)
C(16)	0.1406(17)	0.5085(23)	0.3743(10)	0.086(7)
C(17)	0.1342(17)	0.4100(24)	0.3427(10)	0.088(7)
C(18)	0.1265(20)	0.3030(30)	0.3556(10)	0.099(8)
C(19)	0.1260(15)	0.2674(19)	0.4092(9)	0.066(6)
C(20)	0.1540(18)	0.5888(23)	0.4682(10)	0.092(8)
C(21)	0.1082(20)	0.1451(26)	0.4273(10)	0.102(9)

TABLE 14.24(a): Final atomic co-ordinates of the *non*-H atoms for $Mn_2(CO)_8(CNBu^t)_2$(V)

Atom	x/a	y/b	z/c
Mn(1)	0.1180(0)	0.3937(0)	0.4005(1)
Mn(2)	0.1375(0)	0.2059(1)	0.2125(1)
N(1)	0.0292(2)	0.2521(3)	0.6014(4)
N(2)	0.1298(2)	0.3125(3)	0.5985(4)
O(3)	0.0998(2)	0.5944(3)	0.5652(4)
O(4)	0.0071(2)	0.4510(3)	0.2073(4)
O(5)	0.2092(2)	0.5108(3)	0.2090(4)
O(6)	-0.0061(2)	0.1786(3)	0.2330(5)
O(7)	0.1559(2)	0.0095(3)	0.0383(5)
O(8)	0.1203(2)	0.3645(3)	-0.0285(4)
O(9)	0.1521(2)	0.0868(3)	0.4897(4)
O(10)	0.2780(2)	0.2668(3)	0.2221(5)
C(1)	0.0615(2)	0.3083(3)	0.5244(5)
C(2)	0.1890(2)	0.3428(3)	0.5219(5)
C(3)	0.1067(2)	0.5144(4)	0.5032(5)
C(4)	0.0493(2)	0.4272(4)	0.2816(5)
C(5)	0.1743(2)	0.4632(3)	0.2622(5)
C(6)	0.0488(2)	0.1911(4)	0.2266(5)
C(7)	0.1494(3)	0.0867(4)	0.1055(5)
C(8)	0.1270(2)	0.3042(4)	0.0652(6)
C(9)	0.1464(2)	0.1374(4)	0.3863(5)
C(10)	0.2242(2)	0.2444(4)	0.2208(5)
C(11)	-0.0095(2)	0.1854(4)	0.7001(5)
C(12)	0.0363(4)	0.1165(8)	0.7777(11)
C(13)	-0.0424(5)	0.2743(8)	0.8040(11)
C(14)	-0.0610(4)	0.1347(8)	0.6106(10)
C(15)	0.2788(2)	0.2655(4)	0.6953(5)
C(16)	0.3024(6)	0.3614(8)	0.7880(11)
C(17)	0.3305(5)	0.2198(12)	0.631(10)
C(18)	0.2444(3)	0.1827(6)	0.884(9)

TABLE 14.24(b): Final atomic co-ordinates and isotropic temperature factors of the hydrogen atoms, *for* $Mn_2(CO)_8(CNBu^t)_2$(V)

Atom	x/a	y/b	z/c	U(Å²)
H(12A)	0.060(5)	0.163(8)	0.831(10)	0.21(5)
H(12B)	0.008(3)	0.079(5)	0.852(6)	0.97(2)
H(12C)	0.047(4)	0.066(7)	0.701(10)	0.20(4)
H(13A)	-0.012(3)	0.305(6)	0.849(7)	0.11(3)
H(13B)	-0.086(5)	0.286(8)	0.729(11)	0.24(5)
H(13C)	-0.062(4)	0.219(6)	0.875(8)	0.17(3)
H(14A)	-0.083(4)	0.121(6)	0.550(8)	0.15(4)
H(14B)	-0.027(3)	0.088(5)	0.552(7)	0.13(3)
H(14C)	-0.088(3)	0.095(5)	0.677(6)	0.11(2)
H(16A)	0.275(7)	0.338(11)	0.899(14)	0.34(7)
H(16B)	0.334(4)	0.406(7)	0.702(10)	0.20(4)
H(16C)	0.332(3)	0.340(5)	0.828(7)	0.10(2)
H(17A)	0.311(3)	0.151(5)	0.577(8)	0.13(3)
H(17B)	0.362(3)	0.193(6)	0.651(7)	0.12(2)
H(17C)	0.346(4)	0.272(7)	0.532(8)	0.16(3)
H(18A)	0.278(4)	0.151(6)	0.861(8)	0.14(4)
H(18B)	0.244(4)	0.134(6)	0.715(9)	0.16(4)
H(18C)	0.209(4)	0.221(6)	0.843(8)	0.16(3)

TABLE 14.25: Final atomic co-ordinates, and isotropic temperature factors of the non-C atoms, for $Mn_2(CO)_6(CNC_6H_3Me_2\text{-}2,6)_4$ (VI)

Atom	x/a	y/b	z/c	U(Å²)
Mn	0.1443(2)	0.2607(2)	0.6082(1)	
N(1)	0.135(1)	0.163(1)	0.499(1)	
N(2)	0.128(1)	0.012(1)	0 658(1)	
O(1)	0.165(1)	0.362(1)	0.712(1)	
O(2)	-0.062(1)	0.315(1)	0.608(1)	
O(3)	0.183(1)	0.499(1)	0.562(1)	
C(1)	0.159(1)	0.321(2)	0.672(1)	0.062(5)
C(2)	0.021(1)	0.291(1)	0.608(1)	0.061(5)
C(3)	0.174(1)	0.404(1)	0.580(1)	0.052(5)
C( )	0.140(1)	0.195(1)	0 541(1)	0.059(5)
C(5)	0.134(1)	0.105(1)	638(1)	0.053(4)
C(6)	0.132(1)	0.141( )	0.446(1)	0.063(5)
C(7)	0.120(1)	0.234(2)	0.413(1)	0.072(6)
C(8)	0.121(1)	0.210(2)	0.360(1)	0.087(7)
C(9)	0.131(2)	0.093(2)	0.343(1)	0.101(8)
C(10)	0.143(2)	-0.002(2)	0.376(1)	0.096(7)
C(11)	0.142(2)	0.023(2)	0.430(1)	0.081(6)
C(12)	0.109(2	0.383(2)	0.434(1)	0.087(7)
C(13)	0.155(2)	-0.082(2)	0.467(1)	0.095(8)
C(14)	0.122(1)	-0.100(2)	0.683(1)	0.056(5)
C(15)	0.119(1)	-0.103(2)	0.737(1)	0.068(6)
C(16)	0.118(2)	-0.218(2)	0.758( )	0.087(7)
C(17)	0.119(2)	-0.322(2)	0.728( )	0.097(8)
C(18)	0.121(2)	-0.319(2)	0.675( )	0.079(8)
C(19)	0.122(1)	-0.203(1)	0.65 ( )	0.058(5)
C(20)	0.124(1)	-0.193(2)	0.54( )	0.070(6)
C(21)	0.119(2)	0.010(2)	0.7( )	0.095(7)

TABLE 14.26: Anisotropic temperature factors ($\AA^2$) for the non-C atoms of $Re_2(CO)_9(CNBu^t)$(I)

Atom	U11	U22	U33	U23	U13	U12
Re(1)	0.0434(4)	0.0352(3)	0.0425(6)	-0.0001(4)	-0.0050(4)	0.0002(3)
Re(2)	0.0429(4)	0.0499(4)	0.0461(6)	0.0024(4)	-0.0002(4)	-0.0021(4)
O(1)	0.103(11)	0.063(9)	0.117(12)	0.010(9)	-0.007(10)	-0.019(8)
O(2)	0.062(8)	0.074(9)	0.086(10)	-0.023(8)	0.016(8)	0.003(7)
O(3)	0.110(11)	0.084(10)	0.065(11)	0.018(8)	-0.033(9)	-0.019(9)
O(4)	0.127(13)	0.130(13)	0.075(12)	0.026(10)	-0.037(10)	0.043(11)
O(5)	0.132(12)	0.075(9)	0.094(11)	0.034(9)	-0.023(10)	-0.009(10)
O(6)	0.086(10)	0.143(15)	0.082(11)	-0.023(10)	-0.020(9)	-0.022(10)
O(7)	0.082(9)	0.112(12)	0.102(12)	-0.013(10)	0.040(10)	0.001(9)
O(8)	0.062(8)	0.069(9)	0.107(11)	0.015(9)	-0.019(8)	0.002(6)
O(9)	0.084(10)	0.124(12)	0.044(9)	-0.022(8)	0.000(8)	-0.014(8)
N	0.049(8)	0.041(8)	0.057(10)	-0.013(7)	-0.003(8)	0.002(7)

TABLE 14.27: Anisotropic temperature factors ($\AA^2$) for the non-C atoms of $Re_2(CO)_8(CNC_6H_3Me_2\text{-}2,6)_2$(II)

Atom	U11	U22	U33	U23	U13	U12
Re(1)	0.0419(2)	0.0475(3)	0.0433(3)	0.0020(2)	-0.0106(2)	0.0054(2)
Re(2)	0.0444(2)	0.0441(3)	0.0471(3)	-0.0008(2)	-0.0117(2)	0.0092(2)
N(1)	0.046(4)	0.061(6)	0.055(5)	0.011(5)	-0.004(4)	0.010(4)
N(2)	0.055(5)	0.072(6)	0.045(5)	-0.000(5)	-0.006(4)	0.005(4)
O(1)	0.094(6)	0.074(6)	0.123(7)	0.041(6)	-0.022(5)	-0.012(5)
O(2)	0.060(4)	0.101(7)	0.104(6)	-0.004(5)	-0.027(4)	0.027(4)
O(3)	0.083(5)	0.067(5)	0.082(6)	0.023(5)	-0.007(4)	0.005(4)
O(4)	0.100(6)	0.113(7)	0.077(6)	-0.041(5)	-0.032(5)	0.036(5)
O(5)	0.099(6)	0.057(5)	0.131(8)	-0.013(5)	-0.043(5)	0.008(4)
O(6)	0.085(5)	0.054(5)	0.099(6)	-0.011(5)	-0.016(4)	0.003(4)
O(7)	0.104(6)	0.091(6)	0.050(5)	0.010(4)	-0.012(4)	0.017(5)
O(8)	0.049(4)	0.083(6)	0.143(7)	-0.007(5)	-0.044(4)	0.021(4)

TABLE 14.28: Anisotropic temperature factors ($Å^2$) for the non-C atoms of $Re_2(CO)_7(CNMe)_3$(III)

Atom	U11	U22	U33	U23	U13	U12
Re(1)	0.0418(3)	0.0408(4)	0.0341(3)	-0.0001(3)	0.0001(2)	0.0053(2)
Re(2)	0.0374(3)	0.0392(3)	0.0461(3)	0.0003(3)	-0.0001(2)	0.0007(2)
O(1)	0.079(8)	0.149(15)	0.143(11)	0.011(11)	0.006(8)	0.069(9)
O(2)	0.093(8)	0.049(9)	0.149(12)	0.000(8)	-0.019(8)	-0.004(7)
O(3)	0.071(8)	0.071(10)	0.212(15)	0.009(11)	-0.008(9)	-0.014(7)
O(5)	0.070(7)	0.093(11)	0.0203(15)	0.001(12)	-0.000(9)	0.023(8)
O(6)	0.148(12)	0.101(12)	0.087(9)	-0.022(8)	-0.038(8)	-0.021(9)
O(7)	0.117(10)	0.096(12)	0.114(10)	0.037(9)	0.046(8)	-0.009(8)
N(2)	0.058(7)	0.065(10)	0.052(7)	0.006(7)	0.010(5)	-0.008(6)
N(3)	0.071(8)	0.075(11)	0.052(7)	0.022(7)	-0.009(6)	-0.019(7)

TABLE 14.29: Anisotropic temperature factors ($Å^2$) for the non-C atoms of $Re_2(CO)_6(CNC_6H_3Me_2\text{-}2,6)_4$(IV)

Atom	U11	U22	U33	U23	U13	U12
Re	0.0560(6)	0.0587(6)	0.0289(5)	0.0034(3)	0.0020(3)	0.0054(4)
N(1)	0.045(10)	0.075(12)	0.067(10)	-0.010(8)	0.009(8)	0.006(8)
N(2)	0.061(11)	0.161(18)	0.025(7)	0.032(9)	-0.007(7)	0.012(11)
O(1)	0.043(10)	0.131(14)	0.095(12)	0.014(9)	0.003(8)	-0.004(9)
O(2)	0.107(14)	0.197(19)	0.034(7)	0.044(9)	0.001(8)	-0.018(13)
O(3)	0.125(15)	0.074(10)	0.076(10)	-0.008(8)	0.012(9)	0.017(10)

TABLE 14.30: Anisotropic temperature factors ($\AA^2$) for the non-H atoms of $Mn_2(CO)_8(CNBu^t)_2$(V)

Atom	U11	U22	U33	U23	U13	U12
Mn(1)	0.0412(3)	0.0444(3)	0.0614(4)	0.0003(3)	-0.0047(3)	-0.0014(2)
Mn(2)	0.0530(3)	0.0529(4)	0.0584(4)	-0.0039(3)	-0.0000(3)	-0.0001(3)
N(1)	0.048(2)	0.063(2)	0.067(2)	0.003(2)	0.004(2)	-0.004(2)
N(2)	0.048(2)	0.067(2)	0.063(2)	0.008(2)	-0.009(2)	-0.001(2)
O(3)	0.094(3)	0.072(2)	0.124(3)	-0.043(2)	-0.013(2)	0.011(2)
O(4)	0.074(2)	0.100(3)	0.119(3)	0.010(2)	-0.040(2)	0.017(2)
O(5)	0.092(3)	0.084(3)	0.109(3)	0.020(2)	0.013(2)	-0.038(2)
O(6)	0.054(2)	0.104(3)	0.143(4)	-0.006(3)	-0.009(2)	-0.015(2)
O(7)	0.162(4)	0.082(3)	0.099(3)	-0.041(3)	0.002(3)	0.018(3)
O(8)	0.111(3)	0.100(3)	0.082(3)	0.025(2)	-0.012(2)	0.003(2)
O(9)	0.092(2)	0.069(2)	0.076(2)	0.011(2)	-0.008(2)	-0.006(2)
O(10)	0.053(2)	0.112(3)	0.135(4)	0.015(3)	0.012(2)	-0.002(2)
C(11)	0.043(2)	0.054(2)	0.055(3)	-0.007(2)	-0.009(2)	0.004(2)
C(2)	0.048(2)	0.048(2)	0.062(3)	-0.005(2)	0.006(2)	-0.009(2)
C(3)	0.053(2)	0.063(3)	0.076(3)	-0.007(3)	-0.010(2)	0.001(2)
C(4)	0.059(3)	0.056(3)	0.086(3)	-0.001(2)	-0.002(2)	-0.000(2)
C(5)	0.058(2)	0.047(2)	0.075(3)	0.004(2)	-0.011(2)	-0.005(2)
C(6)	0.068(3)	0.061(3)	0.077(3)	-0.006(2)	-0.011(2)	-0.007(2)
C(7)	0.087(3)	0.075(3)	0.065(3)	-0.002(3)	-0.001(3)	0.005(3)
C(8)	0.062(3)	0.082(3)	0.073(3)	-0.002(3)	-0.005(2)	-0.002(3)
C(9)	0.054(2)	0.059(3)	0.065(3)	-0.007(2)	-0.002(2)	-0.008(2)
C(10)	0.063(3)	0.066(3)	0.063(3)	0.008(2)	0.006(2)	0.007(2)
C(11)	0.054(2)	0.064(3)	0.067(3)	0.001(2)	0.009(2)	-0.010(2)
C(12)	0.107(5)	0.097(5)	0.110(6)	0.032(5)	0.002(5)	-0.001(4)
C(13)	0.111(6)	0.117(6)	0.114(6)	-0.023(5)	0.045(6)	-0.012(5)
C(14)	0.091(5)	0.124(7)	0.116(6)	-0.003(5)	-0.003(5)	-0.052(5)
C(15)	0.050(2)	0.083(3)	0.059(3)	0.012(2)	0.007(2)	-0.004(2)
C(16)	0.152(8)	0.131(7)	0.115(7)	0.015(5)	-0.084(7)	-0.033(6)
C(17)	0.088(5)	0.201(12)	0.109(6)	0.045(8)	0.012(5)	0.065(7)
C(18)	0.081(4)	0.120(6)	0.092(5)	0.045(5)	-0.003(4)	0.006(4)

TABLE 14.31: Anisotropic temperature factors ($Å^2$) for the non-C atoms of $Mn_2(CO)_6(CNC_6H_3Me_2\text{-}2,6)_4$ (VI)

Atom	U11	U22	U33	U23	U13	U12
Mn	0.081(2)	0.033(1)	0.049(1)	-0.001(1)	-0.001(2)	-0.008(1)
N(1)	0.096(13)	0.051(9)	0.050(10)	0.001(8)	-0.005(11)	-0.025(9)
N(2)	0.105(13)	0.040(7)	0.074(12)	0.007(8)	0.012(11)	-0.023(8)
O(1)	0.142(16)	0.110(11)	0.050(9)	-0.028(9)	-0.008(10)	-0.013(11)
O(2)	0.074(10)	0.080(9)	0.103(11)	-0.011(10)	0.004(10)	0.011(7)
O(3)	0.132(12)	0.034(6)	0.087(11)	0.012(7)	0.001(10)	-0.016(7)

XV. THE REACTION BETWEEN DIRHENIUM DECACARBONYL AND PHOSPHINE LIGANDS

15A. Introduction

This chapter deals with aspects of the reaction between $Re_2(CO)_{10}$ (and $Mn_2(CO)_{10}$) with phosphine ligands. The synthetic methods (Thermal, photochemical, NMe_3O-assisted), and the products obtained for the reaction between $Re_2(CO)_{10}$ and PR_3, have been reviewed in section 10.2. Section 15B discusses the characterization of the $Re_2(CO)_{10-n}(PR_3)_n$ ($n = 1$-4) products obtained, and in particular, the use of IR spectroscopy in the assignment of substitution geometry. Kinetic and mechanistic studies reported for the reaction of $M_2(CO)_{10}$ (M = Re,Mn) with PR_3 are covered in Section 15C.

In Section 15D, the catalytic synthesis and characterization of a range of $Re_2(CO)_{10}(PR_3)_n$ (n = 1,2) complexes is presented. This work is an extension of the Pd-catalysed substitution of $Re_2(CO)_{10}$ by RNC ligands (ch. XI) to the bulkier PR_3 ligands. The preparation of isomers of $Re_2(CO)_8(PR_3)_2$ by alternate synthetic routes is also presented. The $Re_2(CO)_8(PR_3)_2$ products are discussed in relation to complexes of this type reported in the Literature, and a rationalization of the formation of isomers is given.

Finally, the Crystal and Molecular X-ray structure of diax$[Re_2(CO)_8(PMe_2Ph)_2]$ is presented in Section 15E. This structure determination was undertaken to establish the molecular geometry, and to investigate the structural effect of replacing the isonitrile ligand (see ch. XIV) with the more sterically demanding phosphine ligand.

15B. Discussion of the IR spectral data of $Re_2(CO)_{10-n}(PR_3)_n$ (n = 1-4) complexes

15B.1 Introduction

The reaction (both thermal and photochemical) between $Re_2(CO)_{10}$ and PR_3 has been investigated by many groups (see section 10.2) and in most cases, the product(s) obtained was either ax-$Re_2(CO)_9(PR_3)$, and/or diax-$Re_2(CO)_8$-

$(PR_3)_2$. In some reactions, sideproducts such as mer-trans-$HRe(CO)_3(PR_3)_2$ were also obtained. There have, however, also been reports of the synthesis of equatorially-substituted $Re_2(CO)_{10-n}(PR_3)_n$ (n = 1,2) products, as well as $Re_2(CO)_7(PR_3)_2$ and $Re_2(CO)_6(PR_3)_4$ products. It is thus apparent that potentially a wide range of complexes (both expected and unexpected) have been observed from the reaction between $Re_2(CO)_{10}$ and PR_3.

Techniques which have been employed in the characterization of products from the reaction of $Re_2(CO)_{10}$ with PR_3, include IR spectroscopy, ^1H NMR and ^{31}P NMR spectroscopy, mass spectroscopy, elemental analysis and chemical reactivity. In general, elemental analysis is used to establish the molecular formula of the compound (but this would not differentiate between, for instance, $Re_2(CO)_{10-2n}(PR_3)_{2n}$ and $HRe(CO)_{5-n}(PR_3)_n$ (n = 1,2)). In some cases mass spectroscopy has been used to obtain the parent ion, and establish that the species in fact a dimer. Cleavage reactions may give information relating to the substitution geometry, in particular the number of phosphine ligands on each metal atom. ^1H NMR and, more recently, ^{31}P NMR spectroscopy has been used to obtain information on the sites occupied by the phosphine ligands (from the number and position of the resonances). IR spectroscopy, however, is the most ubiquitous, and sometimes the only, means of product identification. The number and intensity of the ν(CO) bands in the IR spectrum relates to the molecular geometry. However, IR spectroscopy is not highly reliable in this regard, as the number of ν(CO) bands predicted from Group Theory Analysis often does not correspond to the number observed in practice, as band overlap may occur, resulting in fewer bands. Alternately, there may be more bands, due to a Raman band which gains some weak IR intensity, or to a lowering of the molecular symmetry from the ideal point group symmetry as a result of internal asymmetry of the molecule.

Although X-ray Crystallography remains the ultimate technique for molecular structure determination, no X-ray

studies of $Re_2(CO)_{10-n}(PR_3)_n$ (n = 1-4) complexes have been reported in the Literature to date. Several $Mn_2(CO)_{10-n}(PR_3)_n$ (n = 1,2) X-ray structures have, however, been reported, and these will be used to establish a correlation between IR data and molecular geometry, to aid in the structural interpretation of the IR spectra of $Re_2(CO)_{10-n}(PR_3)_n$ (n = 1,2) complexes.

Despite the limitations of the IR spectral methods as a tool for structure assignment, especially when used alone, it has been used extensively in the Literature, but in view of the confusion which exists over the characterization of certain of the substituted products, the existing IR spectral data for $Re_2(CO)_{10-n}(PR_3)_n$ (n = 1-4) complexes will be reviewed here, and an attempt made to relate IR spectra to substitution geometry. Where relevant, reference will also be made to certain $Mn_2(CO)_{10-n}(PR_3)_n$ (n = 1,2) complexes which aid in the structural interpretation of the IR data.

15B.2. $\underline{Re_2(CO)_9(PR_3)}$ complexes

Complexes of the type $M_2(CO)_9(L)$ have two possible geometries, (Fig. 15.1), viz. ax(IA) or eq(IB). Although $\underline{eq}$-$M_2(CO)_9(L)$ (IB) is the electronically favoured isomer (see ch.XII), with bulky phosphine ligand L, steric factors may dominate, resulting in $\underline{ax}$-$M_2(CO)_9(PR_3)$ (M = Re,Mn), (IA).

According to Group Theory, $\underline{ax}$-$M_2(CO)_9(L)$, of molecular symmetry D4d, should exhibit 5 IR active ν(CO) bands, while $\underline{eq}$-$M_2(CO)_9(L)$, of molecular symmetry Cs, should have 9 bands. However, in practice, many $\underline{eq}$-$Mn_2(CO)_9(L)$ complexes[222] have only 6 ν(CO) bands in the IR spectrum, owing to band overlap.

Table 15.1 lists IR spectral data of some reported $M_2(CO)_9(PR_3)$ (M = Mn,Re) derivatives. In general, the degree of substitution is based on elemental analysis, and in some cases, a mass spectrum, while ^1H NMR and/or IR spectroscopy is used to determine the molecular geometry (ie. *(IA)* or *(IB)*).

The IR spectrum of $\underline{ax}$-$Mn_2(CO)_9(PMe_2Ph)$,[223] the

axial substitution (IA) of which has been confirmed by an X-ray crystallographic structure,[224] with 5 ν(CO) bands, (Table 15.1) is typical of a wide range of ax-$Mn_2(CO)_9(PR_3)$ and ax-$Mn_2(CO)_9(AsR_3)$ complexes.[223] Since the structure of these complexes is reliably known, the IR spectral pattern can be taken as typical of complexes of the type (IA).

In the reaction of $HMn(CO)_5$ with $AsPh_3$[216] in the presence of O_2 at -10°C, both the isomers ax-$Mn_2(CO)_9(AsPh_3)$ and eq-$Mn_2(CO)_9(AsPh_3)$ were reported as being produced. However, the compound identifications were based on elemental analyses only. The IR spectra of these complexes gave 5 and 7 bands respectively in the carbonyl region (see Table 15.1). Both complexes gave very similar ^1H NMR spectra.

Reports of $Re_2(CO)_9(PR_3)$ products are less numerous than those of $Re_2(CO)_8(PR_3)_2$ complexes, as the thermal reaction between $Re_2(CO)_{10}$ and PR_3 tends to give $Re_2(CO)_8(PR_3)_2$, even when only one equivalent of phosphine is used. There have been several reports of the synthesis of ax-$Re_2(CO)_9(PPh_3)$.[181-2] The IR spectrum, in various solvents, is given in Table 15.1. In toluene,[181a] there are 5 ν(CO) bands, as expected. However, in certain solvents, eg. cyclohexane,[181b] and decalin,[181a] there is an additional weak band at ca. 1975 cm^{-1}, a shoulder to the very strong band at ca. 1998 cm^{-1}. This band (B2) gains some intensity in the IR spectrum by the lowering of the local symmetry induced by the triphenylphosphine ligand.[181a] In $CHCl_3$,[182a] the weak peak at ca. 1960 cm^{-1} is absent, but this may be due to band weakness or overlap. The IR spectrum in $CHCl_3$ of ax-$Re_2(CO)_9(PMePh_2)$[184] has a similar pattern (Table 15.1). However, $Re_2(CO)_9(PMe_2Ph)$ (identified by elemental analysis) has a different IR spectrum and its geometry has been assigned as eq-$Re_2(CO)_9(PMe_2Ph)$[183] on the basis of the 7 ν(CO) bands in the IR spectrum (Table 15.1). There has also been a report of eq-$Re_2(CO)_9(PPh_3)$.[182] The only evidence for this, however, is an IR spectrum (Table 15.1). It is to be noted that the spectra of these

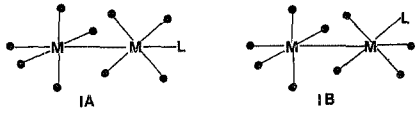


Figure 15.1: Possible isomers for $M_2(CO)_9(L)$ complexes ($\bullet$ = CO) (IA) ax and (IB) eq.

two reported eq-isomers do not correspond to that of eq-$Mn_2(CO)_9(AsPh_3)$, or those of eq-$Mn_2(CO)_9(L)$ complexes[222] either (eg. eq-$Mn_2(CO)_9(py)$, IR(hexane), ν(CO): 2091(w), 2017(s), 2006(s), 1980(vs), 1960(m), 1940(m) cm^{-1}),[222] or those of the eq-$Re_2(CO)_9(CNR)$ complexes (ch. XI), and thus must be regarded with circumspection. The product $Mn_2(CO)_9\{P(OCH_2)_3CEt\}$ obtained from the reaction of $Mn_2(CO)_{10}$ with $P(OCH_2)_3CEt$, [IR(benzene), ν(CO): 2094(w), 2020(ms), 1995(vs), 1980(m), 1965(m), 1930(sh) cm^{-1}] was concluded on the basis of ^1H NMR data to be a mixture of ax-and eq-isomers![59] In the complex IR spectrum of $Mn_2(CO)_9(PF_3)$[IR(hexane), ν(CO): 2110(s), 2038(s), 2015(vs), 2002(m), 1992(2), 1980(m), 1960(w), 1954(m) cm^{-1}], formed from the reaction of $Mn_2(CO)_{10}$ with PF_3, assigned as ax-$Mn_2(CO)_9(PF_3)$,[188] there appear to be several unexplained peaks. The $Re_2(CO)_9(PF_3)$ product is reported as being analogous.[188]

TABLE 15.1: IR spectral data of $M_2(CO)_9(L)$ (M = Mn, Re, L = AsR_3, PR_3) complexes

Complex	Solvent	ν(CO)/cm^{-1}	Ref
ax-$Mn_2(CO)_9(PMe_2Ph)$	benzene	2094(w),2016(s),1993(vs),1969(sh),1938(m)	223
ax-$Mn_2(CO)_9(AsPh_3)$	hexane	2098(m),2020(s),2000(vs),1977(s), 1943(s)	258
eq-$Mn_2(CO)_9(AsPh_3)$	CCl_4	2102(w),2085(w),2028(vs),2002(sh),1995(s),1940(sh),1920(s)	258
ax-$Re_2(CO)_9(PPh_3)$	toluene	2104(m),2032(w),1991(vs),1960(s), 1960(w),1934(m)	181a
	cyclohexane	2107(2),2034(w),1998(vs),1976(w,sh),1968(m),1941(m)	181a
	decalin	2106(w),2034(w),1998(vs),1973(w,sh),1967(m),1941(m)	181b
	$CHCl_3$	2100(s),2080(w),2030(w), 2000(vs), 1940(s)	182a
eq-$Re_2(CO)_9(PPh_3)$	$CHCl_3$	1963(s),1912(m),1897(m), 1880(sh)	182a
ax-$Re_2(CO)_9(PMePh_2)$	$CHCl_3$	2060(w),2000(m),1972(sh),1945(s,br),1910(m)	184
eq-$Re_2(CO)_9(PMe_2Ph)$	$CHCl_3$	2090(w),2020(m),2010(sh),1995(sh),1975(s) 1940(s),1915(sh)	184
ax-$Mn_2(CO)_9(AsMe_2Ph)$	benzene	2092(m),2020(s),1991(vs),1968(sh),1936(m)	223

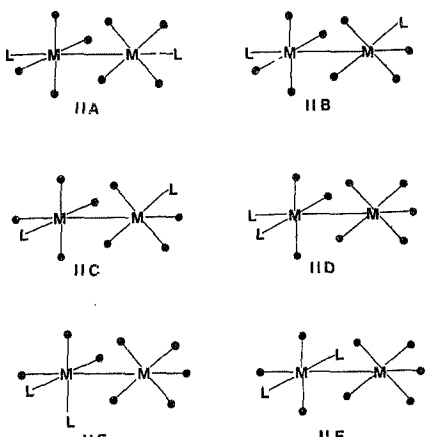


Figure 15.2: Possible isomers for $M_2(CO)_8(L)_2$ complexes (rotamers not shown; • = CO)
(IIA) diax, (IIB) 1,2-ax,eq, (IIC) 1,2-eq,eq,
(IID) 1,1-ax,eq, (IIE) 1,1-cis-dieq, and
(IIF) 1,1-trans-dieq.

TABLE 15.2: IR spectral data of $M_2(CO)_8(L)_2$ (M = Mn,Re ; L = AsR_3, PR_3) complexes

Complex	Solvent	ν(CO)/cm^{-1}	Ref
diax-$M_2(CO)_8(PMePh_2)_2$	benzene	1983(w),1954(vs)	223
1,2-eq,eq-$Mn_2(CO)_8(AsMe_2Ph)_2$ [a]	benzene	2056(w),1989(s),1956(s),1914(m)	223
diax-$Re_2(CO)_8(PPh_3)_2$	$CHCl_3$	2010(w),1960(vs)	182a
1,2-ax,eq-$Re_2(CO)_8(PMe_2Ph_2)$ [b]	CCl_4	2100(w),2060(mw),2000(s),1955(s,br),1905(s)	183
1,2-ax,eq-$Re_2(CO)_8(PMePh_2)_2$ [b]	benzene	2090(w),2058(m),2000(s),1955(s,br),1925(s)	184
1,2-ax,eq-$Re_2(CO)_8(AsMe_2Ph)_2$ [b]	CCl_4	2105(w),2060(mw),2005(s),1945(s,br),1905(s)	183
1,2-ax,eq-$Re_2(CO)_8(PBu^n_3)_2$	hexane	2068(mw),2006(m),1971(s),1928(s),1917(s)	170
1,2-ax,eq-$Re_2(CO)_8(PPh_3)_2$	toluene	2069(mw),2012(m),1964(vs,br),1934(m),1921(m)	170
1,2-eq,eq-$Re_2(CO)_8(PMe_3)_2$	toluene	2063(w),2005(m),1959(s),1925(w),1910(m)	170
1,2-eq,eq-$Re_2(CO)_8[P(OMe_3)]_2$	toluene	2077(w),2024(ms),1986(s),1968(sh),1946(w),1918(ms)	170
1,2-eq,eq-$Re_2(CO)_8[P(OPh_3)]_2$	toluene	2081(w),2032(m),1994(s),1976(sh),1954(w),1931(m)	170
1,2-eq,eq-$Re_2(CO)_8[Ph_2PCH_2PPh_2]$	toluene	2073(m),2020(m),1980(s),1956(w),1940(w),1915(m)	170,198
1,2-eq,eq-$Re_2(CO)_8[Me_2PCH_2PMe_2]$	toluene	2067(m),2012(s),1980(sh),1971(vs),1947(m),1934(sh),1914(s)	198
1,2-eq,eq-$Re_2(CO)_8[Ph_2PCH_2CH_2PPh_2]$	toluene	2070(m),2017(m),1983(s),1944(m),1915(s)	198
1,2-eq,eq-$Re_2(CO)_8[Me_2PCH_2CH_2PMe_2]$	toluene	2066(w),2010(m),1973(s),1938(m),1911(s)	198
1,1-$Mn_2(CO)_8(PHPh_2)_2$ [c]	CH_2Cl_2	2070(=),2060(sh),2022[sh),1989(vs),1945(vs),1914(s)	189
diax-$Re_2(CO)_8(PHPh_2)_2$	CH_2Cl_2	1994(m),1946(s)	189

[a] eclipsed conformation

[b] Incorrectly characterized in references as 1,2-eq,eq-isomer (see text)

[c] See text for a discussion of the substitution geometry

The vast majority of reported $M_2(CO)_9(PR_3)$ (M = Re, Mn) complexes are undoubtedly axially substituted, having the characteristic 5-band ν(CO) IR spectrum exemplified by ax-$Mn_2(CO)_9(PMe_2Ph)$. Indeed, there does not appear to be any convincing evidence for the existence of eq-$Re_2(CO)_9(PR_3)$ isomers. Further, $Mn_2(CO)_9(AsMe_2Ph)$[223] is the ax-isomer (IA), with an IR spectrum (Table 15.1) analogous to that of ax-$Mn_2(CO)_9(PMe_2Ph)$,[221] although $Mn_2(CO)_8(AsMe_2Ph)_2$[225] is equatorially substituted (vide infra).

15B.3 $Re_2(CO)_8(PR_3)_2$ complexes

The possible isomers for $M_2(CO)_8(L)_2$ complexes are shown in Fig. 15.2. Not considering rotamers, there are six possible isomers, viz. (IIA)diax, (IIB)1,2-ax,eq, (IIC)1,2-eq,eq, (IID)1,1-ax,eq, (IIE)1,1-cis-dieq, and (IIF)1,1-trans-dieq - $M_2(CO)_8(L)_2$.

An X-ray crystallographic structure of $Mn_2(CO)_8(PMePh_2)_2$[225] has shown the substitution geometry to be diax(IIA). From Group Theory, diax-$M_2(CO)_8(L)_2$ (staggered conformation), of molecular symmetry D4d, is predicted to give 2 ν(CO) bands in the IR spectrum. As the spectrum of diax-$Mn_2(CO)_8(PMePh_2)_2$ (Table 15.2) shows, this is indeed found to be the case. This spectrum, typical of diax-$M_2(CO)_8(L)_2$ substitution, is observed for a wide range of $Mn_2(CO)_8(PR_3)_2$ complexes.[221,189]

The related complex, $Mn_2(CO)_8(AsMe_2Ph)_2$, has been shown by an X-ray crystallographic structure[225] to have *1,2-eq,eq-substitution*. *However, the conformation is* eclipsed, not staggered as for the diequatorially substituted isonitrile derivatives of $M_2(CO)_{10}$ (M = Mn,Re) (ch. XIV), *owing to steric congestion (see section 15B.2).* The IR spectrum is different having 4 ν(CO) bands (see Table 15.2). This is the number predicted by Group Theory for eclipsed 1,2-dieq-$M_2(CO)_8(L)_2$ (molecular symmetry C2h.)). Although the IR spectrum (in cyclohexane) of $Mn_2(CO)_8(AsMe_3)_2$ is analogous,[223] that of $Mn_2(CO)_8(AsEt_3)_2$, which presumedly has the same structure, has an additional weak band at 1927 cm^{-1} [IR(cyclohexane), ν(CO): 2055(w), 1990(s), 1952(s),

1927(w), 1915(m) cm^{-1}].[213]

There have been reports of diax-$Mn_2(CO)_8(AsR_3)_2$ complexes,[249a] with the typical IR spectrum (eg. diax-$Mn_2(CO)_8(AsPh_3)_2$, IR(CS_2), ν(CO): 1982(w), 1953(vs) cm^{-1}).[250a] This indicates that the steric bulk (cone angle) of the AsR_3 ligand determines the substitution geometry; the longer Mn-As than Mn-P bond facilitates eq-substitution, where the steric bulk of the AsR_3 ligand is not too great.

A third type of arsine-complex, $[Mn_2(CO)_8(\mu\text{-}AsR_2)_2]$, has been reported as the product of the so-called "Lambert's reaction" (ligand fragmentation at high temperature).[250] This product may be distinguished by elemental analysis, and IR spectral data (eg. $[Mn_2(CO)_8(\mu\text{-}AsPh_2)_2]$, IR ($CS_2$), νCO: 2042(s), 1983(sh), 1978(s), 1965(m) cm^{-1}),[249a] ie. 4 νCO peaks, as compared to 2 for diax-, and 4 or 5 (intensity pattern: w,s,s,(w),m) for dieq-$Mn_2(CO)_8(AsR_3)_2$.

The large majority of direct reactions (thermal, photochemical) between $Re_2(CO)_{10}$ and PR_3 are reported to yield diax-$Re_2(CO)_8(PR_3)_2$ (PR_3 = PPh_3[188-92,186,189] $PHPh_2$,[189] $P(OPh)_3$,[193] $P(C_6H_{11})_3$,[192-6] $P(C_6H_4Me\text{-}p)_3$,[185] $P(OC_6H_4Me\text{-}o)_3$,[185] $P(OC_6H_4Cℓ\text{-}p)_3$[187]), as the sole or major product. These complexes all have one weak and one very strong band in the carbonyl region of the IR spectrum, characteristic of diax-$M_2(CO)_8(L)_2$ complexes (IIA). The IR spectrum of a typical example, the much-studied diax-$Re_2(CO)_8(PPh_3)_2$, is shown in Table 15.2.

There has been one report of diequatorially-substituted $Re_2(CO)_8(PR_3)_2$ complexes obtained from the direct reaction (thermal or photochemical) of $Re_2(CO)_{10}$ with PR_3 (PR_3 = PMe_2Ph,[193] $PMePh_2$[194]). The $Re_2(CO)_8(PR_3)_2$ products were characterized by elemental analyses, ^1H NMR and IR spectra, and cleavage reactions, and on the basis of IR spectral data (see Table 15.2), the geometry was assigned as 1,2-eq,eq-$Re_2(CO)_8(PR_3)_2$(IIC) (but see below). The IR spectrum of the related $Re_2(CO)_8(AsMe_2Ph)_2$ complex [8] (Table 15.2) is analogous.

Reaction of (μ-H)(μ-olefin)$Re_2(CO)_8$ complexes with

PR_3 ligands[178] yields 1,2-eq,eq-$Re_2(CO)_8(PR_3)_2$ (IIC) (R = $P(OMe)_3$, PMe_3, $P(OPh)_3$) or 1,2-ax,eq-$Re_2(CO)_8(PR_3)$ (IIB) (R = Bu^n, Ph), depending on the size of the PR_3 ligand (Tolman cone angles[65]: $P(OMe)_3$, 107°; PMe_3, 118°; $P(OPh)_3$, 121-128°; PBu^n_3, 132°; PPh_3, 145°). The latter products, 1,2-ax,eq-$Re_2(CO)_8(PR_3)_2$, isomerize spontaneously in toluene solution at room temperature to the well-known diax-$Re_2(CO)_8(PR_3)_2$ isomers (IIA). The 1,2-eq,eq-$Re_2(CO)_8(PR_3)_2$ products appear to be stable to isomerization. Bidentate phosphine ligands, $(P)_2$, also gave 1,2-eq,eq-$Re_2(CO)_8(P)_2$ products ($(P)_2$ = $Ph_2PCH_2PPh_2$,[176,198] $Me_2PCH_2PMe_2$,[198] $Ph_2PCH_2CH_2PPh_2$,[198] $Me_2PCH_2CH_2PMe_2$[198]). Here the chelating nature of the $(P)_2$ ligand imposes a restriction on the product geometry; the Tolman cone angles for the $(P)_2$ ligands (half chelate)[65a] are in the range 105-125°. The 1,2-ax,eq-$Re_2(CO)_8(PR_3)_2$ products were characterized by ^{31}P NMR spectroscopy, and the 1,2-eq,eq-$Re_2(CO)_8(PR_3)_2$ products by ^1H NMR spectroscopy, and the similarity of the IR spectra of these products to the pattern observed for 1,2-eq,eq-$Re_2(CO)_8(py)_2$[176] [IR(toluene), ν(CO): 2062(w), 2006(m), 1950(s,br), 1917(sh), 1905(m) cm^{-1}]. IR spectral data for these $Re_2(CO)_8(PR_3)_2$ and $Re_2(CO)_8(P)_2$ products are given in Table 15.2.

An examination of the IR data for the $Re_2(CO)_8(PR_3)_2$ complexes in Table 15.2 shows that the 1,2-ax,eq-$Re_2(CO)_8(PR_3)_2$ (R = Bu^n, Ph) complexes have 5 ν(CO) bands, and the 1,2-eq,eq-$Re_2(CO)_8(PR_3)_2$ (R = OMe, Me, OPh) complexes have 6 or 5 (R = Me) ν(CO) bands, but the intensity patterns are quite different. Note the strong similarity of the IR spectra of the 1,2-eq,eq-$Re_2(CO)_8(PR_3)_2$ complexes to that of 1,2-eq,eq-$Re_2(CO)_8(CNC_6H_3Me_2\text{-}2,6)_2$ [IR(hexane), ν(CO): 2053(w), 2028(m), 1985(s), 1952(w), 1943(ms) cm^{-1}] (see ch. XI). Further, the 5 ν(CO) band pattern for the $Re_2(CO)_8(L)_2$ (L = PMe_2Ph, $PMePh_2$, $AsMe_2Ph$) complexes resemble that for the above 1,2-ax,eq-isomers rather than that for the above 1,2-eq,eq-isomers. Hence these $Re_2(CO)_8(L)_2$ complexes may have been incorrectly assigned.[185,24] as the 1,2-eq,eq-isomers (IIC), instead of the 1,2-ax,eq-isomers (IIB). This

seems likely in view of the size of the PMe_2Ph and $PMePh_2$ ligands (Tolman cone angles[83] of 122° and 136° respectively).

However, there would appear to be a seeming anomaly, in that $Re_2(CO)_8(PMePh_2)_2$[186] and $Re_2(CO)_8(PMe_2Ph)_2$[183] were prepared by the thermal reaction of $Re_2(CO)_{10}$ with $PMePh_2$ or PMe_2Ph under forcing conditions (xylene, 140°C, 15 h, 30%, and petroleum ether, 80-100°C, 60 h (4%) or 96 h (46%), respectively), while <u>1,2-ax,eq</u>-$Re_2(CO)_8(PR_3)_2$ (R = Bu^n, Ph) isomerizes spontaneously in toluene solution at 25°C to <u>diax</u>-$Re_2(CO)_8(PR_3)_2$, with a half-life of 10 h (PPh_3) or 1-2 days (PBu^n_3).

Further, traces of <u>1,2-ax,eq</u>-$Re_2(CO)_8(PR_3)_2$ isomers were observed, in addition to the major <u>diax</u>-$Re_2(CO)_8(PR_3)_2$ products, in the Pd-catalysed (140°C) and the mild Me_3NO-*assisted* (CH_2Cl_2, 40°C) reactions of $Re_2(CO)_{10}$ with PR_3 (PR_3 = PMe_2Ph, $PMePh_2$, $P(CH_2C_6H_5)_3$, PMe_3, $P(OMe)_3$) (see section 15D.1). However, in the PdO-catalysed reaction of $Re_2(CO)_{10}$ with PPh_3, no <u>eq</u>-isomers were observed. Hence the stability of the <u>eq</u>-isomers would appear to be governed by the size of the PR_3 ligand. The role of the ligand size and synthetic route in determining product geometry *will be discussed in section* 15D.1.

Mixture of <u>ax</u>-and <u>eq</u>-isomers have been claimed to have been obtained for $[Mn_2(CO)_8\{P(OCH_2)_3CEt\}_2]$[239] and $[M_2(CO)_8(PF_3)_2]$(M = Mn,Re)[196] products. (The IR spectra are complex). With a small phosphine ligand such as PF_3 (Tolman cone angle[83] of 104°), a mixture of isomers probably reflects steric versus electronic control of product geometry.

Of note is the complex $Mn_2(CO)_8(PHPh_2)_2$,[169] which has a different IR spectrum (Table 15.2), and has been shown by ^{55}Mn NMR spectroscopy to have the structure $(CO)_5Mn\text{-}Mn(CO)_3(PHPh_2)_2$, with both phosphine ligands on the <u>same</u> Mn-atom. Thus there are three possible geometries for the complex, viz. 1,1-ax,eq(IID), 1,1-cis-dieq(IIE) or 1,1-trans-dieq(IIF).

Oxidation of $Mn_2(CO)_8(PHPh_2)_2$ *with* $NOPF_6$ gives $[Mn(CO)_5(PHPh_2)][PF_6]$ and also <u>cis</u>-$[Mn(CO)_4(PHPh_2)_2][PF_6]$.[189]

This would seem to exclude (IIF), the 1,1-trans-dieq-isomer, which is unlikely on electronic grounds, in view of the cis-labilization effect (see ch. XII).

An example of (IID), the 1,1-ax,eq-isomer, is $Mn_2(CO)_8(C_4H_6)$[222] [IR(hexane), ν(CO): 2083(m), 2028(s), 1994(vs), 1975(s), 1953(m) cm^{-1}], and examples of the 1,1-cis-dieq-isomer, (IIE), are $Mn_2(CO)_8(CNBu^t)_2$ [IR(hexane), ν(CO): 2055(m), 1999(vs), 1977(vs), 1963(w), 1952(m), 1935(m) cm^{-1}] (see ch. XI), $Mn_2(CO)_8(phen)$[229] [IR(diethyl ether), ν(CO): 2051(s), 2018(vs), 1987(ms), 1954(w), 1908(w) cm^{-1}], $Re_2(CO)_8(phen)$[228] [IR($CH_2Cℓ_2$), ν(CO): 2073(m), 2012(s), 1992(m), 1959(m), 1915(m), 1889(m) cm^{-1}] and $Re_2(CO)_8(biquin)$[228] [IR($CH_2Cℓ_2$), ν(CO): 2076(m), 2020(s), 1986(m), 1958(m), 1915(m), 1889(m) cm^{-1}]. On the basis of this IR data, the reported 1,1-$Re_2(CO)_8(CH_3NH_2)_2$[167] [IR(THF), ν(CO): 2070(m), 1990(s), 1955(s,br), 1883(m), 1867(m) cm^{-1}] appears to be the 1,1-ax,eq-isomer(IID). There is a greater resemblance of the IR spectrum of $Mn_2(CO)_8(PHPh_2)_2$ to that of the (IID) isomer than to that of the (IIE) isomer.

The (IIE) isomer, 1,1-cis-dieq, is the most electronically favoured isomer, expected in the absence of steric constraints. The most sterically favoured of the 1,1-isomers would be expected to be (IIF). This 1,1-trans-dieq-isomer, although electronically disfavoured, cannot be excluded entirely, as cleavage and subsequent ligand rearrangement could account for the cis-$[Mn_2(CO)_4(PHPh_2)_2]$ product. No examples of isomer (IIF) are known, to allow for comparison of IR data. The 1,1-ax,eq-isomer (IID) seems likely, as, with small phosphines (Tolman cone angle[88] of $PHPh_2$: 128°), (IID) could be formed instead of (IIA), in accordance with the proposed mechanism of phosphine substitution, shown in Fig. 15.4 (see section 15D.1).

Note that the rhenium analogue, $Re_2(CO)_8(PHPh_2)_2$, has the typical diax spectrum (Table 15.2) of isomer (IIA). To date no complexes of the type $(CO)_5Re\text{-}Re(CO)_3(PR_3)_2$ have been reported.

15B.4 $Re_2(CO)_7(PR_3)_3$ complexes

There are six geometrical isomers of $M_2(CO)_7(L)_3$ (Fig. 15.3), if each metal-atom M has at least one ligand L bound to it (as expected on steric grounds for bulky phosphine ligands), viz. (IIIA) 1-ax,2,2-trans-dieq, (IIIB) 1-eq,2,2-ax-eq, (IIIC) 1-eq,2,2-trans-dieq, (IIID) 1-ax,2,2-ax,eq, (IIIE) 1-ax,2,2-cis-dieq and (IIIF) 1-eq, 2,2-cis-dieq.

The most extensive investigation of $Re_2(CO)_7(PR_3)_3$ complexes was a study of the photochemical reaction of $Re_2(CO)_{10}$ with PPh_3 under vacuum,[184] which yielded three isomers of $Re_2(CO)_7(PPh_3)_3$, identified by ^{31}P NMR as isomers (IIIA) (35%), (IIIB) (15%) and (IIIC) (5%). The IR spectra of these complexes are listed in Table 15.3.

Photochemical reactions of $Re_2(CO)_{10}$ with PMe_2Ph,[183] $AsMe_2Ph$ [183] and $PMePh_2$,[184] yielded $Re_2(CO)_7(PMe_2Ph)_2$(IIIC), $Re_2(CO)_7(AsMe_2Ph)_3$(IIIC), and two isomers of $Re_2(CO)_7(PMePh_2)_3$,(IIIA) and (IIIC), in essentially equal amounts (ca. 10%). These isomers were identified from IR spectra (see Table 15.3).

There has been one report of a (IIID) isomer. The $Re_2(CO)_7[P(OPh)_3]_3$ product obtained from the thermal reaction of $Re_2(CO)_{10}$ with $P(OPh)_3$[185] was assigned as (IIID) on the basis of the IR spectrum (Table 15.3). This isomer (IIID) might be expected to be the product of further reaction of diax-$Re_2(CO)_8(PR_3)_2$ with PR_3.

Mixtures of isomers (complex IR spectra) have been obtained for the products $[Mn_2(CO)_7\{P(OCH_2)_3CEt\}_3]$[230] (identified by elemental analysis) and $[M_2(CO)_7(PF_3)_3]$ (M = Mn,Re)[193] (^1H NMR evidence), but these were not isolated.

No $Re_2(CO)_7(PR_3)_3$ (or $Mn_2(CO)_7(PR_3)_3$) isomers corresponding to (IIIE) and (IIIF) have been reported. Note that (IIIF) has the same structure as the $Re_2(CO)_7(CNR)_3$ complexes (see ch. XIV).

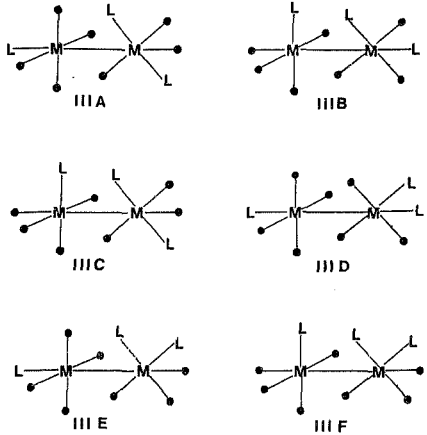


Figure 15.3: Possible isomers for 1,2,2-$M_2(CO)_7(L)_3$ complexes. (rotamers not shown; • = CO)
(IIIA)1-ax,2,2 -trans-dieq, (IIIB)1-eq,2,2 -ax,eq
(IIIC)1-eq,2,2-trans-dieq, (IIID)1-ax,2,2-ax,eq
(IIIE)1-ax,2,2-cis-dieq and (IIIF)1-eq,2,2-cis-dieq

TABLE 15.3: IR spectral data of $Re_2(CO)_7(PR_3)_3$ complexes

Complex	Solvent	ν(CO)/cm^{-1}	Ref
1-ax,2,2-trans-dieq-$Re_2(CO)_7(PPh_3)_3$	$CHC\ell_3$	2050(w),2022(w),1959(s),1920(s),1897(s)	186
1-eq,2,2-ax,eq-$Re_2(CO)_7(PPh_3)_3$	$CHC\ell_3$	2098(m),2082(w),2015(w),2010(s),1990(m),1959(s),1930(s)	186
1-eq,2,2-trans-dieq-$Re_2(CO)_7(PPh_3)_3$	$CHC\ell_3$	2038(m),2007(vs),1957(s),1927(sh),1917(s),1889(m)	186
1-eq,2,2-trans-dieq-$Re_2(CO)_7(PMe_2Ph)_3$	$CC\ell_4$	2018(w),1995(ms),1940(s),1918(sh),1910(s),1885(s)	183
1-eq,2,2-trans-dieq-$Re_2(CO)_7(AsMe_2Ph)_3$	$CHC\ell_3$	2030(w),1990(ms),1945(s),1920(sh),1900(s),1840(s)	183
1-ax,2,2-trans-dieq-$Re_2(CO)_7(PMePh_2)_3$	C_6H_6	2043(w),1994(s),1930(w),1907(s),1877(m)	184
1-eq,2,2-trans-dieq-$Re_2(CO)_7(PMePh_2)_3$	C_6H_6	2021(w),1995(s),1990(s),1938(s),1910(s),1885(m)	184
1-ax,2,2-ax,eq-$Re_2(CO)_7[P(OPh)_3]_3$	$CHC\ell_3$	2065(w),2000(sh),1980(s),1962(s),1912(m)	185

15B.5 $Re_2(CO)_6(PR_3)_4$ complexes

Very few reports exist for $Re_2(CO)_6(PR_3)_2$ complexes, and the evidence for these complexes is tenuous. An early claim to the preparation of $Re_2(CO)_6(PPh_3)_4$[186b] from the thermal reaction of $Re_2(CO)_{10}$ with PPh_3 was later proved incorrect when the product was identified as the monomeric hydride, $HRe(CO)_3(PPh_3)_2$,[186] with an IR spectrum (benzene, ν(CO): 1930 cm^{-1}) typical of mer-trans-$HRe(CO)_3(PR_3)_2$.[182a] Another product prepared similarly and identified as cis-$[Re(CO)_3(Ph_2PCH_2CH_2PPh_2)]_2$[186b] is probably also $HRe(CO)_3(Ph_2PCH_2CH_2PPh_2)$, as the IR spectrum (benzene, ν(CO): 1910(s), 1850(s), 1800(s) cm^{-1}) resembles that of fac-$HRe(CO)_3(PR_3)_2$ complexes.[182a]

The photochemical reaction of $Re_2(CO)_{10}$ with PPh_3 under vacuum yielded, in addition to $Re_2(CO)_7(PPh_3)_3$ isomers, a trace product tentatively identified as $Re_2(CO)_6(PPh_3)_4$[166] [IR($CHCl_3$), ν(CO): 1948(s) cm^{-1}]. Again the simplicity of the spectrum suggests the complex may be mer-trans-$HRe(CO)_3(PPh_3)_2$.[182a] However, MS data are consistent with the tetramer $Re_2(CO)_6(PPh_3)_4$.[166] It has been suggested[186b] that these complexes exist as dimers in the solid state and as monomers in solution. The compound $[Re(CO)_3(PPh_3)_2]_2$ was reported to give several ν(CO) bands in Nujol, but only one in benzene solution[186b] (vide supra).

A mixture of isomers of $[Mn_2(CO)_6(P(OCH_2)_3CEt)_4]$[259] has been reported, (identified by elemental analysis), and the IR spectrum is complex. Attempts to separate the isomers were not successful. A compound tentatively identified as $Mn_2(CO)_6(PF_3)_4$[199] has been reported [IR(hexane), ν(CO): 2078(m), 2034(w), 2012(vs), 1994(m), 1977(w), 1953(vw) cm^{-1}].

15B.6 Conclusions

From the foregoing analysis it is apparent that the vast majority of $Re_2(CO)_8(PR_3)$ complexes reported correspond to the ax-isomer. Only a few isolated examples of

eq-$Re_2(CO)_9(PR_3)$ complexes have been reported, and the evidence (elemental analysis and/or IR spectra) for these is tenuous.

Regarding $Re_2(CO)_8(PR_3)_2$ complexes, at least four different isomers have been reported, viz. diax, 1,2-ax,eq, 1,2-eq,eq and 1,1 isomer, although the majority of products are diax-$Re_2(CO)_8(PR_3)_2$. Combining the data for these complexes with that for the $M_2(CO)_8(CNR)_2$ (M = Re,Mn) complexes (see ch. XI), it is possible to relate IR data to structure for all the known isomers of $M_2(CO)_8(L)_2$ (see Table 15.4).

With the data for the $Re_2(CO)_7(PR_3)_3$ isomers, together with that for $Re_2(CO)_7(CNR)_3$ (ch. XI), it is also possible to relate IR spectra to substitution geometry, although examples of tri-substituted derivatives are not numerous. Further, such complexes, backed up by X-ray crystal structure data, would be useful in establishing a reliable correlation between IR data and geometric isomers.

There is no reliable evidence for $Re_2(CO)_6(PR_3)_4$ complexes, and in cases where such products have been postulated, it has not been possible to assign the substitution geometry on the basis of IR data alone. The lack of $Re_2(CO)_6(PR_3)_4$ (or more highly substituted) products must reflect synthetic limitations of the direct method of PR_3 substitution on $Re_2(CO)_{10}$, and not steric constraints, since $Re_2[P(OMe)_3]_{10}$ (Tolman cone angle[85] for $P(OMe)_3$: 107°), has been prepared by indirect methods.[213]

15C. A Survey of Kinetic and Mechanistic Studies

In consequence of the controversy surrounding the mechanism of substitution reactions of $M_2(CO)_{10}$ (M = Mn,Re) with phosphines yielding $M_2(CO)_{10-n}(PR_3)_n$ (n = 1,2), the kinetics of this reaction have been studied by several groups over the past twenty years.

Two main schools of thought emerged: In 1966, Wawersik and Basolo[261] suggested that substitution of $Mn_2(CO)_{10}$ proceeds via rate-determining CO-dissociation, and that Mn-Mn bond

TABLE 15.4: Correlation between IR data and molecular geometry for $M_2(CO)_8(L)_2$ complexes[a]

Isomer[b]	No. of ν(CO) IR bands: Calculated[c]	Observed[d]	Intensity pattern of ν(CO) IR bands[e]	Example
(IIA) diax	2	2	w,vs	$Re_2(CO)_8(PMe_2Ph)_2$ [f,g]
(IIB) 1,2-ax,eq	8	5	w,m,s,s,s	$Re_2(CO)_8(PBu^n_3)_2$ [179]
(IIC) 1,2-eq,eq (staggered)	8	5(6)	w,m,s,(sh),w[h],ms	$Re_2(CO)_8(CNC_6H_3\text{-}Me_2)_2$ [f,g]
1,2-eq,eq (eclipsed)	4	4(5)	w,s,s,(w),m	$Mn_2(CO)_8(AsMe_2Ph)_2$ [f,221]
(IID) 1,1-ax,eq	8	5	m,s,vs,s,m	$Mn_2(CO)_8(C_4H_6)$ [222] f,h
(IIE) 1,1-cis-dieq	8	6	m,vs,vs,w,m,m	$Mn_2(CO)_8(CNBu^t)_2$ [f,h]
(IIF) 1,1-trans-dieq	8	–	no examples known	–

[a] Staggered molecular geometry, unless otherwise stated.

[b] See Fig. 15.2

[c] Calculated from Group Theory Analysis; the Local Symmetry Approximation was assumed to hold.

[d] The number of bands could be affected by the solvent.

[e] On the basis of known examples (see section 15B.2).

[f] Crystal structure reported

[g] This work

[h] This weak band is sometimes not visible in the IR spectrum.

cleavage does not occur even at 200°C. Hopgood and Poë[239] responded by proposing a mechanism involving homolytic fission of $Mn_2(CO)_{10}$, to give $Mn(CO)_5$· radicals. Basolo's proposal recently received support from Sonnenberger and Atwood,[262] on the basis of their kinetic studies of the reaction of the mixed metal carbonyl, $ReMn(CO)_{10}$, with PR_3. The disagreement regarding the interpretation of kinetic results, resulted in a continuing dispute in the literature between Poë and Atwood[263], the main protagonists. A summary of the main arguments and results follows.

Over a period of twenty years, Poë and co-workers have studied the kinetics of the reaction of $M_2(CO)_{10}$ with PR_3 in decalin at 140°C under N_2 and O_2 (M = Mn,[264a] Tc,[264b] Re[264c]). The results have been interpreted in terms of a substitution mechanism involving reversible homolytic fission of $M_2(CO)_{10}$ to give $M(CO)_5$· radicals (equation 15.1). Substitution of the 17-electron radical $M(CO)_5$·, (equation 15.2) is thought to be rapid, occuring through an associative (SN2) process). Recombination of radicals gives the $M_2(CO)_{10-n}(PR_3)_n$ (n = 1,2) products (equations 15.3 and 15.4).

$$M_2(CO)_{10} \rightleftharpoons 2M(CO)_5\cdot \qquad (15.1)$$

$$M(CO)_5\cdot + PR_3 \rightleftharpoons M(CO)_4(PR_3)\cdot + CO \qquad (15.2)$$

$$M(CO)_5\cdot + M(CO)_4(PR_3)\cdot \rightleftharpoons M_2(CO)_9(PR_3) \qquad (15.3)$$

$$2M(CO)_4(PR_3)\cdot \rightleftharpoons M_2(CO)_8(PR_3)_2 \qquad (15.4)$$

An associative substitution process is supported by substitution studies of $Mn(CO)_5$·,[265a] and $Re(CO)_5$·[265b] radicals. Further, an associative process has been found for the substitution of PPh_3 by $P(OPh)_3$ in $[Mn(CO)_5(PPh_3)]$.[265c]

Brown and co-workers have studied the photochemical reaction of $M_2(CO)_{10}$ (M = Re,[266a] Mn[266b]) with PR_3 in hexane. The radical chain mechanism proposed involves initial photolytic cleavage of the M-M bond, followed by rapid substitution of the $M(CO)_5$· radicals, with subsequent recombination of the substituted radicals (equations 15.1 - 15.4). Studies of $Mn(CO)_5$· radicals[266c] indicate that the substitution of the

17-electron metal carbonyl radicals occurs via an associative pathway. This proposed mechanism is essentially the same as that put forward by Poë for the thermal substitution reactions of $M_2(CO)_{10}$ (vide supra).

From a study of the photochemistry of $MM'(CO)_{10-n}(PPh_3)_n$ ($M = M' = Re$, Mn, $n = 0$; $M = Mn$, $M' = Re$, $n = 0$; $M = M' = Mn$, $n = 1,2$) compounds, Wright and Ginley[219a] concluded that homolytic metal-metal bond cleavage occuring from an excited state derived from a $\sigma \rightarrow \sigma^*$ one-electron transition associated with the metal-metal bond is consistent with the observed results.

Wawersik and Basolo[267] reported kinetic studies of $Mn_2(CO)_{10}$ and $Mn_2(CO)_9(PR_3)$ with PR_3 in *p-xylene* (120°C), and interpreted the rate data as being consistent with a mechanism involving rate-determining CO-dissociation with no metal-metal bond cleavage (equations 15.5 to 15.8).

$$Mn_2(CO)_{10} \rightleftharpoons Mn(CO)_9 + CO \qquad (15.5)$$

$$Mn_2(CO)_9 + PR_3 \rightleftharpoons Mn_2(CO)_9(PR_3) \qquad (15.6)$$

$$Mn_2(CO)_9(PR_3) \rightleftharpoons Mn_2(CO)_8(PR_3) + CO \qquad (15.7)$$

$$Mn_2(CO)_8(PR_3) + PR_3 \rightleftharpoons Mn_2(CO)_8(PR_3)_2 \qquad (15.8)$$

Cox and Davis[188] have rationalized the wide range of products obtained from the thermal reaction between $Re_2(CO)_{10}$ and PPh_3 in xylene (140°C) in terms of a dissociative mechanism. Apart from $Re_2(CO)_{10-n}(PR_3)_n$ ($n = 1$-2) products, complexes of the type $HRe(CO)_{5-n}(PR_3)_n$ ($n = 1,2$) were obtained. However, no $HRe(CO)_5$ was observed. This was taken as an indication that *homolytic fission of the parent carbonyl* $Re_2(CO)_{10}$ is not an important process in the reaction, and that phosphine substitution precedes radical formation. It was suggested that the hydrides are formed by reaction of unstable radical intermediates, $[Re(CO)_{5-n}(PR_3)_n]$ ($n = 1,2$), with the solvent. This type of reaction is known.[268]

From a kinetic study of the substitution of $MnRe(CO)_{10}$ by PR_3 *in decane (130°C), Sonnenberger and Atwood*[262] have reported three observations claimed to be inconsistent with

a free radical mechansim:-

(i) the predominance of the Re-substituted product, $(CO)_5MnRe(CO)_4(PR_3)$.

(ii) the failure of the Mn-substituted complex, (PR_3)-$(CO)_4MnRe(CO)_5$, to isomerize to $(CO)_5MnRe(CO)_4(PR_3)$ when isolated in the pure state, and

(iii) the lack of isomerization to Mn_2 and Re_2 species.

In terms of the proposed mechanism, CO-dissociation from $MnRe(CO)_{10}$ to form $MnRe(CO)_9$ is the rate-determining step. Since dissociation from Mn is expected to be 100 times faster than from Re (owing to the stronger Re-CO than Mn-CO bond[172]), the proposed mechanism involves CO-dissociation from the Mn-centre, and an intermediate with a CO-bridged dimer in which no metal-metal bond cleavage has occured, followed by subsequent phosphine substitution on the Re-atom, to give the observed product, $(CO)_5MnRe(CO)_4(PR_3)$.

Further support for a dissociative mechanism, with no metal-metal bond cleavage, was provided by the report of Basolo and co-workers[269] that the scrambling reaction (equation 15.9) between $Mn_2(CO)_{10}$ and $Re_2(CO)_{10}$, to give the mixed-metal carbonyl $MnRe(CO)_{10}$, does not occur in decalin (130°C) under an atmosphere of CO, and only very slowly in the absence of CO.

$$Mn_2(CO)_{10} + Re_2(CO)_{10} \rightleftharpoons 2MnRe(CO)_{10} \qquad (15.9)$$

However, Poë and co-workers[17] have reported that the scrambling reaction (15.9) occurs in decalin (170°C) under CO, to reach a stable equilibrium.

Muetterties and co-workers,[227] using isotopic labelling and mass spectroscopic product analysis, have demonstrated that Mn-Mn bond scission in $Mn_2(CO)_{10}$ phosphine thermal substitution reactions is not a significant process. Mixtures of $Mn_2(CO)_{10}$ and $Mn_2(^{13}CO)_{10}$ were reacted with PR_3 in octane (120°C) under ^{13}CO atmosphere. Mass spectral analysis of the product, $Mn_2(CO)_9(PR_3)$, showed no evidence of Mn-Mn bond scission. This is consistent with a dissociative mechanism

(equations 15.5-15.6). However, Mn-Mn bond scission was found to be a major process during the photochemically initiated ligand exchange reaction of $Mn_2(CO)_{10}$ at 25°C. Recent laser photolysis studies[121] of $Mn_2(CO)_{10}$ in matrices have indicated that the primary process is CO-dissociation from $Mn_2(CO)_{10}$ to give $Mn_2(CO)_9$ rather than Mn-Mn bond scission, for about 30% of the reacting $Mn_2(CO)_{10}$. The CO-bridged $Mn_2(CO)_9$ reacts with PR_3 ligands to give $Mn_2(CO)_9(PR_3)$.

Similar results have been obtained by Muetterties and Stolzenberg[171] for the reactions of $Re_2(CO)_{10}$ with PR_3. Thus in the thermal reaction of $^{185}Re_2(CO)_{10}$ and $^{187}Re_2(CO)_{10}$ with PR_3 in octane (150°C) under CO atmosphere, mass spectral analysis of the product, $Re_2(CO)_9(PR_3)$, showed no scrambling indicative of Re-Re bond cleavage, in support of a CO-dissociative mechanism. Similar results were obtained for the thermal reaction of $Re_2(CO)_9(PR_3)$ with PR_3 to give $Re_2(CO)_8(PR_3)_2$. However, the photochemically initiated reactions at 25°C led to complete scrambling within short reaction times, indicating that the primary mode of reaction for $Re_2(CO)_{10}$ under photolysis conditions involves Re-Re bond scission as an elementary step.

Thus Muetterties and co-workers have demonstrated unambiguously and via non-kinetic arguments that the mechanism of the thermal reaction (140°C) of $M_2(CO)_{10}$ (M = Mn,Re) with PR_3 under CO atmosphere to give $M_2(CO)_9(PR_3)$, does not involve metal-metal bond cleavage. The results are consistent with the CO-dissociative mechanism, proposed by Basolo, and supported by Atwood. However, Muetterties and co-workers have shown that for the photochemically initiated reaction, metal-metal bond cleavage is implicated as an initial step. This is in accord with the homolytic fission and radical chain mechanism proposed by Brown and co-workers, based on the results of kinetic studies of the photochemical reaction between $M_2(CO)_{10}$ and PR_3. Hence the mechanism for the thermal reaction of $M_2(CO)_{10}$ with PR_3 under CO is represented by equations (15.5 to 15.8), while

that for the photochemical reaction between $M_2(CO)_{10}$ and PR_3 is represented by equations (15.1 to 15.4). Note that metal-metal bond scission has also been excluded for the thermal reaction of $Re_2(CO)_9(PR_3)$ with PR_3 to give $Re_2(CO)_8(PR_3)_2$.[277]

15D.1 Synthesis and characterization of $Re_2(CO)_{10}(PR_3)_n$ (n = 1,2) derivatives

As part of an extension of the Pd-catalysed reaction of $Re_2(CO)_{10}$ with isonitriles (ch. XI) to other ligands, the reaction of $Re_2(CO)_{10}$ with phosphine ligands was investigated. The thermal reaction between $Re_2(CO)_{10}$ and phosphines was found to be extremely sluggish even at elevated temperatures, eg. after 10 h reflux at 140°C, the reaction between $Re_2(CO)_{10}$ and 2 equivalents PMe_2Ph yielded 80% recovered $Re_2(CO)_{10}$, and small amounts of $Re_2(CO)_9(PMe_2Ph)$ and $Re_2(CO)_8(PMe_2Ph)_2$, together with other trace products which were not characterized.

Use of Pd-catalysts, eg. Pd/C (10%), $Pd/CaCO_3$ (10%), or PdO, considerably improves the reaction, yielding mono- and di-substituted phosphine derivatives in poor to good yields after moderate reaction times (Table 15.5). PdO was found to be a more active catalyst than Pd/C (10%) (or $Pd/CaCO_3$ (10%)) for this reaction (although this probably reflects the greater Pd-content for the same mass of catalyst). In favourable cases, the di-phosphine complex can be obtained in good yield as the sole reaction product after relatively short reaction times, eg. 84% $Re_2(CO)_8(PMe_2Ph)_2$ after 1 h (xylene, 140°C).

In the cases of PR_3 = $PMePh_2$, PMe_2Ph, trace products were also isolated, and identified as fac-$HRe(CO)_3(PMePh_2)_2$ [IR($CHCl_3$), ν(CO): 2000(s,sp), 1910(s), 1870(s) cm^{-1}] and fac-$HRe(CO)_3(PMe_2Ph)_2$ [IR($CHCl_3$), ν(CO): 2030(s,sp), 1946(s), 1883(s) cm^{-1}] by comparison with the IR spectrum of fac-$HRe(CO)_3(PPh_3)_2$ [IR($CHCl_3$), ν(CO): 2009(s), 1960(s), 1900(r) cm^{-1}].[278] Such products could have been formed with other PR_3 ligands also but in many cases product decomposition on silica plates was observed, and minor product

isolation not achieved.

Comparison of the IR data for the $Re_2(CO)_{10-n}(PR_3)_n$ (n = 1-2) products (Table 15.6) with that of ax-$Mn_2(CO)_9$-(PMe_2Ph) [IR(benzene), ν(CO): 2074(w), 2016(s), 1993(vs), 1969(sh), 1938(m) cm^{-1}][223] and diax-$Mn_2(CO)_8(PMePh_2)_2$ [IR(benzene), ν(CO): 1983(w), 1954(vs) cm^{-1}],[223] for which axial substitution has been established by X-ray crystallographic structures,[224,255] indicates that the products are ax-$Re_2(CO)_9(PR_3)$ and diax-$Re_2(CO)_8(PR_3)_2$. An X-ray crystal and molecular structure of the $Re_2(CO)_8$-(PMe_2Ph)$_2$ complex (section 15E) confirmed the diaxial substitution.

These $Re_2(CO)_8(PR_3)_2$ products can be prepared independently by the NMe_3O-assisted reaction ($CH_2Cℓ_2$, 40°C) between $Re_2(CO)_{10}$ and PR_3, which yields the major products ax-$Re_2(CO)_9(PR_3)$ (ca. 40%) and diax-$Re_2(CO)_8(PR_3)_2$ (ca. 30%), as well as a minor product, identified as $CℓRe(CO)_3(PR_3)_2$ (ca. 10%). The IR spectra of the latter complexes (Table 15.7) show three strong bands in the carbonyl region. This pattern is characteristic of that of fac-$XRe(CO)_3(PR_3)_2$ complexes (X = H, halogen) [eg. $HRe(CO)_3(PPh_3)_2$, [IR($CHCℓ_3$), ν(CO): 2009(s), 1960(s), 1900(s) cm^{-1}].[102a] This IR spectrum is quite distinct from that of mer-trans-$HRe(CO)_3(PPh_3)_2$ [IR($CHCℓ_3$), ν(CO): 1935(s) cm^{-1}].[102a] The products are probably the chloride, fac-$CℓRe(CO)_3(PR_3)_2$, since the reaction was conducted in $CH_2Cℓ_2$ and the hydrogen in $HRe(CO)_3(PR_3)_2$ is readily replaced by chlorine.[88b] That the fac-isomer, the kinetic product, is obtained, rather than the mer-trans-isomer (mer-trans-H $M(CO)_3(PR_3)_2$, M = Re,[180,182,183] Mn[223,259] obtained by other workers from the thermal reaction of $M_2(CO)_{10}$ with PR_3 (140°C)), probably reflects the mild reaction conditions (40°C) of the Me_3NO-route, as fac-$XRe(CO)_3(PR_3)_2$ isomers readily isomerize to the mer-trans-$XRe(CO)_3(PR_3)_2$ isomers.[259,271]

An attempt was made to prepare arsine derivatives of $Re_2(CO)_{10}$, as the complex $Mn_2(CO)_8(AsMe_2Ph)_2$ has been shown by an X-ray crystallographic structure to have 1,2-dieq substitution.[253] The Me_3NO-assisted reaction

TABLE 15.5: Details of catalytic syntheses of $Re_2(CO)_{10-n}(PR_3)_n$ (n = 1,2) complexes

PR_3	Catalyst	Reaction time/h	Product	Yield (%)
PPh_3	Pd/C(10%)	9	$Re_2(CO)_9(PPh_3)$	20
			$Re_2(CO)_8(PPh_3)_2$	20
$PMePh_2$	Pd/C(10%)	6	$Re_2(CO)_9(PMePh_2)$	20
			$Re_2(CO)_8(PMePh_2)_2$	40
	PdO	3	$Re_2(CO)_8(PMePh_2)_2$	60
			$HRe(CO)_3(PMePh_2)_2$	3
PMe_2Ph	Pd/C or $Pd/CaCO_3$(10%)	2	$Re_2(CO)_9(PMe_2Ph)$	2
			$Re_2(CO)_8(PMe_2Ph)_2$	82
			$HRe(CO)_3(PMe_2Ph)_2$	3
	PdO	1	$Re_2(CO)_8(PMe_2Ph)_2$	84
$P(CH_2C_6H_5)_3$	Pd/C(10%)	8	$Re_2(CO)_{10}$	14
			$Re_2(CO)_9(P(CH_2C_6H_5)_3)$	15
			$Re_2(CO)_8(P(CH_2C_6H_5)_3)_2$	12
PMe_3	PdO	2	$Re_2(CO)_9(PMe_3)$	14
			$Re_2(CO)_8(PMe_3)_2$	18
$P(OMe)_3$	Pd/C(10%)	4	$Re_2(CO)_9(P(OMe)_3)$	55
			$Re_2(CO)_8(P(OMe)_3)_2$	25

TABLE 15.6: IR spectral data for the $Re_2(CO)_{10-n}(PR_3)_n$ (n = 1,2) derivatives

Complex	ν(CO)/cm^{-1} ($CHC\ell_3$ solution)
$Re_2(CO)_9(PPh_3)$	2114(w,sp),2040(w,sp),1998(vs),1964(sh),1940(m)
$Re_2(CO)_9(PMePh_2)$	2111(w,sp),1040(w,sp),1995(vs),1962(sh),1938(m)
$Re_2(CO)_9(PMe_2Ph)$	2108(w,sp),2038(m,sp),1990(vs),1960(sh),1932(m)
$Re_2(CO)_9[P(CH_2C_6H_5)_3]$	2110(w,sp),2034(w,sp),1998(vs),1962(sh),1938(m)
$Re_2(CO)_9(PMe_3)$	2108(w,sp),2040(m,sp),1990(vs),1956(sh),1929(m)
$Re_2(CO)_9[P(OMe)_3]$	2108(w,sp),2040(w,sp),1994(vs),1952(sh),1930(m)
$Re_2(CO)_9(AsMe_2Ph)$	2112(w,sp),2052(m,sp),1998(vs),1964(w), 1930(m)
$Re_2(CO)_8(PPh_3)_2$	2000(sh),1958(vs)
$Re_2(CO)_8(PMePh_2)_2$	2015(w,) 1954(vs)
$Re_2(CO)_8(PMe_2Ph)_2$	2010(w), 1949(vs)
$Re_2(CO)_8[P(CH_2C_6H_3)_3]_2$	2010(sh),1954(vs)
$Re_2(CO)_8(PMe_3)_2$	2000(sh),1943(vs)
$Re_2(CO)_8[P(OMe)_3]_2$	2000(sh),1970(vs)

TABLE 15.7: IR spectral data for the $C\ell Re(CO)_3(PR_3)_2$ complexes

Complex	ν(CO)/cm^{-1} ($CHC\ell_3$ solution)
$C\ell Re(CO)_3(PMePh_2)_2$	2030(s,sp),1954(s),1895(s)
$C\ell Re(CO)_3(PMe_2Ph)_2$	2044(s,sp),1957(s),1896(s)
$C\ell Re(CO)_3[P(CH_2C_6H_3)_3]_2$	2024(s,sp),1940(s),1900(s)
$C\ell Re(CO)_3(PMe_3)_2$	2036(s,sp),1950(s),1894(s)
$C\ell Re(CO)_3(P(OMe)_3]_2$	2040(s,sp),1970(s),1910(s)
$C\ell Re(CO)_3(AsMe_2Ph)_2$	2050(s,sp),1960(s),1914(s)

between $Re_2(CO)_{10}$ and $AsMe_2Ph$ yielded only $Re_2(CO)_9(AsMe_2Ph)$ (74%) and fac-$C\ell Re(CO)_3(AsMe_2Ph)_2$ (15%). The IR spectrum of $Re_2(CO)_9(AsMe_2Ph)$ [IR($CHC\ell_3$), ν(CO): 2112(w,sp), 2052(m,sp),1998(vs),1964(w),1930(m) cm^{-1}] indicates ax-substitution. This is also the case for $Mn_2(CO)_9(AsMe_2Ph)$[23] [IR(benzene), ν(CO): 2094(w), 2016(s),1993(vs),1969(sh), 1938(m) cm^{-1}].

The Me_3NO-assisted reaction between $Re_2(CO)_{10}$ and PR_3 in $CH_2C\ell_2$ (40°C) or $CHC\ell_3$ (20°C, PR_3 = PPh_3)[173] *yielded* axially substituted $Re_2(CO)_{10-n}(PR_3)_n$ (n = 1,2) products. However, it was found that when the Me_3NO-assisted reaction between $Re_2(CO)_{10}$ and PMe_2Ph was conducted in acetonitrile, MeCN, (see section 15D.2.3) instead of $CH_2C\ell_2$, a cream product was obtained (80°C, 2 h), with a complex IR spectrum [IR(hexane), ν(CO): 2078(mw,sp),2000(m,sp),1974(sh),1964(vs, br),1932(s),1916(s) cm^{-1}]. *This product analysed as* $Re_2(CO)_8(PMe_2Ph)_2$ [C: 33.5%, H: 2.7%, cf. Calc. for $Re_2C_{24}H_{22}O_8P_2$, C: 33.0%, H:2.5%; Found for diax-$Re_2(CO)_8(PMe_2Ph)_2$, C: 33.3%, H: 2.6%; mp: 142-44°C, cf. 108-109°C for diax-$[Re_2(CO)_8(PMe_2Ph)_2]$. The similarity to the IR spectrum of 1,2-ax,eq-$Re_2(CO)_8(PPh_3)_2$ [IR(toluene), ν(CO): 2069(mw), 2012(m),1964(vs,br),1934(m),1921(m) cm^{-1}][176] suggests that the product is the isomer, 1,2-ax,eq-$Re_2(CO)_8(PMe_2Ph)_2$. Attempts to obtain crystals suitable for an X-ray crystallographic study of this complex to confirm the substitution geometry have to date not been successful.

The reaction which led to the formation of this product did not follow the usual procedure for the Me_3NO-route (see section 15D.2.2) in that the Me_3NO was added before the PMe_2Ph, and the reaction was conducted in MeCN, not $CH_2C\ell_2$. Reaction, presumedly to dieq-$Re_2(CO)_9(NCMe)_2$ [dieq-$Re_2(CO)_8(NCMe)_2$ has been prepared by the amine-oxide assisted route [IR(NCMe), ν(CO): 2070(w),2015(w),1962(s), 1909(m) cm^{-1}].[175] From the IR data of Table 15.4 for $M_2(CO)_8(L)_2$ complexes, this spectrum would appear to be that of a 1,2-eq,eq-isomer (IIC)), was instantaneous, as evidenced by the colourless solution becoming yellow. On

subsequent addition of the PMe_2Ph ligand, reaction occured with displacement of the NCMe ligands, to give 1,2-ax,eq-$Re_2(CO)_8(PMe_2Ph)_2$, steric consideration determining 1,2-*ax,eq*- rather than 1,2-eq,eq-substitution. (Tolman cone angle[65] of PMe_2Ph: 122°).

It is significant to note that sidebands are often observed in the IR spectra of diax-$Re_2(CO)_8(PR_3)_2$ complexes. For diax-$Mn_2(CO)_8(PR_3)_2$, Lewis et al [77] have ascribed these to *Raman active bands which gain weak IR intensity. However,* this cannot be the case, as these sidebands disappear on recrystallization, eg. single crystals of diax-$Re_2(CO)_8(PMe_2Ph)_2$, *used in the* X-ray study (section 15E), exhibited no sidebands in the IR spectrum ($CHCl_3$). An IR spectrum run on a crude sample of diax-$Re_2(CO)_8(PMe_2Ph)_2$ (toluene solution) had sidebands at 2070(w),2020(m),1930(sh) and 1920(sh) cm^{-1}, in addition to the very strong band at 1950 cm^{-1}. On heating in toluene solution (80°C) for 4 h, these sidebands were observed to grow in intensity, and a shoulder to the main 1950 cm^{-1} band developed at ca. 1965 cm^{-1}. It will be observed that these sidebands correspond to the ν(CO) bands of the 1,2-ax,eq-$Re_2(CO)_8(PMe_2Ph)_2$ isomer (vide supra). As the diax-$Re_2(CO)_8(PMe_2Ph)_2$ and 1,2-ax,eq-$Re_2(CO)_8(PMe_2Ph)_2$ products run together on TLC, separation of the isomers could not have been effected.

The formation of some 1,2-ax,eq-$Re_2(CO)_8(PME_2Ph)_2$ in the Pd-catalysed and Me_3NO-assisted (CH_2Cl_2 solvent) reactions, as evidenced by the above "sidebands", and the partial isomerization described above (ie. growth of sidebands on heating), are consistent with a report of the formation of eq-substituted isomers, $Re_2(CO)_8(PMe_2Ph)_2$ [IR(CCl_4), ν(CO): 2100(w), 2060(mw),2000(s),1955(s,br),1905(s) cm^{-1}][67] and $Re_2(CO)_8(PMePh_2)_2$[IR(benzene), ν(CO): 2090(w),2058(m), 2000(s), 1955(s,br),1925(s) cm^{-1}],[68] in the thermal reaction of $Re_2(CO)_{10}$ with PR_3 at elevated temperatures and for extended reaction times (eg. PMe_2Ph[67]: petroleum ether, 80-100°C, 60-96 h; $PMePh_2$[68]: xylene, 140°C, 15 h). These isomers were originally assigned as 1,2-eq,eq-$Re_2(CO)_8(PR_3)_2$[67,68]

but from the IR data appear to be 1,2-ax,eq-$Re_2(CO)_8(PR_3)_2$ (see section 15B.3). Following the published procedure[184] (see section 15D.2.4), the thermal reaction of $Re_2(CO)_{10}$ with excess $PMePh_2$ (xylene, 140°C, 15 h) yielded a yellow product, characterized by IR data [IR(xylene), ν(CO): 2095(w),2060(m),2000(s),1950(s),1922(m) cm^{-1}] as 1,2-ax,eq-$Re_2(CO)_8(PMePh_2)_2$ [Tolman cone angle[85] of $PMePh_2$: 136°].

Note that for the large phosphine ligand, PPh_3 (Tolman cone angle[85] of 145°), there were no sidebands in the IR spectrum of the crude diax-$Re_2(CO)_8(PPh_3)_2$ product from the Pd-catalysed reaction. Hence the size of the phosphine ligand, ie. steric factors, would appear to determine whether eq-substituted isomers are stable.

According to the mechanism of phosphine substitution on $Re_2(CO)_{10}$, to give diax-$Re_2(CO)_8(PR_3)_2$,[182] $Re_2(CO)_{10}$ undergoes monosubstitution to yield ax-$Re_2(CO)_9(PR_3)_2$, steric considerations presumedly determining the final axial position of the PR_3 ligand. In consequence of the cis-labilization effect (see ch XII), a CO cis to the PR_3 ligand is more easily lost, but the second incoming PR_3 cannot take up the cis position on the same metal because of steric interactions. A vacancy is created on the second metal via a bridging carbonyl mechanism, and the PR_3 ligand occupies the axial site, giving diax-$Re_2(CO)_8(PR_3)_2$, steric factors again governing axial substitution (see Fig. 15.4).

However, equatorially-substituted $Re_2(CO)_8(PR_3)_2$ isomers have been formed by several methods:-

(i) Reaction of (μ-H)(μ-olefin)$Re_2(CO)_8$ complexes with PR_3 ligands, resulting in the formation of 1,2-eq,eq-$Re_2(CO)_8(PR_3)_2$ (R = Me, OMe, OPh) or 1,2-ax,eq-$Re_2(CO)_8(PR_3)_2$ (R = Bu^n, Ph),[176] depending on the size of the phosphine ligand [Tolman cone angles[85]: $P(OMe)_3$, 107°; PMe_3, 118°; $P(OPh)_3$, 121-128°; PBu^n_3, 132°; PPh_3, 145°]. Bidentate phosphine ligands, $(P)_2$, also gave 1,2-eq,eq-$Re_2(CO)_8(P)_2$ products ($(P)_2$ = $Ph_2PCH_2PPh_2$,[170,188] $Me_2PCH_2PMe_2$, $Ph_2PCH_2CH_2PPh_2$, $Me_2PCH_2CH_2PMe_2$).[188] [The Tolman cone angles (half chelates)[85a] for these $(P)_2$ ligands range from

Author Harris Gillian Wendy
Name of thesis Chemical And Structural Studies Of Substituted Transition Metal Carbonyl Complexes. 1984

PUBLISHER:
University of the Witwatersrand, Johannesburg
©2013

LEGAL NOTICES:

Copyright Notice: All materials on the University of the Witwatersrand, Johannesburg Library website are protected by South African copyright law and may not be distributed, transmitted, displayed, or otherwise published in any format, without the prior written permission of the copyright owner.

Disclaimer and Terms of Use: Provided that you maintain all copyright and other notices contained therein, you may download material (one machine readable copy and one print copy per page) for your personal and/or educational non-commercial use only.

The University of the Witwatersrand, Johannesburg, is not responsible for any errors or omissions and excludes any and all liability for any errors in or omissions from the information on the Library website.